Impact of Vegetation in Open Channels on Flow Resistance and Solute Mixing

James D. Shucksmith

Department of Civil and Structural Engineering

University of Sheffield

Thesis Submitted in Partial Fulfilment of the Requirements for the Degree of Doctor of Philosophy

Date: February 2008

Summary : This thesis has investigated the impacts of vegetation on flow resistance and mixing in open channel flow. Existing methods and models proposed by previous research which predict flow and mixing in vegetated channels have been presented and discussed. The most pressing issues have been identified as a lack in understanding of how vegetation affects solute mixing, and a lack of verification of existing flow resistance models in situations involving real rather than simulated vegetation.

To address these issues, a detailed laboratory study has been undertaken. This involved growing real vegetation in the laboratory environment and conducting tests whilst the vegetation grew in size, density and stiffness. Two vegetation types (Carex and Phragmites Australis) were used to provide an indication of how different plant species affect flow and mixing.

Experiments involved the collection of flow resistance, velocity, turbulence and transverse and longitudinal mixing data at different stages of plant growth and whilst the vegetation was in both emergent and submerged states. This involved the use of an acoustic Doppler velocity probe to measure velocity and turbulence. Measurements of mixing were made using CYCLOPES-7 fluorometers with fluorescent tracer used as solute.

The presence of vegetation increased the channels flow resistance. As the vegetation grew the resistance increased. In emergent conditions direct measurements of velocity and Reynolds stress were retarded compared to non vegetated experiments and reduced longitudinal mixing was observed. In submerged conditions more complex profiles of velocity and Reynolds stress were measured and longitudinal mixing was dependant on the canopies submergence ratio and the rate of vertical mass transport between the flow above and within the canopy. Results were compared with predictions made by existing vegetated flow models. New models and methodologies for predicting flow and mixing in vegetated canopies have been presented and tested against the data with good results.

Contents

List of Figures

List of Tables

Notation

Latin

A	=	Cross sectional flow area	(m^2)
A_c	=	Area of free flow zone	(m^2)
A_i	=	Frontal area of vegetation element	(m^2)
b	=	Channel width	(m)
c	=	Concentration	(kg/m^3)
c'	=	Deviation in concentration	(kg/m^3)
C	=	Ensemble average concentration	(kg/m^3)
C_1	=	Empirical coefficient based on vegetation density	(-)
C_2	=	Empirical coefficient based on vegetation stiffness	(-)
C_c	=	Concentration within cell	(kg/m^3)
C_i	=	Inflowing concentration	(kg/m^3)
C_d	=	Drag coefficient	(-)
C_{di}	=	Idealised drag coefficient of a cylinder in 2D flow	(-)
C_d'	=	Vegetal drag coefficient	(m^{-1})
C_h	=	Chèzy coefficient	(m/s^2)
C_q	=	Discharge coefficient	(-)
D_s	=	Average grain size	(m)
D_x	=	Longitudinal dispersion coefficient	(m^2/s)
Df	=	Dispersive fraction	(-)
d_c	=	Depth of mixing/shear layer	(m)
d_b	=	Depth of flow influenced by the boundary	(m)
e_i	=	Turbulent diffusion coefficient / eddy diffusivity (in i direction)	(m^2/s)
e_c	=	Wake zone diffusivity	(m^2/s)
E	=	Modulus of elasticity	(N/m^2)
f	=	Darcy-Weisbach friction factor	(-)
F	=	Force	(N)
F_d	=	Drag Force	(N)
g	=	Acceleration due to gravity	(m^2/s)
h	=	Flow depth	(m)
h_c	=	Height of vegetation (canopy height)	(m)
h_{ac}	=	Depth of free flow zone	(m)
I	=	Second moment of area	(m^4)
k_d	=	First order decay rate coefficient	(-)
k_0	=	Roughness height	(m)
K_y	=	Transverse mixing coefficient	(m^2/s)
k_p	=	Roughness parameter of plants	(m)
J_i	=	Mass flux in i coordinate	(kg/m^2s)
l	=	Mixing length	(m)
L	=	Length scale	(m)
L_x	=	Lagrangian distance	(m)
m_t	=	Measured concentration level at time t	(kg/m^3)
M	=	Mass	(kg)
M_i	=	$_i$ th moment of distribution	(-)
M_o	=	Momentum	(kgm/s)
n	=	Manning's roughness coefficient	($s/m^{1/3}$)
n_b	=	Manning's roughness coefficient (contribution from bed only)	($s/m^{1/3}$)
n_c	=	Manning's roughness coefficient of canopy top	($s/m^{1/3}$)
N	=	Stem density (stems per unit area)	($stems/m^2$)

p_t	=	Concentration level predicted by the model at time t	(kg/m^3)
P	=	Wetted perimeter	(m)
P_D	=	Pressure drop	(m)
Q	=	Discharge	(m^3/s)
Q_c	=	Discharge in canopy layer	(m^3/s)
q_i	=	Fractional thickness of zone i relative to the flow depth	(-)
R	=	Hydraulic radius	(m)
R_c	=	Hydraulic radius of canopy zone only	(m)
R_{ac}	=	Hydraulic radius above the canopy (free flow zone)	(m)
R_x	=	Lagrangian autocorrelation function	(-)
Re	=	Flow Reynolds number	(-)
Re_{st}	=	Stem Reynolds number	(-)
Rt^2	=	Goodness of fit	(-)
s	=	Time differential	(s)
s_p	=	Vegetation spacing	(m)
s_s	=	Distance between roughness strips	(m)
Sc	=	Schmidt number	(-)
S_o	=	Bed slope	(-)
S_d	=	Stem diameter	(m)
Sr	=	Submergence ratio	(-)
t	=	Time	(s)
Δt	=	Time step	(s)
$\bar{t}_i$	=	Centroid of concentration distribution at site i	(s)
T	=	Residence time	(s)
$\overline{T}$	=	Travel time	(s)
T_d'	=	Timescale for cross sectional mixing over the flow depth	(s)
T_w'	=	Timescale for cross sectional mixing over the flow width	(s)
T_x	=	Lagrangian timescale	(s)
U	=	Average cross sectional velocity	(m/s)
u*	=	Shear velocity	(m/s)
u^*_{hc}	=	Shear velocity at canopy top	(m/s)
Δu	=	Average difference in velocity between flow zones	(m/s)
U_c	=	Average velocity through the canopy layer	(m/s)
U_{ac}	=	Average velocity above the canopy (free flow zone)	(m/s)
U'	=	Cross sectional mean of velocity deviation	(m^2/s)
u_i	=	Longitudinal velocity of zone i	(m/s)
u	=	Longitudinal velocity	(m/s)
v	=	Transverse velocity	(m/s)
w	=	Vertical velocity	(m/s)
u'	=	Velocity deviation from temporal average in x dimension	(m/s)
v'	=	Velocity deviation from temporal average in y dimension	(m/s)
w'	=	Velocity deviation from temporal average in z dimension	(m/s)
X	=	Position of origin	(-)
x	=	Longitudinal distance	(m)
y	=	Transverse distance	(m)
z	=	Vertical distance	(m)
z'	=	Canopy deflection under flow	(m)
V_c	=	Cell volume	(m^3)
V_e	=	ADZ volume (Dead zone volume)	(m^3)
V_R	=	Total volume in the reach	(m^3)

Greek

ε	=	Eddy viscosity	(Ns/m^2)
η	=	Molecular diffusion coefficient	(m^2/s)
θ	=	Angle of slope	(degrees)
κ	=	Von Karman's constant	(-)
λ	=	Channel porosity (fraction of control volume taken up by water)	(-)
μ	=	Dynamic viscosity	(Ns/m^2)
ρ	=	Fluid density	(kg/m^3)
σ^2	=	Variance of distribution	(-)
τ	=	Cell time delay	(s)
τ_0	=	Boundary shear stress	(N/m^2)
$\tau_{R(i,j)}$	=	Reynolds stress (in (i,j) plane)	(N/m^2)
τ_c	=	Reynolds stress in the wake zone	(N/m^2)
τ_t	=	Total shear stress	(N/m^2)
τ_v	=	Viscous shear stress	(N/m^2)
ν	=	Kinematic viscosity	(m^2/s)
φ	=	Centroid of distribution	(-)
Ψ	=	Inter-zone transfer coefficient	(s^{-1})
ω	=	Vegetation Index	(N/m^2)

Other Symbols

$\langle\ \rangle$	=	Spatial Average
$\bar{\ }$	=	Temporal Average

Chapter 1 - Introduction

Effective water management is of rapidly increasing global importance. Global water demand is increasing as nations grow and develop. Seventy percent of current water supply is used for agriculture, as the global population increases (forecast to be 8.9 billion people by 2050) this demand will rise (Berrittella et al., 2007). Water consumption will also grow if developing countries aspire to western diets and lifestyles (see Table 1).

Table 1 – Water demand around the world in litres/day (World Water Council, 2007)

Average African Citizen	UN recommended minimum	Average European	Average American or Japanese
10-20	50	200	350

To make effective use of existing water supplies the effect of water pollution needs to be fully understood. In newly industrialised nations the pollution in natural waterways is increasing, as the amount of polluted water grows, the amount of usable water declines. The need to understand the full impact of contamination on water quality places increased demand on water quality models to accurately predict the fate of pollutants in natural channels.

Increasing urbanisation in developed nations, together with a higher risk of severe weather events due to the impacts of climate change highlight the need for the effective flood forecasting of waterways. To do this the flow resistance of each channel must be accurately quantified.

Aquatic and semi aquatic vegetation has been recognised as an important and increasingly valuable resource for numerous reasons such as

- Dissipating stream energy: Vegetation and root systems dissipate stream energy, resulting in less soil erosion and a reduction in flood damage.
- The ability to trap sediment: Reduce suspended sediments creates less turbid water and replenishes soils and build stream banks.
- The enhanced filtration of pollutants and thus improvement of water quality.
- Provision of wildlife habitats, increasing biodiversity and forage for wildlife and livestock.
- Increasing aesthetic appeal.

The use of in-channel treatment systems based on the use of semi aquatic plants such as

common reeds (*Phragmities Australis*) is becoming also more popular (Jadhev and Buchberger, 1995). By planting reed beds downstream of sewer outfalls these systems help improve water quality in the channel. However the presence of in-channel vegetation has an impact on the flow resistance of waterways.

1.1 Vegetation and Flow Resistance

Accurate determination of hydraulic resistance is important in evaluating the flow capacity of a channel. Vegetation is a significant cause of hydraulic resistance, slowing the flow and increasing the flow depth relative to a non vegetated channel (Wilson et al., 2005). Much work (Stone and Shen, 2000, Wu et al., 1999) has been performed attempting to quantify this additional flow resistance. Plant flexibility, density and height all have impact on the flow resistance of the channel but all are difficult to acquire without a full survey of the channel in question. The biomechanical properties of vegetation vary from species to species making idealised laboratory studies using artificial vegetation of limited use when the findings are applied to actual channels (Green, 2005).

Figure 1-1 Flow in a Vegetated Watercourse (River Lathkill, Derbyshire, UK)

1.2 Vegetation and Mixing

Growing environmental concern regarding waterways generates an increased demand on water quality models to accurately predict pollution levels in natural watercourses. There is a need to understand the fate of pollutants once they enter watercourses and for this an understanding of mixing processes in open channel flow is imperative (Guymer, 1998). The science of river mixing is used to solve a variety of environmental problems such as designing outlet structures to comply with water quality criteria, evaluating the environmental impact of potential and

actual pollutant spills and gauging the ecological potential of watercourses. One area of research that has been largely overlooked is the influence of in channel vegetation on the mixing characteristics of the flow. How does the presence of vegetation impact on the magnitude and nature of mixing taking place? Understanding the influence of vegetation on mixing is also important in trying to evaluate the spread of nutrients and pollutants through in channel treatment facilities which feature vegetation. As a first step towards understanding pollution transport in vegetated flow, the work in this thesis is restricted to the study of the mixing of neutrally buoyant pollutants.

1.3 Aim of Thesis

The aim of this thesis is to experimentally investigate the impact of vegetation in open channel flow on flow resistance and mixing processes.

1.4 Thesis Structure

This thesis is organised according to the following structure

1. Introduction to the concepts of open channel flow, including flow resistance, turbulence and mixing in open channels

2. A review of existing theory which seeks to describe flow resistance, turbulence and mixing in vegetated open channels.

3. An identification of the existing research questions in regard to flow resistance and mixing in vegetated flow

4. A description of the experimental procedure which was undertaken to answer the research questions identified

5. A presentation and discussion of the results arising from the experimental program

6. A review of the performance of existing predictive techniques when tested against the experimental data, together with the development of new methods.

7. A presentation of the main conclusions of the thesis as well as recommendations for future work.

Chapter 2 - Open Channel Flow Theory

The aim of this chapter is to introduce the principles of flow, turbulence and mixing in open channels.

2.1 Concepts of Flow

2.1.1 Steady and Unsteady Flow

Water flowing though open channels is subject to both gravitational force driving flow downstream, and resistance from drag and shear as the flow travels over channel boundaries and past obstacles in the channel (such as vegetation). Flow can be classified into three different types.

- Steady uniform (or Normal) flow: Depth is constant with time and distance.
- Steady non uniform flow: Depth varies with distance but not time.
- Unsteady Flow: Depth varies with distance and time.

Normal flow occurs when flow resistance is in equilibrium with gravitational forces (Chow, 1959). This condition rarely occurs in natural channels. However, in practice normal flow conditions are often assumed because it considerably simplifies flow calculations. Channels with insignificant or no resistance from vegetation or other sources (such as other in-channel objects) are only subject to resistance from the frictional effects of the channel boundary. Whilst the basic concepts of flow and mixing are introduced, it will be assumed that all resistance comes from the channel boundary and that all flow is uniform.

2.1.2 Governing Equations

A set of equations exist to describe flow in open channels which are based on the principles of conversation of mass, energy and momentum. When applying the principle of conservation of mass over a given length of channel, if there are no flow inputs or outputs, discharge must remain constant. Considering the longitudinal flow direction the continuity equation is defined as

$$Q = UA \qquad \text{Equation 2-1}$$

Where: Q = Discharge (m^3/s)

U	=	Average cross sectional velocity	(m/s)
A	=	Cross sectional area	(m^2)

For a given discharge, the area, A (and hence flow depth) will increase as flow velocity decreases. To estimate flow velocity and hence depth in open channel flow engineers have derived equations of motion which balance gravitational and frictional forces within open channels. However such equations also require an understanding of the basic properties of fluids and flow.

2.1.3 Fluid and Flow Properties

2.1.3.1 Viscosity

Viscosity represents the resistance of a fluid to deformation. The molecular (or dynamic) viscosity can be defined as 'The internal friction of a fluid that resists forces tending to cause flow' (Robert, 2003). In a fluid the relationship between the applied force, the rate of fluid shear and the dynamic viscosity (resistance to shear) can be expressed as

$$\tau_v = \mu \frac{du}{dz} \qquad \text{Equation 2-2}$$

Where	τ_v	=	Viscous shear stress	(N/m^2)
	μ	=	Dynamic viscosity	(Ns/m^2)
	u	=	Velocity parallel to shearing force	(m/s)
	z	=	Distance from applied force	(m)

Hence the application of shear stress (i.e. a force applied over a given area) to a fluid will produce a change in velocity relative to the distance from the origin of the stress. In most open channels, shear stress is applied by the frictional effects of the channel boundaries, producing a change in velocity relative to the channel bed and banks. The rate of change of velocity is dependent on the viscosity of the liquid being considered. So, for a given shear stress the greater the viscosity, the smaller the velocity gradient within the flow. Viscosity can also be expressed in kinematic terms.

$$\nu = \frac{\mu}{\rho}$$ Equation 2-3

Where ν = Kinematic viscosity (m^2/s)

ρ = Fluid density (kg/m^3)

In a Newtonian fluid such as water the viscosity of a fluid varies only with temperature (Table 2), in a non Newtonian fluid the viscosity may also vary with the rate of shear.

Table 2 –Dynamic Viscosity of Water (Robert, 2003)

Temperature, (degrees C)	Dynamic Viscosity, μ (Ns/m^2)
0	0.018
10	0.0131
20	0.00998

2.1.3.2 *Laminar, Transitional and Turbulent Flow*

The existence of distinct flow regimes was first investigated by Osborne Reynolds in 1883. By conducting experiments injecting filaments of dye into a flow though a glass tube, three distinct flow regimes (laminar, transitional and turbulent) were observed as the flow rate increased (Figure 2-1).

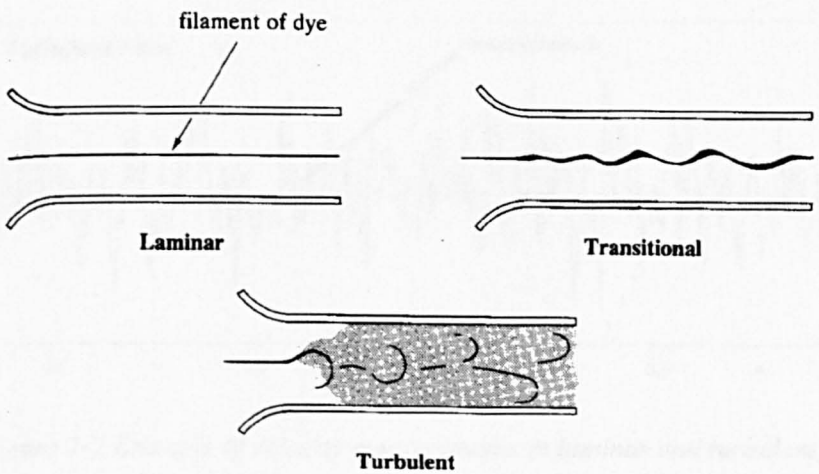

Figure 2-1 Filament of dye in laminar, transitional and turbulent flow (Chadwick and Morfett, 1994).

In laminar flows the relationship between the shearing force, fluid viscosity, and velocity gradient can be described by Equation 2-2. Such flow can be considered as a series of very fine layers sliding over each other, with no mixing between them. The layer closest to the boundary

is assumed to be stationary, with subsequent layers sliding over one another subject to shearing action with the layer below. Hence, in laminar flow fluid travels in a series of independent layers and the velocity of each layer remains constant with time. However, if the overall fluid velocity is increased this ordered pattern of flow begins to break down.

In transitional flow the effects of local disturbances in the flow begin to become apparent, and the distinct flow layers begin to mix. If the flow velocity is increased further the flow enters a turbulent regime in which distinct flow layers in the flow are no longer visible. The motion of a fluid particle in the flow will be unsteady, its velocity and direction will vary with time (Figure 2-2). Flow in this regime is dominated by turbulent eddies which transport mass and momentum throughout the flow. A substance injected into turbulent flow will be transported throughout the flow by turbulent eddies, mixing rapidly in comparison to laminar flow. Turbulent flow can still be classified as uniform (despite its unsteady nature over short timescales) if the temporal mean velocity remains constant with time.

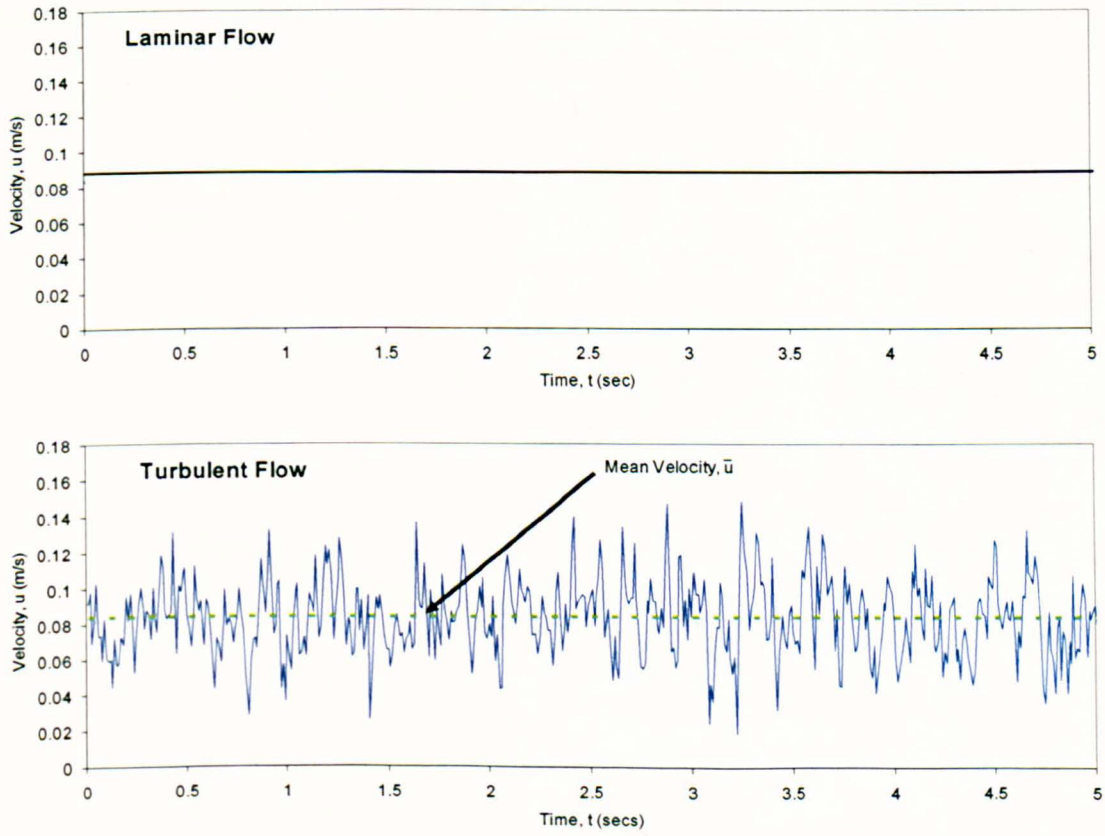

Figure 2-2 Example of velocity measurements in laminar and turbulent flow

Flow can be classified as laminar, transitional or turbulent by the determination of the flow Reynolds number which is a ratio between the inertia force and viscous force acting on the flow. A dimensionless Reynolds Number Re, as defined by Chadwick and Morfett (1994), may be expressed as

$$\mathrm{Re} = \frac{UL}{\upsilon}$$ Equation 2-4

Where L = Length Scale (m)

To derive flow Reynolds number, the length scale, L is most commonly taken as flow depth in open channel flow. Using this definition flow regimes can be classified according to Table 3.

Table 3 –Flow Regimes for open channel flow (Robert, 2003)

Reynolds Number	Flow Regime
Re < 500	Laminar
500< Re < 2000	Transitional
Re>2000	Turbulent

In the vast majority of open channel flows experienced in nature, Re >> 2000, and hence flow is fully turbulent.

2.2 Flow Resistance

As explained in section 2.1.2, by balancing the forces in an open channel (Figure 2-3) a flow resistance equation can be determined.

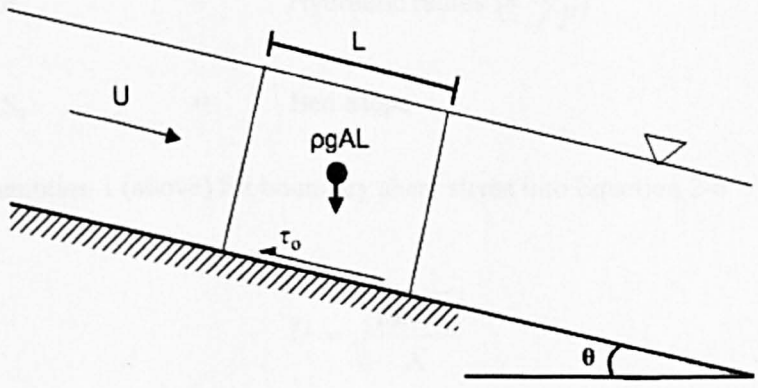

Figure 2-3 Force diagram in uniform flow conditions.

2.2.1 Chèzy's Equation

The Chèzy formula was developed by Anotine Chèzy in 1769 and verified by testing on the Courpalet Canal and the Seine River. It can be derived theoretically based on two assumptions.

1. The force resisting flow per unit area of the bed is proportional to the square of the average velocity. ($F = KU^2$, where K = constant.)

2. The gravity force is equal to the flow resistance (i.e. Uniform flow conditions)

Based on assumption 2

$$\rho g A L \sin\theta = \tau_o P L \qquad \textit{Equation 2-5}$$

Where	g	=	Acceleration due to gravity	(9.81 m^2/s)
	L	=	Length considered	(m)
	θ	=	Angle of slope	(degrees)
	τ_0	=	Boundary shear stress	(N/m^2)
	P	=	Wetted perimeter	(m)

As slopes in rivers are generally shallow $\sin\theta \approx \tan\theta \approx S_o$, therefore the boundary shear stress can be defined as

$$\tau_o = \rho g R S_o \qquad \text{Equation 2-6}$$

Where	R	=	Hydraulic radius $\left(= A/P\right)$	(m)
	S_o	=	Bed Slope	(-)

Substituting assumption 1 (above) for boundary shear stress into Equation 2-6

$$U = \sqrt{\frac{\rho g R S_o}{K}} \qquad \text{Equation 2-7}$$

Taking the Chèzy coefficient, C_h to be

$$C_h = \sqrt{\frac{\rho g}{K}} \qquad \text{Equation 2-8}$$

Average channel velocity can be determined by

$$U = C_h\sqrt{RS_o} \qquad \text{Equation 2-9}$$

Equation 2-9 is easy to use provided an accurate value for the Chèzy resistance coefficient (C_h) can be determined. The Chèzy coefficient is dependent on both bed roughness and Reynolds number and has the dimensions of acceleration (i.e. m^2/s). Several methods for estimating the Chèzy coefficient based on parameters such as bed roughness, slope and hydraulic radius have been proposed. The reader is referred to Chow (1959) for details on these methods.

2.2.2 Manning's Equation

In 1889 Robert Manning proposed a flow resistance formula based on both previous flow resistance equations and experimental observation. Essentially Manning proposed that the Chèzy coefficient can be evaluated by

$$C_h = \frac{R^{1/6}}{n} \qquad \text{Equation 2-10}$$

Where n = Manning's roughness coefficient ($s/m^{1/3}$)

Manning's roughness coefficient (n) is an empirical value determined by the resistance of the bed. Empirically derived Manning's n values for flow over various surfaces can be found in Chadwick and Morfett (1994) and Chow (1959). Substituting Equation 2-10 into Equation 2-9 gives the Manning's equation.

$$U = \frac{R^{2/3}S_o^{1/2}}{n} \qquad \text{Equation 2-11}$$

As the Manning's n value is dependant from boundary roughness alone, it is easier to determine than the Chèzy coefficient. Therefore because of its simplicity of use and accurate results the Manning's equation has become the most widely used open channel flow resistance formula (Chadwick and Morfett, 1994). The Manning's (and Chèzy) equation is only applicable in uniform flow conditions (spatially constant flow depth, flow area, and cross sectionally averaged velocity) in the case of fully rough turbulent flow. However, in practice it is frequently used by engineers for a variety of flow conditions.

2.3 Turbulent Flow

The basic principles of turbulent flow were introduced in section 2.1.3.2. The complex nature of turbulence means that a complete, accurate mathematical description of turbulence based on the laws of mass, energy and momentum continuity is still beyond the capabilities of modern computers for all but the simplest of problems (Douglas et al., 2005). To investigate turbulent flow scientists and engineers have developed a number of statistical tools capable of describing turbulence in open channel flow. The advent of laser and acoustic Doppler instruments in recent years has enabled engineers to accurately measure turbulence in open channels directly. This enables the examination of turbulent flow structures within the flow. These structures or eddies can be defined as swirls of fluid with irregular shapes and sizes which are in a continuous state of development and decay. They are crucial for understanding the transfer of mass and momentum throughout the flow.

Turbulence is generated from velocity shear, and hence levels of turbulence will be greatest in area where the velocity gradient is highest (i.e. around sources of flow resistance, such as the channel bed, or other obstacles in the flow). Energy (from the gravitational force driving the flow) originates within the flow as large eddies (which are responsible for most of the mass and momentum transport within the flow), which slowly decay as energy cascades down to the smallest eddies, finally to be dissipated as heat energy (Pope, 2000). This continuous loss of energy means that turbulence is not self sustaining, energy must be continually provided, otherwise the flow will revert to laminar conditions.

2.3.1 *Describing Turbulence*

When discussing turbulence it is useful to define the Cartesian axes and velocity components relative to an open channel (Figure 2-4).

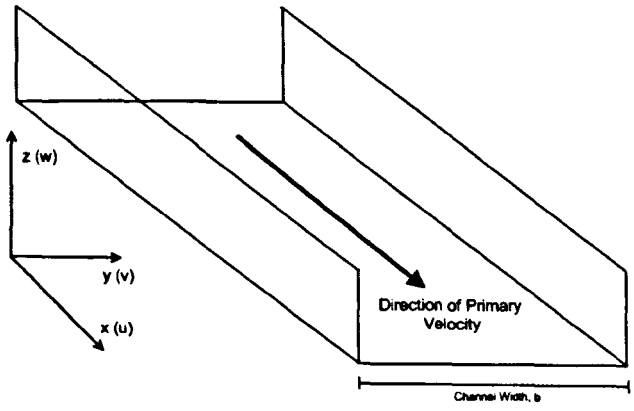

Figure 2-4 Cartesian axes and velocity components relative to an open channel

2.3.1.1 Turbulence Intensity

The velocity at any point in the flow can be decomposed into three perpendicular velocities (Figure 2-4), downstream velocity u, transverse velocity v, (parallel to the channel bed, but normal to the downstream flow), and vertical velocity, w (normal to the downstream flow and the channel bed). In turbulent flow each component of the velocity will not be constant but will vary continuously with time (Figure 2-2). If however the overall flow rate is constant the temporal average of each flow component ($\bar{u}, \bar{v}$ and $\bar{w}$) will be constant. Hence the instantaneous components of velocity at any time can be expressed as

$$u = \bar{u} + u' \qquad \text{Equation 2-12}$$

$$v = \bar{v} + v' \qquad \text{Equation 2-13}$$

$$w = \bar{w} + w' \qquad \text{Equation 2-14}$$

Where u, v and w	=	Instantaneous velocities in x, y and z directions	(m/s)
$\bar{u}, \bar{v}$ and $\bar{w}$	=	Temporally averaged velocities in x, y and z directions	(m/s)
u', v' and w'	=	Velocity deviation in x, y and z directions	(m/s)

Positive or negative deviations of the velocity from the temporally averaged value can give a measure of the turbulence at that position at that point in time.

To obtain a value for the turbulence 'intensity' at a particular position in the flow these deviations must be measured at a frequency and over a length of time sufficient to capture the growth and decay of the flow structures present in the channel. The deviations will form a distribution with a mean value of 0 (i.e. the average velocity measured has a deviation of 0 from the temporal mean). By measuring the spread or standard deviation of the velocity deviations an idea of the average intensity of turbulence at each particular point in the flow is obtained. These are commonly expressed as 'Root Mean Squared' (RMS) values in each coordinate direction

$$RMSu = \sqrt{\overline{u'^2}} \qquad \text{Equation 2-15}$$

$$RMSv = \sqrt{\overline{v'^2}}$$ Equation 2-16

$$RMSw = \sqrt{\overline{w'^2}}$$ Equation 2-17

Turbulence can be classified depending on whether it varies spatially or temporally. Turbulence can be classified as stationary if its intensity constant with time, homogeneous if it does not vary with position in the flow and isotropic if it is equal in each coordinate direction.

2.3.1.2 Reynolds Stress

In section 2.1.3.1 a relationship was established between shear stress and fluid deformation in laminar flow conditions. Shear stress is related to momentum exchange by Newton's second law

The rate of change of momentum of a body is proportional to the resultant force acting on the body and is in the same direction (Newton, 1687).

Hence the shear stress (force per unit area) acting on the fluid is proportional to the rate of change of momentum. In turbulent flows momentum is transferred not only by viscous shear stresses (Equation 2-2) but also by the fluctuating velocity field. Hence by considering the momentum transferred by fluctuations in the velocity field (Equation 2-12 to Equation 2-14) an additional shear stress (termed Reynolds stress) can be determined.

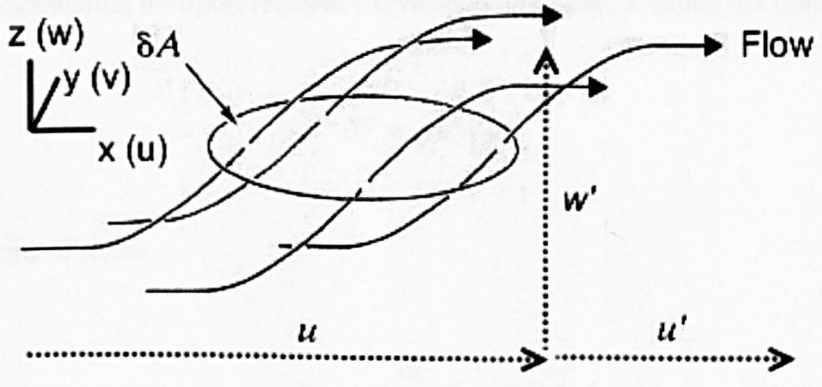

Figure 2-5 Reynolds Stress model (adapted from Chadwick and Morfett, 1994)

Consider two dimensional flow (x and z components only) with velocity fluctuations in the two dimensions represented by u' and w' (Figure 2-5). The mass of fluid passing through a small horizontally aligned element (with area δA) somewhere within the flow during the time interval δt can be represented by

$$\rho w' \delta A \delta t$$ Equation 2-18

Where t = Time (s)

The mass has a horizontal velocity u + u' hence its momentum, δM_o is

$$\delta M_o = \rho w' \delta A \delta t (u + u')$$ Equation 2-19

The rate of transport of momentum (momentum transfer) at this time is

$$\frac{\delta M_o}{\delta t} = \rho w' \delta A (u + u') = \rho \delta A w' u + \rho \delta A w' u'$$ Equation 2-20

To determine the average rate of transport the averaged velocities of the fluid particles must be considered. The average value of the individual velocity fluctuation (w') is zero (see section 2.3.1.1) however the average value of the product (w'u') may not be zero. Hence Equation 2-20 becomes

$$\frac{\overline{\delta M_o}}{\delta t} = \rho \overline{u' w'} \delta A$$ Equation 2-21

The rate of momentum transport requires a corresponding force, F within the fluid

$$\delta F = \rho \overline{u' w'} \delta A$$ Equation 2-22

Hence in terms of stress

$$\tau_{R(xz)} = \frac{\delta F}{\delta A} = -\rho \overline{u' w'}$$ Equation 2-23

Where $\tau_{R(i,j)}$ = Reynolds stress (in (i,j) plane) (N/m^2)

Studies of turbulence in open channel flow (such as Kironoto and Graf, 1994) show that most of the momentum transport is provided either by fast flow moving downwards (towards the bed)

to a slower region of flow (termed a "sweep event") or a slow flow moving upwards into a faster region of flow (termed an "ejection event"). In both of these cases the product w'u' will be negative. Hence Reynolds stresses are conventionally expressed with a negative sign.

By the same process deriving Reynolds stress in the horizontal plane gives

$$\tau_{R(xy)} = \frac{\delta F}{\delta A} = -\rho\overline{u'v'} \qquad \text{Equation 2-24}$$

By combining viscous shear stress Equation 2-2 and Equation 2-3) and Reynolds shear stress the total shear stress, τ_t, at any point in the flow can be determined. In the vertical plane, the total shear stress is given by

$$\tau_t = \tau_v + \tau_R = \rho\nu\frac{du}{dz} - \rho\overline{w'u'} \qquad \text{Equation 2-25}$$

Where τ_t = Total Shear Stress (N/m^2)

In fully turbulent flow the viscous shear stress is insignificant compared to the Reynolds stress and is neglected, conversely in laminar flow the velocity fluctuations in the flow vanish (as explained in 2.1.3.2) and shear stress is solely dependent on the viscous shear stress.

Equation 2-25 describes the shear stress at any point in the flow, although the viscous stress can be easily determined (if the fluid viscosity is known), the Reynolds stress term cannot be mathematically evaluated. Boussinesq (1877) suggested that similarly to viscous stresses the Reynolds stress can be related to the gradient in mean velocity, hence Equation 2-25 becomes

$$\tau_t = \tau_v + \tau_R = \rho\nu\frac{du}{dz} + \rho\varepsilon\frac{du}{dz} = \rho(\nu + \varepsilon)\frac{du}{dz} \qquad \text{Equation 2-26}$$

Where ε = Eddy Viscosity (Ns/m^2)

Whereas dynamic viscosity, ν, is a property of the fluid, eddy viscosity is a property of the flow, Eddy viscosity depends on the size and intensity of the turbulent eddies. In turbulent flow the viscous stresses are often ignored and the equation reduces to

$$\tau_t = \rho\varepsilon\frac{du}{dz}$$ Equation 2-27

2.3.1.3 *Prandtl's Mixing Length Hypothesis*

Prandtl (1925) attempted to quantify the eddy viscosity in turbulent flow. He introduced a characteristic length l, termed the mixing length. If homogeneous turbulence is assumed

$$u' \approx w' \approx l\frac{du}{dz}$$ Equation 2-28

In turbulent flow (i.e. viscous stresses insignificant) Equation 2-25 becomes

$$\tau_t = \rho l^2\left(\frac{du}{dz}\right)^2$$ Equation 2-29

Hence a relationship between the eddy viscosity and the mixing length can be determined

$$\varepsilon = \rho l^2\frac{du}{dz}$$ Equation 2-30

2.3.2 *Boundary Layer Theory*

Open channel flow conditions are usually considered as boundary layers, that is flow where the resistance and therefore the turbulence is generated from a boundary over which the fluid travels. The presence of this boundary creates a spatially varying velocity profile perpendicular to the boundary, with the influence of the boundary resistance decreasing (and hence velocity increasing) with distance from the boundary. In most open channel flow problems the flow considered is much wider than it is deep. Hence for the majority of the flow it is the resistance from the bed rather than the channel banks that will have the most impact on the resistance, velocity distribution and turbulence characteristics of the channel. This assumption allows us to consider two dimensional flow (x,z) over the majority of the flow width.

2.3.2.1 Velocity Distribution in Turbulent Boundary Layers

Using Prandtl's eddy approximation as outlined in section 2.3.1.3, it is possible to derive a relationship between depth and velocity above a boundary in turbulent flow. Although it involves assumptions regarding the eddy size, l, it has been successfully verified by experimental data and accurately describes the velocity profile in the boundary region (i.e. the region where the velocity is influenced by the presence of bed roughness). Assuming that $l = \kappa z$ where κ = constant (i.e. assuming a linear relationship between mixing length and distance from the boundary) and taking $\tau_t = \tau_0$ Equation 2-29 can be written as

$$\frac{\tau_0}{\rho} = (\kappa z)^2 \left(\frac{du}{dz}\right)^2 \qquad \text{Equation 2-31}$$

The parameter $\sqrt{\tau_0/\rho}$ is known as the shear or friction velocity, u*. In terms of u*

$$u^* = \kappa z \frac{du}{dz} \qquad \text{Equation 2-32}$$

Equation 2-32 can be written as

$$du = \frac{u^*}{\kappa}\frac{dz}{z} \qquad \text{Equation 2-33}$$

And u can be described as

$$u = \frac{u^*}{\kappa} \ln\left(\frac{z}{k_0}\right) \qquad \text{Equation 2-34}$$

Equation 2-34 is conventionally written as

$$\frac{u}{u^*} = \frac{1}{\kappa} \ln\left(\frac{z}{k_0}\right) \qquad \text{Equation 2-35}$$

Where κ = Von Karman's Constant (assumed = 0.4) (-)

k_0 = Equivalent roughness height (in rough channels) (m)

The parameters κ and k_0 have been defined experimentally (Bakhmeteff; 1936, Hinze; 1964, Middleton and Southard; 1984). κ is normally taken as a constant (0.4) and k_0 (the height above the bed where the velocity predicted by Equation 2-35 is zero) is dependent on the roughness of the bed. In cases where the boundary is very smooth the roughness parameter k_0 is determined by the shear velocity and fluid viscosity. In cases where the boundary is rough k_o is commonly determined from bed material. For example, for flow over granulated material, Robert (2003) suggests

$$k_0 = \frac{D_s}{30.1} \qquad \text{Equation 2-36}$$

Where D_s = Average grain size (m)

This logarithmic law of the wall (Equation 2-35) is only valid in the region were the assumption $l = \kappa z$ holds, this is strictly only true in one region of the boundary layer (approximately the bottom 20% of the flow, Robert, 2003), however in engineering terms it has proved to be accurate in describing flow over the entire depth and has been verified by experimental testing (Graf and Altinakar, 1998).

Low velocities present close to the bed means a laminar layer of flow (termed the viscous sub layer) can exist adjacent to the channel bed. However, in flow with rough beds and high Reynolds numbers this layer can be neglected as it is very small.

2.3.2.2 *Shear Stress Distribution*

Turbulence and momentum transport throughout the flow is linked to shear stress by Newton's second law (see section 2.3.1.2) therefore in boundary layer flow it is important to quantify shear stress over the flow depth. In open channel flow through simple rectangular channels, resistance is provided by the frictional effects of the channel boundaries. Equation 2-6 provides a theoretical value for bed shear stress based on easily obtainable physical characteristics. In wide channels hydraulic radius can be substituted with flow depth, h (i.e. $R \approx h$). Shear or friction velocity, u^* (introduced in section 2.3.2.1) can be defined as

$$u^* = \sqrt{\frac{\tau_o}{\rho}} = \sqrt{gRS_o} \approx \sqrt{ghS_o} \qquad \text{Equation 2-37}$$

Where h = Flow depth (m)

In channels the friction (or shear) velocity can also be determined by measurements of velocity or Reynolds stress, either by

1. The measured velocity profile in conjunction with the logarithmic law Equation 2-35)
2. In fully rough turbulent flow (i.e. negligible viscous stresses) the Reynolds stress distribution can be measured. This can be converted to shear velocity by Equation 2-37.

Experiments by Babaeyan-Koopaei et al. (2002) in a natural channel found that shear velocity values derived using these three methods (i.e. the two measurement methods plus Equation 2-37) coincided to within 30%.

Assuming a logarithmic velocity profile as defined in Equation 2-35 shear stress in boundary layer flow follows a linear relationship between the maximum value (Equation 2-6) at the bed and zero at the free surface, therefore at any point in the flow depth shear stress can be determined by

$$\tau_t = \rho u^{*2}\left(1 - z/h\right) \approx -\rho\overline{u'w'} \qquad \text{Equation 2-38}$$

Experiments by Kironoto and Graf (1994) have shown that the shear stress is well approximated by the Reynolds stress in high Reynolds number flow, varying as predicted in Equation 2-38.

2.4 Solute Mixing in Open Channel Flow

Mixing studies are used to investigate the concentration of solutes in watercourses. Most commonly these are used to predict levels of contaminant downstream of a pollution incident. As such it is of importance to those who are seeking to design or monitor potential pollution discharges into rivers (Rutherford, 1994).

Due to the complex nature of river mechanics, a complete description of mixing processes by purely mathematical methods is not at present possible. However, a number of semi-empirical models which can describe mixing do exist, given that coefficients which define the rate of mixing are provided. Before such models are introduced it is necessary to explain the key

concepts and processes of mixing.

2.4.1 Scales of Mixing

Consider an instantaneous injection of solute originating from a single point in a typical open channel. Once injected the solute will begin to spread vertically over the channel depth, transversely across the width, and longitudinally along the channel. Open channels have a length much greater than their width and a width much greater than their depth. The solute will therefore first achieve well mixed conditions (i.e. constant concentration levels across the plane) across the vertical (z) plane in what is known as the near field zone, followed by the transverse plane (y) in the mid field zone, before spreading over the longitudinal plane (x) in the far field zone. Once the tracer cloud has become well mixed over the vertical and/or transverse planes then the concentration levels can be depth and/or width averaged. This results in depth, or depth and width (cross sectional) averaged concentration profiles. Well mixed conditions across a plane can also be achieved by the use of a non-point injection system, i.e. if the source is released uniformly across the width of the channel (transverse line source) than the cloud will be transversely well mixed immediately after injection. If, instead of an instantaneous release, the tracer is injected continuously at a uniform rate, then after some time concentration gradients will become constant along the length of the channel and mixing in the longitudinal plane can be ignored. In many practical cases, mixing in each dimension is considered separately, the dominant form of mixing being dependent on the zone considered (Figure 2-6).

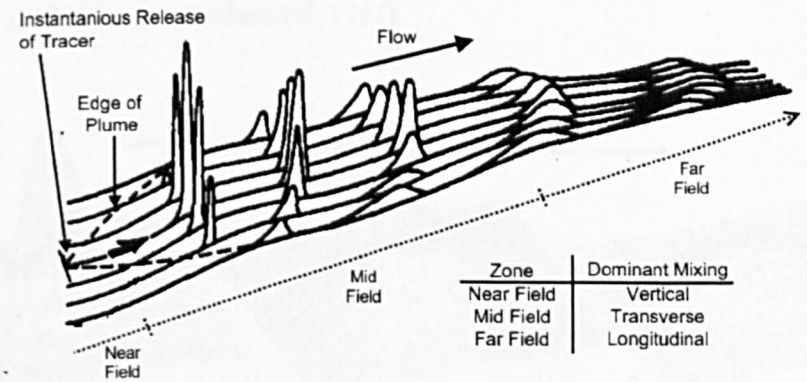

Figure 2-6 Mixing Zones (adapted from Jobson, 1997)

2.4.2 Mixing Processes

The processes that cause a solute to be mixed and transported throughout an open channel are now introduced.

2.4.2.1 Molecular Diffusion

Consider a small still body of water into which a small volume of neutrally buoyant tracer is introduced. Over time, the effects of molecular diffusion will cause the tracer to spread though the body of water until it is evenly distributed throughout the liquid (Figure 2-7). This spreading is due to random molecular motion (known as Brownian motion). This process is very slow, a square millimetre of dye injected into a still body of water would take a round a day to fully mix within a metre cubed of water. The effects of molecular diffusion can be described using Fick's first law. The one dimensional form of Fick's first law is

$$J_x = -\eta \frac{\partial c}{\partial x} \qquad \text{Equation 2-39}$$

Where	J_x	=	Mass Flux in x coordinate	(kg/m^2s)
	c	=	Concentration	(kg/m^3)
	η	=	Molecular diffusion coefficient	(m^2/s)

Put simply, this states that the rate of transfer of tracer between two adjacent regions is proportional to the concentration gradient between those regions. The negative sign denotes diffusion from areas of high to low concentration. The molecular diffusion coefficient is a property of the fluid itself, it is dependent on temperature, but for solutes in water a typical range is 0.5 - 2.0 $*10^{-9}$ m^2/s (Rutherford, 1994).

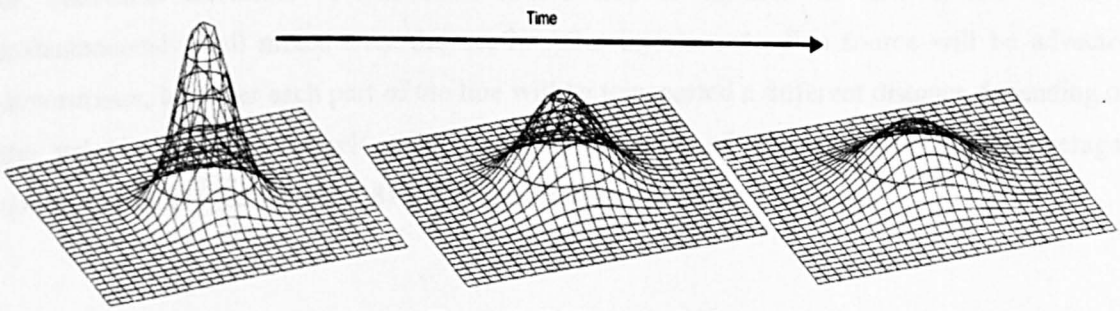

Figure 2-7 2D spread of tracer

2.4.2.2 Advection

In open channels the receiving water into which a solute is injected moves downstream with an average velocity, U. Hence the flow of the river will cause the introduced solute to advect downstream, away from the injection point. Advection will depend on the velocity of the flow at the point of injection. It is important to note that although advection transports the tracer, it

causes no spreading or mixing. If a tracer were to be injected into a channel where the velocity was uniform (i.e. constant at all points in the channel) and no diffusion processes were taking place, then the tracer would simply be transported downstream at the velocity of the channel, undergoing no spreading.

2.4.2.3 *Turbulent Diffusion*

Unlike laminar flow where longitudinal, transverse and vertical velocities are fixed and steady, turbulent flow is characterised by random short term velocity fluctuations around a steady mean value (see section 2.3). In virtually all practical mixing problems, the body of water is subject to turbulence. This turbulence causes the solute to mix much more rapidly and is termed turbulent diffusion. The presence of turbulence does not in itself cause greater mixing, rather its action in shearing the flow causes magnified local concentration gradients and accelerates the process of molecular diffusion. The exact rate of mixing depends on the levels of turbulence present but will typically be several orders of magnitude greater than molecular diffusion.

2.4.2.4 *Shear Dispersion*

Unlike advection and diffusion, dispersion is not a physical property of the flow but a product of the width and depth averaging procedures which account for the effects of velocity shear. Spreading of the profiles of averaged concentration is caused by non-uniform velocity profiles across the width and depth of a channel. Consider a hypothetical channel with typical vertical and transverse velocity profiles (i.e. retarded at the channel edges and at the bed due to the effects of friction from the channel boundaries). Assume that there is no mixing from molecular or transverse diffusion. A transverse line source is injected at time t_0 that becomes instantaneously well mixed over the depth. After injection the line source will be advected downstream, however each part of the line will be transported a different distance depending on the velocity of the channel at that position. A plot of the cross sectionally averaged concentration profile (Figure 2-8) will therefore spread with time/distance.

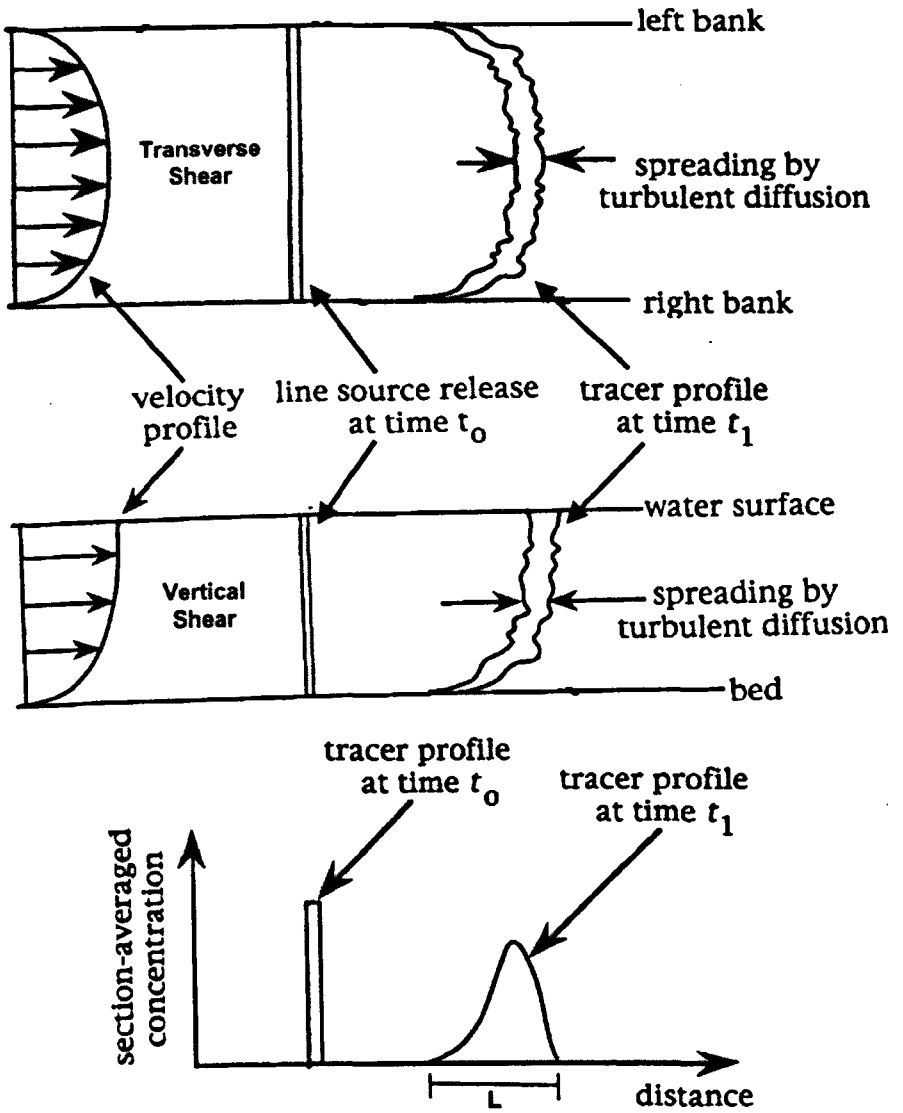

Figure 2-8 Transverse and vertical shear dispersion (adapted from Rutherford, 1994)

In the hypothetical channel there is no mixing due to diffusion, hence each particle remains on its individual flow path and the rate of spreading will depend on the magnitude of the velocity shear. After time, t the distance, L that the trace will be spread over can be stated as

$$L = t\Delta u \qquad \text{Equation 2-40}$$

Where Δu = Difference between the fastest and slowest flow velocities (m/s)

Equation 2-40 suggests that the length of the cloud increases linearly with time. In this case the standard deviation of the cross sectionally averaged concentration distribution will also increase linearly, and the variance will increase as the square of time. In practice, unlike in our hypothetical scenario, the levels of diffusion are not negligible. An important effect of differential advection is the increase of local concentration gradients, and hence the level of

diffusion (by Fick's first law - Equation 2-39). Gradually transverse and vertical differential advection will increase the lateral and vertical concentration gradients up to a point where the magnitude of the diffusion processes will act to encourage uniform concentrations across the channel cross section (and hence move solute into faster or slower velocity regimes). By reducing the quantity of solute travelling at the maximum and minimum channel velocities this process reduces the effects of differential advection, and hence the variance of the tracer cloud does not increase with the square of time as suggested in Equation 2-40. The combined effect of the differential advection and its countering diffusion process is termed shear dispersion.

2.4.2.5 *Trapping Mechanisms*

Valentine and Wood (1977) identified the presence of dead zones or trapping mechanisms in natural channels. A dead zone is a section of channel where the mean longitudinal velocity is zero or very small, and where part of the tracer cloud can become trapped or separated from the main flow, such as in an eddy (see Figure 2-9). When a quantity of tracer becomes trapped in these sections, it will slowly diffuse back into the main flow, increasing the length of the cross sectionally averaged concentration profile and hence increases the spread and mixing of tracer. The significance of dead zones in natural channels will depend on the size and nature of the dead zones themselves.

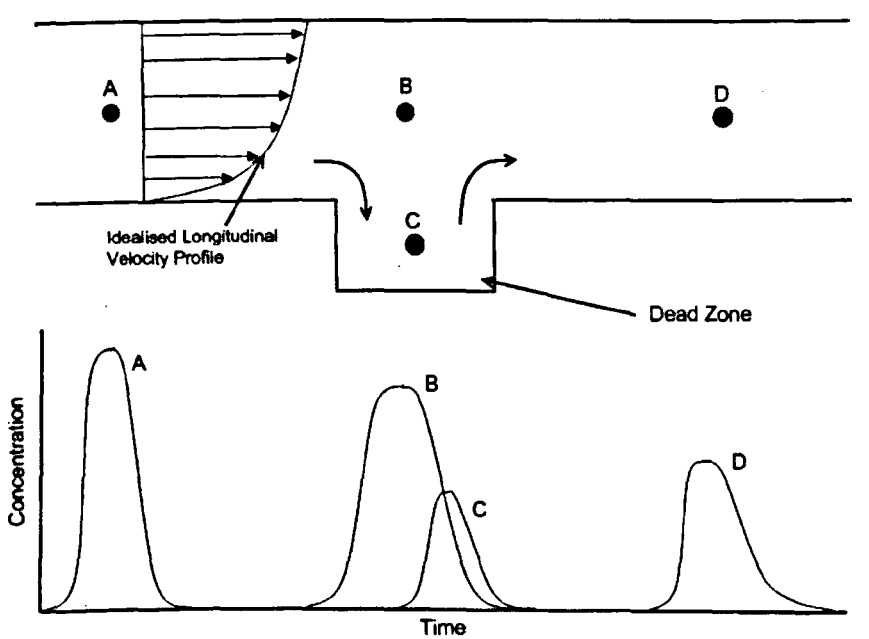

Figure 2-9 Dead Zones in Natural Channels (adapted from Rutherford 1994)

2.4.3 *Governing Equations*

The equations governing mixing in open channel flow are now derived. To simplify the derivation, mixing in laminar flow conditions is initially considered. In open channels featuring

laminar flow conditions, there will be no spreading due to turbulent diffusion, hence in this case it is possible to derive a mixing equation based solely on Fick's first law (Equation 2-39) and the principles of advection.

2.4.3.1 *Molecular Advection Diffusion Equation*

Consider a small element or parcel of fluid within a flow moving at a mean velocity U (Figure 2-10).

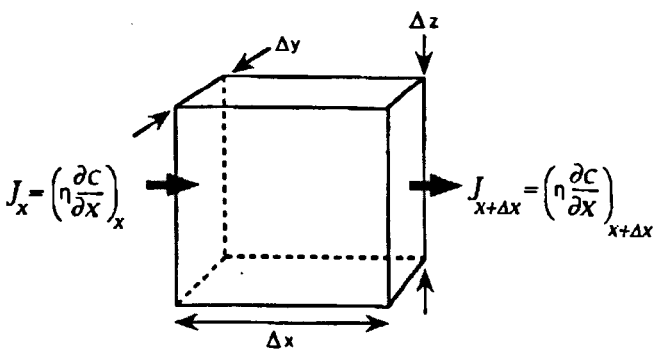

Figure 2-10 Diffusive flux into and out of a small fluid element (adapted from Rutherford 1994)

As solute passes through the boundaries of the element the concentration within the parcel changes. Over a small time period (Δt) this change can be expressed as

$$\frac{(c_{t+\Delta t} - c_t)}{\Delta t}\Delta x \equiv \frac{\partial c}{\partial t}\Delta x \qquad \text{Equation 2-41}$$

Where c_t = Tracer concentration within the parcel at time t (kg/m^3)

$c_{t+\Delta t}$ = Tracer concentration within the parcel at time $t + \Delta t$ (kg/m^3)

By considering conservation of mass along the x-axis it can be shown that the rate of change of mass given by Equation 2-41 must equal the net diffusive flux into and out of the parcel. This change in flux can be written as

$$J_{x+\Delta x} - J_x \equiv \frac{\partial J}{\partial x}\Delta x \qquad \text{Equation 2-42}$$

Therefore by equating Equation 2-41 and Equation 2-42

$$\frac{\partial c}{\partial t}+\frac{\partial J}{\partial x}=0 \qquad \text{Equation 2-43}$$

Combining with Fick's First Law (Equation 2-39)

$$\frac{\partial c}{\partial t}-\frac{\partial}{\partial x}\left(\eta\frac{\partial c}{\partial x}\right)=0 \qquad \text{Equation 2-44}$$

Assuming a constant mixing coefficient with distance, x

$$\frac{\partial c}{\partial t}=\eta\frac{\partial^2 c}{\partial x^2} \qquad \text{Equation 2-45}$$

Equation 2-45 defines the transport of mass by a Fickian diffusion process and is known as the diffusion equation. To apply this equation to open channel flow the parcel of water must be considered within steady laminar flow and expanded to all three dimensions. An advection term must also be included. The expression for total flux in each co-ordinate direction can be given as

$$J_x=uc-\eta\frac{\partial c}{\partial x} \qquad \text{Equation 2-46}$$

$$J_y=vc-\eta\frac{\partial c}{\partial y} \qquad \text{Equation 2-47}$$

$$J_z=wc-\eta\frac{\partial c}{\partial z} \qquad \text{Equation 2-48}$$

Hence, the products uc, vc and wc represent the advective flux in each direction. The change in mass can be expressed as

$$\frac{\partial c}{\partial t}\Delta x\Delta y\Delta z \qquad \text{Equation 2-49}$$

Consider the net flux in each direction

$$(netflux)_x = \left(\frac{\partial J_x}{\partial x}\Delta x\right)\Delta y\Delta z \qquad \text{Equation 2-50}$$

$$(netflux)_y = \left(\frac{\partial J_y}{\partial y}\Delta y\right)\Delta x\Delta z \qquad \text{Equation 2-51}$$

$$(netflux)_z = \left(\frac{\partial J_z}{\partial z}\Delta z\right)\Delta y\Delta x \qquad \text{Equation 2-52}$$

The total flux is equal to the sum of Equation 2-50 - Equation 2-52. This change in net flux must be equal to the change in concentration within the fluid element. Combining Equation 2-49 to Equation 2-52 yields:

$$\frac{\partial c}{\partial t} + \frac{\partial J_x}{\partial x} + \frac{\partial J_y}{\partial y} + \frac{\partial J_z}{\partial z} = 0 \qquad \text{Equation 2-53}$$

Substituting back in the equations for Flux (Equation 2-46 to Equation 2-48) and assuming molecular diffusion, η is uniform in all directions

$$\frac{\partial c}{\partial t} + u\frac{\partial c}{\partial x} + v\frac{\partial c}{\partial y} + w\frac{\partial c}{\partial z} = \eta\left(\frac{\partial^2 c}{\partial x^2} + \frac{\partial^2 c}{\partial y^2} + \frac{\partial^2 c}{\partial z^2}\right) \qquad \text{Equation 2-54}$$

This is known as the advection diffusion equation. The molecular diffusion coefficient is dependent on the fluid properties, i.e. fluid viscosity and temperature. Using this equation it is possible to predict concentration distributions in laminar flow conditions at any point after injection, provided the molecular diffusion coefficient is known.

2.4.3.2 *Properties of the Advection Diffusion Equation*

Equation 2-54 describes the spreading of a conservative solute. If a mass M of tracer is released in an unbounded channel at time t = 0 and position x = y = z = 0, then the concentration at any time and position (provided η, u, v and w are constant) can be described by the solution of

Equation 2-54.

$$c(x,y,z,t) = \left(\frac{M}{(4\pi\eta t)^{3/2}}\right)\exp\left(-\frac{(x-ut)^2+(y-vt)^2+(z-wt)^2}{4\eta t}\right) \quad \text{Equation 2-55}$$

Where M = Tracer Mass (kg)

For any time t > 0, the distribution of solute along the x, y or z axis will form a Gaussian bell shaped curve (i.e. a curve with no 3rd moment/skew). The moments of such a distribution can be found by the following equations (presented here as moments along the x axis)

$$M_0 = \int_1^\infty c_i dx \quad \text{Equation 2-56}$$

$$M_1 = \int_1^\infty (c_i dx) x_i \quad \text{Equation 2-57}$$

$$M_2 = \int_1^\infty (c_i dx) x_i^2 \quad \text{Equation 2-58}$$

$$M_3 = \int_1^\infty (c_i dx)\left(x_i - \left(\frac{M_1}{M_0}\right)\right)^3 \quad \text{Equation 2-59}$$

Properties of the distribution can then be determined.

$$Area = M_0 \quad \text{Equation 2-60}$$

$$Centroid = \varphi = \frac{M_1}{M_0} \quad \text{Equation 2-61}$$

$$Variance = \sigma^2 = \frac{M_2}{M_0} - \varphi^2 \quad \text{Equation 2-62}$$

$$Skew = \frac{\frac{M_3}{M_0}}{\left(\frac{M_2}{M_0}\right)^{3/2}}$$ Equation 2-63

If the variance of the distributions produced by Equation 2-62 are plotted against time, the following trends in spatial variance are found

$$\sigma_x^2 = \sigma_y^2 = \sigma_z^2 = 2\eta t$$ Equation 2-64

Where σ_i^2 = Spatial variance in i direction (m^2)

Hence, the advection diffusion equation predicts that the variance of the concentration distribution increases linearly with time. It is also important to note that solute distributions do not have to be initially Gaussian for the concentration distribution to spread in this fashion. A concentration distribution can be introduced into the channel with an initially skewed distribution (i.e. possessing a non zero 3rd moment). However, from this point on the variance of the distribution will still increase in a linear manner and the skew of the distribution will gradually decrease until the distribution becomes Gaussian.

2.4.3.3 *Turbulent Diffusion*

As discussed in section 2.4.2.3, in the vast majority of open channel flows tracer clouds will be subject to turbulence and hence turbulent diffusion. It is theoretically possible to model turbulent processes using laws derived for laminar flow conditions as diffusion processes are still governed by Fick's law. However, accurate use of Equation 2-54 in turbulent flow would require a detailed evaluation of flow velocities at very small spatial and temporal scales. Such a solution is considered impractical. To incorporate the effects of turbulence, the equations proposed by Reynolds to describe velocity in a turbulent flow (Equation 2-12 to Equation 2-14) are considered and expanded to include concentration.

$$c = \bar{c} + c'$$ Equation 2-65

Where $\bar{c}$ = Temporally averaged concentration (kg/m^3)

c'	=	Deviation in concentration	(kg/m^3)

Incorporating Equation 2-12, Equation 2-13, Equation 2-14 and Equation 2-65 into Equation 2-54 gives

$$\frac{\partial(\bar{c}+c')}{\partial t}+(\bar{u}+u')\frac{\partial(\bar{c}+c')}{\partial x}+(\bar{v}+v')\frac{\partial(\bar{c}+c')}{\partial y}+(\bar{w}+w')\frac{\partial(\bar{c}+c')}{\partial z}=$$
$$\eta\left(\frac{\partial^2(\bar{c}+c')}{\partial x^2}+\frac{\partial^2(\bar{c}+c')}{\partial y^2}+\frac{\partial^2(\bar{c}+c')}{\partial z^2}\right) \qquad \text{Equation 2-66}$$

By taking the ensemble (both spatially and temporally averaged) means, and considering continuity it can be shown that

$$\overset{A}{\frac{\partial\bar{c}}{\partial t}}+\left(\bar{u}\frac{\partial\bar{c}}{\partial x}+\overset{B}{\bar{v}\frac{\partial\bar{c}}{\partial y}}+\bar{w}\frac{\partial\bar{c}}{\partial z}\right)=$$
$$\eta\left(\overset{C}{\frac{\partial^2\bar{c}}{\partial x^2}+\frac{\partial^2\bar{c}}{\partial y^2}+\frac{\partial^2\bar{c}}{\partial z^2}}\right)-\left(\overset{D}{\frac{\partial(\overline{u'c'})}{\partial x}+\frac{\partial(\overline{v'c'})}{\partial y}}+\frac{\partial(\overline{w'c'})}{\partial z}\right) \qquad \text{Equation 2-67}$$

Where expression A represents change of mean concentration with time, B advection of ensemble mean concentration by mean velocity field, C molecular diffusion and D turbulent diffusion. Turbulent transport of the mean concentration is governed by terms involving unknown velocity and concentration distributions. Without knowledge of how the turbulent fluxes are related to a property of average concentration Equation 2-67 is unsolvable.

2.4.3.4 Taylor's analysis

Taylor (1921) published a paper in which he made a theoretical analysis of the spreading of a cloud of tracer particles released into stationary homogeneous turbulence. Taylor adopted a Lagrangian co-ordinate system (where the origin of the coordinate system travels at the mean flow velocity) and examined the processes that cause mixing. If a tracer particle is released at the origin, then after a time t it will be located at a longitudinal distance x, from the moving origin where

$$x(t) = \int_{\xi=0}^{t} u'(\xi) d\xi$$ Equation 2-68

Where ξ = integral time step (s)

If S particles are released then due to the random nature of the turbulent velocity fluctuations they will be at different locations x_i (where i = 1,2,3...S) after time t. It follows that due to the conservation of mass the ensemble mean variance of the resulting tracer cloud is equal to the ensemble mean square displacement of tracer particles. Thus

$$\langle \sigma^2{}_x \rangle = \langle (x - X)^2 \rangle$$ Equation 2-69

Where X = Position of Origin (m)

Angled brackets denote the ensemble average. With a Lagrangian system $\langle X \rangle = 0$, therefore

$$\langle \sigma^2{}_x \rangle = \langle x^2 \rangle$$ Equation 2-70

The ensemble mean size of the tracer cloud is the same as the ensemble mean variance of the displacement of the individual particles from the origin of the Lagrangian coordinate system. Equation 2-68 can therefore be re-written as

$$x^2(t) = \left[\int_{t_1=0}^{t} u'(t_1) dt_1 \right] \left[\int_{t_2=0}^{t} u'(t_2) dt_2 \right]$$
$$= \int_{t_1=0}^{t} \int_{t_2=0}^{t} u'(t_1) u'(t_2) dt_1 dt_2$$ Equation 2-71

The product

$$u'(t_1) u'(t_2)$$ Equation 2-72

is termed the 'auto-covariance' between the velocity of a particle at time t_1 and the velocity of a

similar particle at t_2. Taking the ensemble average of Equation 2-71

$$\langle x^2 \rangle = \int_{t_1=0}^{t} \int_{t_2=0}^{t} \langle u'(t_1) u'(t_2) \rangle dt_1 dt_2 \qquad \text{Equation 2-73}$$

A Lagrangian autocorrelation function, R_x can now be defined. Taylor (1921) assumed turbulence to be isotropic, thus autocorrelation can only depend on the time difference (t_2-t_1)

$$R_x(t_2 - t_1) = \frac{\langle u'(t_1) u'(t_2) \rangle}{\langle u'^2 \rangle} \qquad \text{Equation 2-74}$$

Combining Equation 2-73 and Equation 2-74

$$\langle x^2 \rangle = \langle u'^2 \rangle \int_{t_1=0}^{t} \int_{t_2=0}^{t} R_x(t_2 - t_1) dt_1 dt_2 \qquad \text{Equation 2-75}$$

Which can be rewritten as

$$\langle x^2 \rangle = 2\langle u'^2 \rangle \int_{s=0}^{t} (t - s) R_x(s) ds \qquad \text{Equation 2-76}$$

Where s = (t_2-t_1) (s)

The Lagrangian autocorrelation function cannot be predicted theoretically, but the two limits are known.

$$R_x(0) = 1$$

$$R_x(\infty) = 0 \qquad \text{Equation 2-77}$$

These two limiting cases can now be examined. At very small times, $R_x \approx 1$, and Equation 2-76 becomes

$$\langle x^2 \rangle = \langle u'^2 \rangle t^2$$ Equation 2-78

Thus at very small times the variance of the tracer cloud increases at rates proportional to t^2.

At large times $R_x \approx 0$, the fluctuations in velocity become independent, and Equation 2-76 becomes.

$$\langle x^2 \rangle \rightarrow 2\langle u'^2 \rangle T_x t + constant$$ Equation 2-79

Where T_x = Lagrangian timescale (s)

Equation 2-79 implies that some time (T_x) after the tracer is released into turbulent flow the variance of the tracer cloud will increase linearly with time. The Lagrangian integral timescale is therefore a measure of the time taken for a particle to 'forget' its original velocity. The Lagrangian timescale can be defined as

$$T_x = \int_{s=0}^{\infty} R_x(s) ds$$ Equation 2-80

2.4.3.5 *Fickian Model of Turbulent Diffusion*

It has already been shown in section 2.4.3.2 that Fick's law predicts that the variance of a solute concentration distribution increases linearly with time in laminar flow conditions. Taylor's analysis shows that, after the Lagrangian timescale has been reached, the same relationship holds in turbulent flows. Thus by analogy, after time T_x, Fick's law should also apply to turbulent flows. Hence by analogy to Equation 2-39 the turbulent diffusive fluxes can be described as

$$J_x = u'c' = -e_x \frac{\partial \bar{c}}{\partial x}$$ Equation 2-81

$$J_y = v'c' = -e_y \frac{\partial \bar{c}}{\partial y}$$ Equation 2-82

$$J_z = w'c' = -e_z \frac{\partial \bar{c}}{\partial z}$$ Equation 2-83

Where e_i = Turbulent diffusion coefficient / eddy diffusivity (in i direction) (m^2/s)

Using the same derivation as for the molecular advection diffusion equation provides

$$\frac{\partial \bar{c}}{\partial t} + \bar{u}\frac{\partial \bar{c}}{\partial x} + \bar{v}\frac{\partial \bar{c}}{\partial y} + \bar{w}\frac{\partial \bar{c}}{\partial z} = (\eta + e_x)_x \frac{\partial^2 \bar{c}}{\partial x^2} + (\eta + e_t)_y \frac{\partial^2 \bar{c}}{\partial y^2} + (\eta + e_z)_z \frac{\partial^2 \bar{c}}{\partial z^2}$$ Equation 2-84

In this equation two separate coefficients for turbulent and molecular diffusion are included. However as molecular diffusion is negligible compared to turbulent diffusion in most flows, it is common to use only one term. Either by neglecting molecular diffusion or considering it to be incorporated into the turbulent coefficient, Equation 2-84 becomes

$$\frac{\partial \bar{c}}{\partial t} + \bar{u}\frac{\partial \bar{c}}{\partial x} + \bar{v}\frac{\partial \bar{c}}{\partial y} + \bar{w}\frac{\partial c}{\partial z} = e_x \frac{\partial^2 \bar{c}}{\partial x^2} + e_y \frac{\partial^2 \bar{c}}{\partial y^2} + e_z \frac{\partial^2 \bar{c}}{\partial z^2}$$ Equation 2-85

Unlike the molecular diffusion coefficient (which is a property of the liquid in which the mixing is taking place) the turbulent diffusion coefficient is a property of the flow itself, and is dependent on the amount of turbulence in the flow.

Equation 2-85 is known as the Advection Diffusion Equation (ADE) and it forms the basis for the analysis of mixing problems in rivers. Despite the assumptions involved in its derivation there is a wide body of empirical evidence (Rutherford, 1994) which supports the use of Equation 2-85 to predict the spread of a solute in turbulent flow.

2.4.3.6 *Simplifying the ADE*

Equation 2-85 describes mixing in all three dimensions (x, y and z). However, full use of Equation 2-85 requires detailed knowledge of water depths, velocities and diffusion coefficients. Depending on the mixing zone and type of injection system considered (see section 2.4.1) simplified versions of Equation 2-85 can be produced which are appropriate to describe the dominant form of mixing. For example, if the injection is continuous and steady, concentration levels become independent of time and longitudinal concentration gradients become negligible. Additionally, if the coordinate system is rotated so that the x direction is

aligned with the main flow, net vertical and transverse velocities become negligible. Equation 2-85 becomes

$$\bar{u}\frac{\partial \bar{c}}{\partial x} = e_y \frac{\partial^2 \bar{c}}{\partial y^2} + e_z \frac{\partial^2 \bar{c}}{\partial z^2} \qquad \text{Equation 2-86}$$

If the tracer originates from a transverse line source the transverse concentration gradients become negligible and

$$\bar{u}\frac{\partial \bar{c}}{\partial x} = \frac{\partial}{\partial z}\left(e_z \frac{\partial \bar{c}}{\partial z}\right) \qquad \text{Equation 2-87}$$

Equation 2-87 can be used to analyse vertical mixing problems (in the near-field) downstream of a continuous, steady transverse line source, provided some estimate of the vertical diffusivity, e_z is made.

In the mid-field region the tracer is assumed to be well mixed over the depth, and hence problems focus on transverse and longitudinal changes in the depth averaged concentration gradients. To attain a depth averaged version of Equation 2-85 suitable for analysing such problems, the mixing equation must be integrated over the flow depth. The full mathematical procedure for depth averaging Equation 2-85 can be found in Rutherford (1994). The depth averaged form of the ADE can be written as

$$h\frac{\partial \bar{c}}{\partial t} + \frac{\partial}{\partial x}\left(h\overline{uc}\right) + \frac{\partial}{\partial y}\left(h\overline{vc}\right) = \frac{\partial}{\partial x}\left(-hu'c' + he_x \frac{\partial \bar{c}}{\partial x}\right) + \frac{\partial}{\partial y}\left(-hv'c' + he_y \frac{\partial \bar{c}}{\partial y}\right) \qquad \text{Equation 2-88}$$

c, u, v and the products u'c' and v'c' are now depth averaged. Along with the diffusivity terms, the right hand side of Equation 2-88 now contains u'c' and v'c', which arise as a result of depth averaging and account for mixing due to non uniformities in velocity over the depth. This additional transport is termed dispersion and is the mathematical description of the process discussed in section 2.4.2.4.

Transverse mixing is therefore dependent on diffusivity and dispersion caused by non uniform velocity profiles over the flow depth. The influence of these two processes is discussed in section 2.4.4.2.

In the far-field (see Figure 2-6), the tracer is assumed to be well mixed over the entire cross section. Given an unsteady source and assuming that the vertical and transverse concentration gradients are negligibly small in the far-field, a depth and width averaged form of the ADE can be used. When integrating over the channel cross section, Equation 2-85 becomes

$$A\frac{\partial C}{\partial t}+\frac{\partial}{\partial x}(AUC)=\frac{\partial}{\partial x}\left(-AU'C'+Ae_x\frac{\partial C}{\partial x}\right) \qquad \text{Equation 2-89}$$

Where C = Cross sectionally averaged concentration (kg/m^3)

Taylor's 1921 analysis suggests that at large times ($>T_x$) the dispersion terms u'c' and v'c' in Equation 2-88 and U'C' in Equation 2-89 are proportional to the gradient in depth and cross sectionally averaged concentration respectively. Hence

$$u'c'=k_x\frac{\partial c}{\partial x} \qquad \text{Equation 2-90}$$

$$v'c'=k_y\frac{\partial c}{\partial y} \qquad \text{Equation 2-91}$$

$$U'C'=D_x\frac{\partial c}{\partial x} \qquad \text{Equation 2-92}$$

Where k_y = Transverse dispersion coefficient (from depth averaging) (m^2/s)

k_x = Longitudinal dispersion coefficient (from depth averaging) (m^2/s)

D_x = Longitudinal dispersion coefficient (from cross sectional averaging) (m^2/s)

In open channel flow, longitudinal mixing due to dispersion is much greater than mixing due to diffusivity. The cross sectionally averaged longitudinal dispersion coefficient, D_x is therefore used to account for mixing due to both diffusivity and dispersion. Substituting Equation 2-92 back into Equation 2-89, and considering continuity

$$\frac{\partial C}{\partial t}+U\frac{\partial C}{\partial x}=D_x\frac{\partial^2 C}{\partial x^2} \qquad \text{Equation 2-93}$$

At durations longer than the Lagrangian timescale, the longitudinal spreading of a tracer cloud can be described using Equation 2-93, provided an estimate of the dispersion coefficient, D_x is made.

2.4.4 Theoretical Evaluation of Mixing Coefficients

2.4.4.1 Vertical Mixing

As already shown in section 2.4.3.6 the full ADE can be simplified to analyse near field mixing in situations where vertical spreading is dominant. However, any resulting equation (such as Equation 2-87) requires an estimate of the vertical diffusivity.

Due to the relatively shallow depths of most natural channels, full vertical mixing occurs over a relatively short timescale downstream of the injection and hence near field mixing is often neglected. In plane open channel flow (flow where the influence of the channel walls are negligible), the diffusivity and hence rate of vertical mixing is dependent on the levels of turbulence generated by the influence of the channel bed. As such, the vertical diffusion coefficient can be estimated based on the bed shear stress.

In plane open channel flow, mass and momentum are both transported by turbulent eddies. Reynolds made an analogy which stated that the transfer of mass and momentum is approximately equal, however more specifically one could state that

$$e_z = Sc\varepsilon \qquad \text{Equation 2-94}$$

Where Sc = Schmidt Number (-)

For neutrally buoyant tracers the Schmidt number is usually taken as 1, implying that the transfer of mass and momentum are equivalent (Rutherford, 1994).

Given the linear distribution of shear stress as described in section 2.3.2.2, and the relationship between the Reynolds stress (assumed equal to total stress in turbulent flows) and the flow velocity provided by Prandtl's mixing length hypothesis, an equation for the vertical diffusion coefficient can be provided. Given that

$$\tau_t = \rho\varepsilon\frac{du}{dz} = \tau_o\left(1-\frac{z}{h}\right) \qquad \text{Equation 2-95}$$

Inserting Equation 2-94 into Equation 2-95 (taking Sc = 1) and rearranging the resulting equation

$$e_z = \frac{\left(\tau_0\left(1-\frac{z}{h}\right)\right)}{\left(\rho\frac{du}{dz}\right)} \qquad \text{Equation 2-96}$$

Assuming a logarithmic velocity profile (Equation 2-24) exists, Equation 2-96 can be written as

$$e_z = \kappa u^* z\left(1-\frac{z}{h}\right) \qquad \text{Equation 2-97}$$

Hence, the profile of vertical diffusivity over the flow depth can be determined. Jobson and Sayre (1970a) conducted a study of vertical mixing and found that the predicted concentration profiles were insensitive to the vertical profile of e_z. Hence, in most practical problems it is usual to assume a constant value of e_z over the depth. Averaging e_z over the depth gives

$$\langle e_z \rangle = \frac{\kappa}{6} hu^* = 0.067 hu^* \qquad \text{Equation 2-98}$$

2.4.4.2 *Transverse Mixing*

Transverse mixing dominates the mid field zone (Figure 2-6), prior to the tracer becoming cross sectionally well mixed, but after vertical mixing has taken place. It is especially relevant for point sources of pollution, such as discharges from wastewater treatment works. The rate of transverse mixing determines the timescale until the contaminant reaches the channel boundaries and complete cross sectional mixing occurs.

It is possible to make the analogy with the equation for vertical diffusivity (section 2.4.4.1) to produce an equation for estimating transverse diffusivity.

$$e_y = \frac{\tau_t}{\left(\rho \frac{du}{dy}\right)}$$ Equation 2-99

The practical problem with using an equation such as Equation 2-99 is that in many wide straight channels the transverse velocity gradient is assumed to be zero for the majority of the channel width, and hence Equation 2-99 becomes invalid. At present it is not possible to predict the value of transverse diffusivity theoretically, and therefore all estimates of mixing rates are based on empirical data.

As explained in section 2.4.3.6, transverse mixing is driven by both turbulent diffusion and vertical variations in the transverse velocity. Hence, rates of transverse mixing are dependent on the levels of both turbulence and secondary currents in the channel. Secondary currents are generated by objects in the flow, a non equal distribution of boundary shear stress, or by bends in the channel which create a circular flow, spreading solutes across the cross section. Thus in channels where these features are minor, secondary currents are very weak. However in channels with for example; high sinuosity, secondary currents can be very strong. Transverse mixing rates in such a channel will therefore be much greater than in an equivalent channel where mixing is driven primarily by turbulent diffusion.

It is possible to apply Taylor's analysis (section 2.4.3.4) to transverse mixing, hence given sufficient time has elapsed since injection, the spatial variance of the tracer cloud will increase linearly with time. However, Holly (1985) suggests that in natural, irregular channels, the constantly changing levels of secondary currents will prevent the Lagrangian timescale being reached. Despite this, numerous field and laboratory observations show that the Fickian analogy holds for transverse mixing, and that the spatial variance of the tracer cloud increases linearly with time/distance (Rutherford, 1994). A transverse mixing coefficient (K_y), which accounts for the combined effect of diffusion and secondary currents, can be used to define the rate of mixing.

2.4.4.3 Longitudinal Mixing

Longitudinal mixing is the study of mixing that occurs downstream of an instantaneous injection of solute in channels, after this solute has already become vertically and transversely well mixed, i.e. in the far field (Figure 2-6). Tracer clouds in the far field spread along the channel resulting in a decrease in peak concentrations and an increase in the time of passage past any fixed site.

Due to the fact rivers are much longer than they are wide or deep, full vertical and horizontal mixing will occur within a relatively small timescale. Thus the majority of mixing processes in natural channels are dominated by longitudinal processes. A common use of longitudinal mixing models is to predict pollutant concentrations downstream of a sudden discharge, such as a road tanker crash or industrial accident, or to analyse mixing from temporally varying sources.

Longitudinal mixing is caused by diffusion, shear dispersion and trapping mechanisms. In channels with few trapping mechanisms, shear dispersion dominates, and as shown in section 2.4.3.2 the effects of turbulent diffusion and shear dispersion can be combined in the one dimensional ADE and expressed as a longitudinal dispersion coefficient Equation 2-93), which can then be used once the Lagrangian timescale, T_x, has been reached. The effects that the process of shear dispersion has on the cross sectionally averaged concentration profiles can be examined (Figure 2-11).

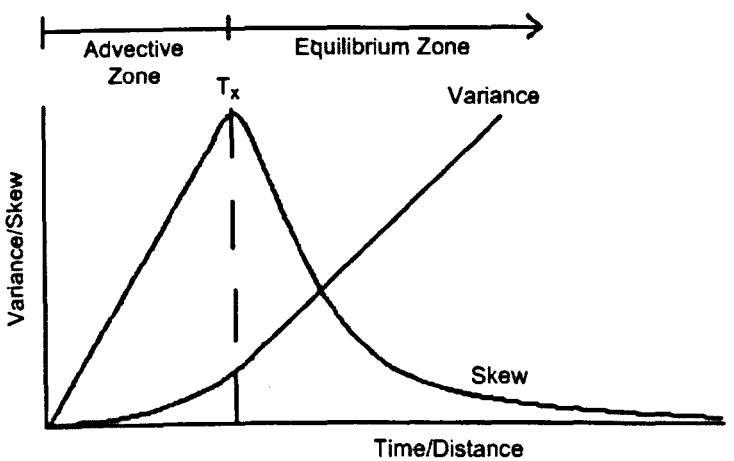

Figure 2-11 Fickian model of changing properties of a concentration profile (Shucksmith et al., 2007).

As stated in section 2.4.2.4, differential advection without a countering diffusion process would cause the variance of the concentration profile to grow in proportion to the square of time. Taylor's analysis predicts this relationship immediately after injection (Equation 2-78). In practice, after injection the effects of differential advection soon increase local concentration gradients; hence diffusion processes increase and act to counter differential advection. Once the effects of diffusion and differential advection are in a state of balance, the solute enters an 'equilibrium' zone. It has been observed (Fischer, 1967) that in this equilibrium zone the variance of the concentration profile grows linearly with time, as predicted by Taylor's analysis after the Lagrangian timescale, T_x has been reached.

The rate of shear dispersion is dependent on the velocity profiles, the greater the variation in velocity across the channel width and depth the greater the effects of shear dispersion and hence mixing. Fischer (1967) showed that in typical open channel flow, transverse velocity shear (i.e.

shear due to the variation in velocity across the channel width) makes a greater contribution to longitudinal mixing than vertical velocity shear (shear due to the variation in velocity across the channel depth). Conversely high levels of diffusivity and/or transverse mixing encourages uniform concentrations across the channel cross section, hence reducing the magnitude of shear dispersion. Fischer (1967) proposed that the rate of transverse and longitudinal mixing were inversely related.

The initial imbalance between differential advection and diffusion within the advective zone (prior to T_x) has the effect of imparting skew into the concentration profile, causing it to become non Gaussian with an elongated tail. During the initial period after injection (when differential advection dominates the mixing process), the skew of the profile grows and the trace spreads in a non Fickian manner. Once the trace enters the equilibrium zone the levels of skew in the profile decrease and the concentration profiles gradually become symmetrical. However, measurements in natural channels almost always result in skewed rather than Gaussian profiles, even if taken at large times after injection (Day and Wood, 1976). This may be because the concentration profiles were taken in or close to the advective zone, and hence the initial skew generated by differential advection has not had time to decay. It may also be because most concentration profiles are not measured instantaneously but rather as the cloud passes a fixed site. Although the assumption (termed a 'frozen cloud' approximation) is usually made that no mixing occurs as the cloud passes the measurement site (Rutherford, 1994), in practice some mixing will occur. The section of the tracer cloud recorded last will be slightly more spread than the section measured first. Hence, this results in a slight skew in concentration profiles measured in this way. It is important to remember that this skew is caused by the measurement procedure rather than by mixing processes.

However, even accounting for this, it is likely that in most channels the profile skew caused by the mixing process is increasing, staying constant, or not decaying as fast as is predicted by the ADE, even at long times after injection. This may be due to the constantly changing cross sections found in natural channels. In this case, equilibrium between differential advection and turbulent diffusion is never fully established and so the skew of the concentration distributions continues to grow. Due to its 1-dimensional nature, the ADE equation will not predict any increase in skew in the concentration profile. Solutions of the ADE will therefore result in profiles with reduced skew and eventually Gaussian shaped concentration profiles. The ADE may therefore not provide a perfect fit to the concentration profiles measured in natural channels (Day and Wood, 1976).

The presence of dead zones or trapping mechanisms (see section 2.4.2.5) also impact on the nature and scale of longitudinal mixing. Valentine and Wood (1977) investigated the effects of

dead zones on longitudinal mixing. Despite the effect of trapping mechanisms elongating the tail of a concentration profile (and hence increasing profile skew, Figure 2-9), Valentine and Wood found that a point is still reached where an equilibrium condition occurs and hence the growth of variance is linear and the skew decays. However, the slow rate of diffusion into and out of dead zones means that the duration for tracer particles to sample the entire flow field is increased. This has the effect of increasing the Lagrangian timescale relative to an equivalent channel with no dead zones. The effect of dead zones to spread the tracer results in an increased rate of longitudinal mixing. Valentine (1978) found that dead zones occupying 4% and 25% of the channel volume increase the longitudinal dispersion coefficient by a factor of 2 and 10 respectively.

2.4.4.4 *Elder's Derivation of Dispersion Coefficient*

As longitudinal mixing in open channels is heavily dependant on shear dispersion it is possible to derive an expression for the longitudinal dispersion coefficient based on the profile of velocity and diffusivity. Elder (1959) theoretically derived an expression for the longitudinal dispersion coefficient in plane shear flow within a infinitely wide channel (i.e. no transverse shear dispersion). This derivation was based on the principle that in such a system longitudinal mixing would be purely caused by vertical velocity shear. Assuming a logarithmic velocity profile and a distribution of diffusivity as described in section 2.4.4.1 the dispersion coefficient can be evaluated as

$$D_x = \frac{0.404}{\kappa^3} hu* + \frac{\kappa}{6} hu* \qquad \text{Equation 2-100}$$

Which, assuming κ can be taken as 0.4 (see section 2.3.2.1), simplifies to

$$D_x = 5.93 hu* \qquad \text{Equation 2-101}$$

Equation 2-101 provides a theoretical value of longitudinal dispersion coefficient in plane boundary layer flow. Elders (1959) result has been used not only to quantify the mixing coefficient, but it also enabled Fischer (1967) to estimate the Lagrangian timescale.

2.4.4.5 *Quantifying the Lagrangian Timescale*

As shown in section 2.4.3.4, the ADE can only be used once the solute has entered the equilibrium zone. To find out when the equilibrium zone occurs and hence the Fickian based

ADE can be applied to model longitudinal mixing, the Lagrangian timescale, as introduced in section 2.4.3.4, must be determined. Fischer (1967) relates the size of the advective zone to the time required for a particle present in the flow to experience the entire flow field. The important parameters are: the nature of the source (line source or point source), the transverse length scale, and the rate of transverse mixing. The Lagrangian timescale, T_x can therefore be evaluated using

$$T_x = \alpha \frac{L^2}{K_y} \qquad \text{Equation 2-102}$$

Where	K_y	=	Transverse mixing coefficient	(m^2/s)
	α	=	Coefficient	(-)
	L	=	Transverse length scale	(m)

The transverse length scale, L, is defined as the transverse distance from the point of maximum velocity to the farthest distance point within the cross section; hence a value of half the channel width is usually taken. The coefficient α depends on the type of source (line or point).

Fischer (1967) derived a theoretical value for α for a transverse line source so that the Lagrangian timescale could be evaluated.

If it is assumed that the mixing can be described by Fickian processes (i.e. linear increase in profile variance with time), the longitudinal mixing coefficient can replace molecular diffusion (section 2.4.3.2) to describe the spatial variance of the concentration profile

$$\sigma_x^{\,2} = 2D_x t \qquad \text{Equation 2-103}$$

Rearranging Equation 2-103 gives

$$D_x = \frac{1}{2}\frac{d}{dt}\sigma_x^{\,2} \qquad \text{Equation 2-104}$$

Combining Equation 2-70 and Equation 2-76 from Taylor's analysis provides

$$\langle \sigma^2{}_x \rangle = 2\langle u'^2 \rangle \int_{s=0}^{t} (t-s) R_x(s) ds \qquad \text{Equation 2-105}$$

Differentiation of Equation 2-105 and incorporating Equation 2-104 provides

$$D_x = \langle u'^2 \rangle \int_{s=0}^{t} R_x(s) ds \qquad \text{Equation 2-106}$$

Fischer (1967) states that the mean turbulence level is sufficiently small compared to the deviations within the cross section of time averaged velocity, so that a good approximation is

$$\langle u'^2 \rangle \approx U'^2 \qquad \text{Equation 2-107}$$

Where U' = Cross sectional mean of velocity deviation (m^2/s)

As s tends to infinity, Equation 2-106 may be written as

$$D_x = U'^2 T_x \qquad \text{Equation 2-108}$$

For two-dimensional plane shear flow the Lagrangian time scale can be evaluated. In such a flow the average value of vertical mixing coefficient, calculated from the distribution of shear and the Reynolds analogy, is given by Equation 2-98.

If Fickian processes are assumed the time scale for the tracer to become well mixed over the depth, T_d' can be expressed as

$$T_d' = \frac{h^2}{e_z} \qquad \text{Equation 2-109}$$

Combining Equation 2-98 and Equation 2-109 gives

$$T_d' = \frac{6}{\kappa}\frac{h}{u*} \qquad \text{Equation 2-110}$$

Averaging the velocity distribution given by the logarithmic law Equation 2-35 gives

$$U'^2 = \left(\frac{u*}{\kappa}\right)^2 \qquad \text{Equation 2-111}$$

Inserting Elder's (1959) result for turbulent diffusion (Equation 2-100), and Equation 2-111 into Equation 2-108 gives

$$T_x = \frac{0.404}{\kappa}\frac{h}{u*} \qquad \text{Equation 2-112}$$

Combining Equation 2-110 and Equation 2-112 gives

$$T_x = 0.068 T_d' \qquad \text{Equation 2-113}$$

Hence, Equation 2-113 provides the relationship between the Lagrangian timescale and time required for complete mixing over the flow depth.

In the transverse plane, if Fickian possesses are assumed, the time scale for the tracer to become well mixed over the width T_w' can be expressed as

$$T_w' = \frac{L^2}{K_y} \qquad \text{Equation 2-114}$$

The transverse mixing coefficient given by Fischer (1967) is

$$K_y = 0.23 h u* \qquad \text{Equation 2-115}$$

Inserting this value into Equation 2-114 and replacing depth with hydraulic radius, R, gives

$$T_w' = \frac{L^2}{0.23Ru*}$$ Equation 2-116

Assuming the relationship between timescales derived in Equation 2-113 also applies to the transverse plane, Equation 2-116 becomes

$$T_x = 0.3\frac{L^2}{Ru*}$$ Equation 2-117

By replacing the Ru* term with the value for transverse mixing coefficient defined by Equation 2-115 the Lagrangian time scale can be derived as

$$T_x = 0.069\frac{L^2}{K_y}$$ Equation 2-118

To verify this theoretical finding, Fischer conducted a series of experiments in a smooth straight laboratory channel. For injection below a horizontal line source it was found that the timescale required for the variance of the tracer cloud to increase linearly with time (i.e. for the equilibrium zone to be established) did not begin until six times the value predicted in Equation 2-118. Fischer's experimental result is effectively $\alpha = 0.414$. It is possible that the source of this contradiction arises in the evaluation of the start of the linear trend of variance of concentration profiles with distance. Using basic experimental procedures, together with the resolution limitations of conductivity probes used in such an experimental study, may have resulted in large errors in variance due to uncertain concentration profile start and end points. This point will be explored in greater detail in the experimental derivation of dispersion coefficients section (section 2.4.5.3).

Several other theoretical and experimental attempts have been made to determine the coefficient α, and hence to estimate the size of the Lagrangian timescale. The results of these studies are presented in Table 4.

Table 4 Estimates of α in a straight, smooth rectangular channel for a transverse line source, (adapted from Rutherford, 1994)

Reference	α	Type
Fischer (1967)	0.069	Theoretical
Fischer (1967)	0.414	Experimental
Fischer (1973)	0.2	Review of Numerical Experiments
Tsai and Holley (1978)	0.4-0.5	Numerical Experiments
Sayre (1968)	0.5	Numerical Experiments
Chatwin (1972)	1	Theoretical

From Table 4 it can be seen that there is considerable uncertainty in the value of α. The Lagrangian timescale is an important parameter in the field of mixing studies, therefore this uncertainty remains a serious problem for practitioners who wish to determine when the ADE Equation 2-93) is valid.

2.4.5 Experimental Evaluation of Mixing Coefficients

As discussed previously, to characterise the rate of transverse and longitudinal mixing the transverse (K_y) and longitudinal (D_x) mixing coefficients must be determined. As these coefficients account for spreading due to several different complex mechanisms (section 2.4.2), there is considerable difficulty in evaluating these coefficients theoretically. For a given mixing reach and flow conditions such coefficients are commonly evaluated by experimental means, i.e. by measuring the rate of mixing of a detectable soluble tracer. The most common way of determining mixing coefficients from the development of observed concentration profiles is the method of moments (Rutherford, 1994). The method of moments works on the principle that the changing properties of concentration distributions can be used to determine mixing coefficients as long as the trace obeys the Fickian laws introduced in section 2.4.3.2. This is achieved by measuring development of the 0^{th}, 1^{st} and 2^{nd} moment of each of the distributions with time or distance.

2.4.5.1 Transverse Method of Moments

If the solute obeys Fickian laws, the appropriate mixing coefficient can replace molecular diffusion (section 2.4.3.2) to describe the spatial variance of the concentration profile (Figure 2-12).

$$\sigma_y^2 = 2K_y t \qquad \text{Equation 2-119}$$

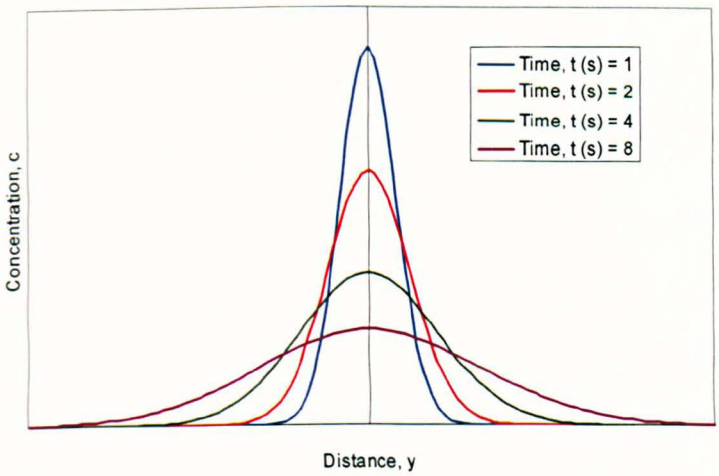

Figure 2-12 Tracer concentration along y axis with time

The transverse mixing coefficient (K_y) can therefore be estimated as

$$K_y = \frac{1}{2}\frac{\Delta\sigma_y^{\,2}}{\Delta t} = \frac{1}{2}\frac{\sigma_y^{\,2}(t_2) - \sigma_y^{\,2}(t_1)}{(t_2 - t_1)} \qquad \text{Equation 2-120}$$

To evaluate the transverse mixing coefficient from field measurements it is more practical to convert time to distance. This can be done simply by substituting a velocity term, hence

$$K_y = \frac{U}{2}\frac{\sigma_y^{\,2}(x_2) - \sigma_y^{\,2}(x_1)}{(x_2 - x_1)} \qquad \text{Equation 2-121}$$

To evaluate the transverse mixing coefficient, several spatial concentration profiles must be collected downstream of a steady point source. To make a reliable estimation several profiles must be collected at different distances. This often requires a large number of measurements.

2.4.5.2 *Other Experimental Methods*

Boxall and Guymer (2001) outlined an empirical method to evaluate transverse coefficients without the need to acquire complete cross sectional profiles. The method evaluates the mixing coefficient based on concentration measurements taken between the initial crossing distance, L_1, and the distance until the profile becomes well mixed, L_2 (Figure 2-13).

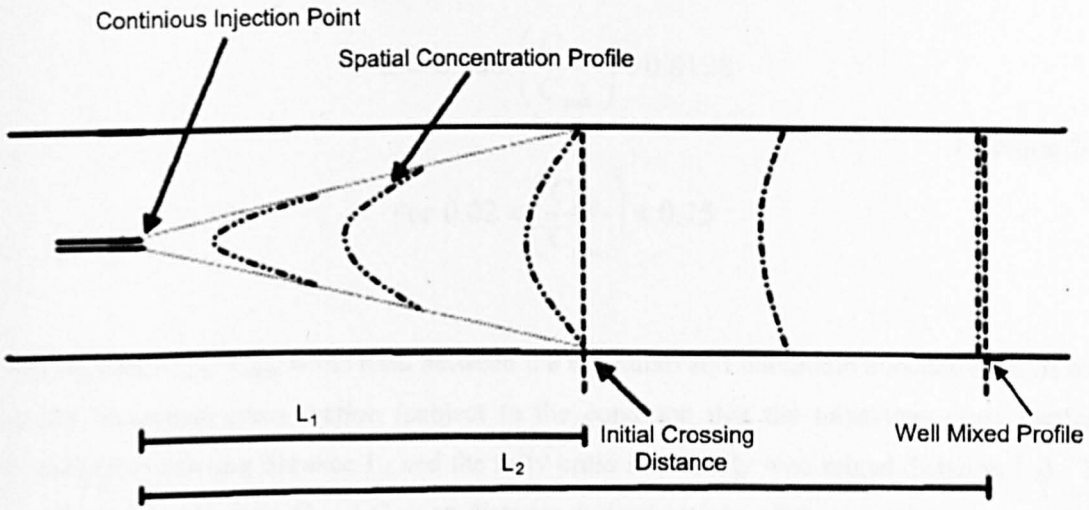

Figure 2-13 Development of Transverse Concentration Profile

Rutherford (1994) presents a simplified expression for the distance to both the initial crossing distance (L_1) and full cross sectional mixing (distance until the profile is well mixed, L_2) of a solute in an open channel based on the depth averaged solution of the advection diffusion equation for a vertical line source (Figure 2-13).

$$L_{1or2} = \alpha \frac{Ub^2}{K_y} \qquad \text{Equation 2-122}$$

Where	b	=	Channel width	(m)
	L_1	=	Initial Crossing distance	(m)
	L_2	=	Distance until full cross sectional mixing	(m)

By substituting L for a distance from injection x, and rearranging Equation 2-122

$$K_y = \alpha \frac{Ub^2}{x} \text{ where } L_1 < x < L_2 \qquad \text{Equation 2-123}$$

The coefficient, α, has been derived theoretically by Boxall and Guymer (2001) for a centreline injection as

$$\alpha = 0.0688\left(\frac{C_{min}}{C_{max}}\right) + 0.0128$$

Equation 2-124

$$\text{For } 0.02 < \left(\frac{C_{min}}{C_{max}}\right) < 0.75$$

The variable C_{min} / C_{max} is the ratio between the minimum and maximum concentration of solute at any transverse cross section (subject to the condition that the transverse cross section is between the crossing distance L_1 and the fully cross sectionally well mixed distance, L_2). Thus by measuring the ratio C_{min} / C_{max} at distance x downstream of the injection point and with knowledge of mean channel velocity and width, a transverse mixing coefficient can be estimated. To use this method it must be assumed that mixing processes confirm entirely to the conditions of the simplified solution of the Fickian mixing equation, i.e. Fickian mixing processes, constant mixing conditions, uniform velocity distribution and idealised reflection of tracer at the channel boundaries.

2.4.5.3 *Longitudinal Method of Moments*

Similarly to the transverse method of moments (Equation 2-120), the longitudinal dispersion coefficient (D_x) can be evaluated as

$$D_x = \frac{1}{2}\frac{\Delta\sigma_x^{\,2}}{\Delta t} = \frac{1}{2}\frac{\sigma_x^{\,2}(t_2) - \sigma_x^{\,2}(t_1)}{(t_2 - t_1)}$$

Equation 2-125

In the case of longitudinal mixing, the development of the cross sectionally averaged concentration profile is of interest (Figure 2-14). Measuring the spatial variance of such a profile is problematic, requiring numerous closely spaced sensors along the channel length. It is far easier to measure a temporal variance, which would require only one sensor (placed at a representative sampling point) measuring the concentration levels as the trace passes the measurement site. In practice the assumption is usually made that

$$\sigma_x^{\,2} = U^2\sigma_t^{\,2}$$

Equation 2-126

Where σ_t^2 = Temporal variance (s^2)

Equation 2-126 is known as the frozen cloud approximation; essentially it assumes that no longitudinal spreading takes place during the time it takes for the tracer to pass the sampling site. This is not strictly valid, as some mixing will obviously take place, especially in cases where the mixing rates are high and the flow velocity low. The frozen cloud assumption is therefore only valid in cases where

$$\frac{x}{U} >> \frac{D_x}{U^2} \qquad \text{Equation 2-127}$$

In most practical cases Equation 2-127 is assumed correct. Hence Equation 2-125 becomes

$$D_x = \frac{U^2}{2}\frac{\sigma_t^{\,2}(x_2) - \sigma_t^{\,2}(x_1)}{\left(\bar{t}_2 - \bar{t}_1\right)} \qquad \text{Equation 2-128}$$

Where $\bar{t}_i$ = Centroid of concentration distribution at site i (s)

Similarly to profile variance, the parameter $\bar{t}_i$ can be determined from the moments of the concentration distribution Equation 2-61). The travel time can then be defined as

$$\overline{T} = \left(\bar{t}_2 - \bar{t}_1\right) \qquad \text{Equation 2-129}$$

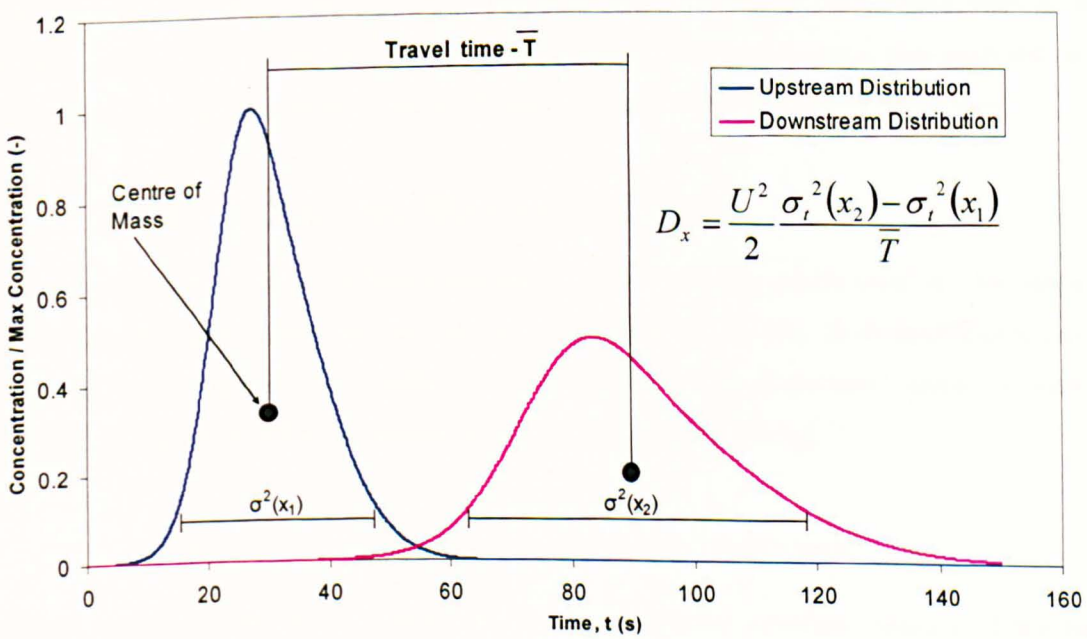

Figure 2-14 ADE Parameter identification

The mixing parameters obtained from the method of moments are, however, susceptible to error. This is because the dispersion coefficient is evaluated from the rate of change of variance of the concentration profiles (Equation 2-128). For the variance of each distribution to be evaluated (Equation 2-62) the 2nd moment needs to be calculated (Equation 2-58). The lever arm term in Equation 2-58 means that the accurate measurement of the edges of the trace is critical in the evaluation of variance. Unfortunately, due to the low concentration levels the edges of the trace are often difficult to distinguish from instrument background noise. Probes therefore need to be very accurate to evaluate 2nd moment and variance precisely. Any inaccuracy can lead to potentially large errors in the estimation of variance, due to the square term in the second moment and even larger errors in skew due to the cube term in the third moment (see section 2.4.3.2). In practice the start and end of measured traces are usually identified as the point where the concentration falls below or rises above a subjective 'cut off' level, which is some percentage of the peak concentration value. Shaw (2000) conducted longitudinal mixing experiments in a natural channel. Longitudinal dispersion coefficients were derived with the method of moments using various levels of tracer cut-off. The resulting dispersion coefficient for an example reach using different levels of cut off are presented in Table 5.

Table 5- Dispersion coefficients measured by method of moments using different levels of trace cut off (Shaw, 2000)

Cut off (% of peak concentration value)	10	1	0.1	0.01
Longitudinal Dispersion Coefficient, D_x (m^2/s)	0.9464	1.2842	2.2294	3.1569

It can be seen that the dispersion coefficient derived from the method of moments is dependent on the level of cut off selected. For most measured concentration profiles it is very difficult to evaluate where the trace starts and ends, where the beginning of the background noise is, and hence to choose the 'correct' level of cut off. This means that experimental data analysed using the method of moments may not give an accurate measure of the dispersion coefficient.

2.4.6 Observed Mixing Coefficients

Numerous researchers have published measured values of mixing coefficients. A wide range of results from different researchers can be found in Rutherford (1994). Such coefficients can be compared to the theoretical estimates, provide reference or comparison values, or used to quantify the impact of different channel and flow properties on mixing.

2.4.6.1 Observed Vertical Mixing Coefficients

Vertical mixing occurs within a relatively short period after injection, because of the short timescales involved, vertical mixing is considered only of marginal importance. Most studies

of river mixing have tended to focus on the transverse or longitudinal planes. Rutherford (1994), however, does present a list of published vertical diffusivities observed in plane shear flow. The published values are presented in Table 6

Table 6- Vertical Diffusivities (Rutherford, 1994)

Reference	Depth, h (m)	Shear Velocity, u* (m/s)	Diffusivity, e_z (m^2/s)	Normalised Diffusivity, e_z/hu^* (-)	Study
Jobson and Sayre (1970b)	0.4	0.049 – 0.136	-	0.063	Laboratory
Schiller and Sayre (1973)	0.071	0.040	-	0.042	Laboratory
McNulty and Wood (1983)	0.039 - 0.076	0.041 - 0.058	1.8	0.067	Laboratory
Nokes and Wood (1986)	0.005 - 0.065	0.014 – 0.016	-	0.067	Laboratory
Rutherford (1994)	2.00 - 2.75	0.066	86 - 155	0.055 – 0.099	Natural Channel

It can be seen from Table 6 that most values of normalised diffusivities agree well with the theoretical value of 0.067 derived in section 2.4.4.1.

2.4.6.2 *Observed Transverse Mixing Coefficients*

Similarly to vertical mixing, transverse mixing is often scaled by flow depth and shear velocity. This is appropriate for wide open channels as turbulence (which drives transverse mixing) is generated by vertical velocity shear due to bed friction, and the flow depth determines the size of the turbulent eddies which transport mass. In natural channels secondary currents also contribute to transverse mixing with sinuous channels encountering larger secondary currents (Boxall, 2000). Rutherford (1994) reviewed reported transverse diffusivities and mixing values from a number of laboratory and field studies. For straight laboratory channels in plane shear flow (i.e. assuming no or negligible secondary currents) transverse diffusivity was in the order of

$$0.1 < \frac{e_y}{hu^*} < 0.26 \qquad \text{Equation 2-130}$$

It is assumed likely that some secondary currents may have been present in some of the experiments. From this reported range Rutherford (1994) suggested a good estimate of transverse diffusivity to be

$$\frac{e_y}{hu^*} \approx 0.13 \qquad \text{Equation 2-131}$$

Although several other researchers such as Elder (1959) and Fischer (1967) have suggested a higher value of 0.23.

In natural channels, mixing occurs due to secondary currents and diffusion and hence reported values are expressed in terms of a transverse mixing coefficient (K_y) which accounts for both processes. Rutherford (1994) also reviewed reported values of transverse mixing in straight natural channels (i.e. those with low secondary currents) which are in the region of

$$0.15 < \frac{K_y}{hu^*} < 0.3 \qquad \text{Equation 2-132}$$

Reported values of transverse mixing in sinuous channels (i.e. those with high secondary currents) are much higher, with K_y/hu^* values up to 10 being reported around sharp bends (Sayre, 1973).

2.4.6.3 *Observed Longitudinal Mixing Coefficients*

Rutherford (1994) reviewed reported longitudinal dispersion coefficients from a number of field studies, finding

$$30 < \frac{D_x}{hu^*} < 3000 \qquad \text{Equation 2-133}$$

It can be seen that the expression derived by Elder (1959) (Equation 2-101) underestimates longitudinal mixing in most natural channels. This is due to the fact that it is derived for plane flow with mixing dominated by vertical shear, and as shown by Fischer (1967) in most channels transverse rather than vertical shear will dominate longitudinal mixing. Valentine and Wood (1977) also showed that in channels featuring trapping mechanisms (i.e. channels with zones of slow flowing water, which is common in many natural channels) the rate of longitudinal mixing is increased (see section 2.4.2.5).

The results reviewed cover a wide range, not withstanding the accuracy of the results this reflects the large influence that different hydraulic parameters have on the mixing coefficient.

For example in a wide channel featuring slow moving flow close to the banks (due to shallow or vegetated areas) the transverse velocity shear will be high and hence so will the rate of longitudinal mixing. Conversely in narrow sinuous channels the transverse velocity shear will be low and the rate of transverse mixing high (due to the secondary currents). In this case a low longitudinal dispersion coefficient would be expected. This variation in mixing coefficients has lead several researchers to link different hydraulic parameters to the mixing coefficient. For example after reviewing observed dispersion coefficients, Rutherford (1994) suggests that D_x/hu^* increases with channel aspect ratio, this is because there is expected to be more variation in transverse velocity (and hence velocity shear) in a wide shallow river than a narrow deep one.

Fukuoka and Sayre (1973) found that in a sinuous laboratory channel D_x/hu^* was inversely proportional to the radius of curvature. This is because the secondary currents which promote transverse mixing (and suppress longitudinal mixing) increase with channel curvature. Boxall (2000) conducted experiments in a sinuous laboratory channel, finding an inverse relationship between longitudinal and transverse mixing rates (transverse mixing being dependent on the levels of secondary currents caused by channel curvature).

Rutherford (1994) suggested that the dimensionless coefficient D_x/hu^* remains constant with discharge for a particular channel. This suggests that the dispersion coefficient should increase with flow. This effect may be caused by greater velocity shear as discharge increases; Rutherford (1994) presented data from experiments conducted in four natural channels at different flow rates to support this. Experiments by numerous researchers such as Fischer (1967) and Boxall (2000), conducted in laboratory channels, also show an increase in dispersion coefficient with discharge. However, Rutherford (1994) also notes that in some rivers increasing discharge may decrease velocity shear by increasing flow velocities in shallow areas. It is not generally possible to generalise how flow will affect mixing in a given river unless the effect of flow on velocity shear can be estimated.

2.4.7 Methods for Predicting Longitudinal Mixing in Shear Dominated Flows

The wide range of observed longitudinal dispersion coefficient values in natural channels (Equation 2-133) means that currently, the most accurate method of obtaining dispersion coefficients for a given reach and flow condition is to conduct experimental trials. However, to avoid this expensive and time consuming process, there are several equations to predict the dispersion coefficient based on river and flow parameters.

2.4.7.1 N - Zone Method

Chickwendu (1986) outlined an approach for predicting dispersion coefficients based on a given velocity profile. By splitting the flow into a series of (N) zones over the vertical, each with a different velocity and a transfer rate for inter zone mixing, a longitudinal dispersion coefficient can be derived mathematically. The two zone model was used as a starting point for the derivation. The concentration levels in each zone are considered to be well mixed. The dispersion equations for each zone are based on the two dimensional form of the ADE. Averaged over each zone and combined with a mass transfer function to describe transport of mass between each zone, the resulting coupled advection diffusion equations for each zone are provided by Chickwendu (1986) as

$$\partial_t c_1 = e_{x1}\partial_x{}^2 c_1 - u_1\partial_x c_1 + \psi\frac{1}{q_1}(c_2 - c_1)$$

Equation 2-134

$$\partial_t c_2 = e_{x2}\partial_x{}^2 c_2 - u_2\partial_x c_2 + \psi\frac{1}{q_2}(c_1 - c_2)$$

Where q_i	=	Fractional thickness of zone i	(-)
u_i	=	Velocity of zone i	(m/s)
Ψ	=	Inter-Zone transfer coefficient	(s^{-1})

This system was solved exactly by Chickwendu (1986) to provide

$$D_x(2) = \frac{(q_1 q_2)^2 (u_1 - u_2)^2}{\psi} + q_1 e_{x1} + q_2 e_{x2}$$

Equation 2-135

The model can then be expanded to use a greater number of zones. After considerable mathematical manipulation the formula for N zones becomes

$$D_x(N) = \sum_{j=1}^{N-1} \frac{(q_1 + q_2 \ldots + q_j)^2 \left[1 - (q_1 + q_2 \ldots + q_j)\right]^2 (u_{1j} - u_{(j+1)N})^2}{\psi_{j(j+1)}} + \sum_{j=1}^{N} q_j e_{xj}$$

Equation 2-136

Chickwendu (1986) defines the inter-zone transfer coefficient between each zone, $\Psi_{j(j+1)}$ as

$$\psi_{j(j+1)} = \frac{2e_{zj(j+1)}}{h^2(q_j + q_{j+1})}$$ Equation 2-137

As N tends to infinity

$$q_1 + q_2 \ldots q_j \longrightarrow \int_0^q dq = q$$ Equation 2-138

and it can be shown that

$$D_x(\infty) = \lim_{N\to\infty} D_x(N) = h^2 \int_0^1 \frac{q^2(1-q)^2}{e_z(q)} [u_f(q) - u_s(q)]^2 dq + \int_0^1 e_x(q) dq$$ Equation 2-139

Considering turbulent open channel flow, the typical logarithmic velocity profile and distribution of diffusivity (as described in section 2.4.4.1) can be split into N discrete zones. For each pair of zones the faster and slower velocity zones (u_f and u_s) can be described as

$$u_f(q) = U - \frac{(1-q)u^*}{q\kappa}\log(1-q)$$

Equation 2-140

$$u_s(q) = U - \frac{u^*}{\kappa}\log(1-q)$$

Given that diffusivity is as evaluated in section 2.4.4.1, Equation 2-139 becomes

$$D_x(\infty) = \frac{hu^*}{\kappa^3} \int_0^1 q^{-1}(1-q)[\log(1-q)]^2 dq + \frac{1}{6}\kappa hu^* = \frac{0.404}{\kappa^3} hu^* + \frac{\kappa}{6} hu^*$$ Equation 2-141

Equation 2-141 provides exactly the same solution as Equation 2-101, i.e. for plane boundary layer flow the Chickwendu (1986) is equivalent to Elders (1959) result. Although the mathematics is arduous, Equation 2-136 can be programmed into a spreadsheet to provide an estimate of the dispersion coefficient for any velocity profile, provided an estimate of the

mixing between the zones (which will be dependent on diffusivity- Equation 2-137) is provided. However, it should be remembered that such a method will only provide an accurate prediction of the dispersion coefficient provided mixing is dominated by shear in one plane only.

2.4.7.2 *Other Methods for Predicting Dispersion Coefficient*

Equations for the estimation of the longitudinal dispersion coefficients based on flow properties have been proposed by several researchers such as McQuivey and Keefer (1974), Lui (1977), Magazine et al. (1988) and Seo and Cheong (1998). Deng et al. (2002) developed a predictive technique based on a triple integration method. Ninety percent of the predicted values were between 0.5 times and 2 times the observed values of dispersion coefficients in natural channels. Boxall and Guymer (2007) present a method which applies the Chickwendu N-zone model to the transverse profile of primary velocities, as opposed to the vertical profile (as presented in section 2.4.7.1), with the transfer coefficient, ψ, based on the transverse mixing coefficient. Predicted values were typically within 20% of the measured laboratory values.

2.4.8 *Concentration Profile Routing Procedure*

It has been established that longitudinal dispersion coefficients derived from theoretical (section 2.4.4.4) and experimental methods (section 2.4.5.3) may not accurately represent the optimum values for a particular reach. In such cases it is often desirable to compare a predicted concentration profile with an observed one. To do this routing procedures have been developed which convert upstream profiles into downstream profiles using mixing coefficients and travel times.

Equation 2-142 is a solution to the one dimensional ADE (Equation 2-93); this solution utilises the frozen cloud approximation as described in section 2.4.5.3 and hence results in temporal concentration distributions which are more easily compared with experimental data (which is more commonly gathered as temporal rather than spatial distributions).

Assuming U and D_x are constant

$$C(x_{ds},t)=\int_{\gamma=-\infty}^{\infty}\frac{C(x_{us},\gamma)U}{\sqrt{4\pi D_x\overline{T}}}\exp\left[-\frac{U^2\left(\overline{T}-t+\gamma\right)^2}{4D_x\overline{T}}\right]d\gamma \qquad \text{Equation 2-142}$$

Where γ = Variable of integration (-)

$C(x_i,t)$ =	Concentration at position i at time t, where *us* or *ds* represent the upstream or downstream measurement locations respectively		(kg/m^3)

Given an upstream temporal concentration profile and values for dispensation coefficient (D_x) and travel time $(\overline{T})$, a simple routing procedure using Equation 2-142 can be performed to predict a downstream concentration distribution from an upstream trace. Equation 2-142 essentially takes each parcel of the upstream concentration distribution, advects it downstream according to the travel time and spreads it out (in a Gaussian manner) depending on the dispersion coefficient.

2.4.9 Development of the Aggregated Dead Zone Model

As stated in section 2.4.4.3, there are existing issues when attempting to apply the Fickian ADE to natural irregular channels in which skewed concentration profiles persist. Day and Wood (1986) suggest that Fickian models are incapable of accurately predicting the concentration distributions observed in most natural channels. In most practical cases Fickian based techniques will only provide an approximate model of the behaviour of tracer. This limitation has meant that there have been several efforts to construct different types of model to predict longitudinal mixing.

The Cells In Series (CIS) method presented by Stefan and Demetracopoulos (1981) is based on the modelling of a series of mixing tanks commonly used in the chemical engineering industry. The mixing reach is simulated as series of well mixed cells. The mass transport of a conservative tracer though each cell is represented by

$$V_c \frac{\partial C_c(t)}{\partial t} = QC_i(t) - QC_c(t) \qquad \text{Equation 2-143}$$

Where	V_c	=	Cell Volume	(m^3)
	C_c	=	Concentration within Cell	(kg/m^3)
	C_i	=	Inflowing concentration (from upstream cell)	(kg/m^3)

Solving Equation 2-143 the tracer concentration in the n^{th} cell can be given by

$$C_{c(n+1)}(t) = \frac{\alpha^n t^n}{n!} \frac{M}{V_c} \exp(-\alpha t) \qquad \text{Equation 2-144}$$

Where	M	=	Mass of tracer injected	(kg)
	α	=	$\frac{1}{T}$	(-)
	T	=	Residence Time (V_c/Q)	(s)

The centroid, variance, and skew of the predicted temporal concentration profiles are all functions of the number of cells used. Although the CIS model is comparatively simple to apply it does have several drawbacks. The terms of the CIS model (number of cells, cell volume) do not have any direct relationship with the reach characteristics. Also the number of cells used determines the advection, dispersion and the amount of skew. These parameters cannot be varied independently and this limits the practical use of the model. Stefan and Demetracopoulos (1981) also report that the CIS model does not offer a significant improvement over the ADE in terms of quality of fit.

Beer and Young (1984) further developed the CIS model. Instead of representing the reach as a series of cells they proposed that all mixing within the reach could be represented by a single aggregated dead zone (ADZ). The term dead zone encapsulates the effects of both pockets of flow which are separated from the main flow, and the other dispersive effects caused by eddies and velocity profiles. This single dead zone is combined in series with a pure advection chamber which introduces a time delay. This arrangement allows the effects of advection and dispersion to be decoupled. The mass balance equation can be expressed as

$$V_c \frac{\partial C_c(t)}{\partial t} = QC_i(t-\tau) - QC_c(t) \qquad \text{Equation 2-145}$$

Where	τ	=	Cell time delay	(s)

Solving Equation 2-145 the tracer concentration in the n^{th} cell can be given by

$$C_{c(n+1)}(t) = \frac{\alpha^n (t-\tau)^n}{n!} \frac{M}{V_c} \exp(-\alpha(t-\tau)) \qquad \text{Equation 2-146}$$

If the centroid of the predicted concentration distribution is calculated then it can be found that the reach travel time is the sum of the time delay (τ) and the residence time, T.

$$\overline{T} = T + \tau \qquad \text{Equation 2-147}$$

Mixing in natural channels is often better described using the standard ADZ model rather than the ADE (Wallis et al. 1989b). For more complex systems, i.e. long reaches with complicated dead zones, higher order versions of the ADZ model may be employed. Such approaches model the reach using different arrangements of cells in series and parallel. Such models require the determination of more than two mixing parameters and models of such complexity are generally not required for most laboratory or simple natural channels. Details of various higher order ADZ models can be found in Richter (2003).

Data is often collected as series of discrete concentration values at set time steps. The discrete time version of Equation 2-145 can be used to route upstream profiles to downstream predictions. For each discrete cell

$$C(x_{ds},t) = -\alpha C(x_{ds},t-1) + (1+\alpha)C(x_{us},t-\delta) \qquad \text{Equation 2-148}$$

Where α	=	$-e^{\left(\frac{-\Delta t}{\overline{T}-\tau}\right)}$	(-)
δ	=	$\frac{\tau}{\Delta t}$	(-)
Δt	=	Time step	(s)

2.4.9.1 *Identifying ADZ parameters*

The ADZ parameters required to solve Equation 2-148 are the normal travel time, $\overline{T}$ (difference between trace centroids) and cell time delay, τ (difference in first arrival times). The identification of these parameters can be achieved by examining measured concentration distributions (Figure 2-15).

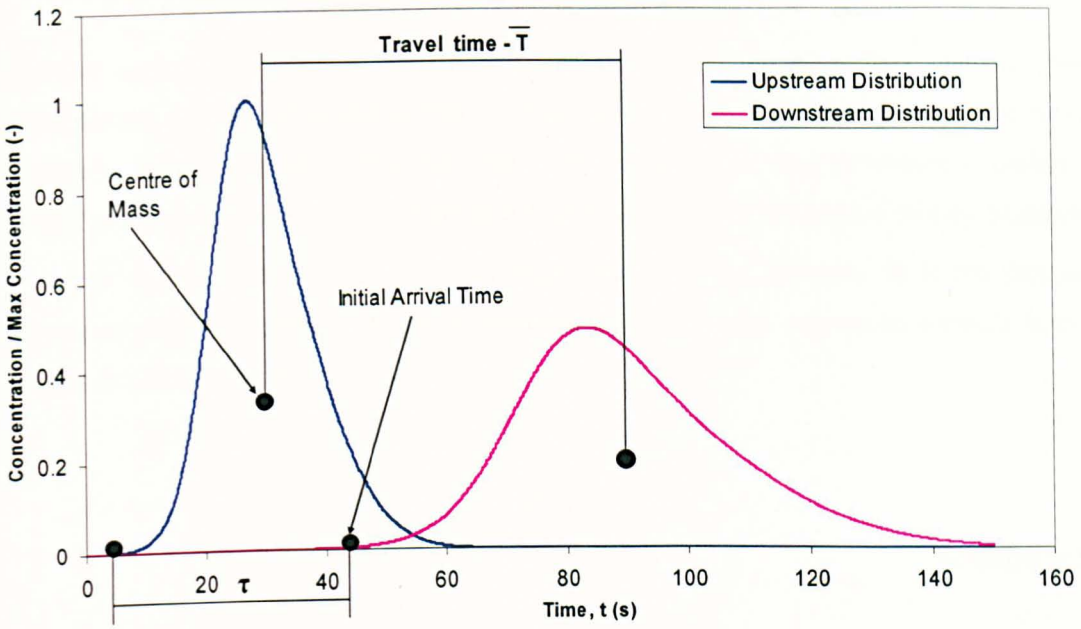

Figure 2-15 Downstream concentration profile at each time step calculated using the ADZ model and two coefficients (τ and $\overline{T}$)

One disadvantage of the ADZ as opposed to the ADE is that it is more difficult to conceptualise the influence of τ and $\overline{T}$ on the rate of mixing compared with a 'simple' mixing coefficient D_x, thus it more difficult to link the physical characteristics of the mixing reach to the ADZ parameters. Some progress has been made, however, a measure commonly used to quantify the level of mixing using the ADZ model is dispersive fraction. The dispersive fraction was first defined by Wallis and Young (1986) as a measure of the ratio between the residence time T and the total time which tracer spends in the reach. Dispersive fraction (Df) can therefore be defined as

$$Df = \frac{V_e}{V_R} = \frac{T}{\overline{T}} = \frac{\overline{T} - \tau}{\overline{T}} \qquad \text{Equation 2-149}$$

Where V_e = ADZ volume (Dead zone volume) (m^3)

V_R = Total volume in the reach (m^3)

Field data conducted in four natural channels by (Wallis et al., 1989b) suggests that the dispersive fraction is approximately constant with discharge. Also, when compared to data from laboratory flumes, (Wallis et al., 1989a) the dispersive fraction is found to be higher in irregular natural rivers than smooth experimental channels.

2.4.10 Parameter Optimisation

Parameter optimisation methods have been successfully used by researchers such as Dennis (2000), Boxall (2000) and Dutton (2004) to improve the accuracy of measured solute mixing parameters. This optimisation procedure works by using the routing procedure explained in section 2.4.8 together with a series of refined searches to identify the pair of mixing parameters (D_x and $\overline{T}$ for the ADE, τ and $\overline{T}$ for the ADZ) that give the optimum fit to the measured downstream profile. Goodness of fit is evaluated by means of a regression formula such as Equation 2-150 (Young et al., 1980).

$$Rt^2 = 1 - \left[\frac{\sum_{t=1}^{n} (m_t - p_t)^2}{\sum_{t=1}^{n} m_t^2} \right] \qquad \text{Equation 2-150}$$

Where	Rt^2	=	Goodness of fit	(-)
	m_t	=	measured concentration level at time t	(kg/m^3)
	p_t	=	concentration level predicted by the model at time t	(kg/m^3)

The regression formula provides an Rt^2 value which represents how well the predicted values represent the measured observations. An Rt^2 of 1 means that the predicted values describe the measured perfectly. Values lower than 1 indicate error between the measured and observed values and a value of zero or less means that the predicted profile fails to describe any part of the measured profile. A program developed by Dennis (2000) works by forming a series of 11 by 11 grids of regression values calculated from running the model with different pairings of mixing parameters. For each pairing the resulting prediction is compared to the measured trace and the resulting Rt^2 is recorded in the matrix (Figure 2-16). To form each matrix 11 values of the two mixing parameters are required. For the first matrix these parameters are based on those identified using the methods outlined in 2.4.5.1. Minimum and maximum values are identified (i.e. a range) and then a step size which will give 11 values in total for each parameter.

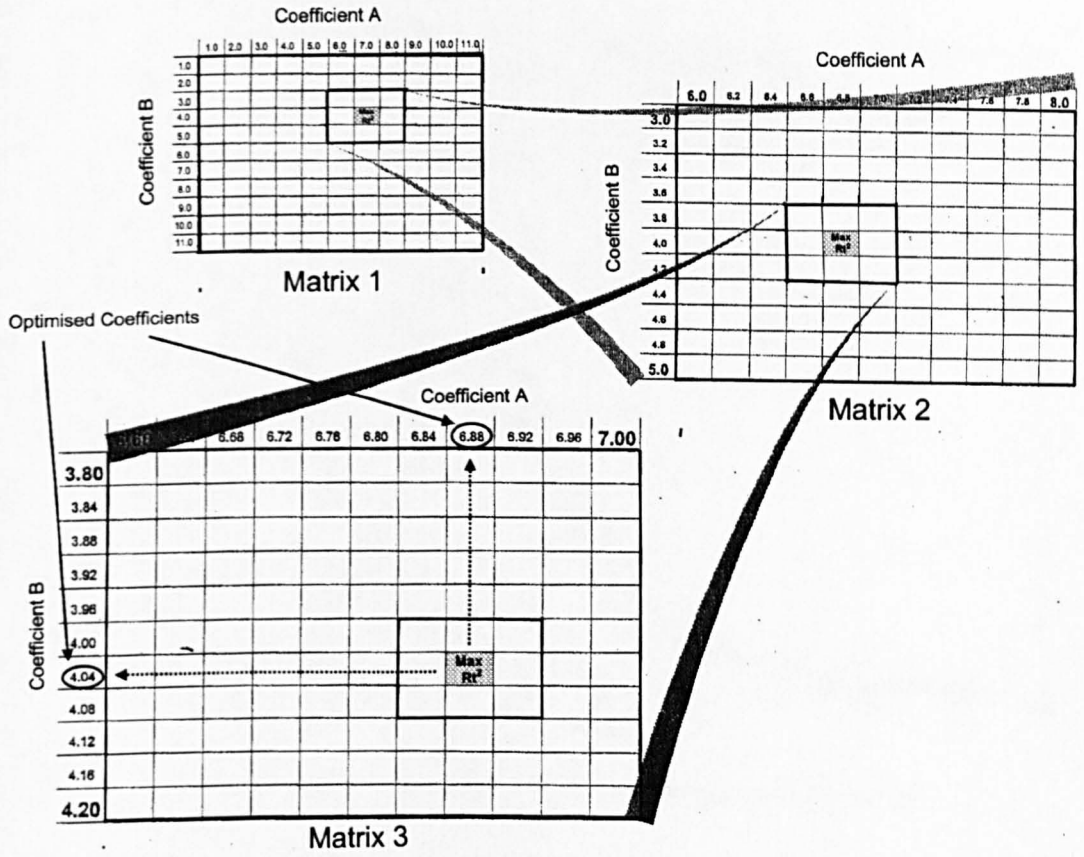

Figure 2-16 Three matrix optimisation procedure (adapted from Dennis, 2000)

Each combination of parameters is then used to produce a grid of Rt^2 values. The best fit combination of parameters (i.e. those whose paring produce the highest Rt^2 value) are then chosen. If the maximum Rt^2 value is found to be on the edge of the grid then it is possible that the maximum value may be outside the range of the parameters chosen. If this is the case the grid is enlarged by increasing the range of the parameters searched, recalculating Rt^2 values and repeating until the maximum Rt^2 is no longer on the perimeter of the grid. The chosen best fit parameters from this grid become the new initial parameters for a new 'refined' grid. This new grid has a smaller range and a smaller step size. The whole process is repeated, the grid becoming smaller when each 'best fit' value is chosen. The final optimised parameter is reached when the step size of the grid becomes sufficiently small, becoming smaller than pre-defined tolerance/final resolution values. An example of the effect of optimisation on the measured ADE parameters and the resulting goodness of fit is shown in Figure 2-17.

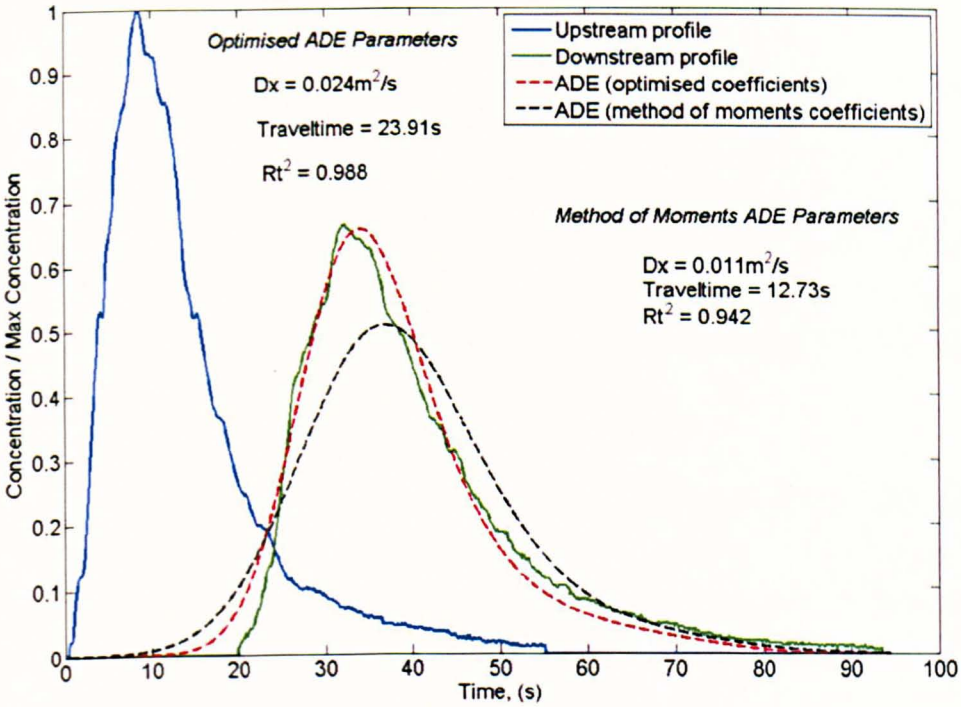

Figure 2-17 Example of the ADE optimisation procedure

Chapter 3 - Vegetated Flow Theory

This chapter reviews existing literature and background theory relating to the impact of vegetation on the conveyance and mixing processes described in Chapter 2. Existing work focuses on either free flowing channels with vegetated banks or cases where vegetation is present across the entire flow width. The need to quantify the resistance of flow though purely vegetated regions and the added complication of differing flow regimes in partially vegetated flow, means that this study is restricted to canopies which occupy the entire flow width.

3.1 Bulk Vegetation Resistance

In channels featuring vegetation, flow resistance comes not only from the bed surface roughness and channel form but also from the vegetation elements. The presence of vegetation in a channel will have an effect on the stage discharge relationship, slowing the flow and reducing the overall flow carrying capacity relative to non-vegetated channels (Hoffman, 2004).

As a result of the relatively large surface area of a vegetation element as opposed to its mass, even a small amount of vegetation can have a large impact on the flow resistance (Nepf, 1999). After a review of existing literature, the primary characteristics of vegetation which affect the magnitude of the vegetated flow resistance have been categorised as:

Stem Density:	Dense vegetation will impart more resistance.
Frontal area:	Large vegetation imparts more resistance than thin sticklike vegetation.
Height:	Vegetation which is taller than the flow depth (emergent) results in a different velocity profile compared with vegetation that is fully submerged.
Stiffness:	Vegetation which bends with the flow becomes more streamlined, experiencing less drag and so imparting less resistance.

In very dense canopies, the physical area taken up by the vegetation elements will noticeably reduce the capacity of the channel, in effect 'constricting' the flow. Previous studies (Li and Shen, 1973; Stone and Shen, 2002) have looked at how changing vegetation density and size affects flow resistance. However, due to the practical problems involved, these studies have mainly used artificial vegetation in laboratory studies rather than real vegetation. These studies have only looked at a limited range of vegetation height to depth ratios, usually used only one stiffness level, and the type of 'vegetation' is kept constant (in most cases the 'vegetation' used were fully rigid cylindrical rods). There is limited understanding of how changing the

vegetation type and stiffness affects the flow resistance. Many studies result in methods which are site specific and non transferable. Difficulties arise when attempting to transfer these models to natural situations where the type, nature and size of vegetation differ from those proven experimentally (Jarvala, 2002).

3.1.1.1 *The Drag Equation*

When considering the flow resistance from elements in the flow it is useful to consider the drag equation. By Newton's third law the force acting on the flow due to an immersed body is equal to the force on a body due to the flow. Force experienced by a body moving through a flow is given by the drag equation, hence this force will be equal and opposite to the flow resistance acting on the flow because of the body. The drag equation is conventionally (Pope, 2000) defined as

$$F_d = 0.5 C_d \rho U^2 A_i \qquad \text{Equation 3-1}$$

Where F_d	=	Drag Force	(N)
C_d	=	Drag Coefficient	(-)
A_i	=	Frontal Area of element	(m^2)

The drag equation is attributed to Lord Rayleigh, who originally used L^2 in place of A_i (L being some linear dimension).

3.1.1.2 *Use of Conventional Models*

The use of conventional resistance equations (such as Manning's equation) in vegetated channels has been criticised because such equations were derived for use in situations where flow is only resisted by boundary shear and not by drag elements extending into the flow (James et al., 2004). For example, the drag experienced by emergent vegetation depends on the flow depth (deeper flow submerges more vegetation, hence resulting in a greater frontal area and more drag), so conventional resistance coefficients (such as Manning's n) also vary with flow depth. An increase in Manning's n with depth is typical for emergent flow either through crops or in floodplains (Chow, 1959). By conducting experiments in a laboratory with harvested vegetation, Jarvela (2002) found that the resistance of emergent (i.e. flow with a depth lower than the plant canopy height) leafless willow tress increased with flow depth.

In submerged vegetation (i.e. flow with a depth greater than the plant canopy height) the height of vegetation resisting the flow remains approximately constant with depth assuming no significant vegetation deformation takes place (see section 3.1.2.4). However, this means that the proportion of flow containing resistance elements decreases with flow depth. Wu et al. (1999) conducted laboratory experiments using dense flexible simulated vegetation. In submerged conditions it was found that as the flow depth increased, the Manning's n value decreased, tending towards an asymptotic constant. This constant was a function of the vegetation height. Wu et al. (1999) suggested that once the proportion of flow passing though the vegetation becomes negligible compared to that which passes above, the vegetation behaves like conventional boundary roughness. Wilson and Horitt (2002) studied the flow resistance of submerged grass linings in a laboratory, finding that the hydraulic resistance decreases as the degree of submergence increases, gradually tending towards a constant value once the flow depth was roughly 3 times the height of the vegetation.

In vegetated flow the use of a single flow resistance coefficient in the forms such as those discussed in section 2.2 will involve significant errors if attempting to determine a stage discharge relationship. The depth dependent nature of flow resistance makes it is convenient to define a submergence ratio (Sr)

$$Sr = \frac{h}{h_c} \qquad \text{Equation 3-2}$$

Where h_c = Vegetation Canopy Height (m)

3.1.1.3 *Velocity within Emergent and Submerged Vegetation*

Researchers (Kouwen et al., 1969, Nepf and Vivoni, 1999) have observed that the primary vertical velocity profile in vegetated channels does not follow the universal logarithmic law (Equation 2-35). In emergent conditions, the velocity profile is much more uniform over the depth (Linder 1982), with the influence of boundary roughness restricted to a small zone near the bed. Profiles may not be entirely uniform if the distribution of mass of the plants is also uneven over the depth (Wilson et al., 2006). In submerged vegetation, a faster layer of flow exists above the vegetation where the flow is not directly resisted by the vegetation. This creates a shear layer at the top of the canopy. The complex 'two layer' effect present in submerged canopies means that flow resistance in this case is seen as more difficult to determine when compared to emergent canopies (Stone and Shen, 2000).

3.1.2 Vegetation Parameters and Flow Resistance

3.1.2.1 Vegetation Density

It has been shown by Einstein and Banks (1950) that total resistance from an array of elements positioned in the flow is equal to the summation of resistance from each individual element. By this principle it follows that an increase in vegetation density will lead to a linear increase of vegetative resistance (assuming all vegetation elements are of the same size and exert the same drag). This is supported by the experiments of Jarvela (2002), who conducted experiments with leafless willows, finding that doubling the stem density resulted in an approximate doubling of the flow resistance.

Total flow resistance is a combination of vegetation resistance (from each individual vegetation element) and resistance from the bed. Also of interest is the relative contribution of both of these sources of resistance towards the total resistance. The contribution of bed resistance toward the total resistance becomes insignificant as vegetation density increases (Temple, 1986). James et al. (2004) conducted experiments using both rigid uniform rods and harvested *Phragmites australis* (Common reeds) stems finding that once stem density satisfies the condition specified in Equation 3-3, resistance from the bed becomes negligible in terms of the total resistance and can be neglected.

$$0.25N\pi S_d{}^2 h > 0.1 \qquad \text{Equation 3-3}$$

Where	N	=	Stem Density	(stems/m^2)
	S_d	=	Stem Diameter	(m)

3.1.2.2 Frontal Area

According to Equation 3-1, flow resistance from an element in the flow will increase linearly with its frontal or projected area. Due to this linear relationship the geometric properties of the vegetation can be linked together with density to provide a 'density index'. For example Nepf et al. (1997) defined the parameter NS_d as a density parameter. Other researchers have used parameters such as channel porosity (Hoffman, 2004) or vegetation projected area (Petryk and Bosmajian, 1975).

3.1.2.3 Planting Configuration

Planting configuration is anther factor which may affect the flow resistance of an array of vegetation elements. Li and Shen (1973) found that resistance elements arranged in a staggered pattern imparted more flow resistance than those arranged in rows. It was explained that when the elements were staggered the resistance from each element was evenly distributed, preventing any part of the flow from accelerating. Whereas in flow with aligned elements the resistance effect was restricted to distinct 'bands', with flow outside these areas passing relatively unhindered. In natural channels most vegetation types grow in a random fashion and hence more closely replicate a staggered vegetation pattern than an aligned one. Most laboratory experiments to date use some form of staggered pattern to simulate this random growth. More recent studies by Nepf (1999) and Ghisalberti and Nepf (2004, 2005) have generated random planting arrangements by using a computer program. Existing models of vegetated flow resistance ignore the effects of different planting configurations.

3.1.2.4 Vegetation Stiffness

Under the influence of the water flow, flexible vegetation elements will bend. Kutija and Hong (1996) proposed that a vegetation element could be modelled as a cantilever element under a uniform load. The degree of bending will depend on the velocity of water, the height and size of the vegetation and the vegetation stiffness. However, due to the wide range of vegetation species and differing degrees of vegetation stiffness, it may not be possible to model the bending of all types of vegetation accurately. Little information currently exists on the biomechanical properties of different types of vegetation (Green, 2005).

The degree of bending of vegetation has two main impacts on flow resistance. Firstly, in submerged flow conditions the more the element is able to flex the more the plants height (and hence cross sectional area and flow resistance) will decrease. Secondly, under the influence of loading, flexible vegetation will adopt a streamlined position. This reduces the drag coefficient of the element, and so the flow resistance. These effects are dependent on the ability of the vegetation element to bend (vegetation stiffness) and the force exerted by the flow (flow velocity, vegetation width and flow depth in the case of emergent vegetation). Jarvela (2002) conducted experiments with submerged grasses and sedges. Flow resistance was observed to decrease with Reynolds number (and hence average channel velocity) due to increased streamlining of the flexible vegetation. Fathi-Maghadam and Kouwen (1997) conducted drag experiments on emergent tree saplings and found that resistance factors varied greatly with the flow velocity due to increased bending. Drag force increased linearly with flow velocity, not with velocity squared as suggested by Equation 2-1. This suggests that increased velocity

decreases drag coefficient and frontal area, and that the assumption of rigid vegetation could lead to large errors in the estimation of roughness.

3.1.2.5 *Drag coefficient*

According to Equation 3-1 the drag on an element in the flow is dependent on the drag coefficient. The drag coefficient of an object in the flow is dependent on its shape and also the flow regime. Consider flow around a uniform cylinder (or a straight uniform vegetation element), a stem scale Reynolds number (Re_{st}) can be defined as

$$\mathrm{Re}_{st} = \frac{US_d}{\nu} \qquad \text{Equation 3-4}$$

As the stem scale Reynolds number increases, the flow regime around the cylinder changes, moving from ideal flow (smooth flow around the cylinder with no separation) to fully turbulent flow with a separation zone behind the cylinder and the formation of wakes (Figure 3-1).

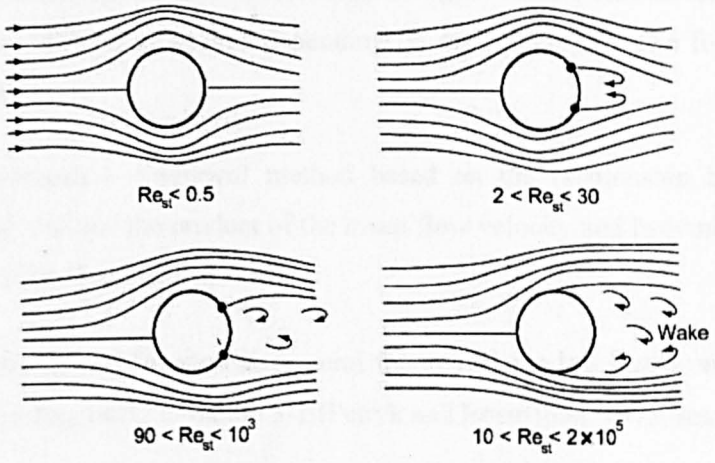

Figure 3-1 Wake formation with increasing stem Reynolds number (from Douglas et al., 2005)

The relationship between Reynolds number and drag coefficient has been investigated by several researchers. Between $100 < Re_{st} < 10^5$ the theoretical value of drag coefficient on an infinitely long cylinder is 1.0 (Pope, 2000). Therefore some researchers (for example Petryk and Bosmajian, 1975) who have modelled vegetation elements as uniform cylinders use a drag coefficient of 1. However, in natural vegetated channels the determination of an accurate drag coefficient is further complicated because

- Most vegetation does not resemble a perfect cylinder. Vegetation will have a higher natural drag coefficient due to the leaves and stems, especially in the case of 'bushy'

vegetation (Jarvala, 2004).

- Vegetation flexes under flow, adopting a more streamlined shape, suggesting a lower C_d with velocity (Tsujimoto et al., 1995; Kouwen and Fathi, 2000),

- In an array of vegetation elements some elements may be sheltered by others, hence the apparent or 'bulk' drag coefficient may be different to one defined for an individual element. This suggests a relationship between C_d and stem density (Nepf, 1999).

Nepf (1999) looks at the relationship between drag coefficient and stem density in an array of emergent dowel rods. As the density gets larger, (past $NS_d^2 \approx 0.01$) a sheltering effect becomes evident, upstream elements effectively sheltering those elements immediately downstream. Hence, as the stem density becomes larger the overall bulk drag coefficient decreases.

3.1.3 *Quantifying Vegetation Resistance*

The requirement for accurate stage discharge prediction in waterways (for activities such as accurate flood forecasting, knowledge of flow velocities and conveyance capacities) has lead to the production of numerous models which estimate vegetated flow resistance. These models can be classified into different groupings depending on their approach. The following groupings have been identified

- n-UR approach – Empirical method based on the relationship between resistance (Manning's n) and the product of the mean flow velocity and hydraulic radius (Ree and Palmer, 1949, Temple et al. 1987).

- Drag Approach – Theoretical or semi theoretical models based on determining total vegetative drag using Equation 3-1 (Petryk and Bosmajian, 1975, James et al., 2004).

- Relative Roughness Approach – Quasi theoretical method for submerged vegetation based on a modified law of the wall (Kouwen, et al., 1969, Kouwen and Unny, 1973).

- Numerical Models – Computational fluid dynamic models which aim to describe flow through vegetated channels (Lopez and Garcia, 2001, Cui and Neary, 2002). Such models require accurate detailed vegetation parameters and boundary conditions which are difficult to acquire for most vegetated flow cases. Due to their complexity a complete description of such models is beyond the scope of this work.

3.1.3.1 n – UR approach

The n-UR approach was first proposed by Ree and Palmer (1949) as a means of predicting Manning's n values for flow through vegetation. It is the first approach to recognise that n-values vary with flow depth and so that selecting a single design n-value for flow through vegetation results in errors. The authors found that n holds a certain relationship with the product of velocity and hydraulic radius. This relationship is characteristic of the vegetation type and height. Vegetation types are classified into five groups dependent on their retardance and experimental curves for n versus UR were produced (Figure 3-2) for each group. Using these curves, the Manning's equation and a trial and error approach, the design capacity of the channel can be determined. The n-UR graphs demonstrate the principle that flow resistance is a function of flow depth. At first resistance increases as more of the vegetation is submerged, but then it decreases as increased flow velocity flattens and streamlines the vegetation, reducing its cross sectional area and drag coefficient. This is in spite of the fact that in conventional flow resistance and drag equations, resistance increases proportionally to the square of velocity. The n-UR curves have been updated to deal with a wide variety of emergent and submerged vegetation and updated versions can be found in Chow (1959) and Temple et al. (1987). Its ease of use means that the n-UR is the most popular method in practice for resistance prediction in vegetated channels. To aid in the design process, best fit equations which represent five curves have been developed by several researchers; equations proposed by Green and Garton, (1983) and Findlay and Ellul (1976) are presented in Table 7.

Table 7 Best Fit Equations for n-UR Curves

Curve	Equation	Example Suitable Vegetation Type and Height (Chow, 1959)	Source
A	$n = 0.44 - 1.674UR$ (if UR<0.1542) $n = 0.46 + \frac{0.0223}{UR}$ (if UR>0.1542)	Very high resistance – Weeping Love Grass, Yellow bluestem ischaemum, $h_c \approx 70cm$	Green and Garton (1983)
B	$n = 0.032 - \frac{0.01545}{UR^{\frac{7}{8}}}$	High Resistance – Bermuda grass, Blue grama, $h_c \approx 30cm$	Findlay and Ellul (1976)
C	$n = 0.03 - \frac{0.00501}{UR}$	Moderate Resistance – Crab grass, Kentucky bluegrass, $h_c \approx$ 25cm	Findlay and Ellul (1976)
D	$n = 0.027 - \frac{0.00534}{UR^{\frac{3}{4}}}$	Low Resistance – Buffalo grass, $h_c \approx 12cm$	Findlay and Ellul (1976)
E	$n = 0.022 - \frac{0.003014}{UR^{\frac{2}{3}}}$	Very Low Resistance – Short grasses, $h_c \approx 3.5cm$	Findlay and Ellul (1976)

However, use of the n-UR curves has been criticized by several researchers and no full scientific justification has been provided for the n-UR approach. Kouwen et al. (1969) demonstrated that for one type of vegetation, plots of n versus UR do not fall on a straight line if the channel slope is varied. The product UR does not uniquely describe a flow condition and the resistance of a channel should not be independent of channel slope (Kouwen, 1990). Several researchers (Jarvala, 2005, Wilson and Horritt, 2002) have commented on the need to replace the n-UR methods with a more theoretically justified approach.

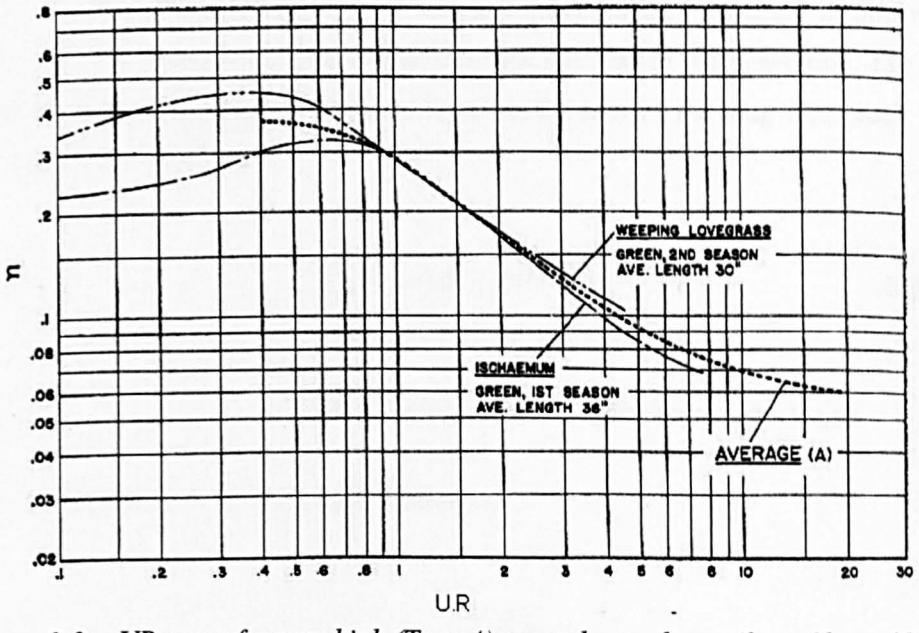

Figure 3-2 n-UR curve for very high (Type A) vegetal retardance (from Chow, 1959)

3.1.3.2 Drag Approach

The Petryk and Bosmajian (1975) model is one of the earliest examples of the drag approach whereby the force resistance generated by the vegetation was calculated by balancing gravitational forces against normal bed friction and a drag force generated by the vegetation. The approach is relatively simple to derive and use, but it contains several simplifications and assumptions which may reduce its accuracy when used with certain types of vegetation. Initially designed for only rigid emergent vegetation, it has been adapted by subsequent authors to include other vegetation types. The method uses the principle of conservation of momentum to balance drag forces acting around the vegetation elements with gravitational force. This type of model has a sound theoretical basis when trying to analyse rigid sticklike emergent vegetation, however, attempts to expand the model to include bending or submerged vegetation both make the model much more complicated and have met with mixed results. The other main drawback with this type of model is that it almost always requires a value of drag coefficient to be derived prior to calculation. This value is very hard to determine unless detailed testing is undertaken

on the vegetation itself (Green, 2005). This drawback has meant that drag approach models have limited appliance in river channel design. Theoretically, from momentum considerations; along a given channel reach, for uniform flow considerations, Petryk and Bosmajian (1975) provide the following force balance equation.

$$\rho g A L S_o = \sum F_d + \tau_0 P L \qquad \text{Equation 3-5}$$

Equation 3-5 is a modified form of the standard force balance equation in uniform flow (Equation *2-5*) with an additional term to account for the drag of the vegetation. The total drag force acting on the vegetation elements is equal to the sum of the drag from each individual plant. Hence from Equation 3-1

$$\sum F_d = 0.5 C_d \rho U^2 \sum A_i \qquad \text{Equation 3-6}$$

Where ΣA_i = Total projected area of vegetation per unit length (m^2)

The boundary shear stress is commonly derived as

$$\tau_0 = \rho g \left(\frac{A}{P}\right) S_0 \qquad \text{Equation 3-7}$$

The Manning's formula is

$$U = \frac{1}{n}\left(\frac{A}{P}\right)^{2/3} S_0^{0.5} \qquad \text{Equation 3-8}$$

Hence by inserting the Manning's formula, the bed shear stress can be given by

$$\tau_0 = \rho g U^2 n_b^2 \left(\frac{P}{A}\right)^{1/3} \qquad \text{Equation 3-9}$$

Where n_b = Manning's n (from bed only) ($s/m^{1/3}$)

Substituting both the new shear stress equation and the drag force equation into the original balance equation leads to a force balance equation

$$\rho gALS_o - 0.5C_d \rho gU^2 \Sigma A_i - \rho gU^2 n_b^{\,2} \left(\frac{P}{A}\right)^{1/3} PL = 0 \qquad \text{Equation 3-10}$$

Solving Equation 3-10 for velocity gives

$$U^2 = \frac{S_0}{\frac{C_d \Sigma A_i}{2gAL} + \frac{1}{n_b^{\,2}} \left(\frac{P}{A}\right)^{4/3}} \qquad \text{Equation 3-11}$$

Expressing the average velocity according to the conventional Manning formula (Equation 2-11) and equating to Equation 3-11, one obtains

$$U^2 = \left(\frac{1}{n}\right)^2 \left(\frac{A}{P}\right)^{4/3} S_0 = \frac{S_0}{\frac{C_d \Sigma A_i}{2gAL} + \frac{1}{n_b^{\,2}} \left(\frac{P}{A}\right)^{4/3}} \qquad \text{Equation 3-12}$$

And Manning's n becomes

$$n = n_b \sqrt{1 + \frac{C_d \sum A_i}{2gAL} \frac{1}{n_b^{\,2}} R^{\frac{4}{3}}} \qquad \text{Equation 3-13}$$

If the flow resistance from the bed, n_b is judged to be insignificant the term containing Manning's n can be ignored and the Equation 3-13 reduces to

$$n = R^{\frac{2}{3}} \sqrt{\frac{C_d \sum A_i}{2gAL}} \qquad \text{Equation 3-14}$$

From Equation 3-14 it follows that if the density of vegetation remains constant with height, Manning's n increases in proportion to the $^2/_3{}^{rd}$ power of the hydraulic radius. Substituting this

into the Manning's formula, the mean velocity can be found by

$$U = \sqrt{\frac{2gAL}{C_d \sum A_i}} S_o^{\frac{1}{2}} \qquad \text{Equation 3-15}$$

The drag coefficient is specified to be 'in the order of 1'. It is worth noting that if the bed is judged to have no influence (in very dense canopies – see section 3.1.2.1) and Equation 3-15 is used, that the flow velocity becomes independent of discharge and flow depth, and is a function only of vegetation size, density and drag. In this case the n-value increases in proportion to the $^2/_3{}^{rd}$ power of the hydraulic radius. This would agree with Temple et al. (1987), who hypothesised that within emergent canopies the mean velocity remains constant with depth. However, this contradicts the empirical n-UR approach (section 3.1.3.1), which generally shows that flow resistance (expressed as Manning's n) does not increase dramatically with hydraulic radius in emergent conditions, leading to an increase in flow velocity with depth. This discrepancy may be due to the fact that the drag approach does not take into account the effects of vegetation streamlining with increasing flow, especially if a constant value of drag coefficient is used.

After the work of Petryk and Bosmajian (1975) several further flow resistance equations based on the force balance have been proposed; the identified models which are based on the drag equation are summarised in Table 8. The model of James et al. (2004) is based on the drag equation but expresses resistance in terms of a new coefficient rather than the conventional Manning's n. This coefficient does not require the resistance coefficient to vary with flow depth because of the form of the Manning's equation. A higher drag coefficient of 1.5 is suggested as the preferred value based on work by Albertson et al. (1960). Compared to the model of Petryk and Bosmajian (1975) the total flow area is reduced to compensate for the area of flow taken up by the plants themselves. Hoffman (2004) developed a similar model to Petryk and Bosmajian (1975), however it includes a extra term which accounts for the fraction of the flow volume occupied by the plants and the 'tortuous flow path'. Hoffman (2004) assumes that the flow resistance from the bed is insignificant and so is neglected. Also, instead of a constant drag coefficient, C_d is based on the theoretical relationship between drag and stem Reynolds number proposed by Taylor et al. (1985).

The models of Stone and Shen (2000) and Jordanova et al. (2006) are based on the force drag concept but are calibrated using experimentally through dowel rods and reed stems respectively.

Table 8 - Drag Flow Resistance Equations

Author	Type	Form	Resistance Equation	Drag Coefficient	Constraints	Notes
Petryk and Bosmajian (1975)	Theoretical	Manning's n - $U = \frac{R^{2/3} S_o^{1/2}}{n}$	$n = n_b \sqrt{1 + \frac{C_d \sum A_i}{2gAL} \frac{1}{n_b^2} R^{\frac{4}{3}}}$	Given as 1 - From previous work by Petryk (1969), Hoerner (1965), and Hsi (1968)	-	Rigid Emergent Vegetation.
Stone and Shen (2000)	Semi Theoretical	$U_c = F\sqrt{hS_0}$ and $\frac{U_c}{U} \approx \sqrt{l^*}$	$F = 1.385\left(S_R^{-1} - \sqrt{NS_d^2}\right)\sqrt{\frac{g}{NS_d h}}$	Included in formula from empirical data	$0.934<\lambda<0.995$ $113<N(/m^2)<2500$ $0.0023<S_d<0.013$ $83<Re_{st}< 7100$ $0.0001<S_0< 0.05$	Emergent and submerged flow conditions. Empirical data from experiments with flow through dowel rods plus previous data.
James et al. (2004)	Theoretical	$U = \frac{1}{F}\sqrt{S_0}$	$\frac{1}{F} = \sqrt{\left(\frac{\left(1 - 0.25N\pi S_d^2\right)}{\frac{gn_b}{h^{1/3}} + C_d 0.25NS_d h}\right) gh}$	1.5 - From Albertson et al. (1960)	-	Investigates relative contribution to total resistance from both bed and vegetation. Manning's n term can be neglected when $(0.25N\pi S_d^2 h > 0.1)$
Hoffman (2004)	Theoretical	Manning's n - $U = \frac{R^{2/3} S_o^{1/2}}{n}$	$n = \frac{C_d(1-\lambda)}{2S_d \lambda g\left(\sqrt{\frac{\pi}{4}} - \sqrt{1-\lambda}\right)^2} R^{2/3}$	If $Re_{st} < 6*10^4$, $\log C_d = -0.125 \log Re_{st} + 0.275$ If $Re_{st} > 6*10^4$, $C_d = 0.6$ From Taylor et al. (1985)	$0.8<\lambda$	Similar to Petryk and Bosmajian but term for flow constriction (i.e. reduced flow area in canopies) included.
Jordanova et al. (2006)	Semi Theoretical	$U = \frac{1}{F}\sqrt{S_0}$	$F = 1.885\left(\frac{s_p}{S_d}\right)^{0.65}\left(\frac{S_d}{h}\right)^{0.07} C_d^{0.48}$	$C_d = \alpha Re_{st}^{-k}$	$0.005<(Q/b)<0.5$ $0.05<s(m)<0.1$ $0.005<S_d(m)<0.02$ $0.0005<S_0< 0.002$	Based on James (2004) model. Tested conducted to determine the $C_d - Re_{st}$ relationship for reeds and bulrushes.

Where U_c = Average Velocity in Stem Layer (m/s), f = Friction Factor (-),
α = Empirical coefficient (-), k = Empirical coefficient (-),
λ = Channel Porosity (-), s_p = Vegetation Spacing (m),

3.1.3.3 Other Derivations of Drag Coefficient

As explained in section 3.1.3.2 one drawback of the drag force approach is the uncertain value of the drag coefficient. Linder (1982) provided a method to compute the effective drag of an array of cylinders. Based on experimental studies with cylindrical elements, an empirical relationship was derived.

$$C_d = \left(1+1.9\frac{S_d}{s_p}C_{di}\right)\left(0.0205+\left(\frac{s_p}{S_d}\right)^{0.46}C_{di}\right)+\left(\frac{2s_p}{s_p-S_d}-2\right) \qquad \text{Equation 3-16}$$

Where C_{di} = Idealised drag coefficient of a cylinder in 2D flow (-)

However, Equation 3-16 is only suitable for ideal cylinders, Jarvala (2002) showed that Equation 3-10 significantly underestimated the drag coefficient of natural plants (in this case willow stems). More recently researchers have measured the drag coefficient of vegetation directly. Wu et al. (1999) conducted flow experiments with simulated vegetation. Although the vegetation was artificial, it was stated that it had a flexibility similar to stiff grasses. The experiments were conducted using a range of slopes and involved emergent and submerged conditions, however, density was not varied. Wu et al. (1999) investigated how the drag coefficient varied with flow depth, Reynolds number and slope. The derivation of drag coefficient was based on the force balance equation used by Petryk and Bosmajian (1975) with the assumption that the effect of the bed is negligible. Making this assumption Equation 3-10 can be written as

$$\rho g A L S_o - 0.5 C_d \rho U^2 \Sigma A_i = 0 \qquad \text{Equation 3-17}$$

By rearranging Equation 3-17, the drag coefficient C_d can then be derived as

$$C_d = \frac{2gS_o}{U^2}\frac{AL}{\Sigma A_i} \qquad \text{Equation 3-18}$$

Wu et al. (1999) goes on to convert the drag coefficient into a vegetated drag coefficient by combining the drag and density terms.

$$C_d' = C_d \frac{\Sigma A_i}{AL} = \frac{2gS_o}{U^2}$$ Equation 3-19

Where C_d' = Vegetal drag coefficient (m^{-1})

The result of this is that the vegetal drag 'coefficient' has units m^{-1}, however this does allow the lumping together of the projected area of vegetation with the drag coefficient. This allows the comparison of new research with previous datasets (such as Ree and Palmer, 1949, Chen, 1976) which may not have recorded vegetation density or porosity values.

In submerged flow it was assumed that the drag becomes dependent on the proportion of flow within the vegetated canopy, leading to the following vegetal drag coefficient formulation for submerged conditions

$$C_d' = Sr \frac{2gS_o}{U^2}$$ Equation 3-20

Wu et al (1999) observed that the vegetal drag coefficient decreased with increasing Reynolds number. Based on Equation 3-18 and Equation 3-20 the following functional relationship was observed.

$$C_d' = \alpha S_0^{\beta} h_c^{\gamma} \mathrm{Re}^{-k}$$ Equation 3-21

Where k = Coefficient based on biomechanical property of vegetation (-)

α, β and γ = Empirical coefficients (-)

Equation 3-21 is similar to that found by Jordanova et al. (2004), as shown in Table 8. In the case of Jordanova et al. (2004) a relationship was found between the unmodified drag coefficient, C_d, and stem Reynolds number, Re_{st}. The slope was not varied and thus remained constant, and conditions were always emergent so $\gamma = 0$.

The derivation of Equation 3-18 and Equation 3-20 assumes that resistance from the bed is negligible, which may not always be the case in sparsely populated canopies. Additionally the derivation of drag in submerged vegetation assumes that drag can be calculated using cross sectionally averaged velocity, if the equation is adjusted by adding the submergence ratio parameter. However, no justification has been provided for this assumption. In submerged flow,

the presence of different flow layers, with a varying profile of velocity over the depth, means that cross sectionally averaged velocity may not provide an accurate estimate of the velocity, and hence drag, acting within the canopy layer (Stone and Shen, 2002). Such assumptions have meant that other researchers have derived equations for drag coefficient which suit their own experimental circumstances. For example, Nepf (1999) derives the drag coefficient using a force balance approach which includes the effects of bed resistance. To avoid using the cross sectionally averaged velocity Stone and Shen (2002) evaluate the drag coefficient in submerged flow using the maximum canopy layer velocity. This was determined by direct measurement of the profiles of primary velocity. Tsihrintzis (2001) summarises various studies of vegetal drag coefficients in emergent vegetation. Previous studies were reanalysed to determine the best fit empirical coefficients for use in Equation 3-21. The resulting coefficients are presented in Table 9.

Table 9 – C_d'-Re relationship through emergent vegetation (adapted from Tsihrintzis, 2001)

Study	Conditions	k	α	β	Vegetation
Kadlec (1990)	S_o = 0.00001 S_o = 0.0001 S_o = 0.001 S_o = 0.01	1.26 1.2 1.15 1.16	25,277,796	0.4	Emergent Marsh Vegetation (sedges)
Chen (1976)	S_o = 0.001 S_o = 0.005 S_o = 0.035 S_o = 0.087 S_o = 0.164 S_o = 0.316 S_o = 0.555	1.33	60,523,602	0.77	Grass
Wu et al. (1999)	S_o = 0.00383 S_o = 0.00533 S_o = 0.01025 S_o = 0.0273 S_o = 0.041	1.0	3,440,000	0.5	Horsehair mattress
Fathi-Maghadam and Kouwen (1997)	S_d=0.06 (Pine) S_d=0.12 (Pine) S_d=0.18 (Pine) S_d=0.24 (Pine) S_d=0.30 (Pine) S_d=0.06 (Cedar) S_d=0.12 (Cedar) S_d=0.18 (Cedar) S_d=0.24 (Cedar) S_d=0.30 (Cedar)	0.26 0.58 0.5 0.48 0.52 0.2 0.61 0.7 0.69 0.77	n/a	n/a	Air flow though tree saplings
Chiew and Tan (1992)	High Density Low Density	1.04 0.98	n/a	n/a	Grass
Hall and Freeman (1994)	High Density Low Density	1.03 1.16	n/a	n/a	Bulrushes
Turner and Chanmeesri (1984)	S_o = 0.0017 S_o = 0.0021 S_o = 0.0034 S_o = 0.0050 S_o = 0.0067 S_o = 0.0084 S_o = 0.01	0.33 0.33 0.36 0.39 0.44 0.46 0.46	78,611	0.86	Emergent Wheat

Observations by Wu et al. (1999) and Tsihrintzis (2001) suggests that the coefficient k is dependent on vegetation flexibility and planting configuration, but is independent on vegetation density. It is suggested by Tsihrintzis (2001) that the coefficient α is directly affected by vegetation density.

3.1.3.4 *Drag Model Comparison*

Few studies have compared existing drag models and/or compared them to experimental data. Hoffman (2004) tested his own model and that proposed by Petryk and Bosmajian (1975) both with the standard drag coefficient (of 1) and with a suitable drag coefficient suggested by the study of Wu et al. (1999) against experimentally gathered data by Elliot (2000). The data was gathered in a laboratory study using 'imitation vines'. None of the models correctly predicted the experimental Manning's n values. The Petryk and Bosmajian (1975) model under-predicted the n values by approximately 40%, Hoffman (2004) under-predicted n by approximately 22%, while the empirical drag coefficient values provided by Wu et al. (1999) over-predicted n by approximately 300%.

James et al. (2004) tested their theoretical model in a laboratory flume with emergent rigid vegetation. The authors report an average error of 11% in the prediction of discharge. The theoretical equation almost always over-predicted discharge, it was suggested that this is because stem drag is underestimated using the standard C_d which was used in their calculations (i.e. 1.5 - from Albertson et al., 1960).

3.1.3.5 *Relative Roughness Approach*

By adjusting the origin intercept and values of the roughness parameter Kouwen et al. (1969) empirically fitted the logarithmic law (Equation 2-35) so that it described the velocity profile above submerged vegetation. Based on this, as well as further research by Gourlay (1970), Kouwen and Unny (1973) and Kouwen and Li (1980) a quasi theoretical approach was developed to determine the average flow velocity through submerged vegetation.

$$\frac{U}{u^*} = C_1 + C_2 Ln\left(\frac{h}{h_c}\right) \qquad \text{Equation 3-22}$$

Where C_1 = Empirical Coefficient based on vegetation density (-)

C_2 = Empirical Coefficient based on vegetation stiffness (-)

The coefficients (C_1 and C_2) were given in tabular format based on experiments conducted with various types and densities of vegetation. A model such as Equation 3-22 is easier to use than the drag approach for submerged vegetation cases. However, it still requires knowledge of the deflected canopy height. Such methods have been criticized because they are limited in their application to the simplest types of plant (Green, 2005) and are unverified in natural conditions. However, this relative roughness approach is sometimes used to model flow through flexible vegetation with a high degree of submergence (Sr>>1).

Kouwen and Unny (1973) conducted laboratory experiments to attempt to link the roughness parameter to the stiffness and density of the plants. Equation 3-21 was adapted to include a density and flexibility term. The resulting relationship relates boundary shear to both the vegetation density, and the degree of vegetation bending which occurs.

$$\frac{h_c}{h_c - z'} = \left(\frac{3.57}{h_c - z'}\right)\left(\frac{NEI}{\rho u^{*2}}\right)^{1/4} - 0.286 \qquad \text{Equation 3-23}$$

Where	E	=	Modulus of elasticity	(N/m^2)
	I	=	Second Moment of Area	(m^4)
	z'	=	Canopy deflection under flow	(m)

The coefficients were determined empirically from experiments using flexible plastic strips within a laboratory flume. The equivalent roughness height (h_c/h_c-z) can be related to commonly used roughness coefficients (Manning's n, Darcy-Weisback friction factor f) by means of a table of empirical values. This method uses the parameter NEI (the product of the stem density N, stem modulus of elasticity E, and the stems second moment of area, I). Although this parameter is simple to derive with plastic artificial vegetation in the laboratory, with natural vegetation the parameter NEI is more difficult to define and quantify. Although the method has been developed further by Kouwen (1988, 1990), including more detailed experimental measurements, the problems of accurately estimating the NEI value persist (Wilson et al., 2005).

Other models which directly involve a vegetation stiffness parameter tend to be too complex to use in practice. For example, Kouwen and Fathi-Moghadam (2000) proposed that Manning's n in emergent vegetation could be evaluated by

$$n = 0.228\left(\frac{U}{\sqrt{\frac{\omega}{\rho}}}\right)^{-0.23}(Sr)^{0.5} \qquad \text{Equation 3-24}$$

Where ω = Vegetation Index (N/m^2)

The vegetation index is dependent on the shape flexibility and biomass of the vegetation. A formula is provided by Kouwen and Fathi-Moghadam (2000) to determine the vegetation index based on the natural frequency of the vegetation. Such a method has limited practical applicability (Jarvala 2004).

3.2 Velocity Structure and Turbulence in Vegetated Channels

There has been a great deal of research on turbulence in vegetated canopies, starting with the studies of air flows through crops by researchers such as Plate and Quraishi (1965). As the study of turbulence is not the primary goal of this study, a complete review of the development of this research is not presented here. This section focuses on the studies and conclusions that are relevant to the present study. For further details the reader is referred to a review of turbulence in vegetated channels presented by Finnigan (2000).

3.2.1 Emergent Conditions

3.2.1.1 Vertical Profiles of Velocity in Emergent Canopies

Resistance in flows featuring emergent canopies is provided over the entire flow depth by the vegetation elements, not just from the bed as in boundary layer flows. Within channels featuring emergent cylinders which have uniform mass distribution over the depth, it has been found that velocity is roughly uniform within the canopy, rather than being depth dependent (Linder, 1982, Tsujimoto and Kitamura, 1990). The influence of the bed roughness is limited to a region very close to the bed (within one stem diameter - Nepf et al., 1997). By balancing the momentum equation and assuming the contribution of bed shear to total resistance is negligible, Lightbody and Nepf (2006) derived an expression to predict the vertical velocity profile inside a vegetated canopy. Assuming the drag coefficient is constant over the depth, this leads to the following relationship.

$$\frac{u(z)}{U} = \sqrt{\frac{A_i}{A_i(z)}} \qquad \text{Equation 3-25}$$

Hence, the velocity at any point above the bed is related to the mass distribution of the vegetation (Figure 3-3). Hence a canopy with a uniform distribution of mass (such as a reed or artificial rod) will have a uniform velocity distribution over the depth.

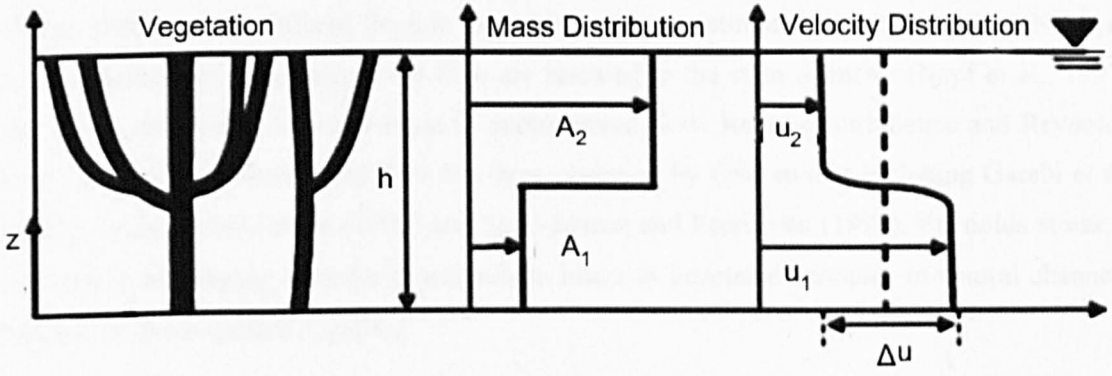

Figure 3-3 Relationship between mass and velocity distribution through emergent vegetation (adapted from Lightbody and Nepf, 2006)

3.2.1.2 Turbulence and Reynolds Stress in Emergent Canopies

Apart from within a region very close to the bed, the majority of turbulence in vegetated flows is generated by water flowing past the vegetated elements rather than from the bed. Nepf (1999) investigated the relationship between stem density and turbulence in an array of emergent dowel cylinders. At very low stem densities ($NS_d^2 < 0.001$) overall turbulence intensities were increased by the presence of vegetation, however as stem density was increased further, the reduction in velocity reduced the magnitude of the turbulent intensities relative to non-vegetated flow.

Momentum is absorbed by the vegetation elements through bending (Velasco, 2000). The momentum equation for vegetated flow (introduced in section 3.1.3.2) can be expressed as

$$\rho g A L S_o = 0.5 C_d \rho \sum A_i U^2 + \tau_0 P L \qquad \text{Equation 3-26}$$

Assuming that viscous stresses are negligible, shear stress can be expressed as Reynolds stress, simplifying to (Ghisalberti and Nepf, 2004)

$$gS_o = 0.5C_d NS_d U^2 + \frac{d\overline{u'w'}}{dz} \qquad \text{Equation 3-27}$$

Momentum is balanced by a combination of vegetative drag and Reynolds stress. Therefore in vegetated channels some momentum is absorbed by the vegetation and the levels of measured Reynolds stress within the canopy are lower than in comparative non-vegetated channels. Negligible levels of Reynolds stress have been observed in emergent canopies by Nepf and Vivoni (2000) using artificial flexible vegetation with an estimated density function (NS_d^2) of 3.3. Turbulent eddies present in the flow are rescaled to the stem diameter (Nepf et al., 1997) and hence are smaller in comparison to unobstructed flow. Reduced turbulence and Reynolds stress relative to non-vegetated flow has been observed by field studies including Gambi et al. (1990), Leonard and Luther (1995) and Sand-Jensen and Pendersen (1999). Reynolds stress is reported to be roughly an order of magnitude lower in vegetated canopies in natural channels relative to non-vegetated canopies.

Turbulence in vegetated channels has been observed to be non isotropic (Nepf 1997, Velasco et al. 2000); turbulence in the horizontal plane being roughly four times greater than in the vertical. This is due to the anisotropic nature of turbulent wakes around the vegetation elements promoting turbulence in the transverse but not vertical plane.

3.2.2 *Submerged Canopies*

Submerged canopy flow can be split into two distinct zones, a slow moving zone through the vegetation and a faster free-flow zone over the top (Righetti and Armanini, 2002). Between these zones a shear layer is established. In the shear layer a number of coherent vortices exist which transfer momentum over the interface between the vegetated and non-vegetated regions. Below the vortices, flow in the canopy or wake zone is governed (as in an emergent canopy) by the balance between water weight and stem drag, in this region (similarly to emergent canopies) turbulence and momentum transport are much reduced relative to non-vegetated flows. Flow above the canopy in the free-flow zone behaves as a turbulent boundary layer. Righetti and Armanini (2002) proposed that the distribution of shear stress above the canopy would follow a linear trend between the canopy top and the free surface. And as found by Kouwen et al. (1969) the velocity profile in this zone can be described by a logarithmic law. However, the velocity profile over the entire depth cannot be described by a single curve (Stephan and Gutknecht, 2002). The characteristics of the shear layer determine the mixing between the two zones and the velocity profile at and above the interface. Raupach et al. (1996) was the first to make the analogy between flow in and above submerged canopies to a turbulent mixing layer.

3.2.2.1 The Shear/Mixing Layer Analogy

In submerged canopies, Raupach et al. (1996) found that flow at the top of the vegetation closely resembles a turbulent mixing layer. A plane mixing layer is a turbulent shear layer formed in the region between two co-flowing streams of different velocities. Mixing layers are characterised by a strong inflection in the mean velocity profile and a maximum Reynolds stress (and hence momentum transfer) at the interface between the two zones, (Figure 3-4). In vegetated canopies this interface (i.e. the inflection point and the peak in Reynolds stress) is observed to occur at the top of the canopy (h_c). Reynolds stress decays towards the free surface and into the canopy. Results from tests in submerged artificial canopies by Gambi et al. (1990), Nepf and Vivoni (2000), Velasco et al. (2000), Poggi et al. (2004), Carollo et al. (2002) all support this analogy.

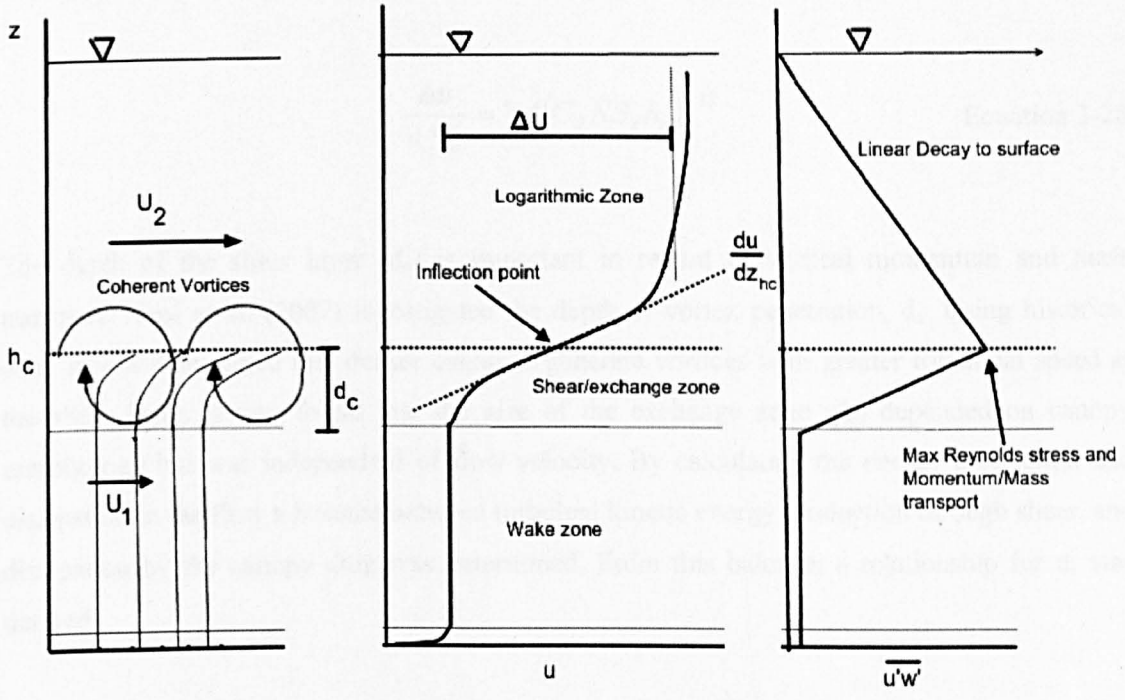

Figure 3-4 Conceptual representation of the mixing layer analogy in submerged vegetated flows

The main parameters of the mixing layer can be defined as

- Difference in velocity between the fast and the slow zone (Δu)
- Size of the mixing/shear layer (how far the eddies penetrate into the canopy) (d_c)
- The magnitude of the inflection $\left(\frac{du}{dz}\right)$ in the velocity profile at the interface (between the canopy and free flow zones)

- Magnitude of the Reynolds stress ($\overline{\rho u' w'_{hc}}$) which occurs at the interface – this can also be expressed in terms of max shear velocity, $u^*_{hc} = \sqrt{\overline{u' w'_{hc}}}$

The parameter Δu is significant since it determines the strength of the inflection in the velocity profile. In turn the magnitude of the maximum Reynolds stress is dependent on the strength of the inflection. Δu is therefore highly significant, to estimate Δu the flow velocity through and over the canopy must be determined. Poggi et al. (2004) found that an increase in stem density forced the flow in the canopy to slow down hence forcing more flow over the top of the canopy, increasing Δu and hence the strength of the inflection and Reynolds stress at the interface. Using data from previous studies using rigid vegetation such as Ghisalberti and Nepf (2005), Nepf et al. (2007) related the velocity difference/shear velocity ratio to the canopy density and drag finding

$$\frac{\Delta u}{u^*_{hc}} = 7.4\left(C_d N S_d h_c\right)^{0.13} \qquad \text{Equation 3-28}$$

The depth of the shear layer (d_c) is important in regard to vertical momentum and mass transport. Nepf et al. (2007) investigated the depth of vortex penetration, d_c. Using historical data, it was determined that denser canopies generate vortices with greater rotational speed at the shear layer. It was found that the size of the exchange zone (d_c) depended on canopy morphology but was independent of flow velocity. By calculating the energy production and dissipation in the flow a balance between turbulent kinetic energy production through shear, and dissipation by the canopy drag was determined. From this balance, a relationship for d_c was derived

$$\frac{d_c}{h_c} \propto \left(C_d N S_d h_c\right)^{-1} \qquad \text{Equation 3-29}$$

Based on a range of experimental data from historical studies, it was determined that in cases where $C_d N S_d h_c < 0.3$, the vortices generated were large enough to penetrate to the bed. In this case the wake zone disappears entirely.

3.2.2.2 *Velocity Profiles above Submerged Canopies*

As stated in section 3.1.3.5, the work of Kouwen et al. (1969) showed that the velocity profile above vegetated channels can be represented by the logarithmic law, provided a suitable value for shear stress and deflection can be found. Various forms of the logarithmic law have been proposed to describe the velocity profile over the canopy, Stephan and Gutknecht (2002) provided a review of the equations (see Table 10).

Table 10 – Methods to describe the velocity profile above vegetation (adapted from Stephan and Gutknecht, 2002)

Author	Vegetation Studied	Velocity Distribution
Plate and Quraishi (1965)	Air flow through flexible plastic strips	$\frac{u}{u^*_{hc}} = \frac{1}{\kappa}\ln\left(\frac{z-h_c}{k_p}\right)$
Kouwen et al. (1969)	Elastic PVC strips	$\frac{u}{u^*_{hc}} = \frac{1}{\kappa}\ln\left(\frac{z}{k_p}\right)+C$
Haber (1982)	Elastic PVC strips	$\frac{u}{u^*_{hc}} = \frac{1}{\kappa}\ln\left(\frac{z}{k_p}\right)+\frac{u_{hc}}{u^*}$
Murota et al. (1984)	Elastic PVC rods	$\frac{u}{u^*_{hc}} = \frac{1}{\kappa_0}\ln(z-(h_c-z'))+C$
Christensen (1985)	Aquatic Vegetation	$\frac{u}{u^*_{hc}} = \frac{1}{\kappa}\ln\left(\frac{z-(h_c-k_s/29.5)}{k_s}\right)+8.5$
Temple (1986)	Bermuda Grass	$\frac{u}{u^*_{hc}} = \frac{1}{\kappa}\ln(z-\alpha h_c)+C$
Watanabe and Kondo (1990)	Cornfield	$\frac{u}{u^*_{hc}} = \frac{1}{\kappa}\ln\left(\frac{z-(h_c-z')}{k_p}\right)$
El-Hakim and Salama (1992)	Branched Strips	$\frac{u}{u^*_{hc}} = A+\frac{1}{B}\ln\left(\frac{z}{k_p}\right)$
Klopstra et al. (1997)	Stiff rods, Reeds	$\frac{u}{u^*_{hc}} = \frac{1}{\kappa}\ln\left(\frac{z-(h_c-z')}{k_p}\right)$
Stephan and Gutknecht (2002)	Fixed aquatic plants in laboratory flume, *Ranunculus, Groenlandia, Berula erecta*	$\frac{u}{u^*_{hc}} = \frac{1}{\kappa}\ln\left(\frac{z-(h_c-z')}{(h_c-z')}\right)+8.5$

Where k_p = Roughness parameter of plants (m)

To use any profiles listed in Table 10, a value of shear velocity (u^*_{hc}) at the interface between the canopy and free flow zone must be determined. This can either be taken directly by measuring Reynolds stress at the interface, or determined by calculation. Shear stress decays linearly from the interface to the free surface (Righetti and Armanini 2002), and several researchers (Jarvela, 2005; Murphy et al., 2007) have used a simple equation to estimate shear velocity at the canopy top.

$$u^*_{hc} = \sqrt{g(h-h_c)S_0} \qquad \text{Equation 3-30}$$

Righetti and Armanini (2002) conducted laboratory experiments with sparsely populated simulated bushes, by measuring Reynolds stress at the canopy top they found the theoretical Equation 3-30) and measured values of canopy top shear stress corresponded to within 8%.

3.3 Effect of Vegetation on Mixing

Comparatively few studies have investigated the effect of the presence of vegetation on dispersion mechanisms and/or dispersion coefficients. Of these, most studies have used artificial or simulated vegetation in place of real vegetation. This section will review the research that has been identified.

3.3.1 Diffusivity

3.3.1.1 Emergent Conditions

As stated in section 2.4.4, turbulent eddies which transport momentum also transport mass, and hence diffusivity will strongly depend on turbulence levels (as discussed in section 2.4). In vegetated canopies, diffusivity will therefore be reduced in comparison to non-vegetated canopies due to lower turbulence levels and reduced eddy scale (Nepf, 1999).

Nepf et al. (1997) developed a random walk model to estimate diffusivity due to mechanical dispersion in a channel populated with emergent cylinders. The model looks at the probability that individual particles will pass through the wake zones created by the cylinder array, and the amount of mass transport that would occur due to this effect. As with turbulence, diffusivity was found to be anisotropic; measured in an array of emergent dowels, vertical diffusivity was found to be approximately four times less than horizontal diffusivity.

Nepf (1999) attempts to link turbulence and hence diffusivity to stem drag through a kinetic energy budget. By balancing force on a cylinder with turbulent kinetic energy dissipation an equation for diffusivity in a canopy was derived as

$$\frac{e_i}{US_d} = \alpha\left(C_d S_d{}^2 N\right)^{1/3} \qquad \text{Equation 3-31}$$

Where α = Coefficient (-)

The accompanying laboratory study involving flow through emergent dowel rods confirms that turbulence intensity and diffusivity is dependent on the product of stem diameter and density. The diffusivity within canopies is non-isotropic, so the coefficient α will depend on whether transverse or vertical diffusion is considered. For vertical diffusivity the coefficient α was found to be between 0.1 and 0.2 in laboratory conditions, for horizontal diffusivity it was measured as 0.9. In the case of very thick dense canopies ($NS_d^2 > 0.1$), an extra term should be added to Equation 3-31 to account for the effects of mechanical diffusion. In all cases, diffusivity within the system is less than in the non-vegetated case due to the smaller eddy scale.

Lightbody and Nepf (2006) conducted a series of mixing experiments in a salt marsh, finding an empirical value for vertical diffusivity

$$e_z = 0.17 US_d \qquad \text{Equation 3-32}$$

Which is effectively considerably higher than the values predicted by Equation 3-31 as derived in Nepf's previous (1999) laboratory study. This is explained by the non-vertical orientation of elements in the field study promoting more turbulence in the vertical plane.

3.3.1.2 Submerged conditions

In submerged canopies the shear layer will create a region of turbulence and high vertical exchange at the top of the canopy (see section 3.2.2.1). In the case of sparsely vegetated, short canopies these vortices will penetrate to the bed and thus vertical mixing will take place rapidly over the depth. In dense tall canopies the vortices will not penetrate to the bed, and a wake zone will exist in the bottom section of the flow. The low turbulence and diffusivity levels in this canopy zone mean the overall timescale for vertical mixing will become much longer compared with canopies where this 'shear layer' penetrates to the bed (Nepf et al., 2007). Actual levels of diffusivity in the shear/exchange zone are dependent on the levels of turbulence, this in turn is

dependent on the strength of the velocity inflection (see section 3.2.2.1). Above the canopy diffusivity should behave as in boundary layer flow (Murphy et al., 2007).

3.3.2 Transverse Mixing

3.3.2.1 Scaling Transverse mixing in Vegetated Flow

Fischer and Hanamura (1975) investigated the effects of the presence of an array of vertical roughness strips on transverse mixing in a laboratory channel. It was proposed that scaling the transverse mixing by hu* is only appropriate in channels were the primary source of hydraulic resistance is the channel bed (i.e. scaling by hu* is not appropriate in vegetated canopies). By assuming a transverse velocity profile based on the arrangement of the strips, an expression for transverse diffusivity, e_y can be determined. Fischer and Hanamura (1975) assume that transverse diffusivity can be evaluated in a similar manner to vertical diffusivity (see Equation 2-99), and because of the roughness strips, shear stress in the vertical plane will vary as

$$\tau_t = \rho\left(\frac{s_s}{2} - y\right)S_0 = \rho e_y \frac{du}{dy} \qquad \text{Equation 3-33}$$

Where s_s = Distance between roughness strips (m)

Then by integration of Equation 3-33, the transverse velocity profile can be determined as

$$u = \left(\frac{gS_0}{2e_y}\right)(s_s - y)y + u_s \qquad \text{Equation 3-34}$$

Where u_s = Velocity though the axis of the strips (m/s)

And the mean velocity, U, is given as

$$U = \left(\frac{gS_0 b^2}{12e_y}\right) + u_s \qquad \text{Equation 3-35}$$

Combining the force balance equation in vegetated flow (Equation 3-10) and the drag force on each cylinder (Equation 3-1), Equation 3-35 can be rearranged to give

$$e_y = \left(\frac{C_d b S_d U}{24L}\right)\left(\frac{U}{U-u_s}\right) \qquad \text{Equation 3-36}$$

Although u_s cannot be predicted a minimum value can be found by setting $u_s = 0$. If b = 1 then

$$e_y = 0.08 S_d U \qquad \text{Equation 3-37}$$

Experiments by Fischer and Hanamura (1975) in a straight channel featuring vertical roughness strips found that

$$0.07 \leq \frac{K_y}{S_d U} \leq 0.14 \qquad \text{Equation 3-38}$$

Where as if transverse mixing is scaled conventionally then

$$0.09 \leq \frac{K_y}{hu*} \leq 0.89 \qquad \text{Equation 3-39}$$

Hence, Fischer and Hanamura (1975) found scaling by strip width and average velocity gives much more consistent answers than scaling by the more conventional hu*.

3.3.2.2 *Effects of Vegetation on Transverse Mixing Rates*

There is a lack of studies which have measured rates of transverse mixing in vegetated channels. Transverse mixing is dominated by turbulence and secondary currents. In vegetated channels it may be expected that secondary currents will be damped somewhat by the presence of vegetation and increased flow resistance. Transverse mixing should therefore be mostly dependent on diffusivity and hence turbulence. Turbulence and Reynolds stress have been observed to be reduced in vegetated canopies (see 3.2.1.2), the main source of turbulence being the stem wakes (Nepf, 1999). Turbulence in vegetated channels has been observed to be non-isotropic, being roughly four times greater in the horizontal plane than in the vertical (Nepf, 1997, Velasco et al., 2000).

Tanino and Nepf (2007), investigated transverse mixing through a dense array of rigid cylinders, for a porosity between 0.65 and 0.95 it was found that transverse mixing varied between

$$0.13 \leq \frac{K_y}{US_d} \leq 0.24 \qquad \text{Equation 3-40}$$

Nepf's (1999) equation (Equation 3-31) predicts an increase in e_y/hu^* with increasing stem density. When compared with the results of the Tanino and Nepf (2007), Equation 3-31 generally over-predicts the value of transverse mixing.

No studies examining transverse mixing in submerged vegetation have been identified.

3.3.3 Longitudinal Mixing

No studies have been identified which determine the applicability of the commonly used mixing models (ADE and ADZ) in vegetated flows, or the impact of vegetated canopies on the Lagrangian timescale and hence size of the advective zone.

3.3.3.1 Effect of Emergent Canopies

Nepf et al. (1997) looks specifically at the effects of vegetation on longitudinal dispersion. The paper introduces the concept of mechanical dispersion, where particles take differing routes around vegetation or other flow obstacles and hence spread. Dead zones behind vegetation elements are also considered, which may become especially prevalent in areas with high levels of vegetation. They suggested that the size of the wakes, and thus the dead zones behind patches of vegetation, will depend on the stem Reynolds number of the flow. Experiments to explain this were conducted using artificial vegetation (rigid dowel cylinders) in a laboratory flume. Three different density levels were considered. The cylinders could be removed to provide a control case and to quantify mixing levels with no vegetation. A decrease in dispersion coefficient was observed with increasing cylinder density and flow velocity (Table 11). It was noted that the presence of simulated vegetation reduced the effect of shear dispersion in the flow by decreasing vertical and transverse velocity shear. Although partly compensated for by increased mechanical dispersion and the increased effect of dead zones, the overall effect was to reduce the dispersion coefficient relative to an un-vegetated flow. No relationship between the strength of the trapping mechanisms (measured from the shapes of the concentration profiles) and the stem Reynolds numbers was found.

Table 11 – Observations of Dispersion Coefficient (m^2/s) though emergent rods (Nepf et al., 1997)

Flow Velocity (m/s)	Stem Population (% of flow area)			
	0	1	1.5	5.5
0.029	0.075±0.008	0.038±0.008	0.022±0.010	0.021±0.008
0.055	0.073±0.010	0.025±0.004	0.024±0.007	0.012±0.004
0.074	0.084±0.010	0.031±0.006	0.029±0.007	0.012±0.009

Lightbody and Nepf (2006) measured longitudinal mixing rates in an emergent salt marsh. Mixing was described as a combination of mechanical and shear dispersion. In this case some vertical shear was present due to the non-uniform mass distribution of the plants over the flow depth. An equation for mechanical dispersion (D_m) was provided based on a mathematical solution of the probability that individual particles would enter trapping mechanisms behind dead zones provided by White and Nepf (2003)

$$D_m = 0.5 C_d^{3/2} U S_d \text{ for } S_d^2 N < 0.1 \qquad \text{Equation 3-41}$$

Prediction of shear dispersion was based on the mass distribution of the plants over the flow depth (Equation 3-31) providing differential velocity and hence vertical shear dispersion. An equation for the dispersion coefficient in emergent flow was given as

$$\frac{D_x}{U S_d} = \frac{e_z}{U S_d}\left[\frac{d}{dz}\sqrt{\frac{C_d A_i}{C_d(z)A(z)}}\right]^2 x^2 + C_d^{3/2} \qquad \text{Equation 3-42}$$

Vertical diffusivity was estimated using Equation 3-32. Longitudinal mixing in the equilibrium zone was not measured and hence Equation 3-42 is unverified.

3.3.3.2 *Effect of Submerged Canopies*

By considering flow in submerged canopies as two separate flow layers (above and below the canopy), Murphy et al. (2007) outlined a model based on the 2-zone equation provided by Chickwendu (section 2.4.7.1) to predict a longitudinal dispersion coefficient (Figure 3-5).

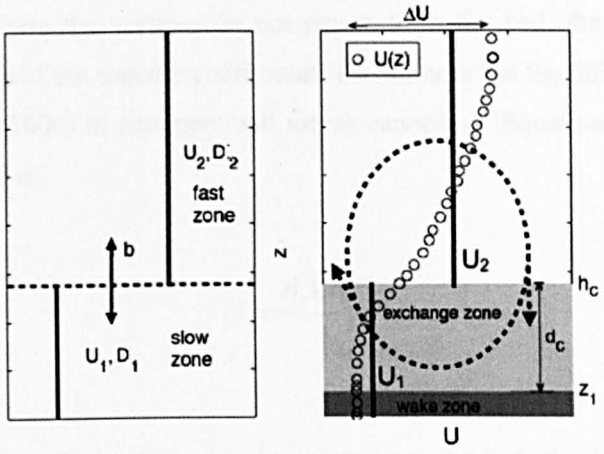

Figure 3-5 2-Zone model applied to submerged vegetated flow (adapted from Murphy, 2007)

Murphy et al. (2007) provides the two-zone form of the Chickwendu model Equation 2-135) as

$$D_x = \frac{(q_1 q_2)^2 (u_1 - u_2)^2}{\psi} + q_1 D_{x1} + q_2 D_{x2} \qquad \text{Equation 3-43}$$

It is suggested that the (u_1-u_2) parameter required for Equation 3-43 can be estimated using the empirical relationship for Δu found by Nepf et al. (2007) (Equation 3-28). Murphy et al. (2007) suggested flow above the canopy could be treated as normal boundary layer flow and hence D_{x2} can be estimated from Elder's (1959) result Equation 2-101). The shear velocity for this boundary layer should be taken from the top of the canopy (i.e. Equation 3-30). D_{x2} can therefore be derived as

$$D_{x2} = 5.93 h u^*_{hc} = 5.93 h \sqrt{\overline{u'w'}_{hc}} = 5.93 h \sqrt{g(h - h_c) S_0} \qquad \text{Equation 3-44}$$

The term involving D_{x1} is expected to be small compared to the other terms and is neglected for simplicity. The transfer coefficient, ψ is dependent on the magnitude of the vortices at the interface. In the case of sparse vegetation, where the vortices penetrate to the bed, the transfer function, ψ is based on the experiments of Ghisalberti and Nepf (2005), who measured an exchange velocity at the interface in submerged experiments using rigid vegetation.

$$\psi = \frac{\Delta u}{40 h_c} \qquad \text{Equation 3-45}$$

In dense canopies, where the vortices do not penetrate to the bed, the wake zone diffusivity controls the magnitude of the transfer coefficient. The authors use the diffusivity value found by Lightbody and Nepf (2006) in emergent salt marsh canopies (Equation 3-32) and the transfer coefficient is provided as

$$\psi = \frac{0.17US_d}{h_c^2} \qquad \text{Equation 3-46}$$

In dense canopies where the vortices do not penetrate to the bed, the rate of vertical transport and hence the transfer coefficient will be lower than if the mixing layer can transport mass over the canopy height. In the case of low vertical transport, the effects of vertical shear dispersion will be greater as a quantity of solute will be trapped in a slow moving layer near the bed, while the faster velocity in the free surface causes the tracer cloud to spread longitudinally. In the case of rapid vertical exchange, solute is transported from the slow to the fast zone rapidly and the effect of the vertical shear is reduced. The authors (Murphy et al., 2007) report good correlation between the model predictions and observed results (Rt^2 = 0.89) when tested in an array of dowel cylinders, however, the model has not yet been verified using natural vegetation.

3.4 Summary of Literature Review

3.4.1 Vegetation and Flow Resistance

There currently exists a variety of approaches to model flow resistance in vegetated channels. They range form the empirical n-UR methods which are likely to be the most easy to use in practice but have scientific shortcomings, to the theoretical drag equations (sometimes used in conjunction with empirical observations of drag coefficient) which seem to work well in laboratory conditions but are largely unverified in natural channels. The practical usability of these drag models has been called into question (Green, 2005), as the drag coefficients of most types of vegetation are unknown and the practicalities of measuring the density and area properties of the vegetation to the degree of accuracy required are problematic. The range of vegetation parameters (such as density, stiffness, and arrangement) which affect the total flow resistance of a channel make their incorporation into a practical, usable model problematical.

The question of how theoretical drag equations, which have been largely derived in laboratory conditions featuring rigid cylinders, can be applied to natural vegetation has been largely left unanswered. It is uncertain whether the additional uncertainties introduced by real vegetation (such as the reduction of drag due to plant flexibility) can be incorporated into the theoretical models. One approach is to attempt to use theoretical drag force models in conjunction with

drag coefficients derived empirically for different types of vegetation. In this case any uncertainty involved in the characterisation of the other parameters used in the model (such as measurement of plant density and frontal area) are included into the calculated drag coefficient for each plant type.

At present these theoretical models work best in the case of emergent vegetation, where complications such as the existence of two flow layers and reduced frontal area due to plant flexibility do not exist. The flow resistance models for submerged vegetation rely on empirical relationships, which have been criticised due to their lack of scientific accuracy (n-UR method) or there practicality (relative roughness method).

In submerged flow conditions, the size of the flow zones in and above the vegetation is dependent on the degree of bending of the plant. Unfortunately little information currently exists on the biomechanical properties of plants which would enable an estimation of the degree of bending. There are however a large number of empirical observations of the velocity profile above vegetated canopies. These profiles are dependent on parameters such as observed roughness height and shear stress at the interface. It is envisioned that a complete velocity profile could be estimated from a combination of a force drag balance inside the canopy, and a logarithmic layer above the canopy. Such a velocity profile could be used to predict flow resistance in submerged canopies.

3.4.2 *Vegetation and Mixing*

There are a number of models available that give a description of mixing in watercourses. These models are based on mathematical principles and apply simplifications to the complex processes that drive mixing. The models require coefficients to define the 'scale' of mixing; these coefficients can be derived either theoretically, from historical data or from empirical data. Although progress has been made, there is still a lack of understanding of how physical conditions such as sinuosity, discharge, and vegetation affect the rate of mixing and thus the suitable choice of mixing coefficient. Compared with the study of flow resistance in vegetated channels, little work has been done on examining the rates of mixing in vegetated channels. However, from a review of the published literature and a consideration of the processes occurring in vegetated channels relative to non-vegetated ones, vegetation may have the following impacts on the mixing and transport processes in natural channels.

3.4.2.1 *Increase in Longitudinal Travel Times*

The added resistance of the vegetation slows down the flow, increasing the flow depth, reducing velocity and increasing longitudinal travel time relative to non-vegetated flows. The magnitude of this effect may increase with increasing plant density.

3.4.2.2 *Effect on Turbulent Diffusion*

Studies by Nepf (1999) and others report non-isotropic turbulence within vegetated canopies with overall levels of turbulence and diffusivity much retarded compared to non-vegetated flow. Levels of diffusivity have been estimated based on theoretical and empirical evidence. Lower levels of diffusivity in canopies would decrease the rates of transverse spreading of tracer due to diffusivity but also increase the effect of velocity shear in spreading tracer. In submerged flow a turbulent shear layer has been observed to exist between the canopy and the 'free flow' layer. This shear layer will have the effect of increasing diffusivity and vertical transport between the in and above canopy zones. Work by Poggi et al. (2004) and Nepf et al. (2007) has linked the size and strength of the turbulent mixing zone to the properties of the vegetation and the depth of flow. However, a study of the shear layer in natural vegetation has not been conducted.

3.4.2.3 *Effect on Shear Dispersion*

In emergent flow the presence of 'elements' retard the usual transverse and vertical variation of longitudinal velocities expected in an open channel flow. The magnitude of differential advection is therefore reduced and hence this also reduces the magnitude of the shear dispersion. This effect would be expected to decrease the magnitude of longitudinal dispersion coefficient relative to a non-vegetated channel. The magnitude of this effect will grow with increasing plant density.

In submerged flow, studies such as Poggi et al. (2004) have shown that in channels featuring submerged vegetation two distinct flow layers of differing velocity exist. The net effect of this is to increase vertical velocity shear relative to emergent conditions. This will increase mixing by trapping dye in the slower moving zone below the main flow and releasing it slowly back into the main flow (effectively acting as a large dead zone). It is likely that in submerged vegetation the effects of vertical shear would become more important than transverse shear in causing longitudinal mixing. The magnitude of the vertical shear will depend on the relative height of the vegetation to the flow depth, the differential velocity caused by resistance of the canopy and the rate of mixing between the two zones (which in turn is affected by the properties of the turbulent shear layer).

3.4.2.4 *Effect on ADE and ADZ models*

The suitability of the ADE and ADZ models to predict mixing in vegetated channels has not been extensively investigated. In canopies, trapping behind vegetation elements may generate extra skew in the concentration profiles, though the efficiency of the trapping mechanisms are at present uncertain. The effect of this may be to increase the time until the Fickian based ADE can be used. However, in vegetated flow overall velocities are greatly retarded and hence Fickian diffusion processes actually occur within a relatively short distance of the injection point. Hence, concentration profiles may approximate to Gaussian profiles relatively soon after the injection point.

In submerged canopies, the wake zone close to the bed may act as a large dead zone, and hence the ADZ may be a more suitable model. However, the effectiveness of this dead zone will depend on numerous factors such as the rate of vertical transfer over the flow depth, the ratio of the flow zones and the velocity difference between the two flow layers. In the case of high overall flow retardance, the concentration profiles may revert to a Gaussian nature a relatively short distance downstream of the injection.

3.4.2.5 *Current State of Research*

Despite a recent focus on mixing in vegetated flow (Ghisalberti and Nepf, 2005, Lightbody and Nepf 2006, Nepf et al., 2007, Murphy et al., 2007), a reliable verified method for predicting mixing in vegetated channels does not at present exist. In emergent flow it is understood that reduced transverse and vertical velocity shear reduces mixing relative to non-vegetated regions, however, existing studies have largely been undertaken in laboratory channels featuring rigid artificial cylinders. Much progress has been made in determining diffusivity levels in canopies, however, existing attempts to measure longitudinal mixing in real canopies have been dependent on measuring the mass distribution of plants over the flow depth, which is difficult in practice and met has with mixed results. At present relationships between vegetation parameters (i.e. stem density and flexibility) and longitudinal mixing are undefined and unverified.

In submerged vegetation, longitudinal mixing appears to be dependent on the properties of the flow, canopy and of the shear layer at the interface between the flow zones. A model has been produced by Murphy et al. (2007) based on the 2-zone model of Chikwendu (1986). Although verified in artificial vegetation the model has not been tested using real flexible vegetation which may have an impact on the properties of the mixing layer.

Chapter 4 - Research Proposal

The aim of this research is to gain understanding of how the presence of vegetation in an open channel impacts both the flow resistance and the nature and scale of longitudinal mixing. To investigate these phenomena, a series of laboratory experiments has been undertaken. To investigate the effects of vegetation on open channel flow and dispersion in the most accurate way possible, real vegetation has been grown and used in the experiments. Different species of vegetation have been used, and this enables a comparison of different vegetation types on conveyance and mixing.

Using this approach detailed experiments have been undertaken in a more realistic manner than have previously been undertaken in a laboratory study. Stage discharge relationships have been investigated as the vegetation grows in height and increases in density and stiffness. A variety of emergent and submerged conditions have been investigated. Existing flow resistance models are assessed for their accuracy and usability, and the influence of the vegetation on the velocity profiles and turbulence levels is investigated.

Mixing through real vegetation has been measured in a controlled environment and the effects of different vegetation parameters on transverse and longitudinal mixing are investigated. Existing methods and models are tested against measured values to determine if previous research conducted though artificial vegetation is accurate when used with real vegetation.

Previous research indicates the presence of a high degree of shear between the flow within and above the canopy (Poggi, 2004). Therefore vertical rather than transverse shear dispersion is likely to dominate mixing in submerged vegetation. Methods exist (Chickwendu, 1986) which estimate the levels of dispersion in shear dominated flows, however their use requires detailed knowledge of velocity profiles as well as the rate of vertical/transverse transport. If accurate velocity profiles can be predicted based on the vegetation parameters, this should enable the estimation of longitudinal mixing coefficients in cases where shear dispersion is the dominant form of mixing. The rate of vertical mass transport is also be an important parameter as it influences the effectiveness of vertical shear dispersion. Vertical transport will have to be determined based on the properties of the mixing/shear layer which exists at the canopy top.

4.1.1 Thesis Objectives

This thesis seeks to answer the following questions.

- How accurate are the existing flow resistance models and are there any which are practical to use?

- Can current mixing models suitably describe mixing in vegetated channels?
- How does the presence of vegetation affect the rate of mixing and so the selection of suitable mixing model coefficient?
- How do the mixing rates vary with the vegetation parameters?
- Can the effect of vegetation on the profiles of velocity and turbulence be predicted and can this information be used to accurately calculate the longitudinal mixing coefficient?

Chapter 5 - Laboratory Setup & Data Collection

This chapter describes the equipment and methodology used to collect and process the data required to fulfil the aims described in chapter 4.

5.1 Laboratory Description

Testing was undertaken within the University of Sheffield hydraulics laboratory. The experiments described were conducted in the facilities main flume which is constructed of reinforced glass fibre panels. The flume has an experimental length of 14.5 metres, a width of 1.22m, and depth of 0.5m and is set at a fixed slope of 0.00123. The slope of the channel was confirmed by measuring the depth of a stationary body of water along the length of the channel. Upstream of the experimental length the flume is fitted with a flow baffle. Downstream of the experimental length the flume is fitted with a tailgate so that uniform flow can be achieved. Discharge down the channel can be controlled by use of a valve regulating flow from the main laboratory header tank. Though not recently used, the channel has its own separate smaller sump (capacity of approximately 18.8m^3) situated directly below (Figure 5-1).

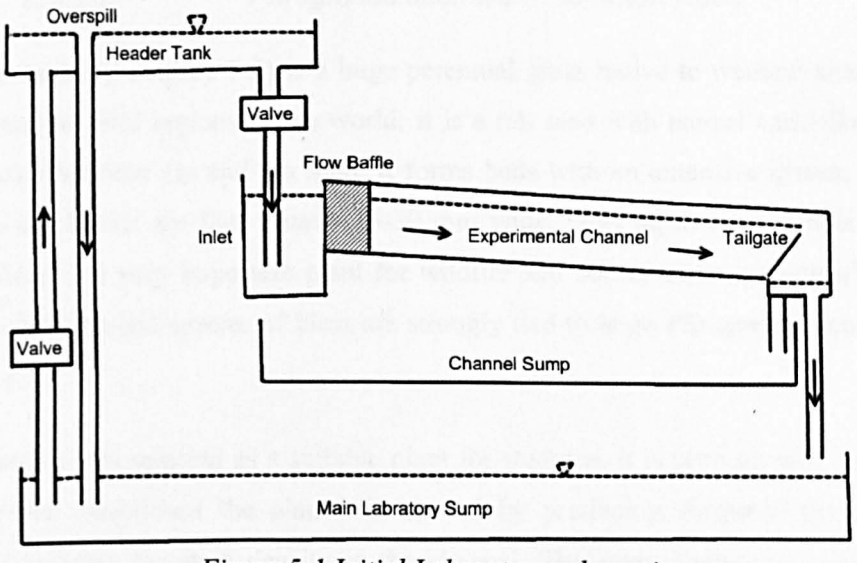

Figure 5-1 Initial Laboratory schematic

5.2 Vegetation Selection and Channel Modification

5.2.1 Selection of Vegetation

Vegetation had to be selected to grow in the channel which would be suitable for the experimental purposes of this project. To measure the impact of differing vegetation types on the flow properties of the channels it was desirable to select and test at least two varieties of

vegetation. Ideally these species would have different biomechanical (i.e. mass, height, flexibility, etc) properties.

5.2.1.1 Requirements of the Vegetation

The main requirements of the vegetation were

1. Suitable simulation of natural river vegetation
2. Rapid growth to enable testing over a wide range of sizes/densities
3. Relatively hardy – able to survive in laboratory conditions
4. Suitable for growth in a medium which can be added to the channel base

After consultation with a number of plant suppliers, two types of semi aquatic vegetation were identified as being suitable, the *Phragmites australis* (or common reed) and the Carex. Their properties are described in the following sections.

5.2.1.2 Phragmites australis – Common Reed

Phragmites australis (Figure 5-2) is a large perennial grass native to wetland sites throughout temperate and tropical regions of the world; it is a tall reed with annual cane-like (round and hollow) stems between 1m and 4m high. It forms beds with an extensive system of perennial rhizomes. Leaf blades are flat, usually 15-30 mm wide, tapering to long slender points. The Common Reed is a very important plant for wildlife and conservation, particularly in Europe and Asia, where several species of birds are strongly tied to large *Phragmites* stands (Clapham et al., 1987).

The *Phragmites* was selected as a suitable plant for study; as it is semi aquatic, hardy and fast growing. Once established the plant will spread by producing rhizomes through the bed, gradually increasing the stem density in the channel. The stems themselves will not greatly increase in stem width. Due to the height of the plants all flow conditions studied will be emergent (with the plants taller than the depth of flow). The stems themselves would be fairly stiff, with a roughly uniform distribution of mass over their height. It was advised by the plant suppliers (Yarningdale Nurseries, Warwick) that the *Phragmites* would require a substrate (such as sand or gravel) of at least 150mm depth for the development of a healthy root system. Throughout this thesis the *Phragmites australis* shall be referred to simply as 'Reeds'.

Figure 5-2 Phragmites in nature (image taken from www.yarnigdale.co.uk)

5.2.1.3 Carex - Sedge

Carex (Figure 5-3) is a genus of plants in the family Cyperaceae, commonly known as sedges. An evergreen perennial rhizomatous herb with solid stems and flat leaves, it can grow to around 0.75m tall with leaves around 7-10mm wide and is common around rivers in the UK and Europe (Clapham et al., 1987).

In contrast to the reeds, the Carex is a dense leafy plant, but shorter and more flexible. This means that the plant could be submerged and highly deflected at high flows. Rather than increasing in stem density with age, the plants themselves grow in size, becoming broader, taller and leafier. The Carex should be capable of surviving in laboratory conditions, though the growth rate was uncertain. Again it was advised that the Carex would require a substrate of at least 150mm depth for the development of a healthy root system.

Figure 5-3 Carex in nature image taken from (image taken from www.yarnigdale.co.uk)

5.2.1.4 Planting Formation

Previous research on the effects of different planting formations on the flow has been conducted by Li and Shen (1973) and is detailed in section 3.1.2.3. To gain the most influence from the vegetation elements it was decided to plant the vegetation in a staggered formation. Based on this and on advice from plant suppliers on the minimum required spacing between plants, it was decided to plant the vegetation in staggered rows of 2 plants and 3 plants per row, with a spacing of 0.2m. This gives an initial planting density of 12.5 plants per metre length of channel. A diagram of the planting arrangement together with further experimental details is presented in Figure 5-16 as part of the vegetation measurement section (section 5.3.5).

5.2.2 Trial Reed Growth

To test that vegetation could be grown successfully in laboratory conditions four sample vegetation buckets were set up. Each contained a rhizome of common reed and was subject to different conditions. One plant was placed in the window and given plant food, another was also in a window but given no food. Two further plants were placed in the shade, one of which was fed and one was not. All reeds were grown in a gravel bed of 150mm depth. After two months the difference in the growth rate was dramatic. The two plants placed in shade had not grown and were in very poor health. The plant in light but with no food was healthy but had experienced very little growth. The plant with both food and light had experienced dramatic growth and could not grow further due to the confines of the bucket (Figure 5-4). The main conclusions of this study were,

1. Growing plants in laboratory conditions is possible.
2. A satisfactory light source must be provided to all plants to ensure healthy growth
3. For rapid growth a source of food is required.

Figure 5-4 Growth of reeds placed in window over 3 months, the plant on the left was supplied with plant food

The most suitable source of nutrients found for the vegetation was Vita Link Hydroponic plant food. This food was recommended by plant suppliers, the recommended dose was added to the water source every week throughout the experimental program.

5.2.3 Channel Modifications

Before adding vegetation to the channel several procedures had to be undertaken to ensure the laboratory setup was suitable for both the growth of vegetation and the testing program.

1. A suitable growth medium had to be added to the channel bed.

2. Normal laboratory water is treated for health and safety reasons and contains high levels of free chlorine, which may be toxic to the vegetation. Therefore a separate sump was used to provide clean (tap) water to the reeds. A separate pumping and flow measurement system was installed.

3. Extra lights had to be fitted to the channel to promote vegetation growth.

4. To test both reeds and Carex in the same testing program the channel was split into two separate sections.

5.2.3.1 Growth Medium

A number of plant suppliers suggested gravel as a suitable growth medium. Several types of aquatic plant can grow in gravels including Phragmites and Carex. In addition, it could easily be contained in the channel by fixing barriers at the top and bottom of the channel and it would not be washed away under high flows experienced in the laboratory channel. It is also readily available from several local suppliers. To achieve a gravel depth of 150mm recommended by the plant suppliers it was calculated that 5 tonnes of gravel would be required to fill the laboratory channel over the experimental length, this gravel (D_s = 10 mm) was supplied by C Paget & Co. Ltd, Sheffield. The gravel was held in place by impermeable boundaries 150mm deep at the top and bottom of the experimental length. In addition to holding the gravel in place these boundaries also minimise the flow through the gravel bed itself ensuring most of the flow passes over the channel bed. The gravel bed was laid with a levelling device to ensure that the along the channel the gravel was as close to an even 150mm depth as possible. This depth of gravel would leave an effective operational channel depth of up to 350mm.

5.2.3.2 Water Supply and Pumping System

To make the water supply suitable for growing plants the channel was reconnected to the smaller channel sump situated directly below the channel. This sump was then filled with tap water which is suitable for vegetation. Advice was sought from the departmental safety officer regarding possible implications of using untreated water in the laboratory. It was advised that using tap water should pose no significant risk to health; but it was recommended that the water be changed regularly. A Flygt in-line pump (model number 2102.041) was placed in the channel sump to pump water into the channel inlet by a pipe (110mm diameter). To accurately measure the flow rate, a Venturi meter with a throat diameter of 86mm (connected to a manometer) was installed in the pipe between the pump and the inlet. According to British Standards, EN ISO 5167-4:2003, a properly calibrated Venturi meter should report the true discharge to within ± 1%.

5.2.3.3 Flow Measurement by Venturi meter

The Venturi meter is a device commonly used to measure discharge in pipelines. Flow is forced through a constriction in the pipeline. By the principle of conservation of mass, velocity though the constriction is increased, and therefore to conserve total energy the pressure is decreased. Therefore the drop in pressure across the constriction is directly related to the discharge in the pipe (Figure 5-5).

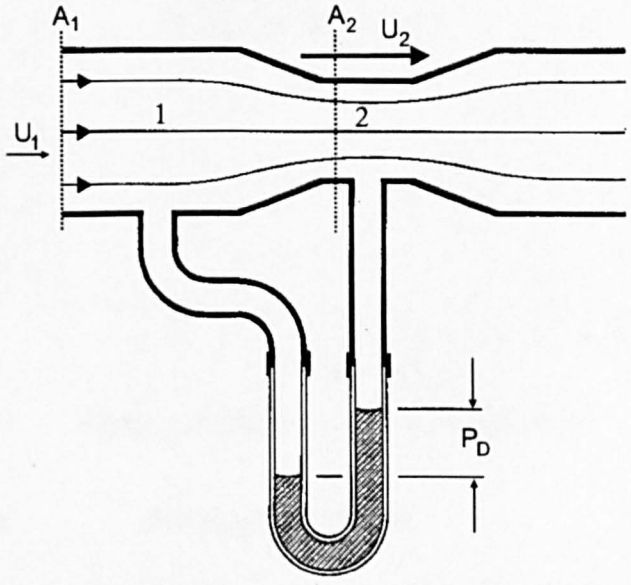

Figure 5-5 Venturi Meter (adapted from Chadwick and Morfett, 1994)

By measuring this pressure drop, discharge can be calculated using Equation 5-1 (Chadwick and Morfett, 1994).

$$Q = \sqrt{\frac{P_D 2gC_q}{\frac{1}{A_2^2} - \frac{1}{A_1^2}}}$$ Equation 5-1

Where P_D = Pressure drop across the Venturi (m)

C_q = Coefficient of Discharge (-)

To determine the coefficient of discharge, C_q a calibration of the Venturi meter was required. Calibration of the Venturi meter was conducted by pumping water from the new channel sump, through the experimental channel and into the laboratory measurement tank, where discharge can be determined by measuring the rate of change of volume with time. Measured discharge can then be related to the observed pressure drop (measured with a mercury manometer) over the Venturi. Figure 5-6 shows resulting calibration curve along with the best fit form of Equation 5-1. The best fit form of Equation 5-1 has a coefficient of discharge of 0.96. This is roughly in line with the expected values for a Venturi flume of this type (0.97-0.99 - from British Standards, EN ISO 5167-4:2003). From this calibration it was established that the pump has a maximum capacity of 29.5l/s.

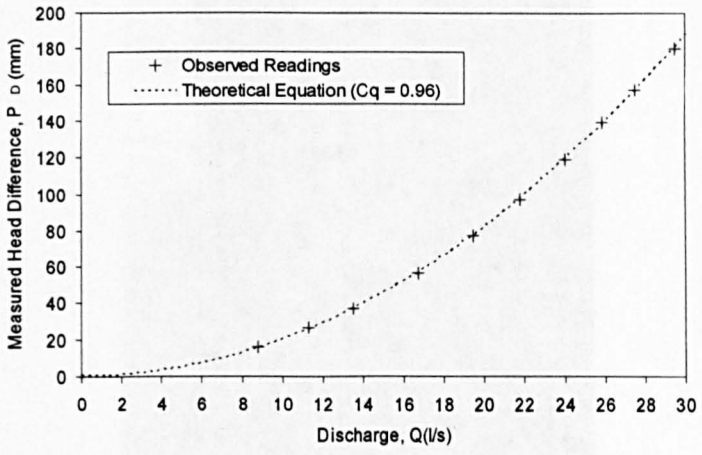

Figure 5-6 Channel pump calibration curve

5.2.3.4 Dividing the Channel

To enable the testing of both types of vegetation simultaneously the channel had to be spilt into two sections. A Perspex divider was made which ran the entire length of the channel. For the vegetation tests this divider was positioned down the channel centreline splitting the channel into two equal widths (of 0.6m). So that the full flow capacity was to be available to each type

of vegetation a simple flow divider was made which blocked one half of the full channel width. The full pump capacity was therefore available for use in each half of the channel.

5.2.3.5 *Channel Lighting*

To provide the plants with sufficient light for growth, three grow lamps were fitted over the channel. The lights chosen were 600 Watt High Pressure Sodium lamps with an output of 90,000 lumens each. The lamps were designed to output a spectrum of light which is suitable for all stages of plant growth. The lights were fitted with reflectors to spread the light over the channel. It was recommended by plant suppliers that the plants should be exposed to the lights for around 10 hours per day, this would simulate natural conditions. Based on visual experimentation with the lamps and the reflectors it was decided to position the lamps 4m, 7.75m and 11.5m down the channel at a height of 2m above the gravel bed. This positioning gave a reasonably even distribution of light, with a slight focus towards the downstream end of the channel. The upstream end of the channel had a greater share of the natural light which fell on the channel, due to the positioning of the laboratory windows. An example of one of the mounted lights is presented in Figure 5-7.

Figure 5-7 Channel Lighting

5.3 Data Collection

To accomplish the aims outlined in chapter 4 the following measurements were made in the channel during the testing program

1. Quantification of vegetation

2. Stage - discharge relationships
3. Vertical and transverse profiles of velocity
4. Vertical and transverse profiles of Reynolds stress
5. Longitudinal mixing
6. Transverse mixing

The methods used to take all of the above measurements are outlined in this section.

5.3.1 Frequency of tests

To establish base case conditions tests 2 to 6 above were first conducted in the absence of vegetation. Once vegetation had been planted time would be allowed for the vegetation to establish itself before further testing. Once the vegetation became established the rate of testing would largely be dictated by the rate of vegetation growth. Each set of tests would be conducted when it was judged that properties of the vegetation had changed significantly (i.e. a noticeable visual increase in vegetation height, size or density). For each set of tests the quantification of vegetation would first be conducted. The other measurements (2-6 outlined above) would then be conducted for five flow rates, each conducted with uniform flow conditions. The full testing program is detailed in section 6.2.3.

5.3.2 Quantification of Vegetation

Measurements of vegetation size and density were taken for each test. This was necessary to link any possible changes in the mixing characteristics or flow resistance of the channel to the changing nature of the vegetation. For each set of tests measurements were taken of the

1. Average stem diameter
2. Undeflected Canopy height
3. Deflected Canopy height (measured at each flow rate)
4. Number of leaves per plant
5. Average leaf width
6. Stem Density

Measurements for each test were carried out on an average of 10 plants randomly spaced over the channel length. In addition to these measurements, a detailed photographic record of the vegetation condition at each test was made with a digital camera.

5.3.3 Stage Discharge Relationships

Stage discharge curves were determined to quantify the flow resistance in the channel, as well as to determine cross sectionally averaged flow velocity. At each flow rate uniform flow (see section 2.1.1) was achieved by the use of the tail gate and five pointer gauges positioned down the channel (at 3.5, 6, 8.5, 11 and 13.5m from the inlet). To ensure accurate measurements the depth was measured to the bottom of laboratory flume rather than to the gravel bed where a definite bed level is harder to define due to the uneven nature of the gravel. The depth of the gravel (150mm) was then subtracted to give a flow depth. For each flow rate, the tail gate was adjusted until the flow depth became uniform. This was judged to have been achieved when the flow depth down the channel as measured by the pointer gauged varied by less than 2mm. Once uniform flow was reached, the flow depth was recorded and the tests 3 to 6 above were conducted. Discharge was determined by a manometer connected to a Venturi meter downstream of the pump (see section 5.2.3.3 for details of discharge measurement).

5.3.4 Velocity and Turbulence Measurements

As described in section 2.4 both velocity shear and turbulence levels have an impact on shear dispersion and therefore mixing. Measurements of velocity and turbulence profiles were taken to quantify the effect of vegetation on these factors. Point velocity measurements were taken using a Sontek Acoustic Doppler Velocitimeter (ADV) Probe (Figure 5-8). The probe is capable of measuring velocities in the x, y and z coordinates simultaneously at a frequency of 25Hz. This data can

1. Be temporally averaged to produce mean velocity measurements in x y and z directions at each measurement position.

2. Provide instantaneous and temporally averaged Reynolds stress (section 2.3.1.2) at each measurement position.

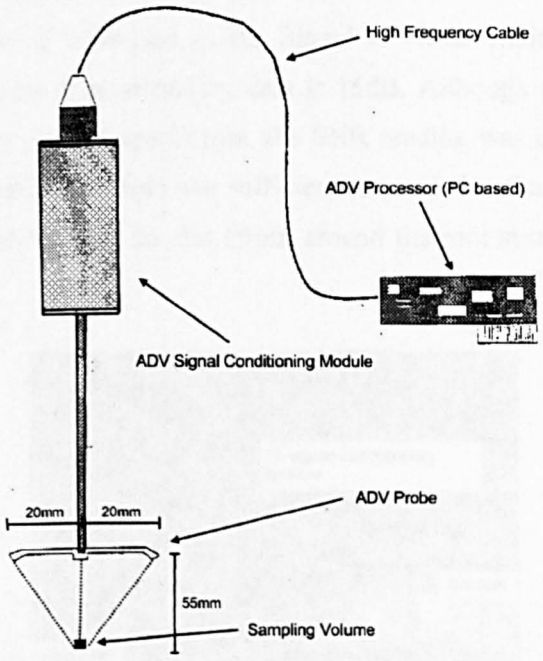

Figure 5-8 ADV System (adapted from Sontek ADV operation manual, 1995)

5.3.4.1 Principles of the ADV probe operation

All information regarding the principles and technical operation of ADV operation are sourced from "Sontek ADV operation manual" (1995).

The ADV probe (shown in Figure 5-9) works on the Doppler principle, named after Christian Doppler who first described the phenomenon of the Doppler effect (Doppler, 1842). The Doppler effect is the shift in frequency and wavelength of waves which result from a source moving with respect to the medium, a receiver moving with respect to the medium, or a moving medium. The concept was first described with reference to astronomy, wavelengths of light received from objects moving towards the earth tend to be compressed, and shifting toward the blue end of the spectrum, while wavelengths of light received from objects moving away are slightly stretched, becoming redder.

The ADV probe utilises the same concept but uses sound instead of light. First a short ultrasonic pulse at a known frequency is transmitted from the acoustic transmitter. When this pulse hits an entrained particle (termed scatter) carried by the flow, the wave is reflected at a new frequency. This echo from the water is received by the three small transducer elements. The frequency shift between the transmit pulse and the received echo is proportional to the water velocity. This echo must be strong enough to allow calculation of the frequency shift. If the echo is weak, the calculation will be statistically noisy and the velocity data will show significant short term variability. The strength of the echo is affected by the amount of scatter in the flow. The amount of scatter is determined by the concentration and size of the particles suspended in the water.

These particles can be suspended sediment, entrained air bubbles or artificially added 'seeding'. The strength of the echo is expressed as the Signal to Noise Ratio (SNR). The minimum recommended SNR to achieve good quality data is 15dB. Although no artificial seeding was added to the flow in any of the experiments, the SNR reading was consistently at a level of 20bB (± 2dB). This indicated that there was sufficient suspended sediment in the water provided from both the gravel particles and the dirt (from around the root system of the vegetation) to provide a good echo.

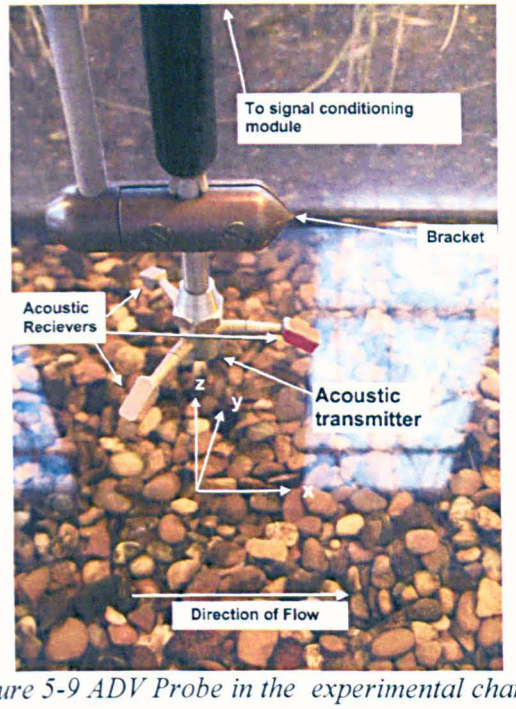

Figure 5-9 ADV Probe in the experimental channel

5.3.4.2 ADV Probe Measurement Limitations

The probe head has a diameter of 40mm (Figure 5-8). The practical implication of this is that when measuring transverse profiles of velocity, the probe cannot measure to within 20mm of the channel boundary. The probe sampling volume is positioned 55mm below the transducer at the centre of the probe. The probe itself must be submerged to take a reading so there is a limitation on the possible measurement locations within the vertical profile, i.e. when the probe is positioned as presented in Figure 5-10, it not possible to take measurements within 55mm of the water surface, although it is possible to take measurements very close to the bed. When acquiring vertical velocity profiles this limitation on the vertical measurement meant that it would be impossible to take a significant section of the vertical velocity profile. To solve this problem, when taking ADV measurements close to the surface, the probe had to be re-aligned to the horizontal plane (Figure 5-11). Data could then be measured to within 20mm of the water surface (half the head diameter).

Figure 5-10 Normally Aligned ADV Probe

Figure 5-11 Horizontally Aligned ADV Probe

This data would then have to be 're-aligned' in the data processing phase so that the coordinates match with the other data sets taken with a normally aligned probe. To ensure that this re-alignment of the probe would not affect the results a test was conducted. The probe first measured a flow velocity over 180 seconds at 25Hz when normally aligned. The probe was then rotated to the horizontal plane and the same position in the flow was measured. A frequency plot of the measured velocity is displayed in Figure 5-12.

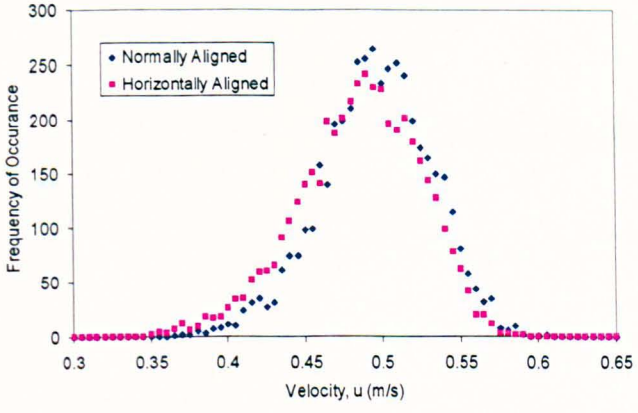

Figure 5-12 Histogram of results from normally aligned and horizontally aligned ADV probe

The results from the normally aligned and horizontally aligned probe show a good similarity. The temporal mean velocity and standard deviation of the data are shown in Table 12.

Table 12 Difference between normally aligned and horizontally aligned probe

	Normally Aligned	Horizontally Aligned	Difference (%)
Average Velocity (m/s)	0.493	0.483	2.12
Standard Deviation	0.036	0.038	5.55

The difference in the mean velocity value between the normally aligned and horizontally aligned probe is 2.1%, the difference in the standard deviation of velocity distribution is 5.5%.

This difference is judged to be sufficiently small. This method was therefore used to measure velocities close to the surface of the flow.

5.3.4.3 *ADV Probe Rotation Error*

The ADV operation manual claims that the probe is accurate to within ± 0.001m/s. In proportion to the minimum measured average flow velocity down the channel (≈ 0.1 m/s, see results 7.2) this is small (≈ 1%). However, when measuring transverse and vertical velocities this value must be taken into consideration. Inaccurate probe alignment may be a source of further error. The probe was visually aligned in the channel; meaning that the nature of the holding bracket makes the probe susceptible to rotation error in the x-y plane (see Figure 5-13).

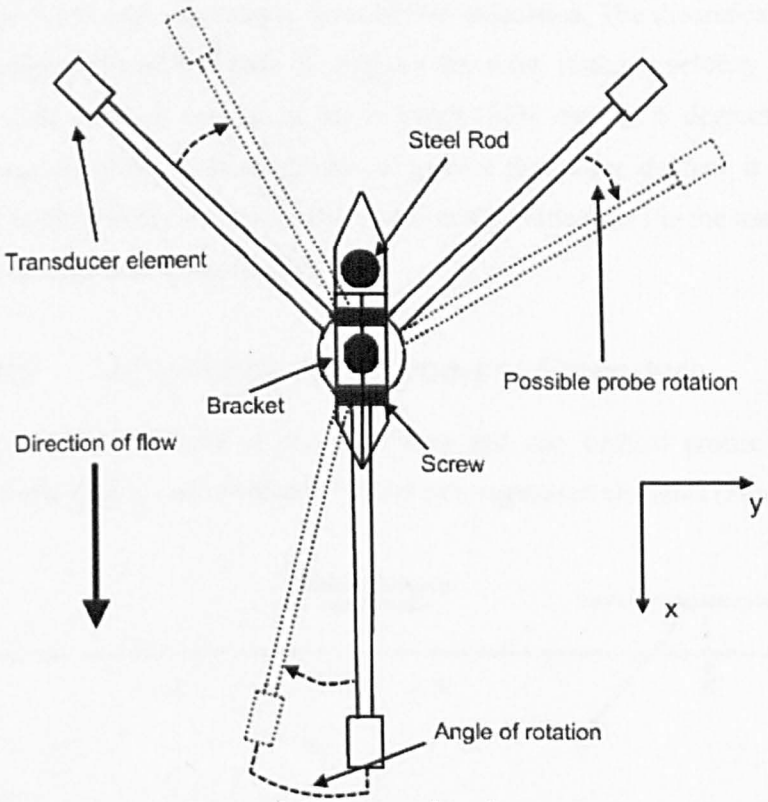

Figure 5-13 Potential probe rotation

If this rotational error is constant over an entire vertical profile, than the data can be analysed and corrected. However, because of the two different probe rotations (section 5.3.4.2) used over each vertical profile this rotational error may change over the depth and such correction is not possible. A theoretical vector analysis was conducted to see what the effect of different degrees of rotation would be on the error in the flow measurements (Figure 5-14 and Figure 5-15).

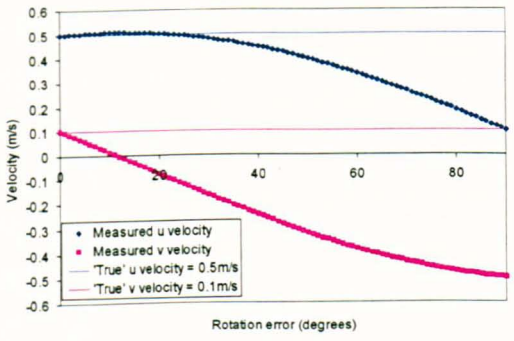

Figure 5-14 Measured velocity against degree of probe rotation

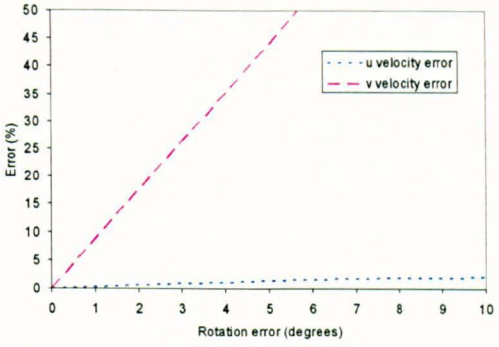

Figure 5-15 Theoretical error against ADV probe rotation

The theoretical error was calculated for a flow with a u velocity of 0.5m/s and a v velocity of 0.1m/s. As the measurement probe is rotated the measured velocity is compared to the 'true' velocity (Figure 5-14) and a percentage error is then calculated. The theoretical analysis shows that for miss-alignments of less than 10 degrees the error in the u velocity is small (<2%). However the error in the v velocity is much larger (50% error at 6 degrees rotation).When visually aligning the probe, a misalignment of greater than three degrees is unlikely. Hence rotation errors in the primary flow velocity (u) are small, while errors in the transverse direction (v) should be considered to be up to 25%.

5.3.5 ADV Probe Measurement Procedure

For each flow rate a minimum of one transverse and one vertical profile was taken. The standard transverse profile was positioned behind two vegetation elements (Figure 5-16).

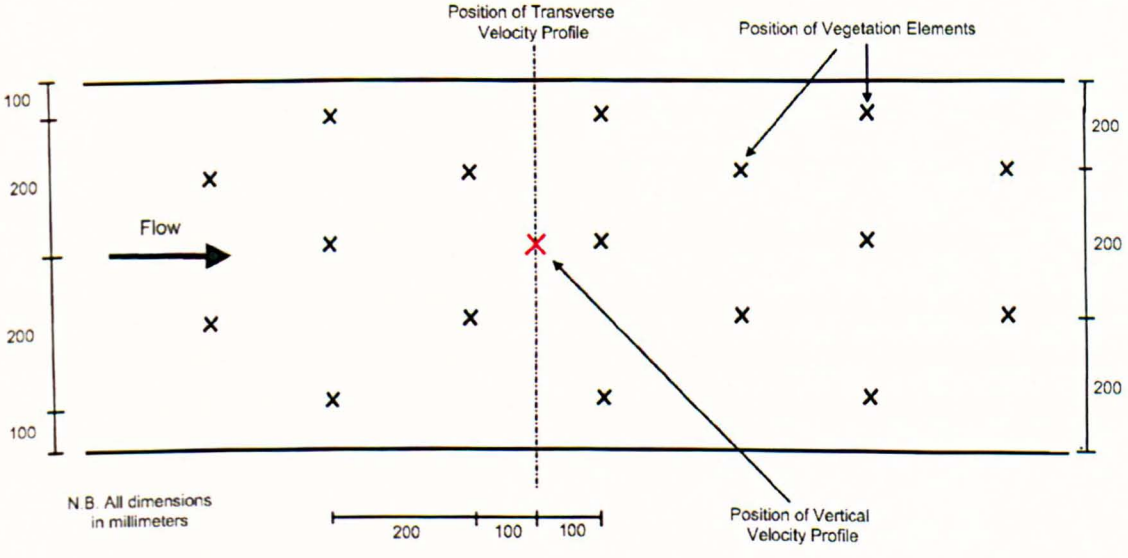

Figure 5-16 Planting diagram

The transverse profile consisted of eight point measurements positioned at 20, 100, 180, 260, 340, 420, 500 and 580mm across the channel. Vertical velocity profiles were taken in greater

detail, especially in the case of submerged vegetation. This was due to the need to accurately quantify the vertical velocity shear, which in the case of submerged vegetation is expected to be the major driver of longitudinal dispersion (see section 3.4.2.3). The number of points in the vertical profile depended on the flow depth but ranged from 5 (for low flow depths) to 21 (for a detailed profile taken at a high flow depth). The velocity section profile was taken close to the middle of the channel length to minimise any possible impact from the inlet or tailgate. The vertical profile of velocity was taken at mid flow width. This position meant that the profile was taken outside the immediate wakes of the nearest vegetation, which meant that the profile should give a good indication on the impact of the vegetation on the bulk of the flow.

5.3.5.1 Turbulence Measurement

The probe is capable of measuring velocities in the x, y and z coordinates simultaneously at a frequency of 25Hz. To obtain accurate turbulence values and reliable mean velocity each point measurement has to be taken over a sufficient length of time to capture the growth and decay of the flow structures present in the channel (see section 2.3). Figure 5-17 is an example of a time series plot which shows how the value of Reynolds stress changes as the length of time over which it is temporally averaged increases.

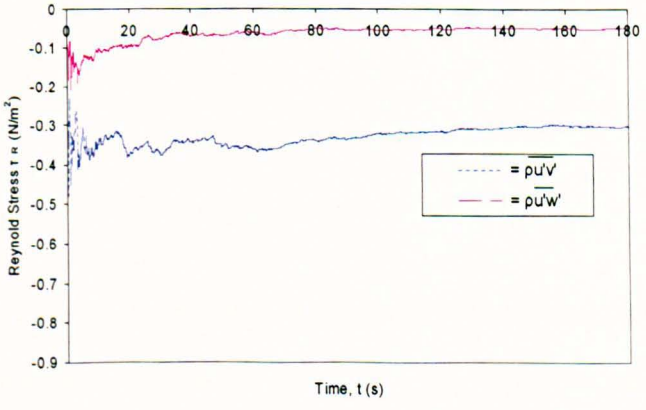

Figure 5-17 Effect of time on temporally averaged Reynolds Stress value

The data was taken within the experimental channel with no vegetation and at the maximum flow rate (29.5l/s). The figure converges to a steady value at around 100-120 seconds. To obtain a reliable mean velocity value and a good representation of the turbulence of the flow each point measurement was taken over 180 seconds.

5.3.5.2 Profiles of Transverse Velocity and Secondary Currents

When measuring vertical profiles of transverse velocity the average value of transverse velocity will be zero (as mass is conserved over the depth). The average will only be non zero if there is

some degree of rotational error (see section 5.3.4.3). In this case, conventionally, vertical profiles of transverse velocity are 'corrected' by adjusting all the velocities in the profile by a fixed amount until the average velocity is zero. However, this method is dependant on all the measurement points being taken with the same degree of rotational error. In the tests conducted in this study some of the measurements are taken with the ADV probe aligned in a different plane (see section 5.3.4.2). Thus, the rotational error may not be constant and so a mass balance correction can not be performed.

Vertical profiles of transverse velocity can still be used to measure the strength of the secondary circulations in the flow. As detailed in section 2.4.4.2, the secondary circulations directly effect the transverse mixing coefficient. Secondary circulations will be dependant on the variation of the transverse velocities over the depth. The variance or standard deviation of the profile can therefore be used to quantify the strength of the secondary circulations. An example of how variance represents the transverse velocities is presented in Figure 5-18.

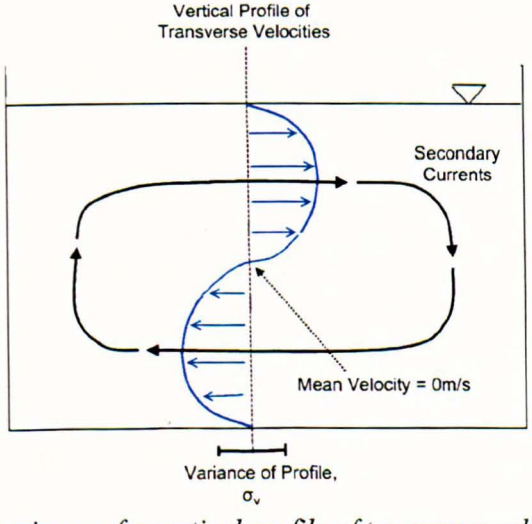

Figure 5-18 Mean and variance of a vertical profile of transverse velocities (theoretical case)

Whilst the mean value the vertical profile in Figure 5-18 is zero, the variance of the profile is directly related to the secondary circulations in the flow.

5.3.5.3 ADV Probe Data Processing

The ADV probe produces velocity data files in a compressed ADV format. This data can be converted into readable CSV files using the WINADV32 program. (WINADV32 Ver 2.022, Wahl, 2002). The files contain instantaneous values of u, v and w velocities. From the CSV files temporally averaged velocity and turbulence values can be produced using simple MATLAB routines. The WINADV software also filters the data in order to remove noise (i.e. data points with poor SNR) or spikes in the reading. Such data points can be caused by vibrations in the

water, or a temporary lack of scatter in the flow. If this data is left it can influence the mean velocity or turbulence values, therefore this erroneous data is removed. Points with a poor signal to noise ratio are simply filtered out. Spikes in the flow are filtered using a phase-space threshold de-spiking algorithm developed by Goring and Nikora (2002) which is automatically programmed into the WINADV32 program. The full method is not reproduced here, however, it can be briefly summarised into two main phases.

1. Spike identification – Based on the concept that there should be a physical upper limit to the change in flow velocity (i.e., the acceleration) that can occur in a flow. Measurements that indicate abnormal accelerations are identified as spikes

2. Spike removal – The spike is replaced by an interpolated value based on a third order polynomial fitted through 12 data points either side of the spike.

5.3.6 Fluorometery Measurements

Transverse and longitudinal mixing in the channel was measured using fluorometery, i.e. by measuring the transport of a traceable soluble material through the channel.

5.3.6.1 Tracer Used

In all mixing experiments Rhodamine WT dye was used as the tracer. When exposed to light of a specific wavelength the dye fluoresces and emits light which is detectable by fluorometers. Rhodamine WT was selected because

1. It is highly detectable. This enabled low injection concentrations which minimised the build up of background levels in the sump.

2. It has a slow rate of decay (much longer than testing period).

3. Prior experience of using Rhodamine WT both personally and in the Department.

Factors affecting the performance of Rhodamine WT are discussed in Smart and Laidlaw (1977). If an accurate calibration procedure (section 5.3.6.2) is performed, all such factors become inconsequential.

5.3.6.2 Fluorometer Calibration

All concentration readings were taken with CYCLOPS-7 analogue submersible fluorometers provided by Turner Designs. Six such instruments were available throughout the main testing

program. The fluorometers work by emitting a particular wavelength of light , when tracers such as Rhodamine WT are exposed to this wavelength they become excited and emit light of a different, higher wavelength. The intensity of the emitted light is dependent on the dye concentration. This light intensity is measured by the fluorometer. The probe outputs a voltage which is dependent on the intensity of the light recorded (provided that the intensity level is within the linear range of the probe measurement values). By calibrating each probe using dye diluted to a range of known concentrations, the relationship between voltage output from the probe and concentration measured can be determined. Figure 5-19 shows that there is a linear relationship between measured concentration and voltage output from each probe.

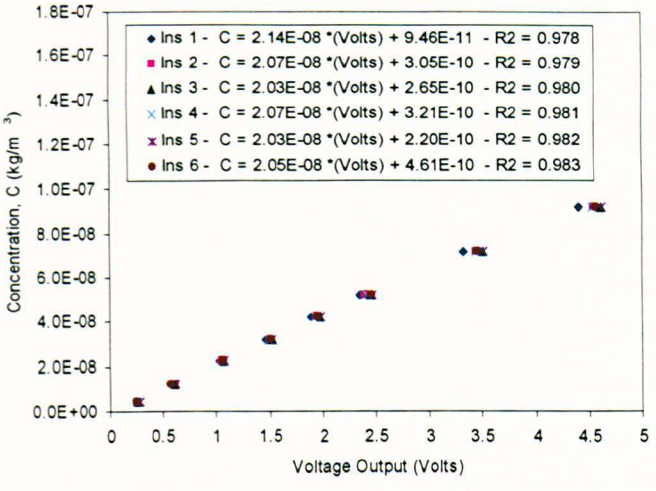

Figure 5-19 Example of six Cyclops-7 fluorometer probe calibration relationships

A PC equipped with a USB voltage measurement device and LABVIEW software continuously monitors and records the voltage output of the probes during each test. The data acquisition software compiled in LABVIEW is based on original software written by Cathy White of Adept Scientific, supplied on the Adept Scientific website (www.adeptscience.co.uk). The software was modified slightly to enable simultaneous measurement from all six fluorometers. Data from each test was gathered in the form of CSV files containing concentration against time plots for each instrument. The data was logged at a rate of 100 Hz; this is much higher than would be actually used in data analysis. However, the data acquisition program became unstable when attempting to use lower rates and the data files could be easily sampled to a more suitable size before analysis. The probes' small dimensions (22mm in diameter) and their submersible nature allowed the fluorometers to be placed directly into the flow at the required measurement location (Figure 5-20).

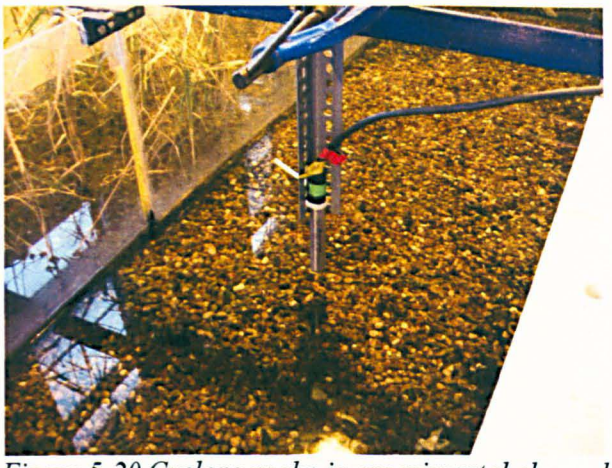

Figure 5-20 Cyclops probe in experimental channel

5.3.6.3 Signal to Noise Ratio (SNR)

Tracer data collected in the laboratory consists of both the actual signal from the fluorescing dye and an element of random noise. The typical magnitude of the noise can be established by examining the signal from the instruments while the concentration of dye is constant. The size of the random fluctuations represents the noise. When measuring low concentrations it can be difficult to differentiate between the actual signal and the noise. Steps taken to minimise the effect of noise on the results are detailed in the respective mixing sections

5.3.7 Longitudinal Mixing

Longitudinal mixing is concerned with the rate of longitudinal spread of a slug or instantaneous release of tracer with time/distance (see section 2.4). For each flow rate longitudinal mixing was measured directly. Five repeat tests were conducted at each flow rate to determine experimental variability.

5.3.7.1 Dye Injection System

To negate transverse and vertical mixing effects (as is necessary for the one dimensional longitudinal dispersion models to accurately describe the tracer cloud), the dye must be well mixed over the channel cross section before it enters the test reach. Through experimentation it was found that the best way to achieve this was to inject the dye using a tipping mechanism laid across the width of the channel (Figure 5-21). When tipped a uniform distribution of dye is introduced across the channel width.

Figure 5-21 Tipping Injection System

5.3.7.2 Fluorometer Placement in the Experimental Channel

Mixing is measured over a distance known as a reach, a fluorometer is placed at the upstream and downstream end of the reach and the rate of mixing between these points is measured. The availability of several fluorometers allows the measurement of mixing over different reaches, i.e. instruments are placed at several different points longitudinally down the channel. Ideally longitudinal mixing should be measured over the longest distance possible to minimise the influence of local variations in the mixing rates. However, as explained in section 2.4 one-dimensional mixing models are only applicable within the equilibrium zone. Before the final longitudinal positions of the instruments were decided, the position of the equilibrium zone would first have to be established. At each longitudinal site fluorometers were positioned to measure the concentration at the middle of the channel cross section (mid width, mid flow depth). Figure 5-22 presents example data from the six fluorometers when positioned at six discrete distances downstream of the injection point.

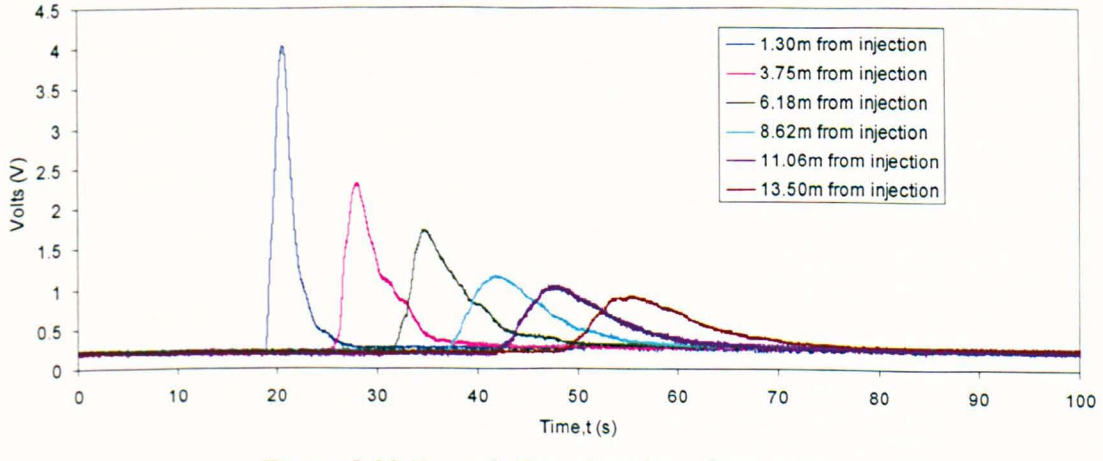

Figure 5-22 Example Raw data from fluorometers

5.3.7.3 Minimising Noise

The presence of noise in the data can cause problems when processing the data, especially when attempting to identify the start and end of each concentration profile (see section 2.4.5.3). To minimise this problem it is important to maximise the signal to noise ratio so that a greater proportion of the trace is easily distinguishable from the noise. In practice the maximum signal to noise ratio decreases with distance away from the injection as the peak levels of dye decrease (Figure 5-23 and Figure 5-24) (assuming the noise from each instrument is roughly equal). To maximise the SNR when conducting tests, the maximum amount of dye was injected that the upstream instrument could record (approx $9.5*10^{-8}$ l/l).

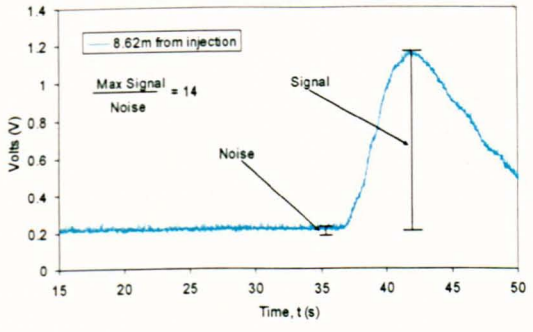

Figure 5-23 Signal to noise ratio

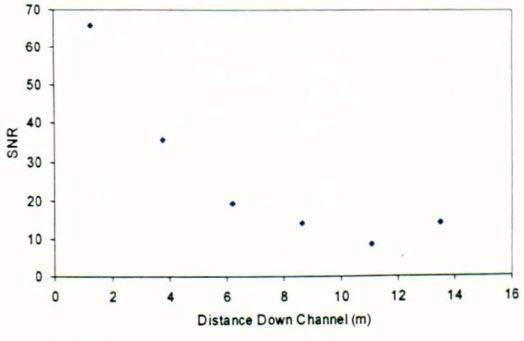

Figure 5-24 Maximum SNR ratio for each distribution (calculated from Figure 5-22)

5.3.8 Longitudinal Mixing Data Analysis

To quantify longitudinal mixing, the measured temporal concentration profiles from each test can be fitted to theoretical results from the ADE and ADZ models outlined in section 2.4. (i.e. use the ADE and ADZ models to predict the downstream trace from the upstream trace). The ADE or ADZ parameters which best describe the measured mixing can then be used to compare mixing between each test. How accurately the models can predict the mixing occurring in the flow will also give some information on the dominant processes at work in the channel. To undertake this analysis a computer program was written in MATLAB.

This program takes the raw data (voltage against time plots) and determines coefficients which can be entered into ADE or ADZ models to describe the mixing occurring in the channel. Throughout the analysis the measured data must undergo the following procedures.

1. Conversion from voltage to concentration plots by calibration curves
2. Removal of the background reading
3. Trace identification and data cut-off

4. Mass balance of concentration profiles

5. Initial parameter identification by method of moments

6. Parameter optimisation

These processes are explained in the sections below.

5.3.8.1 Voltage to Concentration Conversion

The program converts the raw voltage readings into concentration values using the calibration equations previously identified by testing each instrument (section 5.3.6.2).

5.3.8.2 Removal of the Background Reading

The program identifies and removes the background reading present throughout the data files. Background readings will be present due to dye remaining in the channel sump from previous injections. Over the course of each test, the background levels may vary between the start and the end of the trace. This build-up of background is assumed to be a linear function. This background is first identified by examining the reading prior to the trace arrival (i.e. reading from data file before any tracer is injected into the channel) and after the trace has passed (each data file is run for a length of time after the trace has passed through the channel). A linear function is calculated and removed from each trace (Figure 5-25 and Figure 5-26). Background levels can be reduced by replacing the water in the sump. This was done overnight in-between tests.

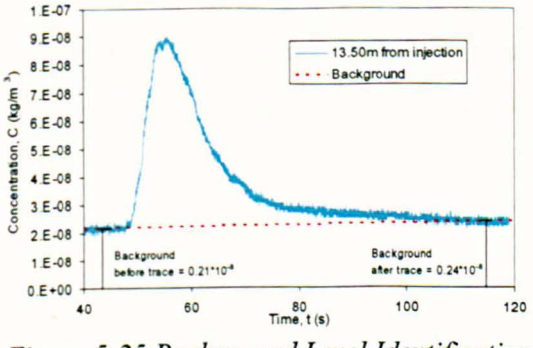

Figure 5-25 Background Level Identification

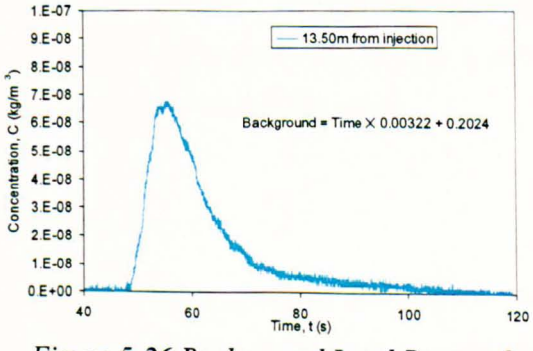

Figure 5-26 Background Level Removed

5.3.8.3 Trace identification

The start and end of each trace must be identified and the data can be clipped to acquire clean start and end points. It is important that this is conducted accurately as the method of moments (which is used to calculate the initial coefficients) is sensitive to error from inaccurate cut off

(see section 2.4.5.3). Unfortunately due to the low concentration values encountered at the start and end of each trace it is difficult to distinguish between the actual trace signal and instrument noise (see section 5.3.6.3). The computer program identifies the start of the trace as when the signal rises above 1% of the peak value for 10 consecutive data points. The end of the trace is defined as when the signal falls below 1% of the peak value for 10 consecutive data points. This level was chosen because visually it gave the most satisfactory levels of cut off (Figure 5-27 and Figure 5-28).

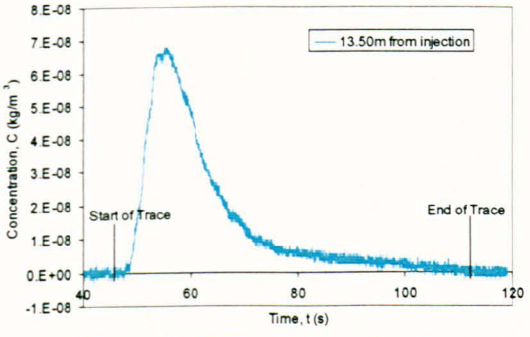

Figure 5-27 Trace identification

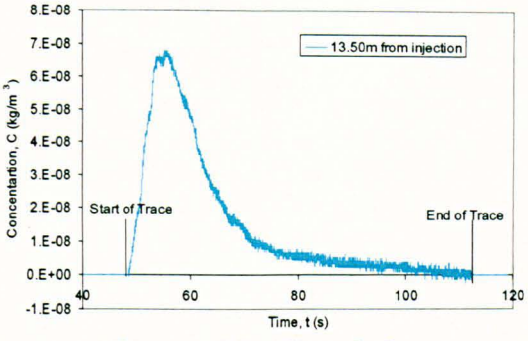

Figure 5-28 'Clipped' data

5.3.8.4 Mass Balance

Assuming that the tracer is conservative and the entire tracer mass measured at the upstream fluorometer was also measured at the downstream fluorometer, the area (and hence tracer mass) of the two concentration profiles should be equal. In practice however, this was rarely the case. Mass balance ratios were generally good however, being in the region of 95-105%; the deviation may be due to errors in the calibration, or uncertain cut off points. The ADE and ADZ models assume a conservation of mass over the reach, therefore it would be inappropriate to compare model predictions that conserve different degrees of mass. The program therefore performs a mass balancing procedure by multiplying the downstream data points by a mass balance factor (Total upstream tracer mass divided by total downstream tracer mass).

5.3.8.5 Parameter Identification

For each longitudinal reach, initial parameter identification is the next step in the program. The ADZ parameters are identified as the normal travel time (difference between trace centroids) and first arrival time (see section 2.4.9.1). The ADE parameters are identified using the method of moments, by measuring the development of the 0^{th}, 1^{st} and 2^{nd} moment of each of the distributions with time/distance. Details of using the method of moments to identify initial parameters are presented in the background section 2.4.5.3. However, when these initial parameters are put back into the models they usually provide a poor description of the mixing.

This is largely due to the errors involved with the evaluation of the parameters of each profile due to uncertain levels of trace cut off (section 5.3.8.3). For example, the change in variance with time is dependent on the trace cut off levels. Figure 5-29 shows how the rate of change of variance is dependent on the cut off rate chosen for an example test reach.

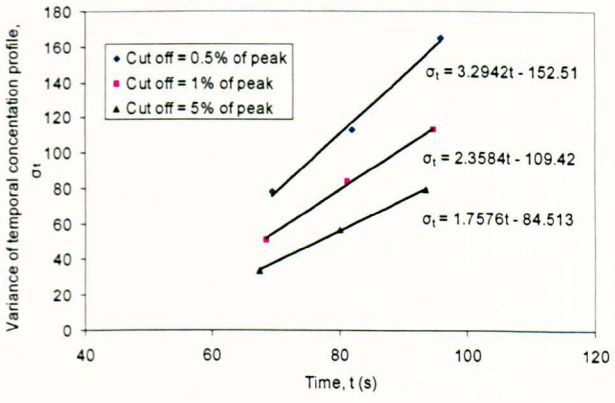

Figure 5-29 Example of how the growth of variance with time is dependent on levels of cut off.

Recently developed optimisation procedures aim to improve the accuracy of the final parameters by eliminating errors in the calculation of variance, first arrival times and centroids. The principles of parameter optimisation are presented in section 2.4.10; such methods can be used to increase the accuracy of mixing parameters. Researchers such as Boxall (2000) and Dennis (2000) suggest that optimised mixing parameters are relatively insensitive to subjective data collection techniques such as the uncertain choice of trace cut off levels. Boxall (2000) suggests that when using optimisation routines, accurate mixing coefficients can still be obtained when using cut off of up to 10% of the peak trace concentration value. The main drawback with the standard approach detailed in 2.4.10 is the length of the computational time required to calculate and compare all of the predictions, particularly if numerous reaches are to be analysed. When the solution requires three 11 by 11 matrices to acquire a sufficiently accurate solution this means the model has to be run and compared 363 times for each reach analysed. Thus the computational run time for optimisation is heavily dependent on the length of time it takes to run each model. The length of run time for each model is dependent on the time each trace is taken over, the frequency of the readings and the defined final tolerance values. To influence the time for each run both tolerance and data sampling rate can be altered. However, doing so may have implications for the accuracy of the parameters found and the quality of fit.

5.3.8.6 Optimisation Tolerance Value Analysis

The computational analysis time of the ADE and ADZ models is dependent on the final grid resolution size (i.e. tolerance) specified. Reducing the resolution of the optimisation grid will

shorten the overall run time as the program will require fewer iterations to reach the required resolution. However, the choice of final resolution values is a compromise between accuracy and computational run time. Choosing a reduced resolution will affect the final parameters because the optimisation will halt once the predicted trace only roughly matches the observed profile. To investigate the effects of the chosen resolution values on the final parameters achieved from the optimisation procedure, a resolution analysis was undertaken. The resolution analysis was undertaken on a test reach in an empty gravel bed channel detailed in section 5.1. Figure 5-30 and Figure 5-31 present example plots from the resolution analysis.

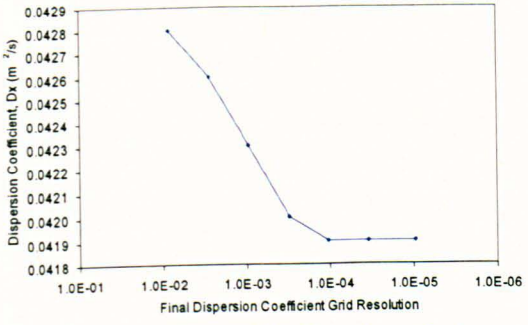

Figure 5-30 Effect of final grid resolution on optimised dispersion coefficient

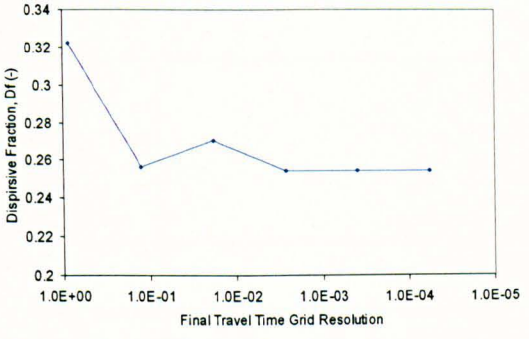

Figure 5-31 Effect of final grid resolution on Dispersive Fraction

It can be seen that the final parameters achieved become constant above a certain grid resolution. Based on this analysis the final grid resolution values were chosen. The final resolution values (which gave a suitably accurate solution) used in the optimisation program are listed in Table 13

Table 13- Final Resolution Values

Model Parameter	Final Resolution
Dispersion Coefficient (D_x) - ADE	$1*10^{-4}$ m^2/s
Travel time, ($\overline{T}$) – ADE and ADZ	$1*10^{-3}$ s
Time delay (τ) - ADZ	$1*10^{-3}$ s

5.3.8.7 Optimisation Data Sampling Analysis

The computational analysis time of the ADE and ADZ models also is dependent on the size of the data files being analysed. Conducting data analysis with the full data set (taken at 100Hz) would be impractical as it would take hours to optimise each test. By sampling the data the computational run time can be shortened. It is however important to be aware that sampling data is a compromise between accuracy and computational run time. Over sampling (i.e. using a much lower frequency) will affect the final parameters because the traces themselves will be less detailed. To investigate the effects of the sampling on the final parameters achieved from

the optimisation procedure, a sampling analysis was undertaken. The effect of over sampling will be more severe in the case of data with a short time of passage. A short time of passage means that data needs to be taken at a high frequency to accurately describe the trace. Therefore data used in the analysis was taken from longitudinal mixing tests taken in the non vegetated channel at the maximum flow rate (29.5 l/s), as it was judged that this would be the worst case scenario. In this case the flow velocity would be highest (adding vegetation will slow the flow) thus the time of passage of each tracer cloud will be short. Figure 5-32 to Figure 5-35 present results from a test reach which shows how the final mixing parameters obtained from the optimisation procedure change when the data is sampled down to different frequencies.

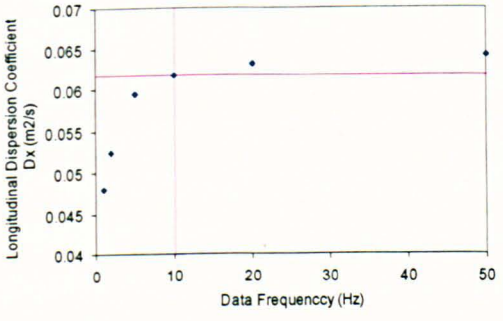

Figure 5-32 Effect of Sampling Frequency on dispersion coefficient

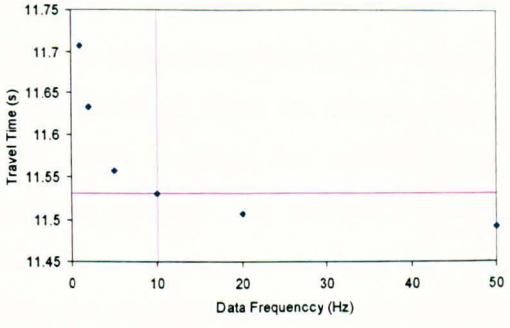

Figure 5-33 Effect of sampling frequency on ADE travel time

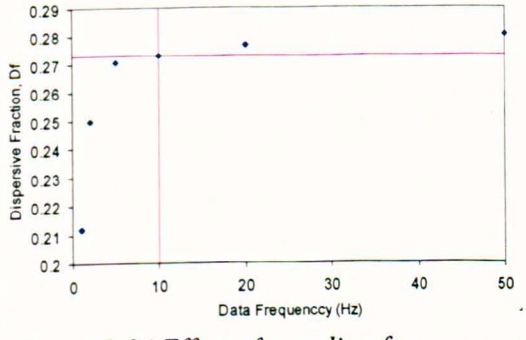

Figure 5-34 Effect of sampling frequency on dispersive fraction

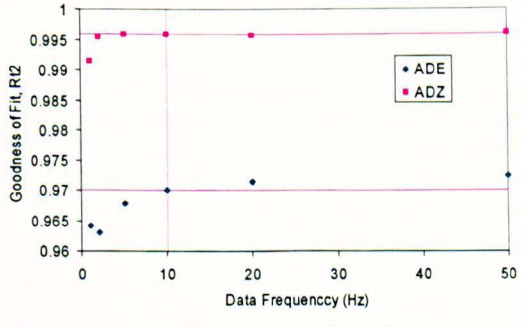

Figure 5-35 Effect of sampling frequency on goodness of fit

As the data becomes less detailed, the parameters diverge from the values achieved when a highly detailed data set is used. If the data is sampled down to a frequency less than 10Hz, then over sampling may have a significant impact (for example Figure 5-32 and Figure 5-34 suggest that sampling down to 1 Hz results in coefficients that are approximately 25% smaller than those measured if the analysis is conducted at 10Hz) on the parameters achieved from the optimisation procedure. Therefore based on this analysis a minimum data frequency of 10Hz was chosen as a balance between computational run time and trace accuracy. From an initial data rate of 100Hz the data was thus sampled at a rate of 1 value in 10 to achieve an analysis data rate of 10Hz. This frequency is not an issue when running the ADZ model as it has a short computational run time. However it was found that when using data at 10Hz the ADE model

can take around 30 minutes to run for each analysis (using typical data sets produced during this project). When analysing a large number of traces this run time is impractical. One solution is reducing the resolution values of the final solution (as listed in Table 13). However this option would also have negative implications on the accuracy of the derived parameters.

5.3.8.8 *Refined Optimisation*

Through experimentation it has been found that the speed of the optimisation solution can be dramatically increased by modifying how the program searches for a solution. Instead of starting with an 11 by 11 grid the new procedure starts with a 3 by 3 grid. After calculation of the regression values for this 3 by 3 grid the position of the maximum Rt^2 is located. If the maximum Rt^2 is situated on the edge of the grid than the parameters searched are enlarged so that all the points adjacent to this maximum are now calculated. Once the maximum point is found to be not on the edge of the 3 by 3 grid, the search is refined and repeated as in the previous method (until the required resolution value is reached). For example Figure 5-36 shows a full 11 by 11 grid of Rt^2 values calculated for an example reach. Each Rt^2 value is calculated from running the model for each pairing of travel time and dispersion coefficient. Traditionally to find the maximum value the program would run for each combination of parameters (i.e. 121 times). The maximum value can then simply be chosen.

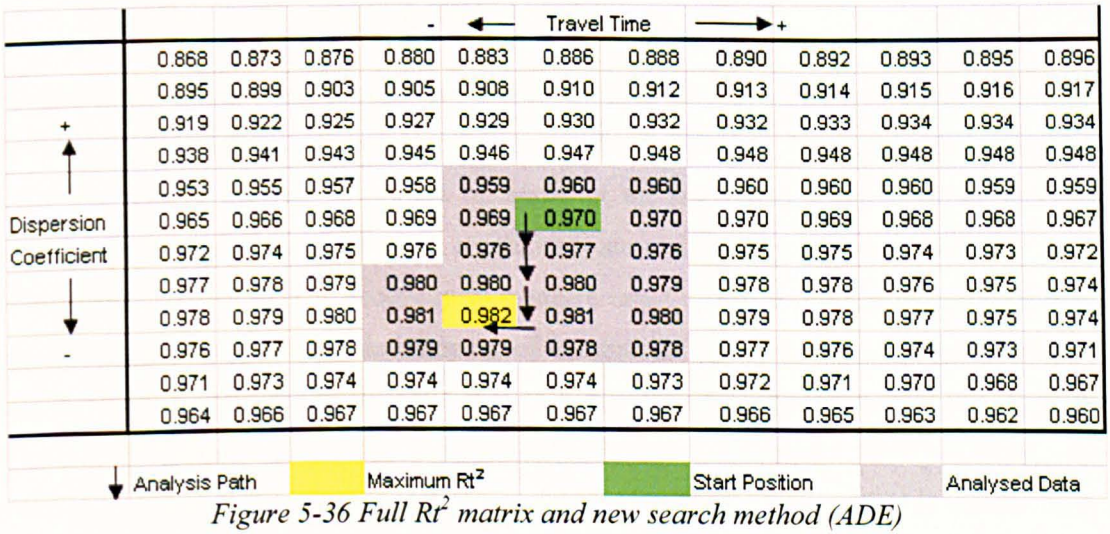

Figure 5-36 Full Rt^2 matrix and new search method (ADE)

The new method calculates the Rt^2 value for the initial parameters (i.e. those identified by the method of moments) and those immediately adjacent to it. In this case a higher Rt^2 value is identified if the dispersion coefficient used is lower. The grid is enlarged to analyse all cases adjacent to this new maximum Rt^2. The search continues until a maximum value is found (i.e. all adjacent pairings produce a lower Rt^2). In this case the program is required to run the ADE model 21 times rather than the 121 times if using the traditional method. This method works as long as there is one unique best solution and the Rt^2 matrix is a smooth function. This was

checked by running the traditional optimisation procedure for a number of sample traces and examining the resulting matrix of Rt^2 values (e.g. Figure 5-37). For all cases a single unique solution was found and identical parameters were produced from the traditional and new optimisation procedure.

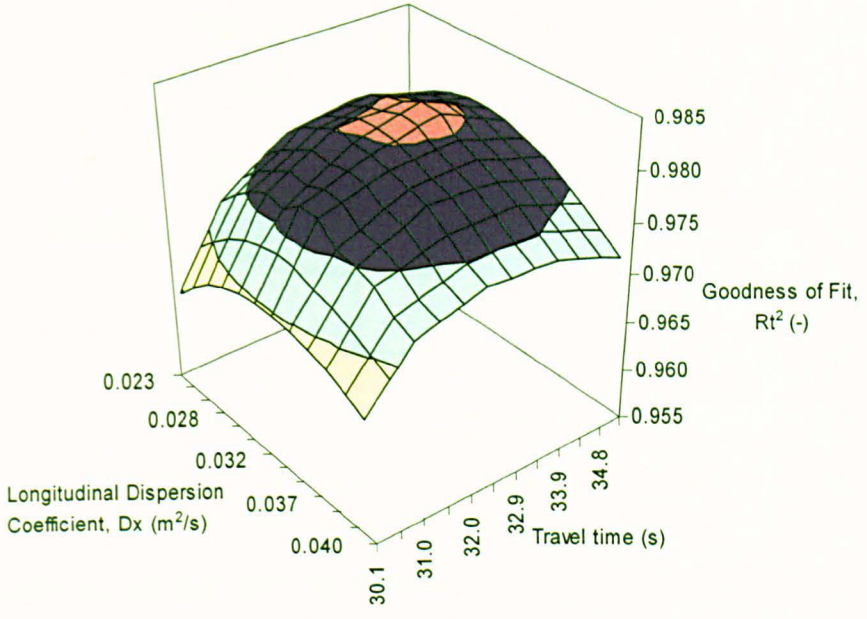

Figure 5-37 Example of how ADE parameters affect the goodness of fit (Rt^2)

5.3.9 Transverse Mixing

The concepts of transverse mixing were introduced in section 2.4. Transverse mixing is caused by the combined effects of secondary currents and turbulence. To empirically evaluate the transverse mixing the rate of spread of tracer in the transverse plane must be measured. Empirically derived transverse mixing coefficients are traditionally evaluated using the method of moments. To do this it is necessary to measure cross sectional profiles of concentration at several longitudinal positions downstream of continuous injection. This method is relatively time consuming compared to the collection of data required for the evaluation of longitudinal mixing coefficients. In this study the method of Boxall and Guymer (2001) is used, which removes the need to acquire complete cross sectional profiles. This method is summarised in section 2.4.5.2. The method requires the use of a continuous point injection system.

5.3.9.1 Constant Head Injection

By using a continuous point source it is possible to neglect the effects of longitudinal mixing as concentration levels can be assumed to be constant with time in the longitudinal direction. Also as all measurement points are downstream of the crossing distance L_1, it can be assumed that the tracer is vertically well mixed. The injection system (Figure 5-38) comprises of a constant

header tank positioned above the channel, which is kept full by a pump sourcing dye from a reservoir.

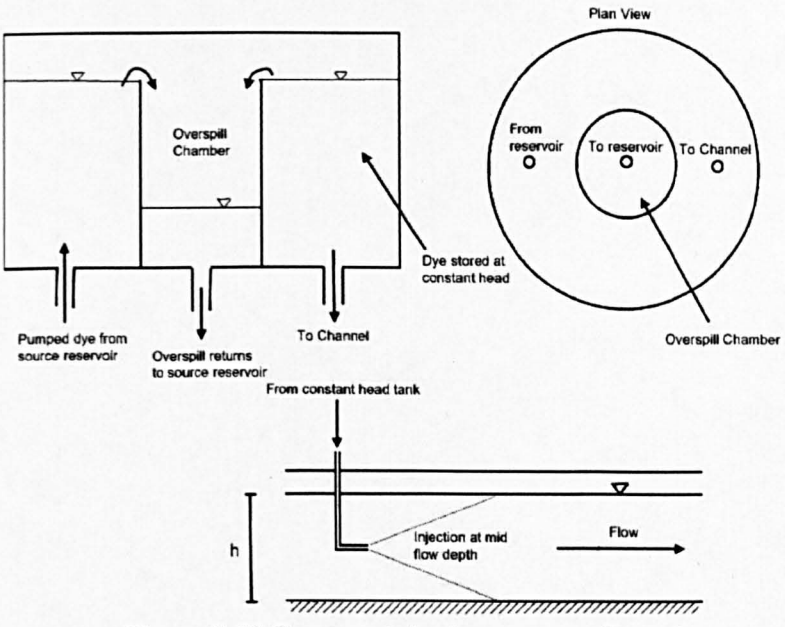

Figure 5-38 Constant injection system schematic

Dye is continuously pumped from the reservoir into the header tank where it is kept at a constant head by means of an overspill chamber (linked by pipe back into the source bucket). From the header tank, the dye is fed into the channel by means of a pipe (diameter of 3mm) aligned with the flow. As the head is constant , the dye therefore enters the channel at a constant rate. The inlet pipe is positioned at mid flow depth to minimise the distance until complete vertical mixing. It is positioned at mid channel width so that the calculation of the α coefficient (Equation 2-124) is as specified in Boxall and Guymer (2001). To minimise additional mixing due to injection momentum, injection velocities which were similar to the main flow velocity could be achieved by positioning the constant head tank at different elevations.

5.3.9.2 Transverse Reach

The Boxall and Guymer (2001) method required a reach where dye, injected from a continuous mid channel point source, reaches all points in the transverse cross section (the crossing distance, L_1), and provides sufficient room downstream of this point for taking measurements (i.e. leaving sufficient measurement clearance upstream of the tailgate, where the flow may not be uniform due to acceleration over the tailgate). The selected measurement reach started 4.3m downstream of the injection, and ended 2.1m upstream of the tailgate. This upstream distance was sufficient to achieve crossing distance, L_1, prior to the reach for each test, and provided sufficient room to take three or four measurements at least 1.22m apart. A diagram of the transverse mixing reach is presented in Figure 6-10.

5.3.9.3 Transverse Mixing Experimental Procedure

For each experiment concentration levels were monitored using the Cyclops probes (described in section 5.3.6.2) positioned mid depth at the centre (C_{max}) and edge (C_{min}) of the laboratory channel at four longitudinal positions downstream of the crossing distance of an continuous injection of soluble tracer (Rhodamine WT as detailed in 5.3.6.1). Measured concentration profiles over the channel width downstream of the continuous injection point confirmed that C_{max} occurred at the mid point of the channel and C_{min} occurred at the channel edge (as in Figure 2-13).

As explained in section 5.3.6.3, data from the Cyclops instruments contains an element of random noise (Figure 5-39). To minimise the effect of the noise, concentration values (C_{max} and C_{min}) should be temporally averaged over a sufficiently large time. The influence of time on the average concentration value can be seen in Figure 5-40. If the temporal average is taken over a short time, than the effects of noise on the reading have a significant impact on the result. As the length of time over which the average value is taken increases, the reading converges to a steady value. Once this steady value has been reached, the effect of noise becomes negligible on the temporal average. Based on this analysis all concentration values used were a temporal average taken over at least 180 seconds.

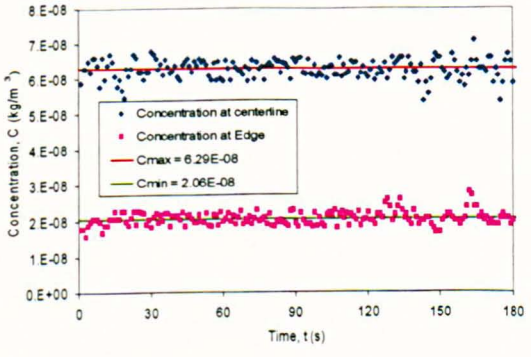

Figure 5-39 Example Data (Background levels removed)

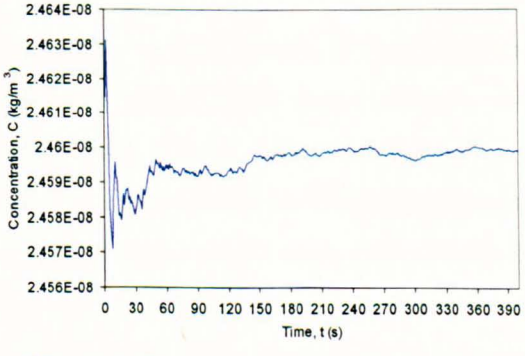

Figure 5-40 Average concentration value converges with time

For each instrument the background levels were removed (using a similar procedure detailed in the longitudinal mixing analysis, section 5.3.8.2) the ratio C_{min} / C_{max} could then be calculated at each of the four measurement positions, and transverse mixing coefficient determined using Equation 2-123 and Equation 2-124 (provided a measurement of average cross sectional velocity was made).

Chapter 6 - Testing Program & Validation of Results

The aims of this chapter are to detail the vegetated testing conditions in the laboratory channel and to justify the procedures adopted to collect and interpret the data. This requires a description of

1. The investigation of the length of the advective zone in the channel
2. Vegetation growth and testing conditions
3. The use of the Boxall and Guymer (2001) method for measuring transverse mixing coefficients
4. The experiments regarding the influence of flow straightners on the velocity and mixing
5. The performance of ADE and ADZ models over the longitudinal mixing reach

6.1 Determination of Advective Zone Length

6.1.1 Aims of Investigation

As explained in section 2.4.3.4 the one-dimensional ADE is only applicable in the equilibrium zone, where the variance of concentration profiles grows linearly with time / distance. This equilibrium zone occurs in uniform flow conditions only after a defined timescale, once differential advection and transverse diffusion reach equilibrium. This investigation examines the theoretical and experimental estimation of the length of the advective zone, and explores the influence of channel and flow regime properties. The aim is to determine where in the experimental channel the ADE can be applied, and hence over what reach to measure longitudinal mixing.

6.1.2 Estimating the Length of the Advective Zone

6.1.2.1 Theoretical Estimation

As described in section 2.4.4.5 the equilibrium zone begins after the Lagrangian timescale (T_x) has passed. Fischer (1967) proposed that the timescale would be related to the time it takes each particle in the flow to sample the entire flow regime and produced an equation to determine this timescale, T_x, (Equation 2-102). Therefore, to determine the length of experimental channel required to reach the equilibrium zone it is necessary to convert the Lagrangian timescale (T_x) to

an advective zone length (L_x). A mean flow velocity term (U) is therefore added to Equation 2-102

$$L_x = \alpha U \frac{L^2}{K_y} \qquad \text{Equation 6-1}$$

The theoretical impact of the channel and flow parameters on advective zone length can now be investigated by considering the following

1. Channel width, b, – Length scale (L) in Equation 6-1 is taken as half the channel width
2. Normalized transverse mixing coefficient (K_y/hu^*)– Directly affects Equation 6-1
3. Discharge – Changing discharge affects both flow velocity and flow depth (which indirectly affects Equation 6-1 through K_y)

The advective zone length will also be dependent on the value of α. In the following calculations three values of α have been used to cover the range of previous studies (see Table 4 is section 2.4.4.5). The minimum theoretical obtained by Fischer (1967), 0.069; a mid range value, 0.5; and a maximum, 1. Using these α values the theoretical effect (using Equation 6-1) of the variation of the other parameters (1 to 3 above) can be investigated (Figure 6-1 to Figure 6-3).

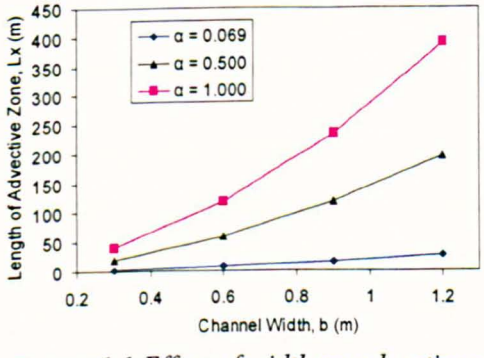

*Figure 6-1 Effect of width on advective zone length. Q/b = 30l/sm, K_y = 0.13hu**

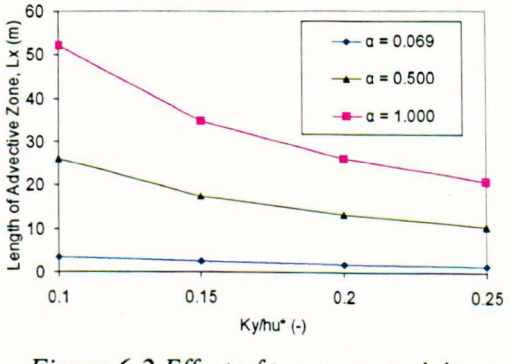

Figure 6-2 Effect of transverse mixing on advective zone length. Q/b = 30l/sm, b = 0.3m

Figure 6-1 shows the theoretical effect of channel width on advective zone length for three values of α. It can be seen that an increasing length of advective zone is predicted with increasing channel width. This may be explained due to the increase in distance each particle has to travel to experience the complete flow regime. Figure 6-2 shows the theoretical effect of the normalised transverse mixing coefficient on advective zone length for three values of α. A decreasing length of advective zone is predicted with increasing rate of normalised transverse

mixing coefficient. An increase in the rate of transverse mixing will increase the rate at which a tracer is moved around a given cross section to experience the complete flow regime.

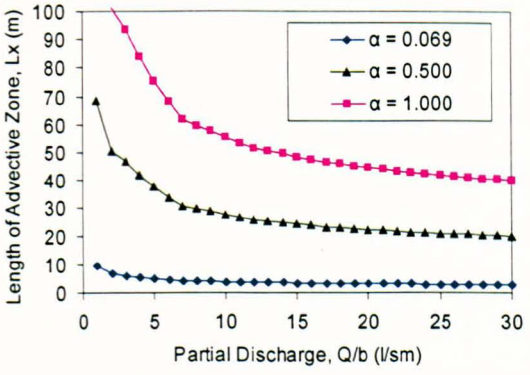

Figure 6-3 Effect of discharge on advective zone length. b = 0.3m, K_y = 0.13hu.*

Figure 6-3 shows the effect of flow rate on advective zone length for three values of α. The theoretical effect of increasing discharge is not as straightforward to evaluate as the effects of width or normalised transverse mixing coefficient. For these calculations it has been assumed that normal flow conditions have been established, and hence that depth of flow can be calculated for each partial discharge by application of Manning's equation, using an 'n' value calibrated to the experimental studies reported here. From depth of flow, continuity can be applied to estimate cross sectional average velocity, hence velocity is proportional h^{-1}. The transverse mixing coefficient as evaluated using Equation 2-132, (assuming $u^* = \sqrt{gRS_0}$), is proportional to $h^{1.5}$. Thus from Equation 6-1 the length of the advective zone is proportional to $h^{-2.5}$. When relating depth to discharge through Manning's equation, it can be seen that this is the form of the relationship shown in Figure 6-3, with increasing discharge leading to decreasing length of advective zone.

From comparison of Figure 6-1 to Figure 6-3 it can be seen that, of the three parameters, over the ranges investigated (which are considered to cover most typical laboratory channels), the channel width (length scale) has the greatest influence on the length of the advective zone. Although the selected value of α may be even more significant than the length scale.

6.1.2.2 *Implications of theoretical study*

The total working length of the experimental channel used for the vegetated flow experiments was 14.5 metres, it has been proposed in section 5.2.3.4 to split the channel in two and hence use a channel width of 0.6m. However, assuming a K_y/hu* value of 0.15 (approximate value for straight laboratory channels, see section 2.4.6.2) and a α of 0.414 (i.e. the experimental value found by Fischer, 1967) and using Equation 6-1 gives an advective zone length in the range of

45m to 60m; over the range of discharges available in the channel. If this theoretical estimate of advective zone length is proved correct the channel would have to be narrowed further to achieve a smaller length scale, which would allow measurements to be performed in the equilibrium zone.

6.1.3 Advective Zone Experimental Program

The main aim of the experimental program was to determine the actual length of the advective zone in the experimental channel and therefore determine if the channel (at its 0.6m width) was suitable for the experimental study of mixing using one-dimensional mixing models such as the ADE. Additionally by measuring the advective zone using a range of channel widths and discharges the suitability of Equation 6-1 could be determined and an accurate value of α derived.

It was assumed that the length of the advective zone would be at its longest before any vegetation was added, in flow over the plain gravel bed (i.e. the base case conditions). The addition of vegetation will slow the flow by increasing flow resistance (see section 3.1), hence decreasing the velocity term in Equation 6-1, and reducing the advective zone length in the presence of vegetation relative to the base case. The base case was therefore judged to be the worst case scenario in terms of length to the equilibrium zone.

Experiments were conducted using the equipment and procedures as detailed in chapter 5. For these experiments the channel width was adjusted by altering the position of the Perspex divider. Four different channel widths were investigated, 0.3m, 0.6m, 0.9m and 1.2m, each for four different flow rates per unit width, 12l/sm, 15l/sm, 20l/sm and 25l/sm. Rhodamine WT fluorescent dye was used as a soluble tracer, monitored at six downstream cross sections (1.30, 3.75, 6.18, 8.62, 11.06 and 13.50 m downstream of the injection) using calibrated Cyclops fluorometers (detailed in section 5.3.6.2). The dye was introduced as a transverse line source at the channel inlet, using a tipping injection system positioned above the water surface as detailed in section 5.3.7.1. For each of the 16 uniform flow conditions five repeat tests were conducted.

6.1.3.1 Evaluating the length of the advective zone

By plotting the development of variance and skew with distance, the point where the tracer cloud enters the equilibrium zone could be established. The variance and skew of each distribution were evaluated by moment analysis (see section 2.4.3.2). The inaccuracies associated with using this technique is that any data error such as identification of the start and end of each trace will lead to potentially large errors in the estimation of variance, due to the square term in the second moment and even larger errors in skew due to the cube term in the

third moment (see section 2.4.3.2). The limits of the concentration profiles have been identified as a percentage of the peak measured concentration for each injection. Unlike when fitting ADE and ADZ models there is no optimisation procedure to eliminate error arising from uncertain trace identification, and therefore the calculations of variance and skew are sensitive to the level of cut off chosen. At low cut offs the inclusion of additional instrument noise in the calculations may provide misleading results while a loss of result sensitivity may be the result of a high cut off level (see section 2.4.5.3). Therefore a range of percentage cut off values were used to provide a clearer estimation of the trends in variance and skew.

6.1.4 Results of Advective Zone Study

From the evaluation of the zero moment it was found that mass was conserved for each of the injections, an average variation of 1.5% was found, which was deemed acceptable. The values of variance and skew for each of the five repeat tests were normalized by the maximum variance or skew value of that test. This was necessary due to a slight difference in the initial variance and skew imparted from the injection system. The average for the five repeat injections was calculated for each reach.

6.1.4.1 Example Plots of Variance and Skew Development

The measured development of variance and skew from the test conducted using a flow rate of 12l/sm and a channel width of 0.3m are presented as examples (Figure 6-4 and Figure 6-5). Each data point on these graphs is the average of the five repeat injections. The figures include the effects of the different cut off values showing the sensitivity of the calculations.

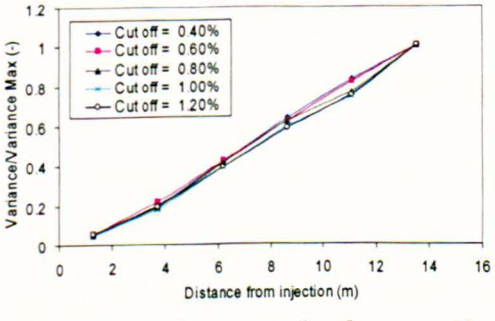

Figure 6-4 2nd moment development (b = 0.3m, Q/b = 12l/sm)

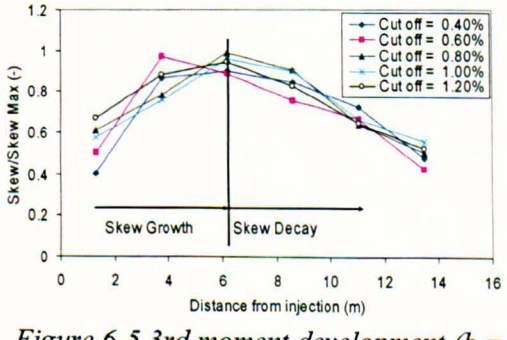

Figure 6-5 3rd moment development (b = 0.3m, Q/b = 12l/sm)

To identify the start of the equilibrium zone, it is necessary to identify where the change in variance becomes linear with distance or where skew stops increasing. From Figure 6-5 it is possible to estimate the location of the peak in skew with some confidence. However identifying the start of linear increase in variance in Figure 6-4 is not as distinct. It appears that linear growth in variance occurs slightly before the peak in skew. By using these plots for each

flow condition it is possible to estimate a point for each condition where the equilibrium zone begins. The start of the equilibrium zone is taken as the point where the skew begins to decay as this point is easier to identify and thus is more accurate. It is suggested that the source of the uncertainty in previously determined α values in the literature (Table 4) is due to the fact that the development of variance was used to determine the advective zone length, rather than skew. Establishing the start of the linear trend in variance is susceptible to error (from the method of moments – section 2.4.5.3) unless the 2nd moment of each profile is determined accurately with high resolution instruments.

6.1.4.2 *Experimental Length of the Advective Zone*

Figure 6-6 shows the change in the length of the advective zone (established from the peak in skew) for each of the experimental conditions. Figure 6-6 shows a general increase in the length of the advective zone with increasing discharge. However, the variation with width (length scale) shown in Figure 6-6 is not consistent across the different discharges, and suggests relatively little impact over the range of widths studied.

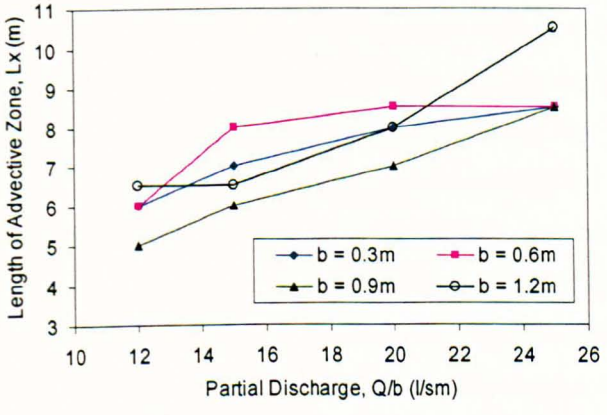

Figure 6-6 Measured length of the advective zone in the experimental channel.

6.1.5 *Discussion of Advective Zone Study*

It is possible to make a comparison between experimental and theoretical derived values for the length of the advective zone by comparing Figure 6-6 with Figure 6-1 and Figure 6-3, and through this explore the relative impact of channel width, discharge and transverse mixing coefficients. Of the range of α values used in Figure 6-1 to Figure 6-3 it is the lower bound value which provides the closest approximation to the experimental values. This represents the value was that obtained entirely theoretically by Fisher (1967). This suggests that the other studies have overestimated the length of the advective zone.

According to Equation 6-1 channel width (i.e. length scale) increases the length of advective zone (Figure 6-1), while the length decreases with increasing normalised transverse mixing coefficient and with discharge. However, the only clear trend shown by the experimental data is an increase in the length of the advective zone with increasing discharge, which directly contradicts the theoretical Equation 6-1 (Figure 6-7 and Figure 6-8).

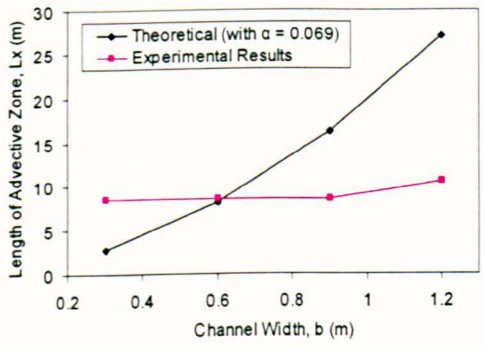

Figure 6-7 Theoretical and Experimental Trend. Q/b = 25l/sm, K_y = 0.13hu, α = 0.069.*

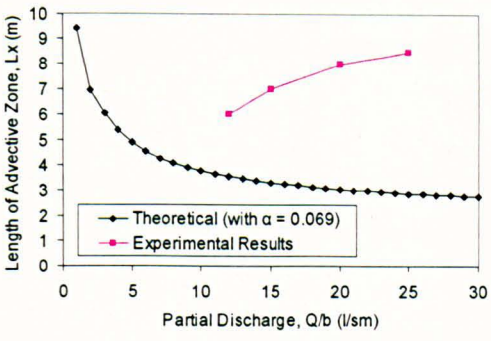

Figure 6-8 Theoretical and Experimental Trend. b = 0.3m, K_y = 0.13hu, α = 0.069.*

It is possible that this lack of agreement is due to changes in the transverse profile of primary velocities and / or the transverse mixing coefficient with width. For example at a fixed partial discharge, decreasing the channel width will keep the same average velocity but will increase dispersion due to the altered transverse profile of primary (longitudinal) velocities (increasing the length of advective zone). But the increased boundary shear of this profile would generate more turbulence increasing the rate of transverse mixing (decreasing the length of the advective zone). Similarly any irregularities in the channel boundaries are more likely to establish secondary flow features also increasing the rate of transverse mixing. If these two effects were equal the net effect would be no change in the length of the advective zone, possibly explaining the observed experimental result. However, in this investigation neither the transverse profile of primary velocities nor the transverse mixing coefficient have been measured, hence this can not be verified.

6.1.6 Conclusions of the Advective Zone Study

The results of the advective zone study are important for both this study and future work because

- The experimental results presented highlight the need to conduct initial longitudinal mixing experiments using multiple measurements at longitudinal locations to ensure that the solute has entered the equilibrium zone.

- When defining the length of the advective zone it is more accurate to examine the development of skew (3rd moment) of concentration time distributions, (where a peak in skew clearly defines the start of the equilibrium zone) than to determine when the development of variance (2nd moment) becomes linear with distance / time.

- The use of α coefficient values in Equation 6-1 provided by previous experimental studies leads to considerable overestimation of the length of the advective zone. The α coefficient value which provides the closest approximation to the experimental values was obtained entirely theoretically by Fisher (1967).

- The experimental data identified a trend which showed an increase in the length of the advective zone with increasing discharge, which directly contradicts the theoretical relationship.

- The study showed that width (length scale) had little effect on advective zone length, therefore it is judged that the experiments can proceed with two channels of 0.6m width, with two differing types of vegetation

- In the experimental channel investigated, the measurement reach for longitudinal mixing should begin no sooner than 7.5 m downstream of the inlet (approximate start of equilibrium zone from Figure 6-6).

6.2 Vegetation Growth and Testing Conditions

Following the study of advective zone length, the mixing reaches could be defined. This section details the mixing reaches together with the rate of plant growth and the resulting testing conditions.

6.2.1 Longitudinal Mixing Reaches

The advective zone study showed that the base case (which was judged to be the worst case scenario) longitudinal experimental reach should begin approximately 7.5 m downstream of the inlet. The end of the reach should also have sufficient clearance from the end of the channel so that the tailgate effects do not influence the measurements. Longitudinal mixing was therefore measured over a 4.88m reach beginning 7.36m downstream of the injection point (Figure 6-9).

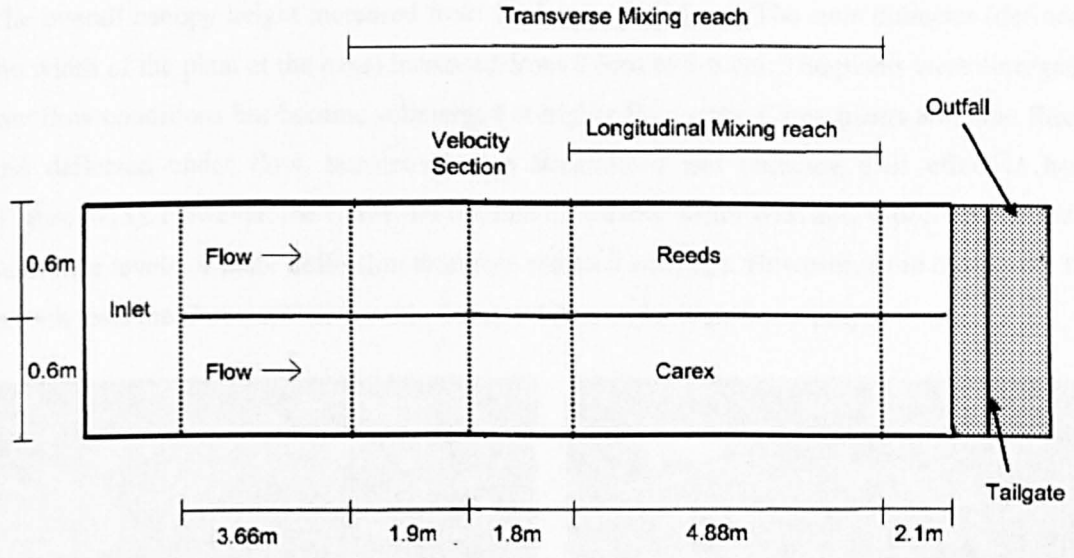

Figure 6-9 Testing setup

Within this reach there were three measurement points positioned at the start, mid distance and at the end of the reach. Effectively this splits the reach into two sub reaches. Sub reach 1 being the upstream half of the zone (2.44m) and sub reach 2 the downstream half of the zone (2.44m). The end of the mixing measurement zone is 2.1m upstream of the tailgate which means any effects which the tailgate has on the main flow should be negligible in the mixing reach (Figure 6-10).

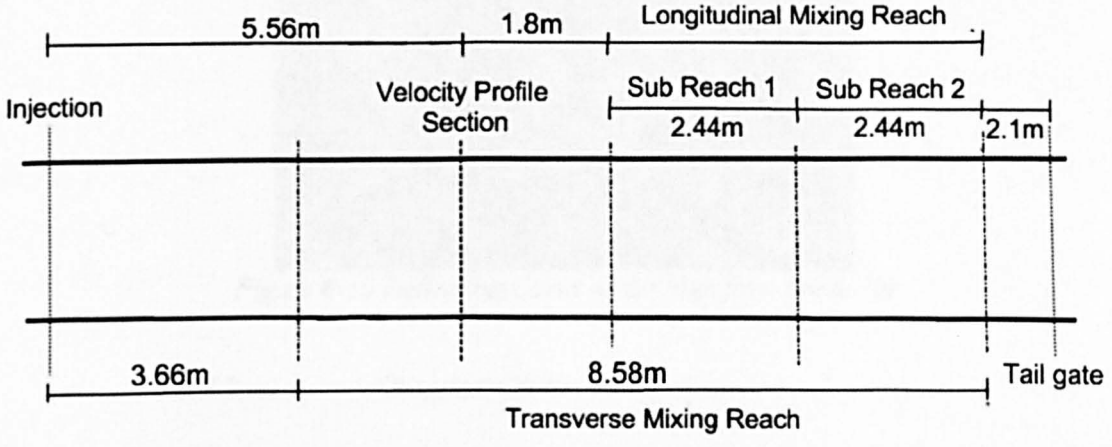

Figure 6-10 Reach diagram

6.2.2 Vegetation Growth

6.2.2.1 Growing Carex

The Carex were first planted in the channel in October 2006. As expected the effective stem density did not increase with age. However, the plants rapidly increased in size and height through to final test, 26 weeks after planting in April 2007 (see Figure 6-11 and Figure 6-12).

The overall canopy height increased from 5-10cm to 30-35 cm. The stem diameter (defined as the width of the plant at the base) increased from 0.5cm to 5-6 cm. The plants were emergent at low flow conditions but became submerged at higher flow rates. Carex plants are quite flexible and deflected under flow, becoming more streamlined and reducing their effective height (Figure 6-13). However, the Carex did became noticeably stiffer with age, especially around the base. The levels of plant deflection therefore reduced with age. However, even during the final growth tests the Carex still noticeably deflected (but under high flows only).

Figure 6-11 Carex at Week 2

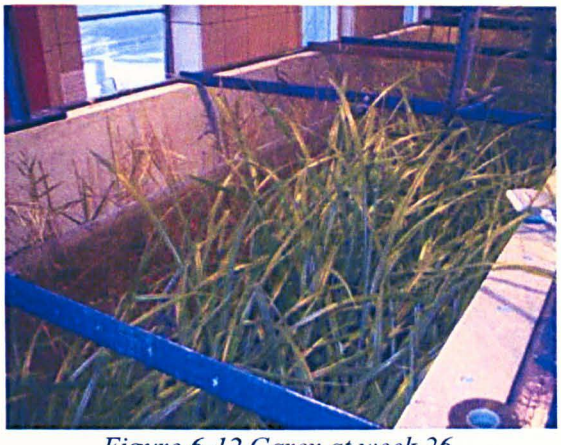

Figure 6-12 Carex at week 26.

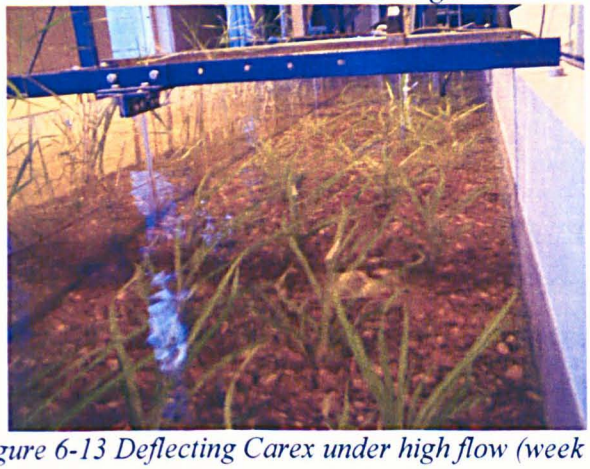

Figure 6-13 Deflecting Carex under high flow (week 10)

6.2.2.2 Cropped Carex

After 26 weeks of growth the added flow resistance of the Carex plants was sufficient to almost cause the channel to overtop (i.e. flow depth > 350mm). To continue testing and to investigate dense but low canopies the Carex were cropped and retested at three different heights, 25cm 13.5cm and 5.5cm (Figure 6-14 to Figure 6-16). These tests were conducted in quick succession so the size (stem diameter, leaf thickness etc) of the plants had changed little between the final growth test at week 26 and the cropped Carex tests. After cropping to 13.5cm and 5.5cm only the dense 'stubs' of the Carex remained. These stubs did not noticeably deflect under flow.

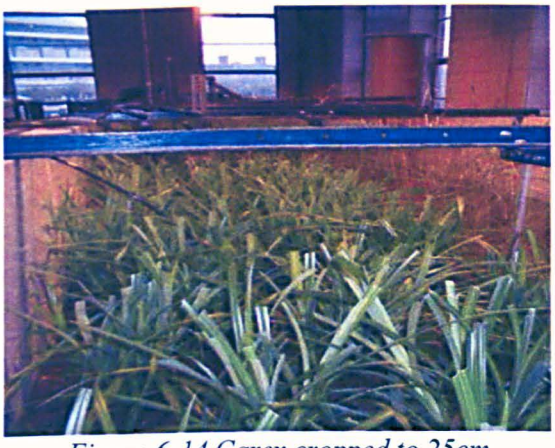

Figure 6-14 Carex cropped to 25cm

Figure 6-15 Carex cropped to 13.5cm

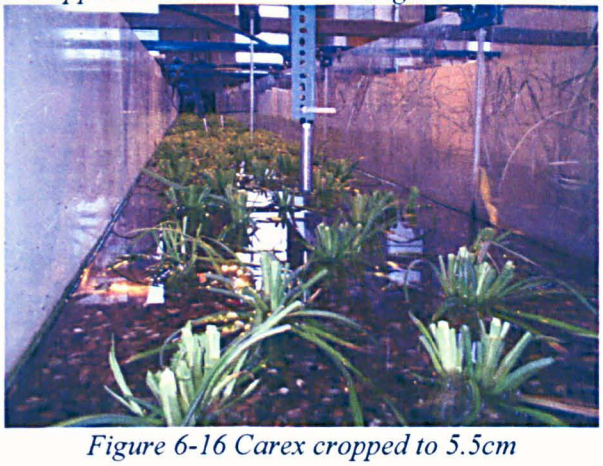

Figure 6-16 Carex cropped to 5.5cm

6.2.2.3 Reeds

The reeds were also first planted in the channel in October 2006. They experienced slower growth than the Carex, however the reeds still increased from a stem density of around 90 stems/m to 200 stems/m (Figure 6-17 and Figure 6-18). The plants were left in the channel until September 2007 when the final test was taken. The reeds were quite stiff and did not noticeably deflect under flow, although the small amount of leaves present on the stems did adopt a more streamlined position under high flows.

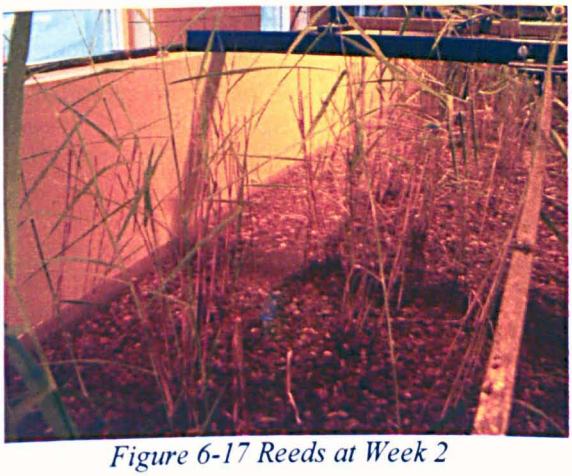

Figure 6-17 Reeds at Week 2

Figure 6-18 Reeds at week 50

6.2.3 Testing Program

Prior to the vegetated tests, a base case test was carried out. Flow resistance, profiles of velocity and Reynolds stress and transverse and longitudinal measurements were taken in a channel featuring no vegetation, in flow over the gravel bed (see section 5.3.1). Table 14 - Table 16 display the plant characteristics measured prior to and during each vegetated test. The age of the plants is expressed as weeks since they were planted into the channel. Tests were not conducted immediately after planting to give the plants time to establish. Plant characteristics are an average of 10 measured plants. Channel porosity, λ has been used as a measure of vegetation size and density by previous researchers such as Hoffman (2004). In this case channel porosity, λ can used to display the rate of growth and to compare growth between species. Channel porosity is estimated as

$$\lambda = 1 - \frac{PlantArea}{FlowArea} = 1 - \left[\frac{NbL\pi\left(\frac{S_d}{2}\right)^2}{bL} \right] = 1 - \left[N\pi\left(\frac{S_d}{2}\right)^2 \right] \qquad \text{Equation 6-2}$$

Both undeflected Carex height and deflected Carex height under maximum flow are presented (the maximum submergence ratio is calculated from this value). The height of the reeds was such that they were always tested in emergent conditions.

Table 14 – Growth Phase Carex Testing Characteristics

Age (weeks)	2	5	7	10	16	20	24	26
Canopy Height (un-deflected) (m)	0.150	0.200	0.250	0.275	0.300	0.300	0.350	0.350
Canopy Height (max deflection) (m)	0.110	0.120	0.160	0.182	0.195	0.220	0.270	0.280
Stem diameter, S_d (m)	0.010	0.015	0.020	0.030	0.040	0.045	0.050	0.055
Leaves/plant	6	10	15	20	30	40	50	50+
Maximum leaf width (m)	0.0050	0.0075	0.0100	0.0100	0.0125	0.0125	0.0150	0.0150
Maximum Submergence Ratio (Sr)	1.59	1.61	1.46	1.43	1.40	1.27	1.26	1.23
Channel Porosity, λ	0.9980	0.9956	0.9921	0.9823	0.9686	0.9602	0.9509	0.9406

Table 15 – Reeds Testing Characteristics

Age (weeks)	2	5	10	20	50
Stem density (Stems/m)	90	150	170	180	200
Stem width (m)	0.0020	0.0020	0.0025	0.0030	0.0030
Channel Porosity, λ	0.9995	0.9992	0.9986	0.9979	0.9976

Table 16 – Cropped Phase Carex Testing Characteristics

Age (weeks)	27	28	29
Canopy Height (undeflected) (m)	0.250	0.135	0.055
Canopy Height (max deflection) (m)	0.230	0.135	0.055
Stem diameter (m)	0.055	0.060	0.060
Leaves/plant	50+	50+	50+
Maximum leaf width (m)	0.015	0.015	0.015
Maximum Submergence Ratio (Sr)	1.40	1.80	2.90
Channel Porosity, λ	0.9406	0.9293	0.9293

6.2.3.1 Vegetation Properties

Figure 6-19 displays the comparative rate of growth of the Carex and reeds expressed as channel porosity (Equation 6-2). The rate of Carex growth was much greater than that of the reeds.

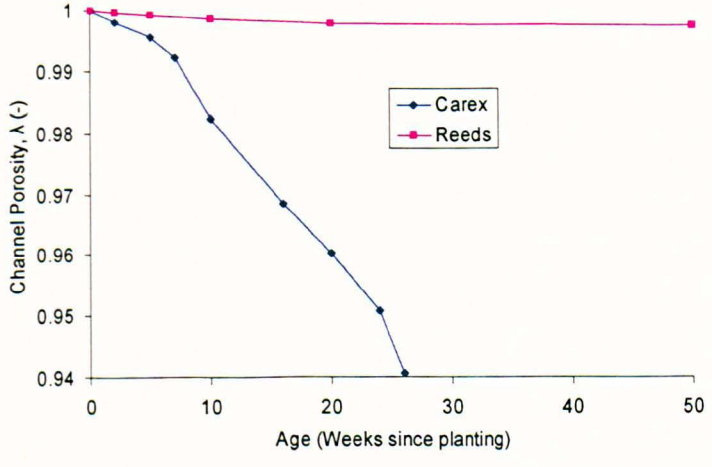

Figure 6-19 Plant Age and Porosity

In submerged conditions the proportion of flow within and above the canopy is also of interest. This proportion can be expressed as the submergence ratio Equation 3-2). The maximum submergence ratio achievable for each test is dependent on the maximum flow rate (fixed at 29.5l/s see section 5.2.3.3) and the height and flow resistance of the vegetation. Figure 6-20 shows the submergence ratio achieved at the maximum flow rate (≈ 29.5l/s) for each Carex test.

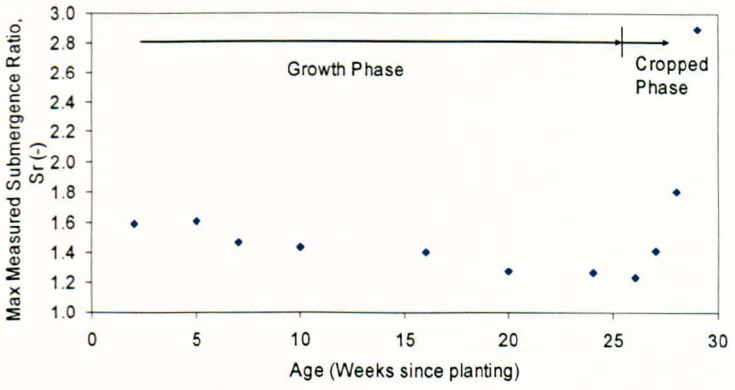

Figure 6-20 Maximum submergence ratio achievable with plant age

Figure 6-20 shows that as the Carex grows in height (with age) the proportion of the flow that is above the canopy at high flow decreases, thus decreasing the maximum achievable submergence ratio. After the vegetation is cropped to lower heights, the maximum achievable submergence ratio increases.

6.3 Measurements of Transverse Mixing Coefficient

Measurements of transverse mixing coefficient were made using the Boxall and Guymer (2001) method, outlined in sections 2.4.5.2 and 5.3.9. With knowledge of the channel average velocity (provided from the measured channel discharge and uniform depth values) and the ratio C_{min}/C_{max} at various discrete longitudinal locations downstream of the initial crossing distance, Equation 2-123 and Equation 2-124 can be used to quantify the transverse mixing coefficient at each location. From these values a mean is taken to represent the transverse mixing rate over the full reach and a standard deviation is taken to represent the experimental variability. Example of the ratio C_{min}/C_{max} at the measurement locations downstream of a continuous mid stream point source are displayed in Figure 6-21 and Figure 6-22.

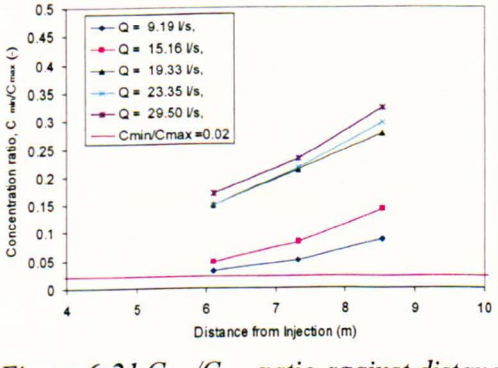

Figure 6-21 C_{min}/C_{max} ratio against distance (Base Case)

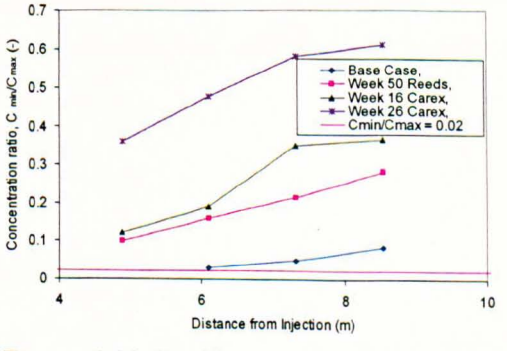

Figure 6-22 C_{min}/C_{max} ratio against distance for different vegetated conditions (Q= 8-10l/s)

As specified by Boxall and Guymer (2001) ratios below 0.02 or above 0.75 are unsuitable and are discarded. In the base case, three ratios were taken that fell within this specified range. In all

other vegetated cases four suitable measurements were taken. Once the C_{min}/C_{max} ratio is determined, the transverse mixing coefficient at each location can then be quantified using Equation 2-124 (Figure 6-23 and Figure 6-24).

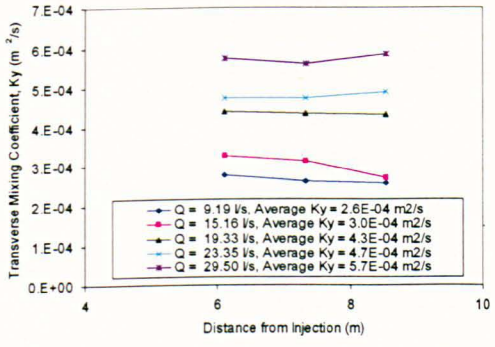

Figure 6-23 Transverse Mixing Coefficient against distance (Base Case)

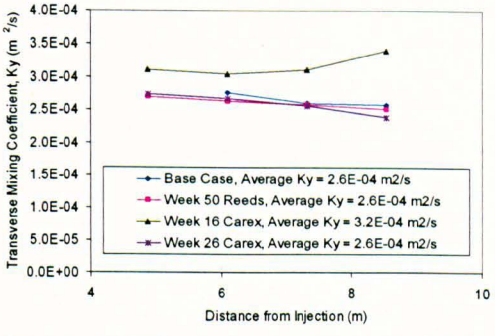

Figure 6-24 Transverse Mixing Coefficient against distance in various vegetated conditions (Q= 8-10l/s)

All transverse mixing coefficients quoted in this study are an average of the values measured in the channel, with error bars set at $\pm$ one standard deviation.

6.4 Flow Straightner Experiments

After conducting five sets of experiments (i.e. 16 weeks after initial planting) on the growing plants it was noticed that the transverse velocity profiles experienced a considerable distortion. Flow down the centre channel boundary was approximately 20% faster than flow down the edge boundary. It was a concern that this distortion may have an effect on the mixing processes in the reach and experimental results up to this point may give misleading values. Testing was suspended whilst this phenomenon was investigated. It was suggested that this distortion may be occurring due to the inlet condition. An additional investigation was undertaken to examine the effect of the inlet condition on the flow profiles and to determine if this has an impact on mixing in the studied reach. To do this transverse longitudinal, and vertical transverse velocity profiles were taken at various longitudinal positions downstream of differing inlet conditions, transverse and longitudinal mixing was also measured.

6.4.1 Inlets Used

Three different inlets were used in the following experiments (Figure 6-25).

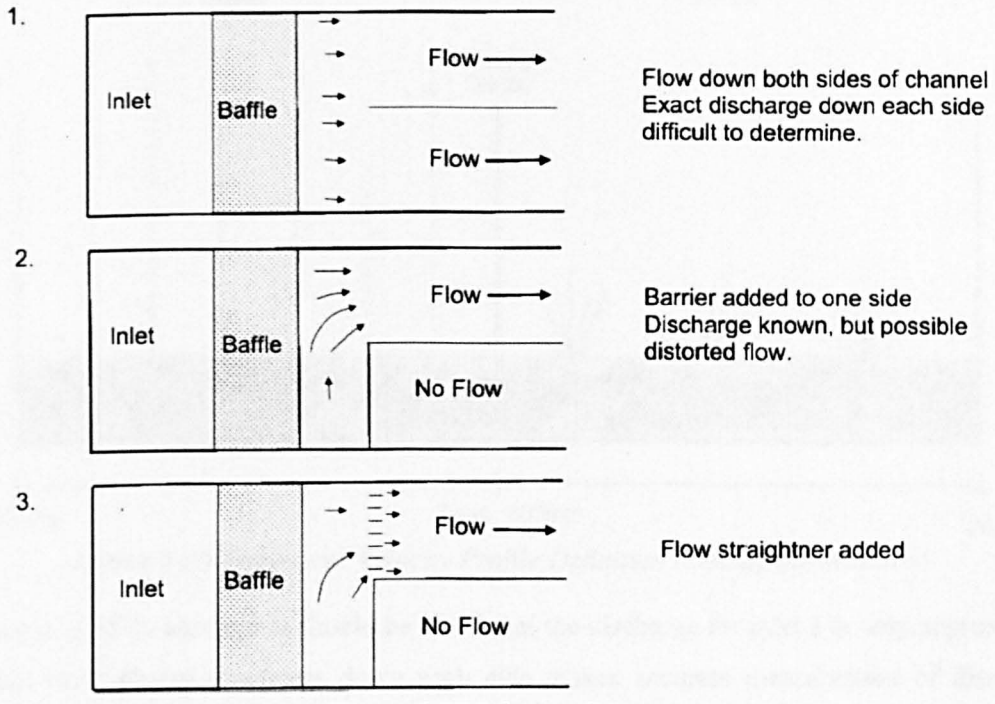

Figure 6-25 Inlet conditions

Experiments to determine the advective zone length (as described in section 6.1) were conducted using inlet 1. However all vegetation experiments up to this point had been conducted using inlet 2. This inlet was preferred to inlet 1 because

1. Higher flow rates are achievable by diverting all available flow down each channel section

2. Flow measured is total flow though the channel. If inlet 1 were used, estimating the flow rate down each side of the channel would involve errors due to the different resistance down each side of the channel.

However, inlet 2 may produce a distorted velocity profile due to the fact that the flow is forced suddenly from a wide flow inlet to a narrow channel. For these experiments a flow straightner (Inlet 3) was constructed. This should minimise any distorted velocity profiles which may be produced by inlet 2.

6.4.2 Impact on Transverse Profiles of Primary Velocity

To study the effect of the different inlets on flow, transverse profiles of velocity were taken at three longitudinal positions using each of the three inlet conditions. Looking down the channel, transverse profiles are taken from right to left. The reed side of the channel is presented here so 0mm is the 'centre' boundary (next to the divider) and 600mm is the edge 'boundary' (Figure 6-26).

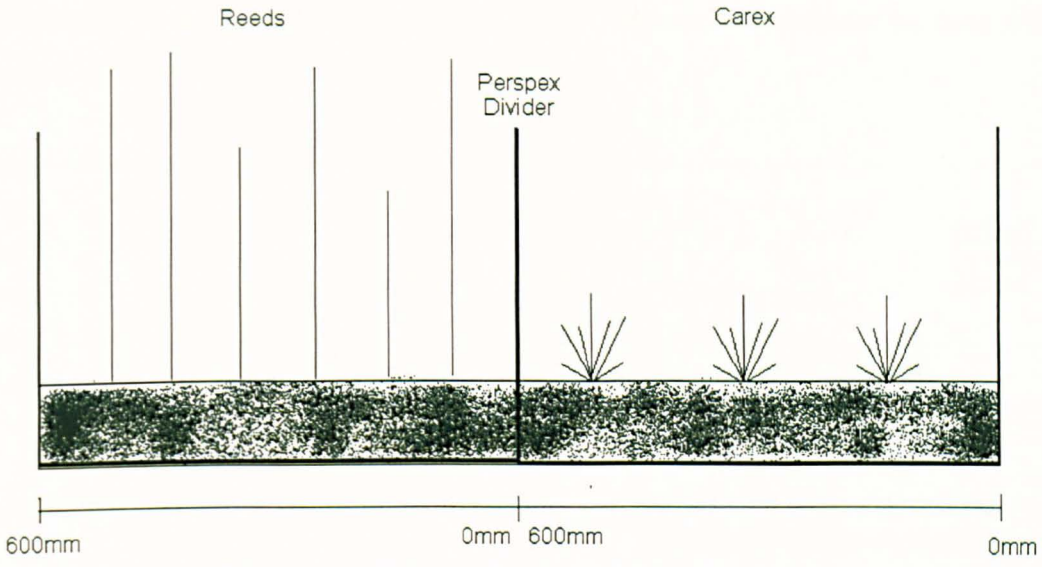

Figure 6-26 Transverse Velocity Profile Definition (looking downstream)

Discharge is 15 l/s although it should be noted that the discharge for inlet 1 is only approximate because the different roughness down each side makes accurate measurement of discharge difficult. Figure 6-27 to Figure 6-29 plot the transverse profiles of primary velocity at each longitudinal location, using each of the three inlet conditions.

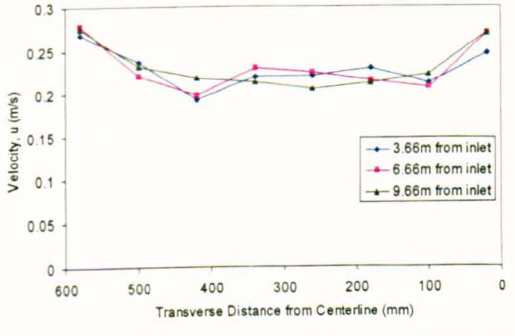

Figure 6-27 Transverse Profiles of Velocity (Inlet 1-Reeds)

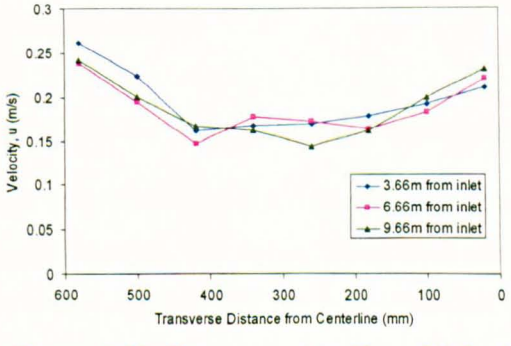

Figure 6-28 Transverse Profiles of Velocity (Inlet 2-Reeds)

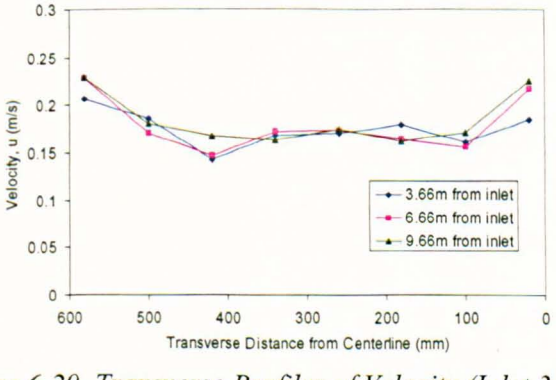

Figure 6-29 Transverse Profiles of Velocity (Inlet 3-Reeds)

Figure 6-27 to Figure 6-29 show that for all inlet conditions the flow is faster along the edge boundary (600mm) than the centre boundary (0mm). Figure 6-30 and Figure 6-31 show the

difference in the measured velocity (in %) at the two boundaries plotted for the three inlets in the reeds and the Carex.

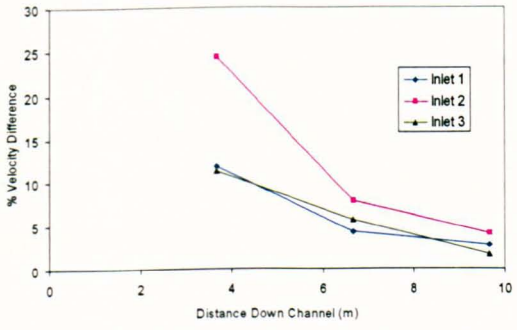

Figure 6-30 Difference in velocities at channel boundaries (Reeds)

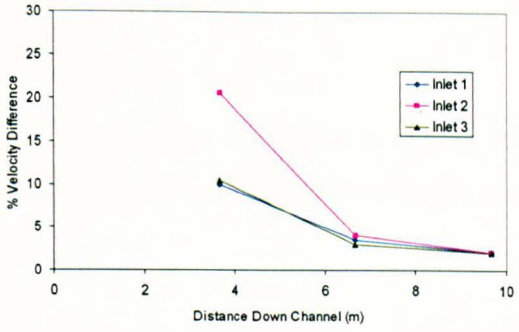

Figure 6-31 Difference in velocities at channel boundaries (Carex)

The levels of distortion decay down the channel, this suggests that the inlet is a major cause of the differential boundary velocity. Some distortion is always present irrespective of the inlet condition. However the problem is largest when inlet 2 is used. The addition of a flow straightner returns the magnitude of the distortion to its original condition (i.e. similar to inlet 1). Once the flow passes half way down the channel the difference is around 5%. After this distance the difference persists down the channel. This difference is probably not caused by the inlet, but a differential roughness between each side of the channel.

6.4.3 Impact on Vertical Profiles of Transverse Velocities

Transverse velocities were measured at the standard velocity section (i.e. 6.66m downstream of inlet) in both the reeds and the Carex for inlet conditions 2 and 3 (i.e. straightner and no straightner). A difference in transverse velocities would indicate that the inlet condition was creating flow structures within the channel, which would have an impact on transverse and longitudinal mixing. Figure 6-32 and Figure 6-33 show the profiles of transverse velocities measured in the reeds and the Carex with and without a flow straightner.

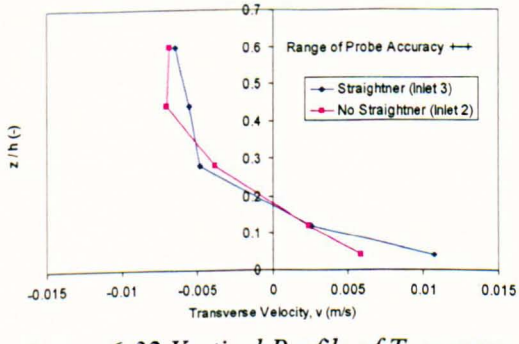

Figure 6-32 Vertical Profile of Transverse Velocities (Reeds)

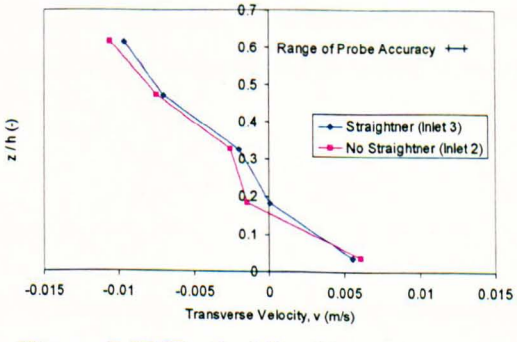

Figure 6-33 Vertical Profile of Transverse Velocities (Carex)

At the standard velocity section there is little difference in the profiles of transverse velocities with or without the flow straightner. The difference between the flow with the flow straightner and without usually falls within the specified error of the ADV probe (± 0.001m/s).

6.4.4 Impact on Transverse Mixing

Transverse mixing is measured using the centre/edge ratio method as detailed in section 5.3.9 and 6.3. Figure 6-34 and Figure 6-35 show the transverse mixing rates measured in the reeds and the Carex with and without a flow straightner.

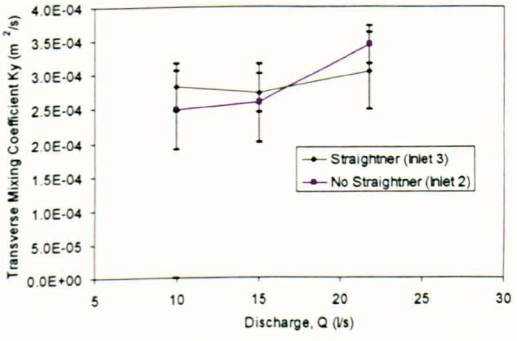

Figure 6-34 Transverse mixing in Reeds

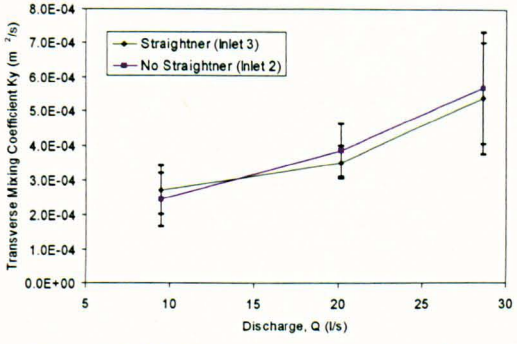

Figure 6-35 Transverse mixing in Carex

For both the reeds and the Carex case there is little significant difference in the values of transverse mixing for the two inlet conditions. Values taken for transverse mixing with no straightner fall within the error bars for the case with a straightner added. Any difference in secondary currents which might have caused differential transverse mixing seem to have decayed before the transverse mixing section has been reached. The addition of a flow straightner may not have changed the turbulence structure in the mixing reach.

6.4.5 Impact on Longitudinal Mixing

Longitudinal mixing experiments were conducted over the full 4.88m reach (as defined in section 6.2.1), quoted dispersion coefficients in Figure 6-38 and Figure 6-43 are an average of 3 repeat experiments, with error bars set at ± one standard deviation. Longitudinal mixing was first measured with the ADE in order to determine if a distorted velocity profile would have any effect on the dispersion coefficient.

6.4.5.1 Impact on the Reeds

Figure 6-36 and Figure 6-37 show example plots of the measured upstream and downstream longitudinal concentration profiles in the reeds, together with the ADE predicted traces (using both method of moments and optimised parameters).

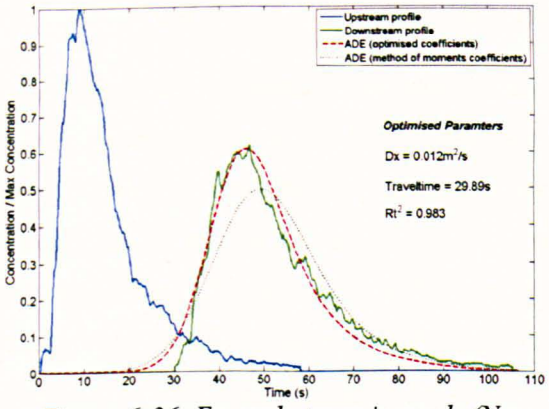

Figure 6-36 Example trace in reeds (No straightner)

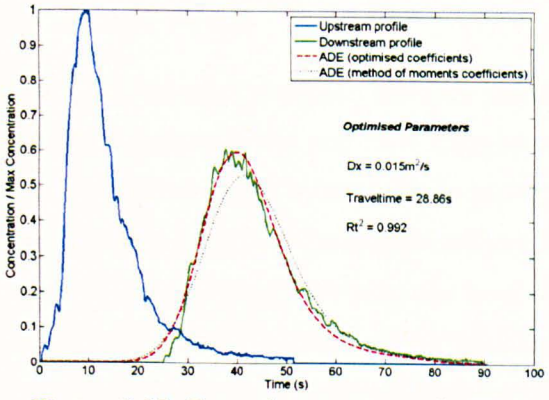

Figure 6-37 Example trace in reeds (With straightner)

Visual examination of the traces shows that the addition of a flow straightner to the channel both reduces the level of skew in the both the upstream and downstream concentration profiles, and improves the predicted traces goodness of fit. This may be because without a straightner the initial non-uniform velocity profile imparts extra initial skew into the concentration profile in the upstream section of the channel. With the straightner fitted any skew present has largely decayed before the trace enters the longitudinal mixing reach and the profiles are more symmetrical. This enables a better fit to the ADE (see section 2.4.4.3). Figure 6-38 shows the measured longitudinal dispersion coefficient in the reeds with and without a flow straightner for all discharges tested.

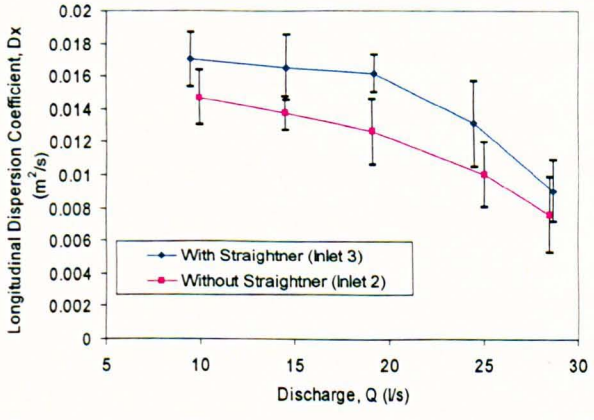

Figure 6-38 Dispersion coefficient in reeds with and without flow straightner

The longitudinal dispersion coefficient is approximately 20% higher when a flow straightner is added. The concentration profiles are more skewed and a lower dispersion coefficient is the result of the optimisation procedure attempting to fit the ADE prediction to such a skewed profile. This suggests that dispersion coefficients measured in the reeds up to this point in the testing program may have a significant error.

6.4.5.2 Skew Development through Reeds

The difference in dispersion coefficients found between the two inlet conditions has been linked to the visually larger levels of concentration profile skew present in the non flow straightner case. Similarly to the advective zone study (section 6.1) the development of skew can be plotted throughout the mixing reach for both inlet conditions. Previous reeds tests (conducted without a straightner) can also be examined. For clarity, in this and future plots of skew only one level of background cut off is displayed (0.8 %). From visual examination of the traces and the resulting skew values this level is judged to be the best compromise between the inclusion of background noise at low cut-offs and loss of result sensitivity at high cut-offs. Figure 6-39 plots the development of profile skew in the reeds tests with and without a flow straightner. Figure 6-40 plots the development of profile skew in all the reeds tests conducted up until the flow straightner experiments (i.e. all tests conducted without a flow straightner).

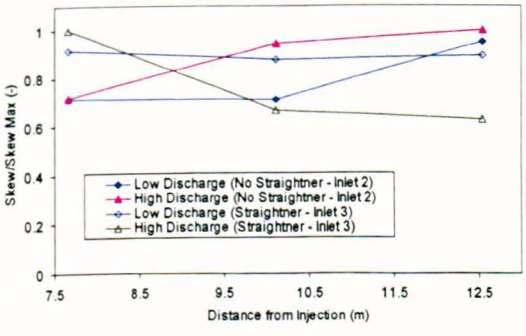

Figure 6-39 Skew development in reeds with and without straightner

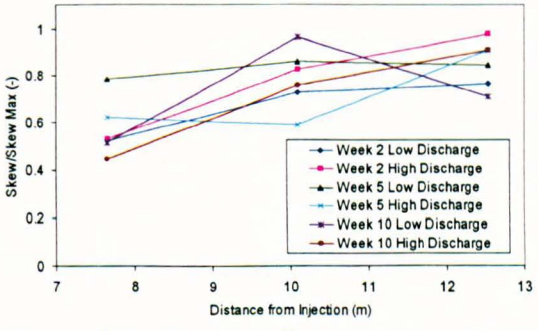

Figure 6-40 Skew development in reeds with age (weeks since planting) i.e. no straightner.

Figure 6-39 and Figure 6-40 show that, for all cases, skew increases in the reach when there is no straightner but decreases when a flow straightner is added. This shows that the inlet 2 condition imparts extra skew which is still developing within the reach.

Looking at the theoretical development of skew (Figure 2-11) it can be shown that adding a flow straightner to the reeds case moves the reach from an advective zone condition (skew increasing - not suitable for ADE analysis) to the equilibrium zone (skew decreasing- suitable for the ADE).

6.4.5.3 Impact on the Carex

Figure 6-41 and Figure 6-42 show example plots of the measured upstream and downstream measured longitudinal concentration profiles taken in the Carex together with the ADE predicted traces (using both method of moments and optimised parameters).

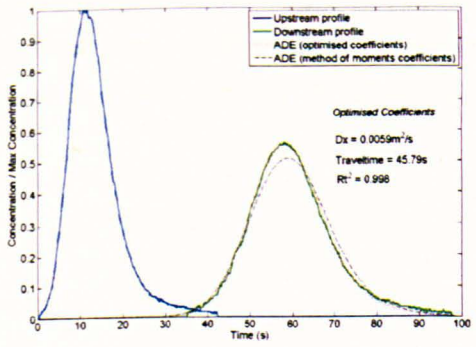

Figure 6-41 Example trace in Carex (No straightner)

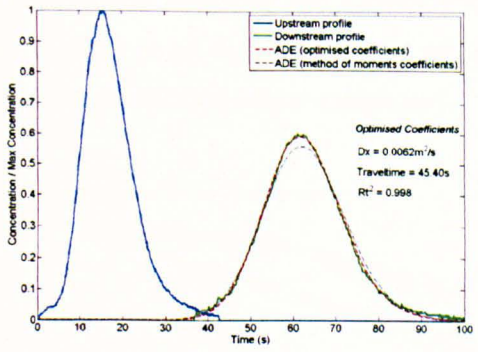

Figure 6-42 Example trace in Carex (With straightner)

Visual examination of the traces shows that with or without flow straightner, the profiles become roughly Gaussian within the reach. Unlike the reeds the Carex have a large volume which dominates the velocity profile. The volume of the Carex may have caused any extra skew created by the inlet to largely decay. Figure 6-43 shows the measured longitudinal dispersion coefficient taken in the Carex with and without a flow straightner for all discharges tested.

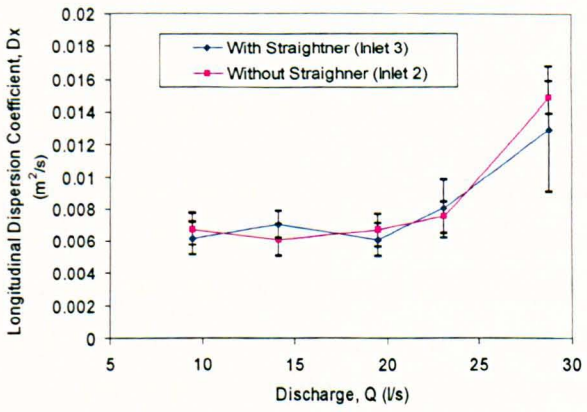

Figure 6-43 Dispersion coefficient in Carex with and without flow straightner

The straightner has no significant impact on the longitudinal dispersion coefficient through the Carex. The average values of dispersion coefficient for the non straightner case lie within the error bars of the straightner case.

6.4.5.4 Skew development in Carex

It is necessary to determine if tests conducted when the Carex plants were significantly smaller are also unaffected by the distorted velocity profile. To do this it is necessary to compare the development of skew in the tests conducted so far. If skew is decaying in the reach then the plants have had sufficient impact to negate the effects of the inlet condition prior to the mixing reach.

Figure 6-44 plots the development of profile skew in the Carex tests with and without a flow straightner. Figure 6-45 plots the development of profile skew in all the Carex tests conducted up until the flow straightner experiments (i.e. all test conducted without a flow straightner).

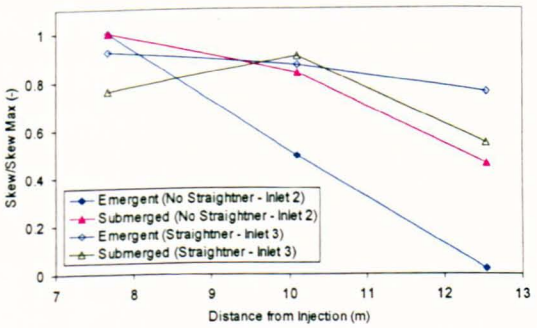

Figure 6-44 Skew development in Carex with and without straightner

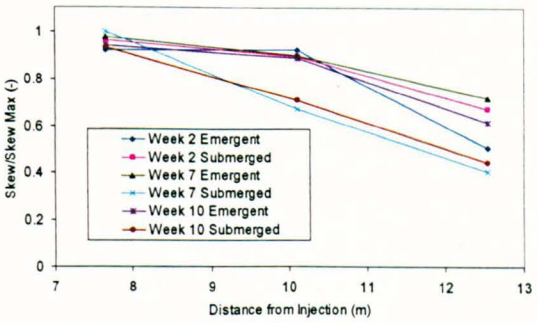

Figure 6-45 Skew development in Carex with age (weeks since planting) i.e. no straightner

In the Carex tests the skew decays for all cases even when the plants have just been planted (and are relatively small). This suggests that extra skew imparted by the inlet is decaying once the dye enters the reach. Therefore the values of dispersion coefficient should not be affected by the inlet condition in any of the Carex cases.

6.4.6 Conclusions of Flow Straightner Experiments

In the reeds case the inlet condition has had an impact on the mixing. Skew imparted by the inlet condition is still evident in the longitudinal mixing reach and mixing coefficients are altered. However, in the Carex case the mixing has not been affected irrespective of the inlet condition. This is probably due to the larger mass of plant causing any extra skew to decay before the mixing reach has been entered. It is therefore judged that the existing data from the Carex experiments are valid to be used. However all dye tracing data from the flow though the reeds up to week 20 is compromised and therefore not presented or used in the subsequent analysis. A revised reed testing timetable is presented (Table 17). Due to the slow growth of the reeds only a low age and a high age case were conducted. Base case tests were retaken with a flow straightner once the vegetation testing program was complete.

Table 17 – Reeds Testing Characteristics (Revised)

Age (weeks)	20	50
Stem density (Stems/m)	180	200
Stem width (mm)	0.003	0.003
Channel Porosity, λ	0.9979	0.9976

Hence, the reeds test at week 20 becomes a 'low stem density' test, and the test at week 50 provides a comparatively 'high stem density' test.

6.5 Model Applicability within the Mixing Reach

This section attempts to determine whether the ADE and ADZ models detailed in section 2.4.2 accurately describe the mixing processes in the base case, reeds, growing Carex and cropped Carex experiments over the mixing reach. Measured mixing coefficients and goodness of fit (Rt^2 –see Equation 2-150) parameters from each experimental case over both sub reaches (see Figure 6-10) are presented. For each condition, presented values are a mean of five repeat tests, with error bars set at one standard deviation. A number of example traces are also presented which show the measured upstream and downstream concentration distributions together with the optimised ADE and ADZ predictions.

6.5.1 Model Applicability in the Base Case

6.5.1.1 Example Traces in the Base Case

Figure 6-46 to Figure 6-49 show example plots of the measured upstream and downstream measured longitudinal concentration profiles taken in the base case with the optimised ADE and ADZ predicted traces. Example traces from both sub reaches conducted at low and high discharges are presented.

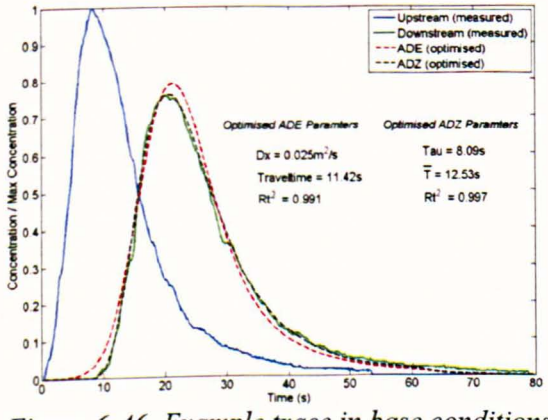

Figure 6-46 Example trace in base conditions (Reach 1, Q= 9.19l/s)

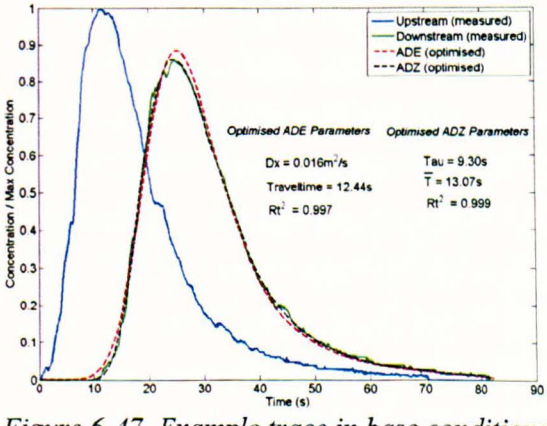

Figure 6-47 Example trace in base conditions (Reach 2, Q= 9.19l/s)

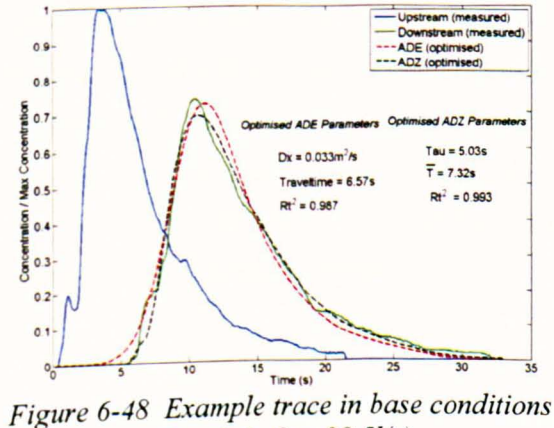

Figure 6-48 Example trace in base conditions (Reach 1, Q = 29.5l/s)

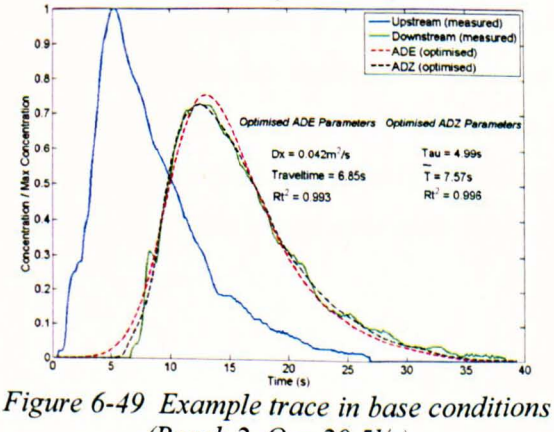

Figure 6-49 Example trace in base conditions (Reach 2, Q = 29.5l/s)

For the examples shown, the ADE and ADZ predicted traces match the observed downstream traces well over both sub reaches and at low and high discharges. To show results for all tests, average mixing and goodness of fit parameters can be examined for all tests conducted in the base case.

6.5.1.2 ADE Performance in the Base Case

Figure 6-50 and Figure 6-51 show the longitudinal dispersion coefficient and ADE goodness of fit over all flow rates tested for both sub reaches in the base case.

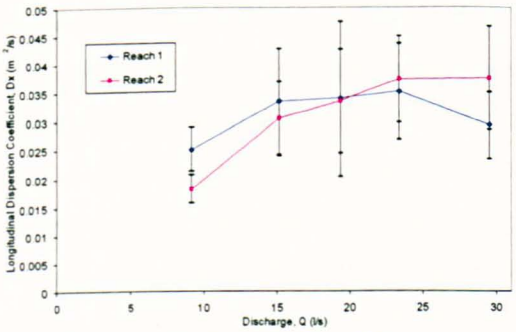

Figure 6-50 Longitudinal Dispersion Coefficient in Reach 1 and 2 (Base Case)

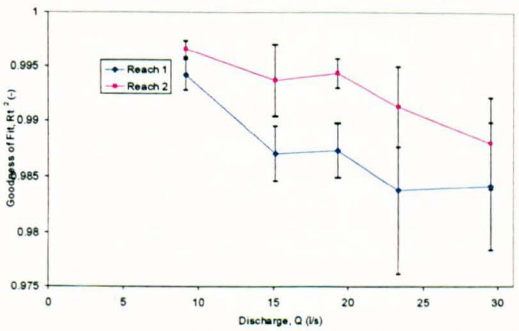

Figure 6-51 ADE 'Goodness of fit' in Reach 1 and 2 (Base Case)

Figure 6-50 shows that there is an observable difference in dispersion coefficient (approximately 15% on average) between sub reach 1 and sub reach 2. Figure 6-51 shows that the ADE produces a better quality of fit over sub reach 2 than sub reach 1 and that the quality of fit decreases with flow rate in both sub reaches. The study of the size of the advective zone (section 6.1) determined that the advective zone ended approximately 7.5 m downstream of the injection, However at high flow rates the advective zone length tended to be greater (approximately 8 - 8.5m in the 0.6m wide channel – see Figure 6-6). It is possible therefore that at the higher flow rates the upstream reach (which begins 7.66m downstream of the injection) may not entirely be within the equilibrium zone, and thus the ADE will not be accurately describing the mixing processes. Within the equilibrium zone the skew of the tracer profiles should decay over the reach (see Figure 2-11). To enable easy comparison of skew development the average percentage rate of skew decay for each test over the two sub reaches can be plotted. If the skew is decaying over the reach (skew decay > 0%) the tracer cloud will be within the equilibrium zone. The skew of each profile is calculated from moment analysis (as in section 6.1) with a cut off rate of 0.8%. In Figure 6-52 the average skew decay over each reach is plotted for each discharge tested.

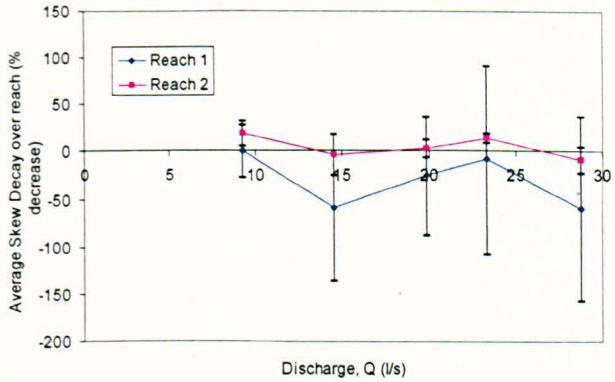

Figure 6-52 Development of skew over each reach (Base Case)

In reach 1 skew is increasing slightly (skew decay < 0) in most cases. In sub reach 2 this change in skew over the reach is smaller and in most cases skew is decaying over the reach. This would indicate that the end of the advective zone in the base case is somewhere within sub reach 1 in most cases. If the skew is increasing over the reach, the ADE will not accurately describe the mixing processes, and this explains why the goodness of fit is worse in sub reach 1 than sub reach 2. This growth in skew also causes the difference in dispersion coefficients over the two reaches as observed in Figure 6-50. This is due to the optimisation program attempting to fit the ADE model to a more skewed distribution with a relatively long tail. The advective zone study (Figure 6-6) and the high goodness of fit values ($Rt^2 > 0.985$ - Figure 6-51) suggest that sub reach 2, which begins 9.94m downstream of the injection, should remain within the advective zone for all flow rates.

6.5.1.3 ADZ Performance in the Base Case

Figure 6-53 and Figure 6-54 show the dispersive fraction and ADZ goodness of fit over all flow rates tested for both sub reaches in the base case.

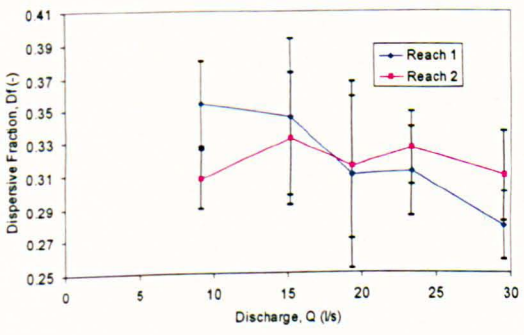

Figure 6-53 Dispersive Fraction in Reach 1 and 2 (Base Case)

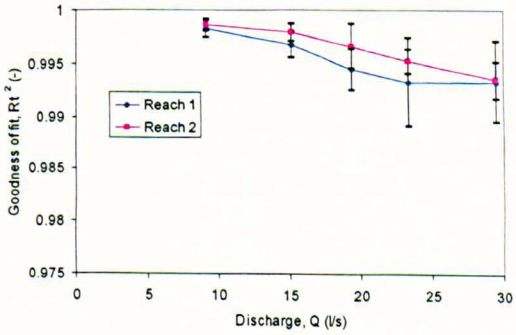

Figure 6-54 ADZ 'Goodness of fit' in Reach 1 and 2 (Base Case)

Figure 6-53 shows that on average there is a 7% difference in dispersive fraction over the two sub reaches. Figure 6-54 shows that Reach 2 provides a slightly better goodness of fit , although

the ability of the ADZ to predict an increase in skew (in sub reach 1) means that the model has an Rt^2 value of close to 1 in all cases (Figure 6-54).

6.5.2 Model Applicability in Reeds

6.5.2.1 Example Traces in Reeds

Figure 6-56 to Figure 6-58 show example plots of the measured upstream and downstream measured longitudinal concentration profiles taken in the reeds tests with the optimised ADE and ADZ predicted traces. Example traces are from sub reach 2, with low and high density reeds, conducted at low and high discharges.

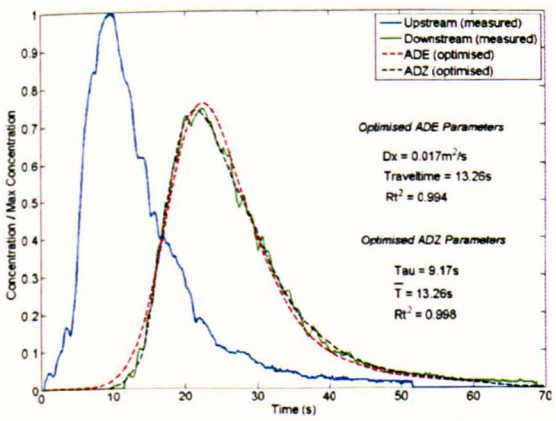

Figure 6-55 Example trace in reeds (Reach 2, Week 20, Q= 9.19l/s)

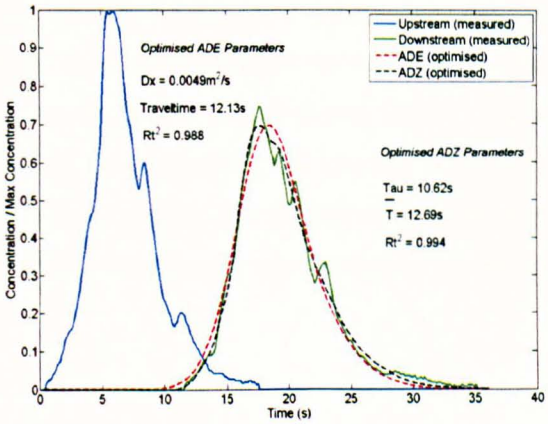

Figure 6-56 Example trace in reeds (Reach 2,Week 20, Q= 28.66l/s)

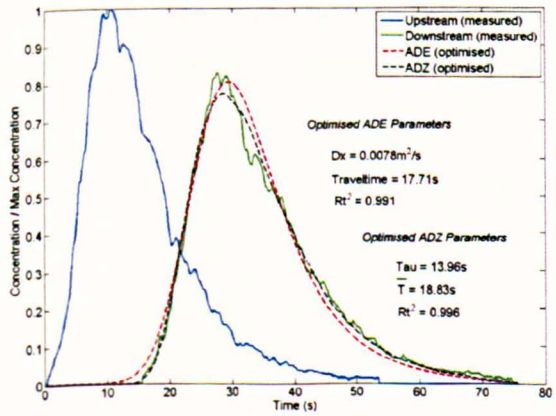

Figure 6-57 Example trace in reeds (Reach 2,Week 50, Q = 9.45l/s)

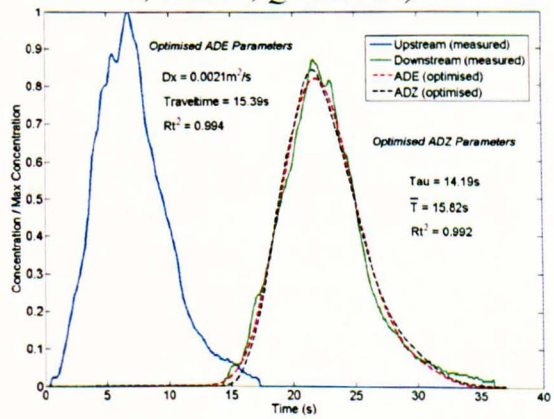

Figure 6-58 Example trace in reeds (Reach 2, Week 50, Q = 28.9l/s)

6.5.2.2 ADE Performance in Reeds

Figure 6-59 and Figure 6-60 show the longitudinal dispersion coefficient and ADE goodness of fit over all flow rates tested for both sub reaches in the low and high age reeds cases.

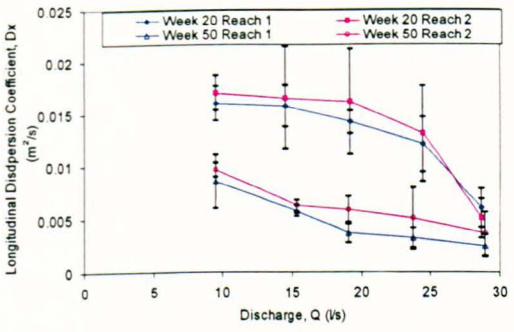

Figure 6-59 Dispersion coefficient in low and high density reeds over reach 1 and 2

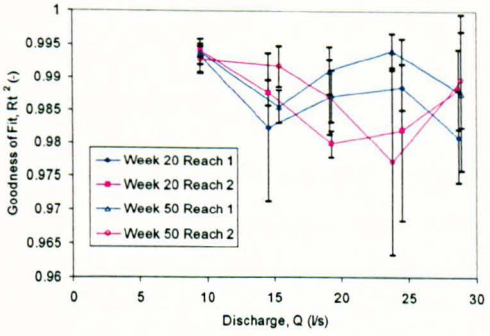

Figure 6-60 ADE 'Goodness of fit' in low and high density reeds over reach 1 and 2

Figure 6-59 shows that there is a 10% average difference between the dispersion coefficients over the two reaches. Figure 6-60 shows that in all cases the mixing in the reach is described accurately by the ADE ($Rt^2 > 0.975$). As shown in section 6.4.5.2 skew decays over the full mixing reach in emergent reeds. This indicates that in emergent vegetation the equilibrium zone occurs closer to the injection point than in base case conditions. This is due to the extra flow resistance provided by the vegetation (see section 3.1), which reduces the average velocity of the flow, causing the advective zone to be shorter (Equation 6-1). The difference in dispersion coefficient values is most likely caused by the natural variation in vegetation characteristics between the upstream and downstream sub reaches.

6.5.2.3 ADZ Performance in Reeds

Figure 6-61 and Figure 6-62 show the dispersive fraction and ADZ goodness of fit over all flow rates tested for both sub reaches in the low and high age reeds cases.

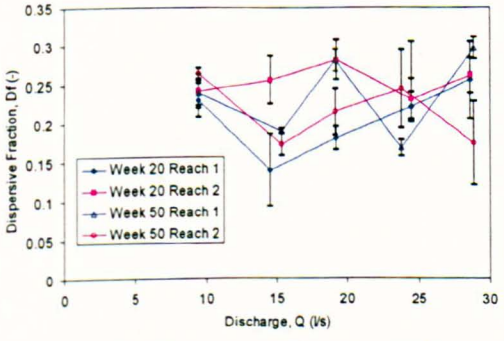

Figure 6-61 Dispersive Fraction in low and high density reeds over reach 1 and 2

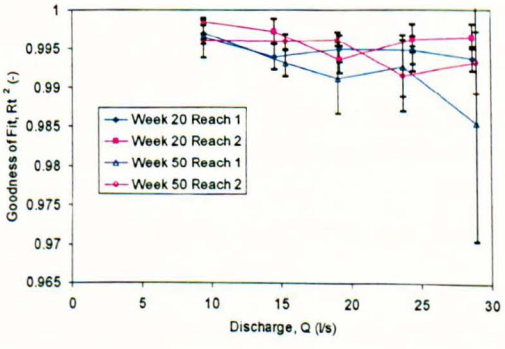

Figure 6-62 ADZ 'Goodness of fit' in low and high density reeds over reach 1 and 2

Figure 6-61 shows that there is a 20% average difference between the dispersive fraction over the two reaches. Figure 6-62 shows that the ADZ accurately describes the mixing processes in emergent reeds in all cases ($Rt^2 > 0.985$). The difference in dispersive fraction values is most likely caused by the natural variation in vegetation characteristics between the upstream and downstream sub reaches.

6.5.3 Model Applicability in Growing Carex

6.5.3.1 Example Traces in Growing Carex

Figure 6-63 to Figure 6-66 show example plots of the measured upstream and downstream measured longitudinal concentration profiles taken in the growing Carex tests with the optimised ADE and ADZ predicted traces. Example traces are from sub reach 2, with low and high density reeds, conducted at low and high discharges.

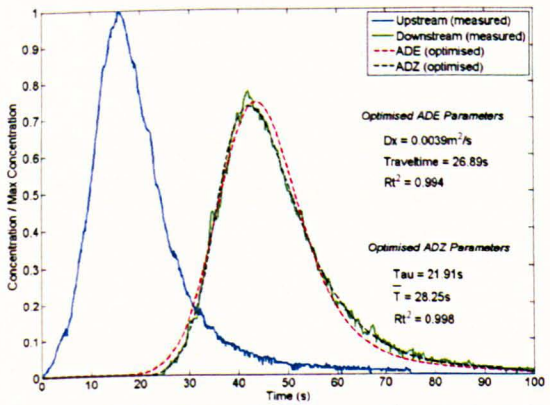

Figure 6-63 Example trace in Carex (Reach 2,Week 7, Q = 10.19l/s- emergent conditions)

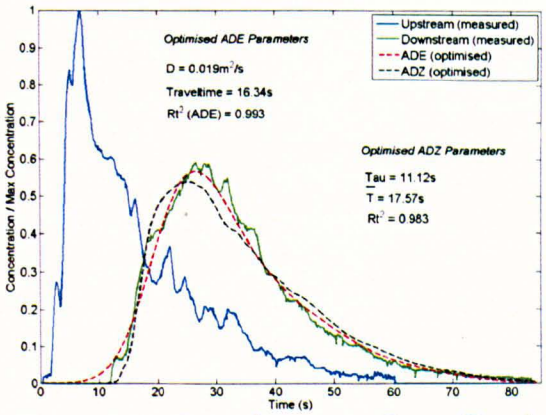

Figure 6-64 Example trace in Carex (Reach 2, Week 7, Q= 28.66l/s-submerged conditions)

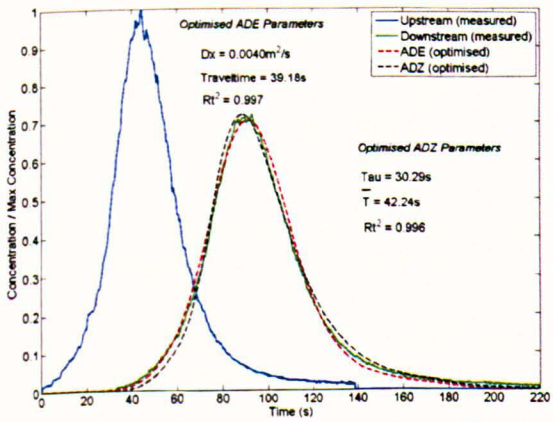

Figure 6-65 Example trace in Carex (Reach 2, Week 24, Q= 8.35l/s- emergent conditions)

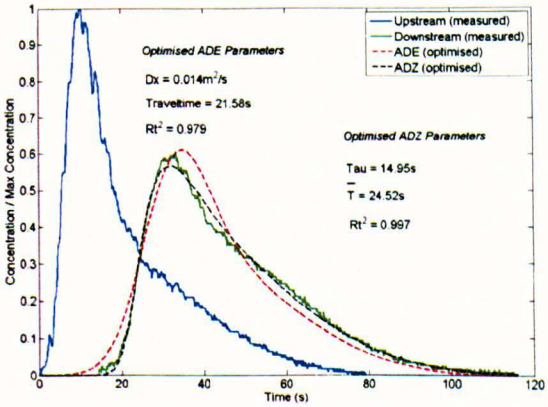

Figure 6-66 Example trace in Carex (Reach 2,Week 24, Q= 29.5l/s-submerged conditions)

At low discharges the Carex were in an emergent condition, whilst at high discharges the plants were submerged. Concentration profile skew in both upstream and downstream traces is noticeably larger in submerged conditions. Section 2.4.4.3 described how one of the initial effects of shear dispersion is to impart skew into the concentration profile. Submerged flow is subject to high levels of vertical shear (due to two layer flow - see section 3.2.2). Therefore the high skew levels present in Figure 6-64 and Figure 6-66 will be imparted into the profile by the presence of high vertical shear caused by two layer flow (however, such profiles can still be described by the ADE provided the skew is decaying over the measured reach). In contrast, the high density emergent Carex concentration profiles are approximately symmetrical, which

suggests that skew imparted by initially dominant differential advection has already almost fully decayed prior to the mixing reach. Due to the slow flow (travel time of approximately 46 seconds over the sub reach in the Carex compared with 12 seconds in the equivalent base case test, see Figure 6-47 and Figure 6-65) skew has had time to decay before the reach is entered. Also, the lack of high vertical shear in the emergent case means that levels of skew initially imparted are likely to be much smaller. This confirms the predictions of Fickian mixing theory as outlined in section 2.4.3.5 which suggest that concentration profiles will eventually become symmetrical if sufficient time has elapsed since injection.

6.5.3.2 ADE Performance in Growing Carex

Figure 6-67 and Figure 6-68 show the longitudinal dispersion coefficient and ADE goodness of fit over all flow rates tested for both sub reaches at two Carex ages (a low and high age Carex are displayed).

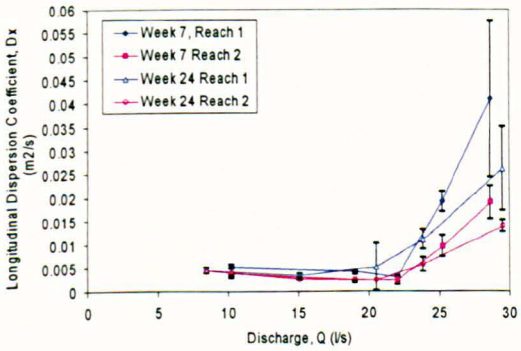

Figure 6-67 Dispersion coefficient in low and high density Carex over reach 1 and 2

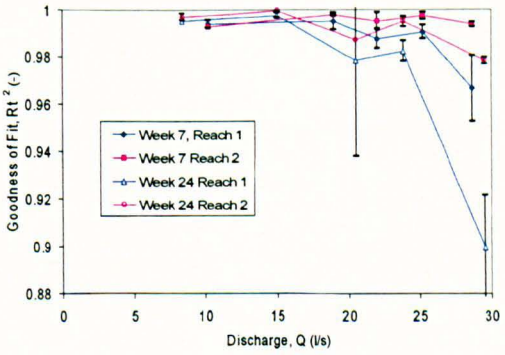

Figure 6-68 ADE 'Goodness of fit' in low and high density Carex over reach 1 and 2

Figure 6-67 shows that at low discharges whilst the Carex is in emergent conditions, the difference in dispersion coefficient between the two sub reaches is negligible. At high discharges the Carex becomes submerged, the dispersion coefficient increases and the measured dispersion coefficient over the two reaches varies significantly (average difference = 50%). Figure 6-68 shows that the ADE model describes the mixing very well in almost all cases ($Rt^2 >$ 0.98). The exception is the highest discharge condition through sub reach 1 ($Rt^2 \approx$ 0.90 and 0.96). The most likely explanation for this is that the upstream reach is on the edge of the advective zone for the maximum flow rate. To explore this variation further, the difference in dispersion coefficients between the sub reaches for all growing Carex tests is now explored. Figure 6-69 plots the average difference in dispersion coefficient between the two sub reaches for all tests conducted in the growing Carex relative to the dispersion coefficient obtained over the entire reach (set at 100%).

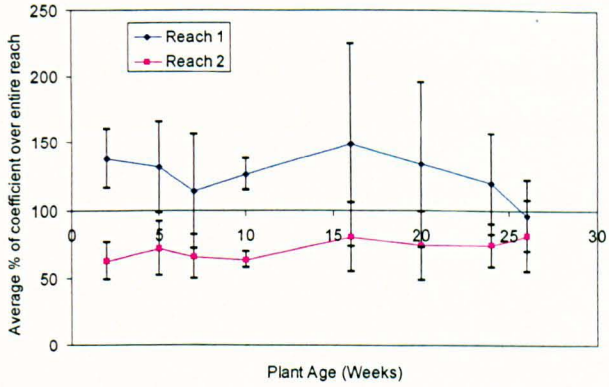

Figure 6-69 Average difference in dispersion coefficient for each sub reach

This shows that the difference in sub reaches is relatively constant with plant age/size. The difference may be due either to differential growth between the two reaches, or that the levels of skew are increasing over sub reach 1. To test this the average rate of skew decay for each test over the two sub reaches has been calculated.

Figure 6-70 and Figure 6-71 plot the average skew decay for all the Carex tests over sub reach 1 and sub reach 2 respectively.

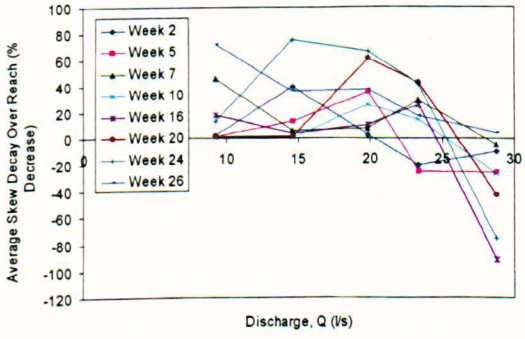

Figure 6-70 Skew decay over reach 1 in growing Carex

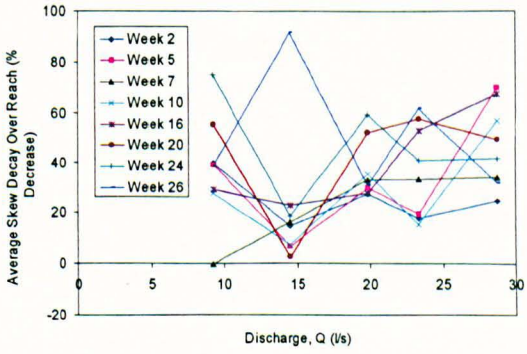

Figure 6-71 Skew decay over reach 2 in growing Carex

In sub reach 1 some tests conducted at higher discharges (i.e. submerged flow conditions) have a skew decay which is less than 0 (i.e. skew is increasing over the reach). At all flow rates in reach 2 skew is decaying over the reach. This suggests that at high discharges (in submerged flow) sub reach 1 is within the advective zone, leading to a poor quality of ADE fit over reach 1.

The advective zone is therefore larger in submerged flow than in equivalent emergent flow conditions. This is due to increased initial skew generation imparted by higher levels of differential advection (caused by two layer flow) and an increased average flow velocity (see section 3.2.2) due to some of the flow travelling above the vegetation (this directly affects advective zone length in Equation 6-1). As the size of the advective zone is increased relative to emergent flow conditions, sub reach 1 may not be entirely within the equilibrium zone.

6.5.3.3 ADZ Performance in Growing Carex

Figure 6-72 and Figure 6-73 show the dispersive fraction and ADZ goodness of fit over all flow rates tested for both sub reaches at two Carex ages (a low and high age Carex are displayed).

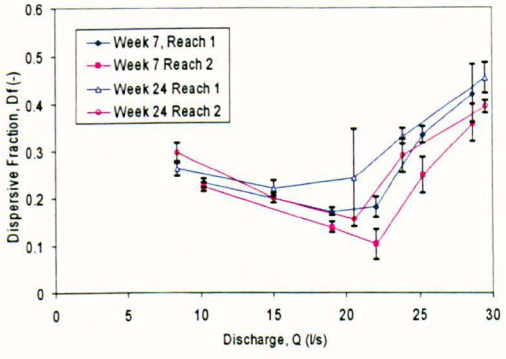

Figure 6-72 Dispersive fraction in low and high density Carex over reach 1 and 2

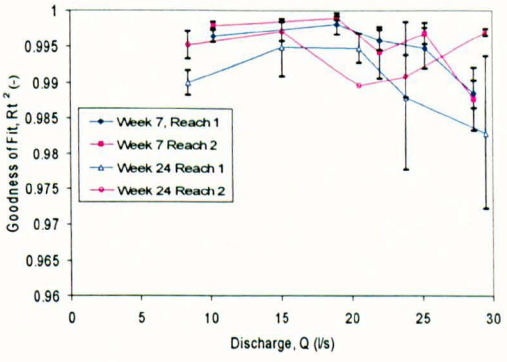

Figure 6-73 ADZ 'Goodness of fit' in low and high density Carex over reach 1 and 2

Figure 6-72 shows that there is a 20% average difference between the dispersive fraction values over the two sub reaches. Figure 6-73 shows that ADZ accurately describes the mixing processes in Carex in all cases ($Rt^2 > 0.97$).

6.5.4 Model Applicability in Cropped Carex

6.5.4.1 Example Traces in Cropped Carex

Figure 6-74 and Figure 6-75 show example plots of the measured upstream and downstream longitudinal concentration profiles taken in the cropped to 13.5cm Carex tests with the optimised ADE and ADZ predicted traces.

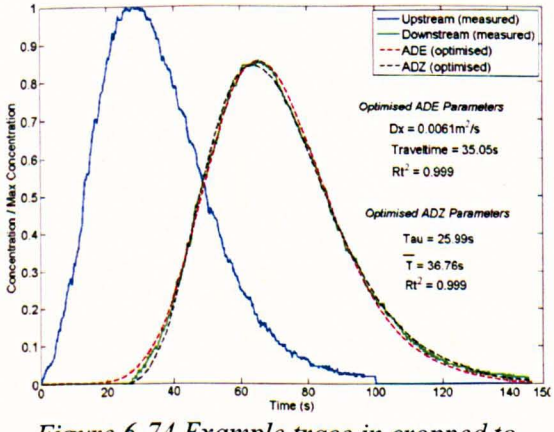

Figure 6-74 Example trace in cropped to 13.5cm Carex (Reach 2, Q= 6.32l/s, emergent conditions)

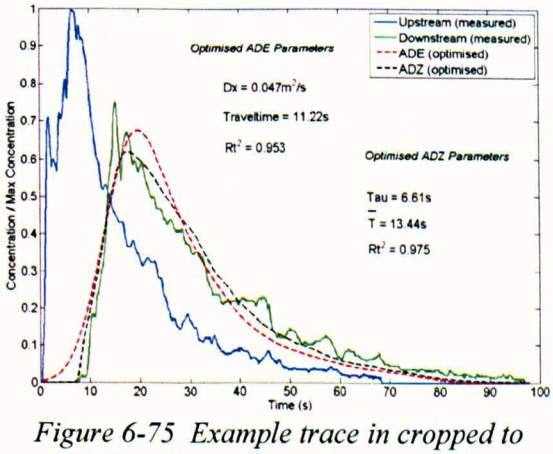

Figure 6-75 Example trace in cropped to 13.5cm Carex (Reach 2, Q= 29.5l/s, submerged conditions)

At low discharges the Carex were in an emergent condition, whilst at high discharges the plants were submerged. Concentration profile skew in both upstream and downstream traces is noticeably larger in submerged than emergent conditions for similar reasons to the submerged growth stage Carex.

6.5.4.2 ADE Performance in Cropped Carex

Figure 6-76 and Figure 6-77 show the longitudinal dispersion coefficient and ADE goodness of fit over all flow rates tested for both sub reaches in cropped to 13.5cm Carex.

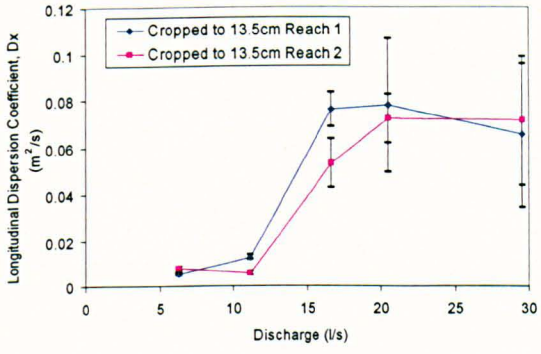

Figure 6-76 Dispersion coefficient in cropped Carex over reach 1 and 2

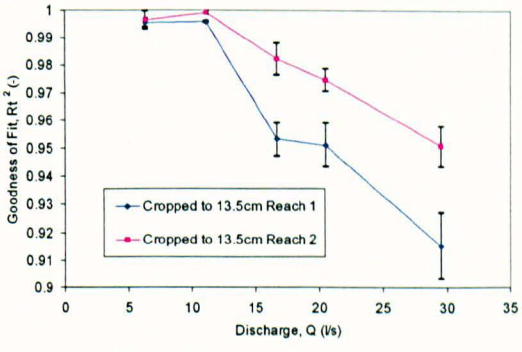

Figure 6-77 ADE 'Goodness of fit' in cropped Carex over reach 1 and 2

Figure 6-76 shows that there is a 25% difference between the dispersion coefficient values between the two sub reaches. Figure 6-77 shows that after the first two flow rates the goodness of fit declines for both sub reaches. Similarly to the previous cases, to determine if the trace is within the equilibrium zone the development of skew over the reach can be plotted. Figure 6-78 plots skew decay for each sub reach in cropped to 13.5cm Carex.

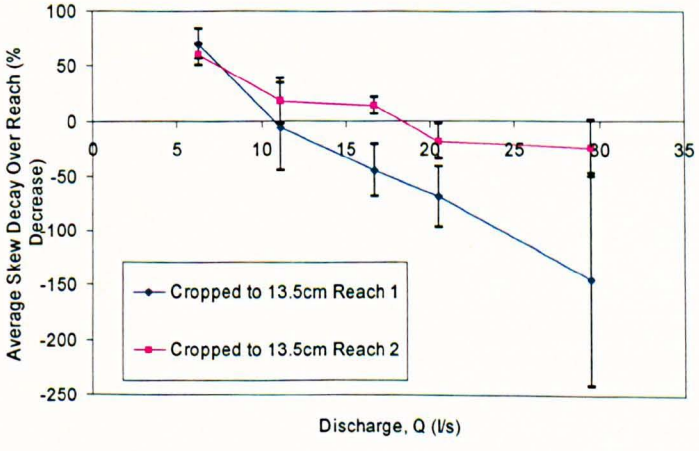

Figure 6-78 Skew decay against discharge (Cropped to 13.5cm Carex)

Skew decay declines with discharge for both reaches, becoming negative and thus unsuitable for the ADE at high flow rates. Similarly to the sub reach 1 growth stage Carex, the ADE goodness

of fit becomes poor when the vegetation becomes submerged. However, in the cropped case this affects both sub reaches. Results for all cropped tests in the downstream sub reach can be examined to determine if this affects all cropped Carex tests. Figure 6-79 and Figure 6-80 plot the goodness of fit of the ADE and the decay of skew for all cropped Carex tests against submergence ratio over sub reach 2.

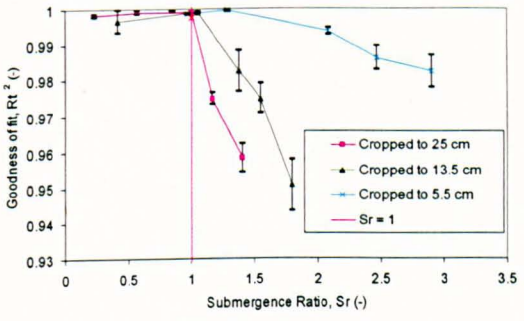

Figure 6-79 ADE 'Goodness of fit' in cropped Carex (sub reach 2)

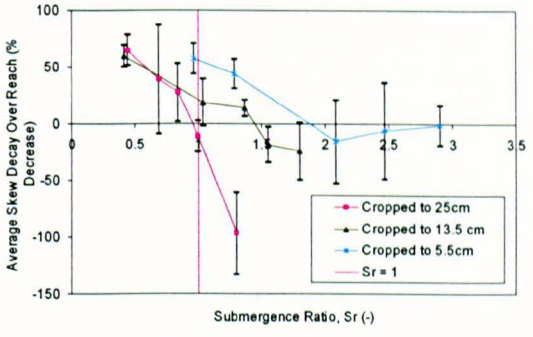

Figure 6-80 Skew decay against submergence ratio in cropped Carex (sub reach 2)

Figure 6-79 shows that after the vegetation becomes submerged the quality of fit declines. Figure 6-80 shows that once the flow becomes submerged and two layer flow is set up the skew begins to increase over the channel reach. This explains why the ADE model does not describe the mixing in the channel when the cropped Carex is in a submerged condition. Unlike in the growth phase this increase in skew affects both sub reaches. Hence, in the cropped Carex case the size of the advective zone is increased beyond that found in the growth Carex phase or the base case.

6.5.4.3 ADZ Performance in Cropped Carex

Figure 6-81 and Figure 6-82 show the dispersive fraction and ADZ goodness of fit over all flow rates tested for both sub reaches in cropped to 13.5cm Carex.

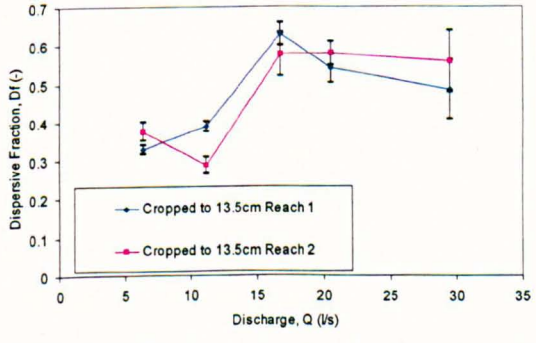

Figure 6-81 Dispersive fraction in cropped Carex over reach 1 and 2

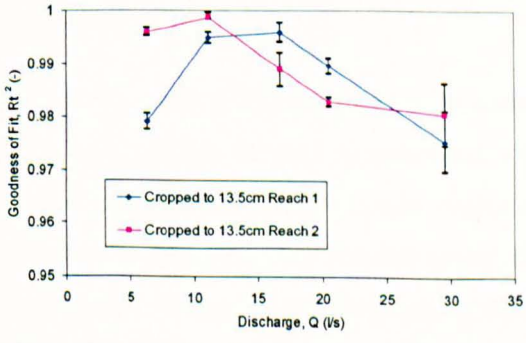

Figure 6-82 ADZ 'Goodness of fit' in cropped Carex over reach 1 and 2

Figure 6-81 shows that there is a 14% difference between the dispersive fraction over the two sub reaches. Figure 6-82 shows that after the first two discharges the goodness of fit declines for both sub reaches. The ADZ model is however, better at describing the mixing in two layer flow in the cropped vegetation phase than the ADE (ADE average $Rt^2 = 0.975$, ADZ average $Rt^2 = 0.988$). Figure 6-83 shows the average goodness of fit of the ADZ for the tests conducted in the cropped Carex.

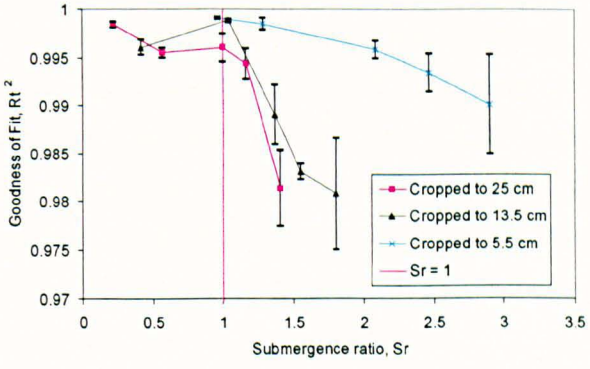

Figure 6-83 ADZ 'Goodness of fit' in cropped Carex (reach 2)

Similarly to the ADE, the quality of fit declines once the cropped Carex becomes submerged. However, the Rt^2 values are significantly higher than the ADE which is due to the capability of the ADZ to predict skew.

6.5.5 Conclusions from Model Applicability Tests

In the base case poor goodness of fit values and increasing concentration profile skew indicate that the trace is not within the equilibrium zone over sub reach 1. However, in sub reach 2 decaying levels of skew suggest that the tracer cloud is within the equilibrium zone. This supports the findings of the advective zone study (section 6.1), which suggested that in the base case channel, set at 0.6m width, the advective zone would end approximately 7.5-8.5 m downstream of the injection point. In the base case the ADE is therefore best used over reach 2 only. The ADZ provides a good quality of fit over both reaches.

In the tests through emergent vegetation (reeds and Carex) mixing follows Fickian processes over the entire reach, the skew of the profiles decay and profiles become symmetrical. The higher resistance and thus slower velocities which occur in vegetated relative to non vegetated flow mean the advective zone is short. In this case skew is decaying over the full reach, the differences in mixing over the two reaches are negligible, and mixing is described well by either the ADE or ADZ models. In the high age Carex tests the flow resistance is very high, resulting in slow flow, as a result traces have sufficient time to become almost symmetrical prior to the mixing reach.

Submerged, two layer flow increases initial skew generation and delays the beginning of the advective zone relative to the emergent cases. Plots of skew development suggest that sub reach 1 is unsuitable for the ADE, but that the trace has entered the equilibrium zone before sub reach 2. The ADE provides a good quality of fit over the downstream sub reach. The ADZ model accurately models mixing over both reaches.

In submerged, cropped vegetation high levels of initial skew generation and faster average flow means that none of the mixing reach is within the equilibrium zone. In this case the ADE fails to describe mixing well over either sub reach. The ADZ predicts mixing more accurately in these conditions however the quality of fit also declines with increasing submergence. To accurately model longitudinal mixing over this reach would require a higher order model as described in section 2.4.9; such higher order modelling is not undertaken in this thesis. Longitudinal mixing coefficients measured in the cropped phase will be used in the results section, however it should be noted that these results may not be representative of coefficients for equilibrium zone mixing.

In the base case and submerged Carex cases the skew of the concentration profiles often increases over sub reach 1. If this reach is considered, it may provide non representative ADE mixing parameters. Therefore from this point onwards, to provide a comparative reach, mixing parameters used to characterise the longitudinal mixing properties of all tests conducted shall be calculated from sub reach 2. Both ADE and ADZ models shall be considered. When comparing results from the cropped tests it should be remembered that the mixing parameters may not be representative of values taken in equilibrium conditions.

Chapter 7 - Summary of Results and Discussion

This chapter presents a summary of the results from the testing program and a discussion on how vegetation influences flow resistance, profiles of velocity, turbulence and transverse and longitudinal mixing in the experimental channel. To provide a measure of plant growth tests are classified by plant age and/or channel porosity as detailed in section 6.2 (Figure 6-19). Further details on how plant age relates to plant size and density parameters can be found in Table 14 (growing Carex), Table 17 (Reeds), and Table 16 (cropped Carex).

7.1 Flow Resistance Results and Discussion

This section investigates the impact of vegetation on the flow resistance of the channel. An understanding of the resistance characteristics of the channel is important for determining the accuracy of the flow resistance prediction methods introduced in chapter 3. Stage discharge relationships and cross sectionally averaged velocity measurements are presented for the experimental cases. Bulk flow resistance and velocity parameters are derived and discussed. Using the measurements taken, there are three possible ways of measuring cross sectionally averaged channel velocity, (U).

1. Using measurements of stage and discharge and the continuity equation (Equation 2-1).
2. Using measurements of optimised travel time over sub reach 2 (from the ADE) and reach length from longitudinal mixing experiments.
3. Spatially averaging ADV probe measurements for each flow rate.

In the travel time method (2), velocities are calculated from an average of 5 travel times from each of the traces conducted at each flow rate, this allows the calculation of error bars which are set at one standard deviation from the mean.

7.1.1 Flow Resistance in the Base Case

This section presents the result of the flow resistance experiments carried out in the base case (i.e. over a gravel bed, (D_s = 10mm) with no vegetation – see section 5.1). Figure 7-1 displays the measurements of average velocity in the base case measured using the three methods.

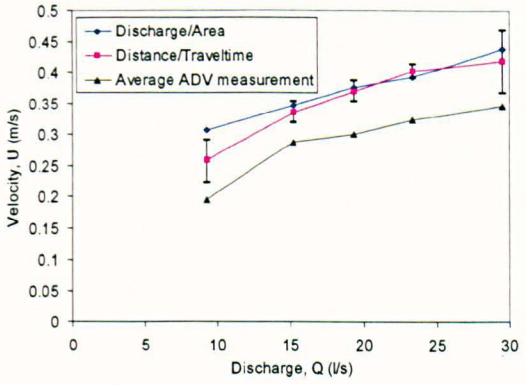

Figure 7-1 Velocity comparison - base case

In all methods the average velocity increases with flow rate. The average difference in the discharge/area method and the travel time method is 4%. The velocity measured using the ADV probe is on average 22% smaller than the discharge area method. Figure 7-2 shows the stage discharge relationship for the base case. The theoretical stage discharge relationship according to the Manning's equation (see section 2.2.2) is also plotted using the best fit 'n' value which in this case was found to be 0.015 (regression value, $R^2 = 0.999$). Figure 7-3 shows that the flow velocity (from the discharge area method) in the base case is proportional to the product $R^{2/3}S_o^{1/2}$ ($R^2 = 0.956$).

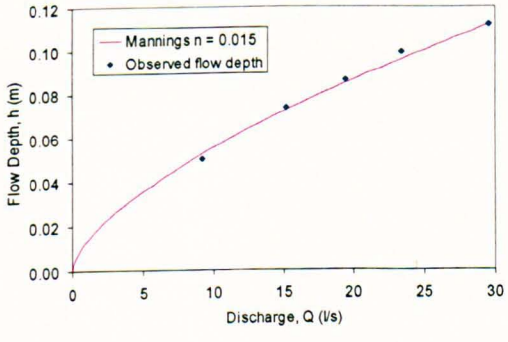

Figure 7-2 Stage discharge in the base case

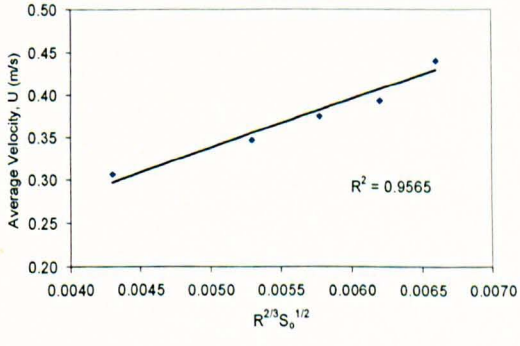

Figure 7-3 Relationship between U and $R^{2/3}S_o^{1/2}$

According to Equation 2-11, a proportional relationship between average velocity and $R^{2/3}S_o^{1/2}$ means that Manning's n will be constant over the flow depth.

7.1.2 Flow Resistance of Reeds

This section presents the result of the flow resistance experiments carried out when reeds were present in the channel. As detailed in section 5.2.1.2 the flow depth is always lower than the height of the reeds and hence the flow condition is always emergent. Figure 7-4 and Figure 7-5 display the measurements of average velocity in the low (i.e. week 20) and high age (i.e. week 50) reeds using the three methods.

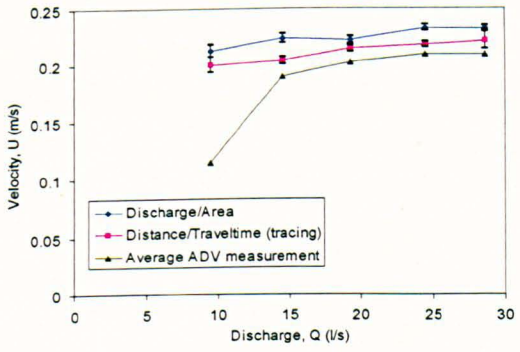

Figure 7-4 Velocity comparison - Reads (Week 20)

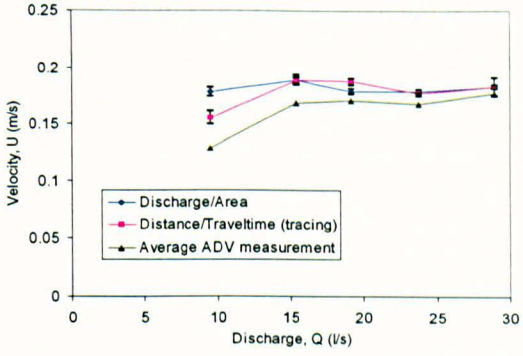

Figure 7-5 Velocity comparison - Reads (Week 50)

The average difference in the discharge/area method and the travel time method is 4%. The velocity measured using the ADV probe is on average 13% smaller than the discharge/area method. The ADV measurement at the lowest discharge is significantly (i.e. ≈ 100%) lower than the other methods. This may be due to local effects of vegetation, or because in this case, the ADV probe was positioned close enough to the bed to be influenced by bed roughness. The flow velocity in the reeds increases only slightly with flow rate in the week 20 reeds, while in the week 50 reeds the velocity is approximately constant with increasing flow rate.

The flow velocity through the high age reeds is lower than in the low age reeds, (week 20 average = 0.224 m/s, week 50 average = 0.182 m/s – using discharge/area method). Figure 7-6 shows the stage discharge relationship measured in low and high age reeds. As a comparison, the best fit Manning's relationship for the base case is also displayed (n = 0.015).

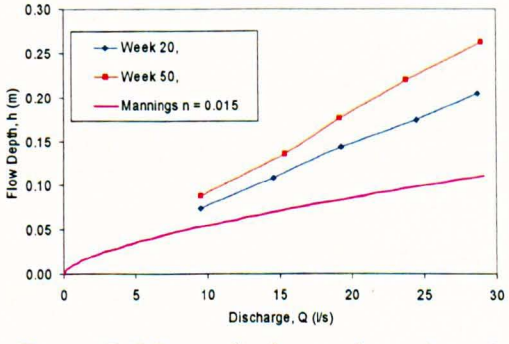

Figure 7-6 Stage discharge through reeds

The (on average) increasing flow depth achieved as the channel condition changes from the base case to low, then high age reeds, indicates that the channel resistance has increased with the addition of and subsequent growth of the reeds.

7.1.3 Flow Resistance of Emergent Carex (Growth)

This section presents the result of the flow resistance experiments carried out when growing Carex were present in the channel and the flow conditions were emergent. Average flow

velocities are displayed over the full flow range within the submerged Carex section. Figure 7-7 shows the stage discharge relationship in the channel at various Carex ages. As a comparison, the best fit Manning's relationship for the base case is also displayed.

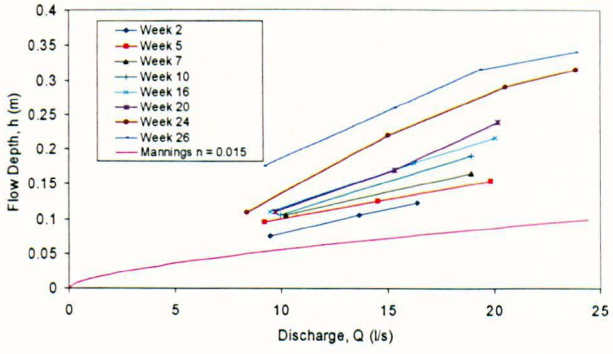

Figure 7-7 Stage discharge through emergent Carex

The higher (on average) flow depth achieved as the Carex increase in age (and size – see section 6.2.2) indicates that the channel resistance increases with Carex growth.

7.1.4 Flow Resistance of Submerged Carex (Growth)

This section presents the result of the flow resistance experiments carried out when growing Carex moved from emergent to submerged conditions. Cross sectionally averaged velocities over the entire flow range are also presented. Figure 7-8 and Figure 7-9 display the measurements of average velocity in the low and high age emergent Carex respectively measured using the three methods.

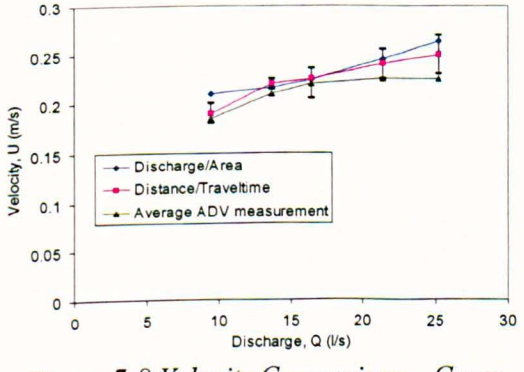

Figure 7-8 Velocity Comparison – Carex (Week 2, submerged at 21.33l/s and 25.22l/s)

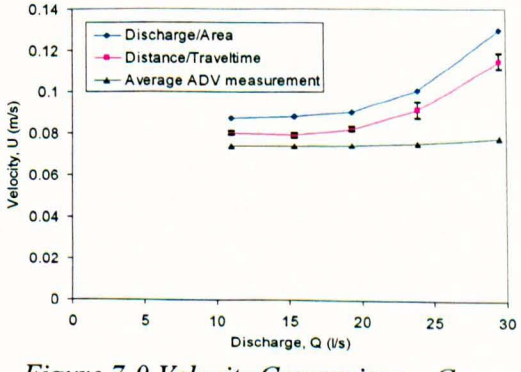

Figure 7-9 Velocity Comparison – Carex (Week 26, submerged at 29.50l/s)

In the low age Carex the velocity increases with discharge over the entire flow range, before and after submergence. In high age Carex, the velocity remains roughly constant with discharge at first, but then increases at higher flow rates when the Carex moves closer to submerged conditions. The average difference between the discharge/area method and the travel time method is 4% in the low age Carex and 10% in the high age Carex. The velocity measured using

the ADV probe is 8% smaller than the discharge area method in the low age Carex; and 23% in the high age Carex. Figure 7-10 shows the stage discharge relationship in the channel at various Carex ages. To give an indication of the effect of submergence, stage is now expressed as submergence ratio (see Equation 3-2). The point of submergence, Sr = 1 is also highlighted.

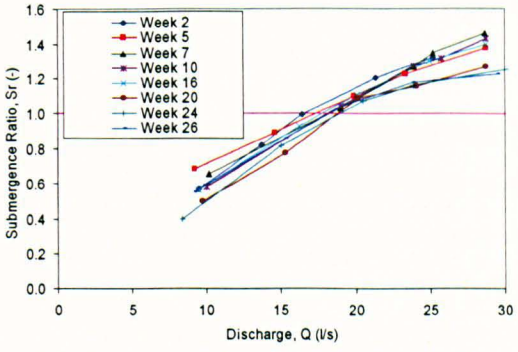

Figure 7-10 Discharge and submergence ratio through Carex

The submergence ratio of the flow is dependant on the flow resistance of the plants (which increases with age), the height of the plants and the flow in the channel.

7.1.5 Flow Resistance of Submerged Carex (Cropped)

The results of the flow resistance experiments conducted in cropped Carex are now presented. To give an indication of the effect of submergence, stage is expressed as submergence ratio. Figure 7-11 shows the stage discharge relationship in the channel after the Carex was cropped to different heights. The point of submergence, Sr = 1 is also highlighted.

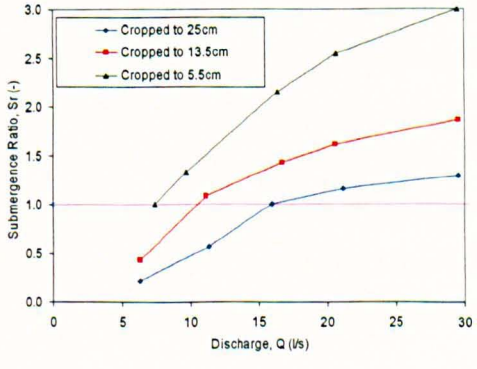

Figure 7-11 Discharge and submergence ratio through cropped Carex

It can be seen from Figure 7-11 that when the vegetation becomes submerged the gradient of the of the stage discharge relationship becomes shallower, suggesting a lower overall flow resistance than when the plants are in an emergent condition.

7.1.6 Discussion of Flow Resistance

7.1.6.1 Velocity Measurement Accuracy

In most cases the three measurement methods show similar trends in cross sectional velocity with discharge. The differences between measurements of velocity using the discharge area method and the travel time are small (<4%) in most cases.

Using the ADV probe to measure cross sectionally averaged velocity may involve significant error as the profile may not be detailed enough (eight velocity measurements are taken over a transverse cross section at a single height) and the profile chosen may not be representative of the entire flow field, especially in two layer flow (i.e. in submerged flow conditions). The ADV profile was measured in one longitudinal location, it may therefore be affected by localised effects of the vegetation. The primary reason for ADV measurements was to characterise local velocities and indicate the effect of vegetation on velocity shear and turbulence. Therefore these values are not used to characterise the cross sectionally averaged velocity.

The measurement of velocity using the ADE travel time is dependent on how well the optimised ADE fits the measured downstream profile. Again, the velocity is measured over a relatively short section of channel (the 2.44m mixing reach), and may therefore be affected by localised effects of vegetation in this channel section. This may explain the comparatively larger variations in velocity measurement in the high age Carex test, as the variations in plant growth over the length of the channel will be at their greatest.

The measurement of velocity using the discharge/area method is subject only to error caused by measurement error (depth or discharge measurement). Discharge measurement from a properly calibrated Venturi is specified to be accurate to $\pm 1\%$ (see section 5.2.3.2), error from measuring depth using the depth gauges should also be small. This method also gives an average reading for velocity over the uniform flow region, and is less affected by variations in resistance along the channel length caused by natural differences in plant growth. Therefore, unless otherwise stated, average velocity values from this point on are calculated using the discharge/area method.

7.1.6.2 Base Case

Section 7.1.1 shows that the flow resistance of the base case channel closely follows the theoretical flow resistance for boundary layer flow as derived in section 2.2. The Manning's equation accurately describes the stage discharge relationship in the channel and one Manning's n value ($n = 0.015$) accurately predicts stage over the flow range of the experiments. According

to Chow (1959) a Manning's n of 0.015 is the minimum value for a lined channel with 'Finished concrete walls and a gravel bed'. Therefore a Manning's n of 0.015 value is roughly in line with expected values for the gravel bed laboratory channel.

7.1.6.3 *Effect of Vegetation*

Figure 7-4 to Figure 7-11 show that if vegetation is added to the channel the stage discharge relationship changes. The presence of vegetation increases flow resistance, retards the flow velocity and hence increases the flow depth relative to a non-vegetated channel. In the first valid tests after planting (week 2 Carex - $\lambda = 0.9980$, week 20 reeds - $\lambda = 0.9979$) the flow depth over the full range of discharges tested was on average 40% higher in the Carex and 60% higher in the reeds than the base case relationship. As both the reeds and Carex increase in density/size the flow resistance of the channel increases and the stage discharge relationship moves further from the base case relationship. The flow depth through the Carex, 26 weeks after planting ($\lambda = 0.9406$), over the full range of discharges tested was on average 220% higher than in the base case. The reeds stage discharge relationship, 50 weeks after planting ($\lambda = 0.9976$), was on average 110% higher than in the base case.

As discussed in section 3.1, the main factors affecting the magnitude of the flow resistance in vegetated channels are plant density, frontal area submerged by the flow (i.e. plant size and flow depth) and flexibility. The plant density, frontal area and flow depth have been measured directly for each test. As detailed in section 6.2 the Carex increased in plant size with age, while the reeds stem density increased with age. To evaluate the increase in resistance with plant growth, and compare between the two vegetation types, the combined effects of stem density and plant size can be expressed as channel porosity (Equation 6-2). Plant flexibility was not measured directly, however the Carex are quite flexible plants which became stiffer with age, whilst the reeds were stiff throughout the testing program. The relationship between flow resistance and both flow depth and plant growth/channel porosity is now investigated.

7.1.6.4 *Flow Resistance and Flow Depth*

Figure 7-12 shows how the Manning's resistance coefficient changes with relative flow depth in the reeds. The Manning's n calculated for the base case is also plotted for comparison. The Manning's n value was calculated for each flow condition by rearranging the Manning's equation (Equation 2-11). Flow depth is normalised by the maximum flow depth achieved in each testing case.

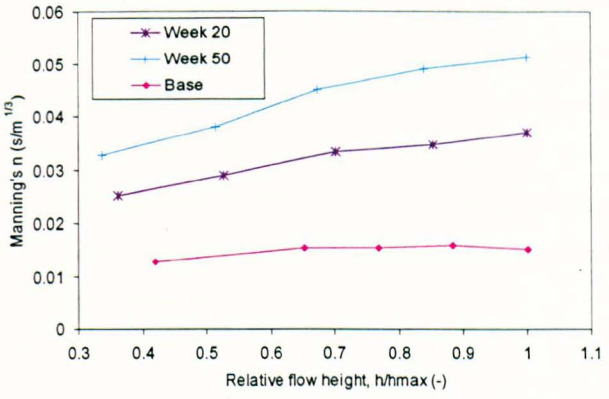

Figure 7-12 Manning's n with flow depth in reeds

The Manning's n value for the base case is roughly constant with discharge, while in the reeds the Manning's n increases with flow depth. This is due to the increasing proportion of each vegetation element becoming submerged and hence providing resistance to the flow. This supports existing studies such as Jarvela (2002) and is predicted by the drag force models first proposed by Petryk and Bosmajian (1975) (see section 3.1.2). Figure 7-12 also shows that the average Manning's n value is greater in the older/ higher density reeds case.

Figure 7-13 shows how the Manning's resistance coefficient changes with submergence ratio in the Carex.

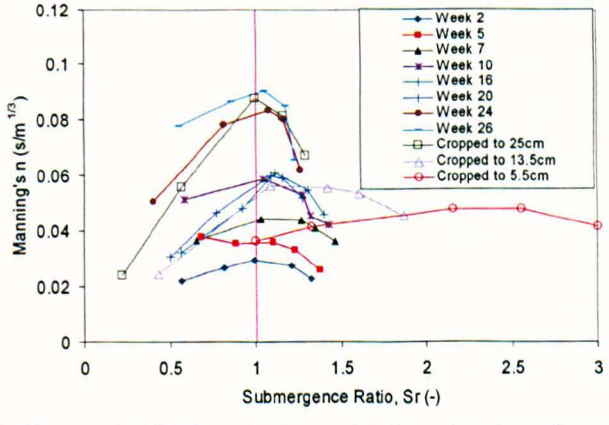

Figure 7-13 Manning's n with flow depth in Carex

In emergent conditions, the Manning's n in the Carex case generally increases with flow depth. As with the reeds, this is due to the increasing proportion of each vegetation element becoming submerged and hence providing resistance to the flow.

Once the flow becomes submerged, the flow resistance (expressed as Manning's n) begins to decrease. The flow resistance declines as the proportion of the flow not resisted directly by the vegetation elements increases. This supports previous studies such as those by Wu (1999) which have shown that the Manning's n value is dependent on the ratio between the canopy height and

the flow depth (see 3.1.1.2). According to Wu (1999), as the proportion of flow above the canopy increases Manning's n should eventually descend to a constant value and the vegetated layer will behave like conventional boundary roughness. For comparison, in experiments conducted using short grass, Wilson and Horritt (2002) found that resistance coefficients became constant when the submergence ratio became greater than approximately 3. For the vegetation states tested, the discharge required to achieve this constant n value is outside the range of the laboratory channel used in these experiments.

7.1.6.5 Flow Resistance and Emergent Vegetation Growth

In emergent vegetated flow, resistance is provided over the entire flow depth, not just from the bed as in boundary layer flow. One effect (as demonstrated in Figure 7-12 and Figure 7-13) of this is that a single Manning's n value does not accurately predict flow depth over the range of discharge in the channel. To describe how resistance changes with plant growth, it is proposed that flow resistance can also be expressed as a function of how rapidly flow depth increases (dh) with discharge (dQ) for each case in the growth phase (for the emergent state). This is mathematically expressed as dh/dQ, and is essentially the gradient of the stage discharge plots (Figure 7-6 and Figure 7-7). This approach assumes that the discharge is proportional to the depth, and thus may be inaccurate in cases where the velocity increases significantly with discharge (i.e. low age Carex). However, over a relatively small range of flow, the dh/dQ parameter should give an indication of how flow resistance changes with plant growth. Figure 7-14 shows the parameter (dh/dQ) for the reeds and the emergent growing Carex (emergent cropped Carex are not plotted because they have a similar porosity and dh/dQ values as the final growth phase test).

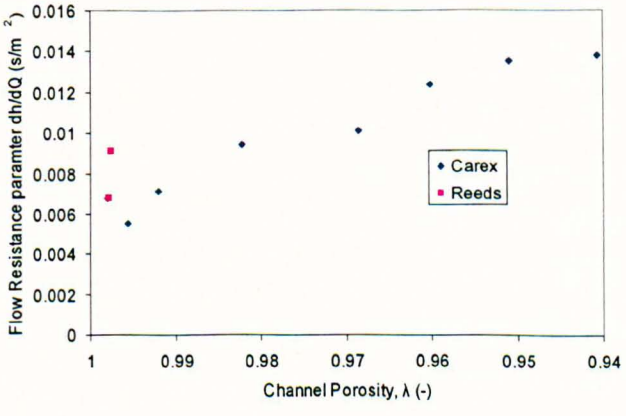

Figure 7-14 Changing flow resistance with porosity

In Figure 7-14 plant growth is expressed in terms of channel porosity so that comparisons can be made between the reeds and Carex. Details of how the channel porosity varies with age for

both the reeds and the Carex can be found in section 6.2. The flow resistance parameter (dh/dQ) increases as channel porosity decreases demonstrating that the addition and subsequent growth of the vegetation increases the flow resistance of the channel. The reeds exerted a greater resistance on the flow than the Carex at high channel porosities. However, due to the lack of Reed growth, the trend between resistance and channel porosity in the reeds case cannot be fully explored.

7.1.6.6 Average Velocity in Emergent Canopies and Plant Growth

In section 3.1.3.2 it was discussed that according to the momentum equation, if the bed resistance is negligible and the drag coefficient is constant with flow rate, flow velocity though an emergent canopy should remain constant with flow (dU/dQ = 0), and flow can be considered by balancing forces from water weight and vegetation drag. The plots of cross sectionally averaged velocity plots show that in some cases (reeds, high age emergent Carex), the velocity is approximately constant with discharge. The dU/dQ parameter can be measured from the velocity/discharge plots and plotted against plant growth (expressed as channel porosity) in emergent conditions (Figure 7-15).

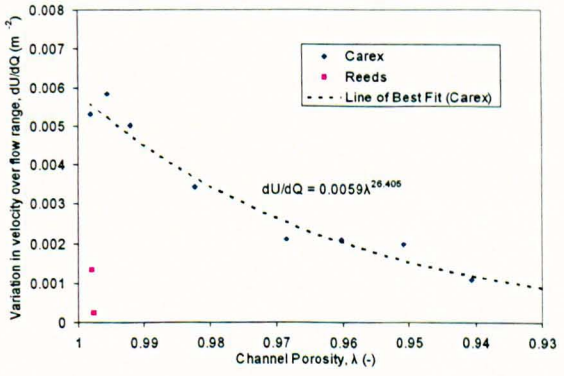

Figure 7-15 Change in velocity over discharge with channel porosity

Figure 7-15 shows that none of the emergent vegetated cases achieve the condition dU/dQ = 0. This may be because either the bed does have a noticeable effect on total resistance or the drag acting on the vegetation is not constant with flow rate. In the case of the reeds, the dU/dQ parameter is close to zero, which means that velocity within the canopy is only increasing slightly with discharge. As the reeds are stiff, the drag coefficient should be roughly constant with flow rate (due to little additional streamlining with increasing flow), however the reeds did not achieve a large stem density and it is assumed that the influence of the bed on total flow resistance was not negligible in this case. The average velocity through the low age / high channel porosity Carex canopy increases with discharge to a greater extent than the reeds even though the calculated porosity values are roughly similar. This effect is due to the greater

flexibility of the Carex as compared with the reeds. As the flow rate increases the plants adopt a more streamlined position, reducing their effective drag coefficient and allowing the velocity to increase (according to Equation 3-1). However, this effect decreases as the plants become stiffer with age and stem diameter. As the vegetation increases in age and density, the flow condition moves closer to the condition whereby the flow velocity remains roughly constant with discharge. If a constant velocity condition were to be assumed, extrapolation of Figure 7-15 shows that to achieve a less than 1% error in depth prediction over a discharge range of 10l/s would require a channel porosity value of 0.885 (in Carex).

7.1.6.7 *The Free Flow Layer (in Submerged Vegetation)*

Once the Carex becomes submerged, two flow layers exist. One layer through the canopy where velocity is resisted by the vegetation, and one free flow layer above. This free flow layer causes the cross sectionally averaged velocity to increase with discharge, even in dense canopies. It has been proposed (Righetti and Armanini, 2002, Kouwen et al., 1969) that the free flow layer can be considered as boundary layer flow, resisted by a shear force acting at the canopy top. It may therefore be possible to consider this layer using conventional resistance models developed for boundary layer flow. To show this, the stage discharge relationships for only the free flow layer can be plotted. The depth of the free flow layer is measured directly as the total flow depth minus the canopy height ($h-h_c$). Discharge in the free flow layer is estimated by subtracting the discharge measured with the flow depth equal to the canopy height from the total discharge ($Q-Q_c$). Figure 7-16 and Figure 7-17 show the stage discharge relationship for flow over the growing and cropped Carex respectively.

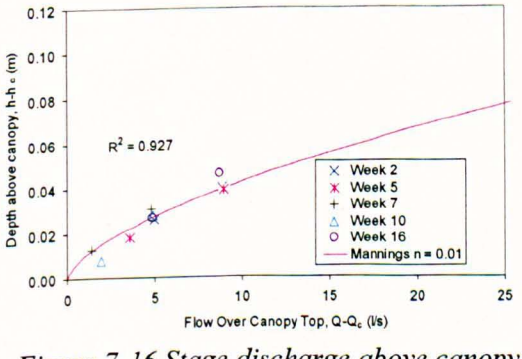

Figure 7-16 Stage discharge above canopy (growing vegetation)

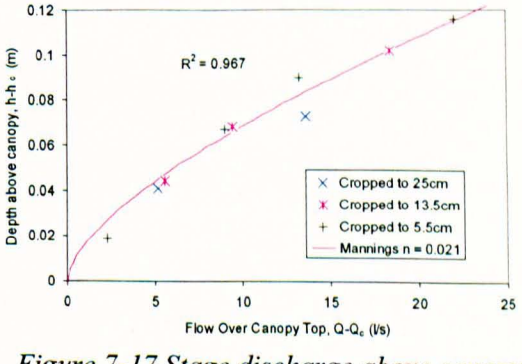

Figure 7-17 Stage discharge above canopy (cropped vegetation)

Figure 7-16 shows that stage discharge relationship over the growing vegetation can be approximated ($R^2 = 0.927$) by a Manning's relationship with a value of 0.01. Figure 7-17 shows that the equivalent value for the cropped phase is significantly higher, around 0.021 ($R^2 = 0.967$). This demonstrates the principle that flow over the top of the canopy can be considered as boundary layer flow which follows a Manning's relationship.

During the growth phase the Manning's n value is low, this is because the top of the canopy is quite smooth due to the natural streamlining effect as the plants bend under high flows. In the cropped phase the plants stay quite rigid and consequently have a higher roughness value (see Figure 7-18 and Figure 7-19). According to Chow (1959) a Manning's n of 0.021 is equivalent to a channel constructed of rough gunite. While a Manning's n of 0.01 is equivalent to a channel constructed of smooth brass or glass.

Figure 7-18 Growing vegetation – Streamlining

Figure 7-19 Cropped vegetation – Little streamlining.

7.1.6.8 Summary of Flow Resistance Discussion

The main conclusions to be considered from the bulk flow resistance section are

- Vegetation increases the flow resistance in the channel.
- Flow resistance increases with depth in emergent conditions, and then decreases after submergence.
- Flow resistance increases as the plants grow in size/ density.
- In the relatively stiff reeds the canopy velocity increases only slightly with flow rate.
- In the flexible Carex, the canopy velocity increases to a greater extent with flow rate (due to plant streamlining). However, the rate of increase declines as the Carex becomes stiffer.
- The free flow zone can be treated as boundary layer flow, with an 'n' resistance value dependent on the roughness of the canopy top.

7.2 Profiles of Velocity Results and Discussion

In this section the transverse and vertical profiles of primary velocities, as well as vertical profiles of transverse velocities obtained from the ADV probe measurements (see section 5.3.4) are presented. As discussed in section 2.4.2.4 velocity shear is a major factor for driving mixing in open channel flow. To quantify the influence of the vegetation on velocity shear it is necessary to measure and compare transverse and vertical profiles of velocity.

Looking downstream, all transverse profiles of velocity are measured from the right hand bank to the left hand bank. As stated in section 5.3.4.2, the maximum height measurable in each vertical profile is 2 cm below the flow depth. Transverse and vertical profiles were taken at the longitudinal position described in Figure 5-16 (with respect to vegetation) and Figure 6-10 (with respect to the laboratory channel).

7.2.1 *Profiles of Velocity in the Base Case*

The velocity profiles for the base case condition are initially presented. Transverse profiles of velocity were taken at one third flow depth, except in the bottom two flow conditions where this was not possible due to insufficient clearance for the operation of the ADV probe. Figure 7-20 shows the transverse profile of primary velocities for each measured flow rate in the base case.

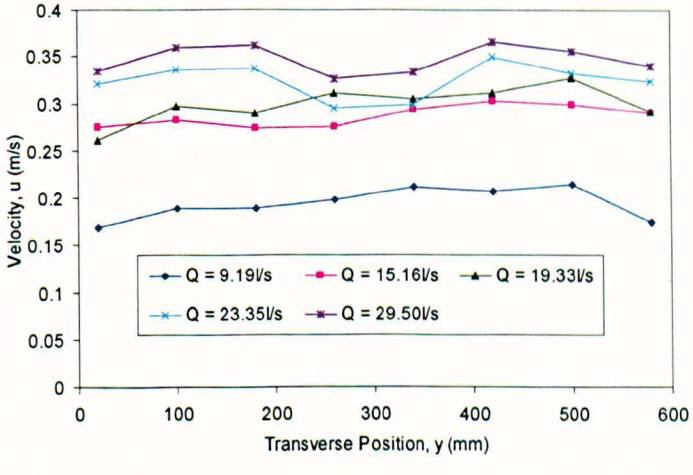

Figure 7-20 Transverse profile of primary velocities (Base Case)

Figure 7-20 shows that there is little variation in flow velocity across the width of the channel. The profiles taken at the two highest flow rates exhibit a slight retardance in the middle of the channel. It is possible that this is due to the formation of secondary currents or irregular flow structures on each side of the channel centreline. However no direct measurements of secondary currents other than at the channel centre have been taken and thus this hypothesis cannot be tested.

Figure 7-21 shows how the vertical profile of primary velocities changes with flow rate in the base case. The vertical profile of velocities of the test taken at 9.19l/s is not displayed due to insufficient measurements taken over the flow depth. Figure 7-22 compares the measured vertical profile of primary velocities at the maximum flow rate with the theoretical law of the wall as described in section 2.3.2.1.

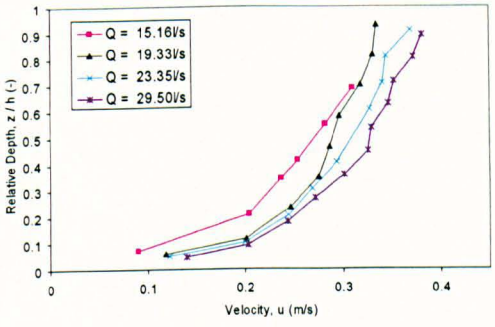

Figure 7-21 Vertical profile of primary velocities (Base Case)

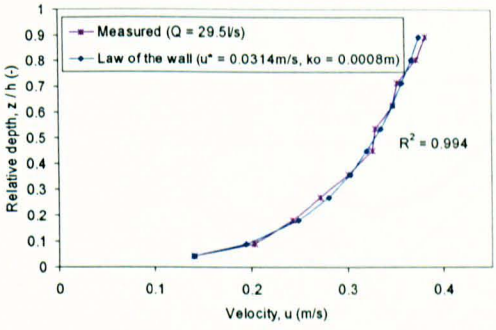

Figure 7-22 Vertical velocity profile compared to the law of the wall

The shear velocity and roughness height parameters required for the theoretical profile are optimised to give the best fit to the measured profile. Only the profile at the maximum flow rate is displayed in Figure 7-22, however the logarithmic law provides a good approximation to the profiles taken at the other flow rates ($R^2 > 0.98$ in all cases).

Figure 7-23 shows the vertical profile of transverse velocities for each flow rate in the base case.

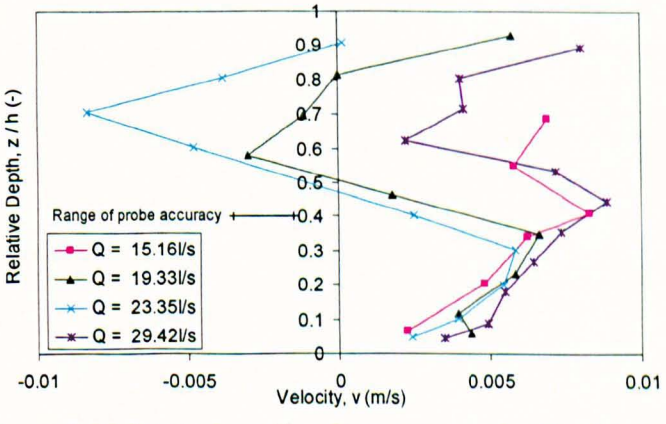

Figure 7-23 Vertical profile of transverse velocities (Base Case)

Figure 7-23 shows that the magnitude of these velocities is small and constant with flow rate (approximately 2% of the average primary flow velocities). The range of accuracy of the ADV probe (as specified in the ADV operation manual) is also displayed.

7.2.2 Velocity Profiles in Reeds

The transverse and vertical profiles of velocity taken in the channel containing reeds are now presented. Transverse profiles of velocity were taken at one third flow depth, except in the bottom flow condition where this was not possible due to insufficient clearance for the operation of the ADV probe. Figure 7-24 and Figure 7-25 show the transverse profiles of primary velocities in the low and high age reeds case respectively for each discharge tested.

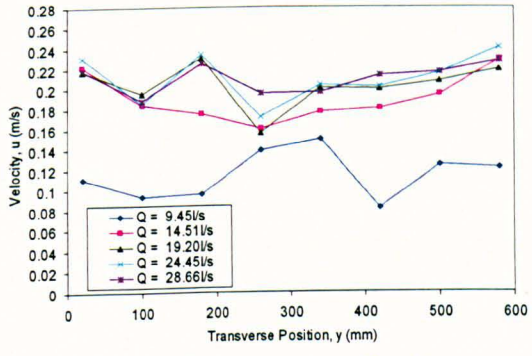

Figure 7-24 Transverse profile of primary velocities (Reeds - Week 20)

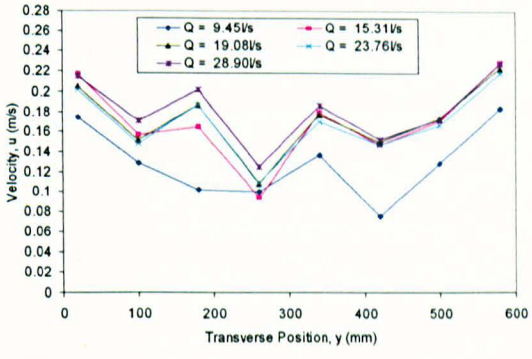

Figure 7-25 Transverse profile of primary velocities (Reeds - Week 50)

The profiles exhibit regions of low velocity which exist due to the presence of wakes behind the vegetation elements. Apart from the tests conducted at 9.45l/s the velocity profiles change only slightly with flow rate.

Figure 7-26 and Figure 7-27 show the vertical profiles of primary velocities in the low and high age reeds case respectively for each discharge tested.

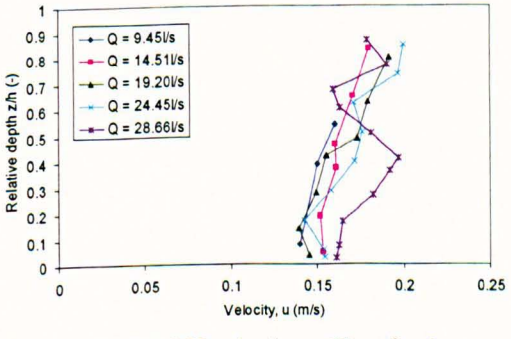

Figure 7-26 Vertical profile of primary velocities (Reeds - Week 20)

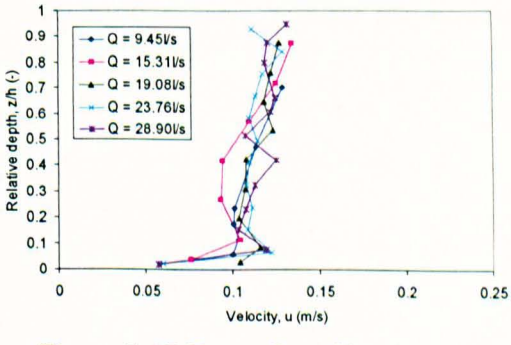

Figure 7-27 Vertical profile of primary velocities (Reeds - Week 50)

Both profiles display roughly uniform flow velocities over the depth, although there is a slight increase over the flow depth in the low density case. As suggested in section 7.1.2, there is little change in average flow velocity with discharge.

Figure 7-28 and Figure 7-29 show the vertical profiles of transverse velocities in the low and high age reeds case respectively for each discharge tested.

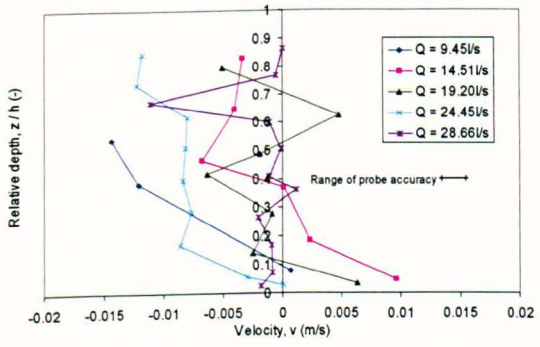

Figure 7-28 Vertical profile of transverse velocities (Reeds - Week 20)

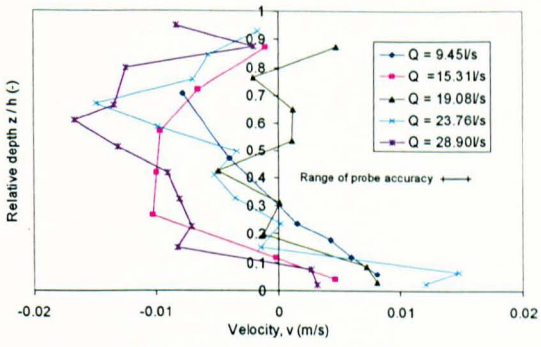

Figure 7-29 Vertical profile of transverse velocities (Reeds -Week 50)

The range of accuracy of the ADV probe is also displayed in both figures. In both cases average transverse velocities are approximately 2% of the average primary flow velocities.

7.2.3 Velocity Profiles in Emergent Carex

The transverse profiles of velocity taken in the channel containing low and high age Carex are now presented. Although at the highest flow rates the Carex are classified as submerged, all profiles displayed here are taken within the canopy and thus are presented here for both completeness and to provide a comparison. Vertical profiles of velocity are displayed as part of the full velocity profiles in the submerged Carex section. Transverse profiles in emergent conditions are taken at one third flow depth whilst in submerged conditions they are taken at third canopy height.

Figure 7-30 and Figure 7-31 show the transverse profile of primary velocities in the Carex for each flow rate, in tests conducted 2 and 24 weeks after planting respectively. Figure 7-32 displays the transverse profile of primary velocities at various Carex ages for the maximum channel discharge (29.5l/s).

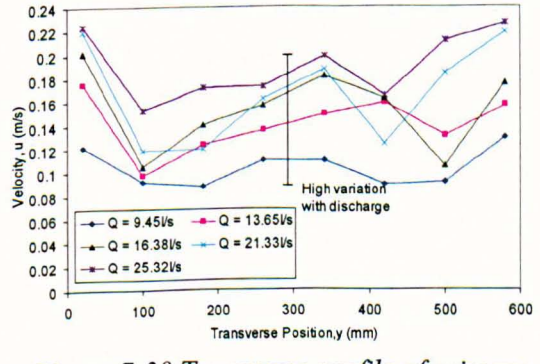

Figure 7-30 Transverse profile of primary velocities (Carex, Week 2- Within Canopy)

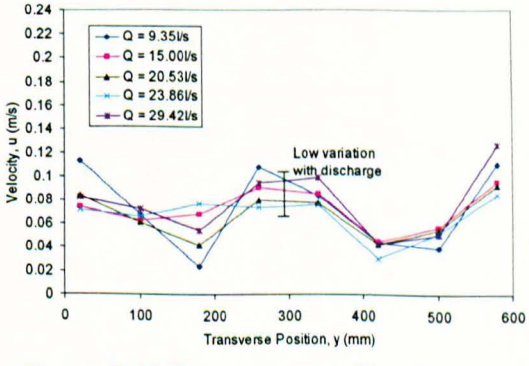

Figure 7-31 Transverse profile of primary velocities (Carex, Week 24- Within Canopy)

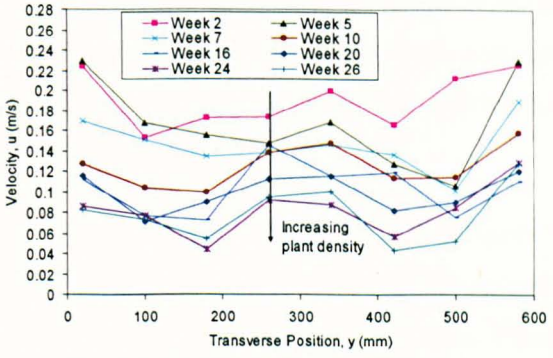

Figure 7-32 Transverse profile of primary velocities (Growing Carex, Q=29.5l/s, Within Canopy)

In Figure 7-30 it can be seen that there is a large variation (0.086m/s, 45.3% over the range of discharge) in velocity with discharge. In Figure 7-31 there is much less variation in velocity with discharge (0.009m/s, 7.3% over the range of discharge). Regions of low velocity exist in the wakes of the vegetation elements in both profiles. In Figure 7-32 a retardation effect can be observed as the plants increase in age therefore and grow in size.

7.2.4 Velocity Profiles in Submerged Carex (Growing)

The transverse and vertical velocity profiles taken in the channel containing low and high age submerged Carex are now presented. In tests conducted at the maximum flow velocity (≈ 29.5l/s) at week 7 and 20, transverse profiles of velocity were taken above, as well as within the canopy. Transverse profiles of velocity taken above the canopy are measured 2cm below the total flow depth. These profiles of velocity taken in the free flow zone can be compared to the velocities measured within the canopy.

Figure 7-33 and Figure 7-34 display the transverse profile of primary velocities in and above the canopy at the maximum flow rate (29.5l/s) in tests conducted 7 and 20 weeks after planting respectively.

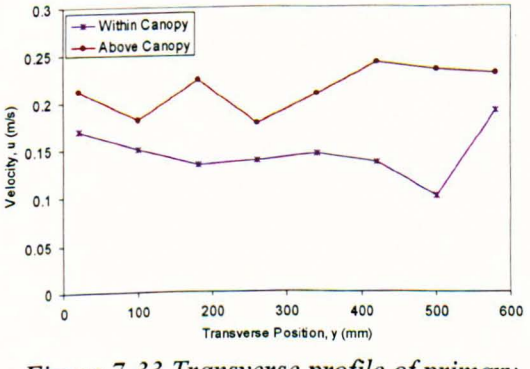

Figure 7-33 Transverse profile of primary velocities in and above canopy, Carex, Week 7

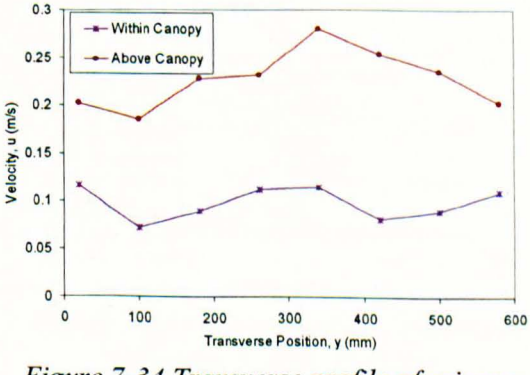

Figure 7-34 Transverse profile of primary velocities in and above canopy, Carex, Week 20

Seven weeks after planting the difference in measured average flow velocity between the flow within and above the canopy is approximately 0.068m/s (30.9% difference). Twenty weeks after planting the difference in flow velocity between the canopy and the faster flow layer is larger, approximately 0.13m/s (56.5% difference).

Full vertical velocity profiles were measured from week 7 onwards. The vertical profiles of primary velocity in submerged flow are plotted in respect to the canopy height, h_c, to provide an indication of the effect of submergence on the velocity profiles. Figure 7-35 and Figure 7-36 display the vertical profile of primary velocities for each flow rate, in tests conducted 7 and 24 weeks after planting respectively.

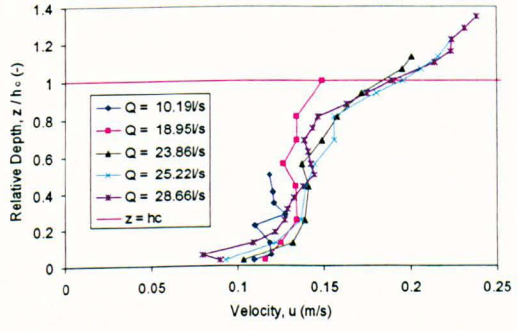

Figure 7-35 Vertical profile of primary velocities (Carex, Week 7)

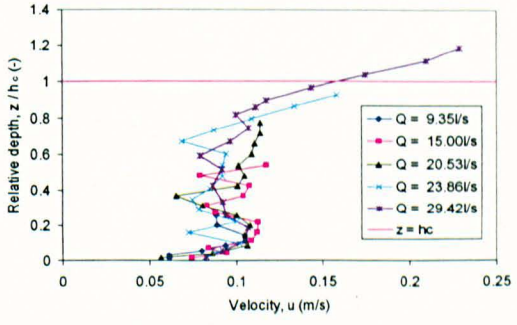

Figure 7-36 Vertical profile of primary velocities (Carex, Week 24)

Except for the region very close to the bed, profiles taken in emergent conditions (10.19l/s and 18.95l/s in week 7, 9.39l/s to 20.53l/s, week 24) exhibit roughly uniform velocity profiles over the flow depth. In submerged cases the velocity increases towards and over the top of the canopy.

Figure 7-37 and Figure 7-38 display the vertical profile of transverse velocities for each flow rate, in tests conducted 7 and 24 weeks after planting respectively.

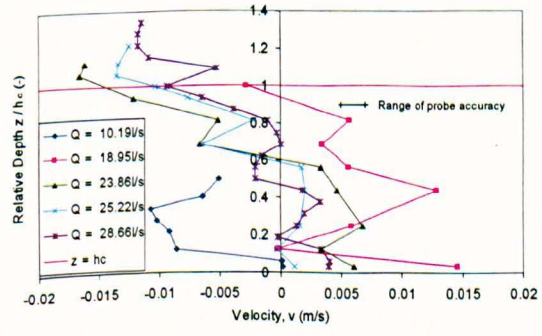

Figure 7-37 Vertical profile of transverse velocities (Carex, Week 7)

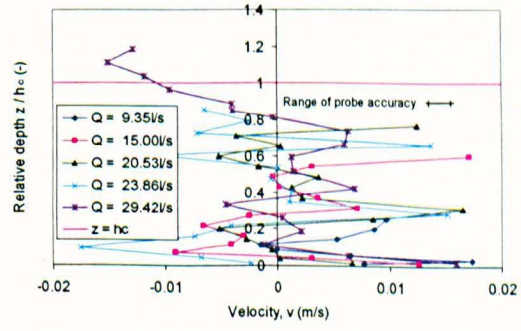

Figure 7-38 Vertical profile of transverse velocities (Carex, Week 24)

In both cases average transverse velocities are approximately 10% of the average primary flow velocities.

7.2.5 Velocity Profiles in Submerged Carex (Cropped)

In this section the vertical profiles of velocity taken in the channel containing cropped Carex are presented. Transverse profiles of velocity are not displayed as the conditions are similar (similar stem diameters, porosities etc.) to the velocity profiles taken at the last test in the growth phase.

Figure 7-39 displays the vertical profile of primary velocities for each discharge tested after the Carex were cropped to a height of 25cm. Figure 7-40 displays the vertical profile of primary velocities for each discharge tested after the Carex were cropped to a height of 5.5cm. The test conducted at 7.41l/s is not displayed due to insufficient measurements over the flow depth.

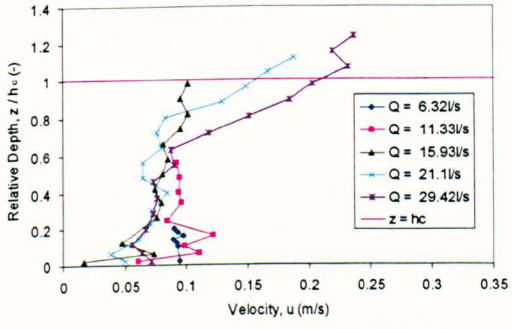

Figure 7-39 Vertical profile of primary velocities (Carex cropped to 25cm)

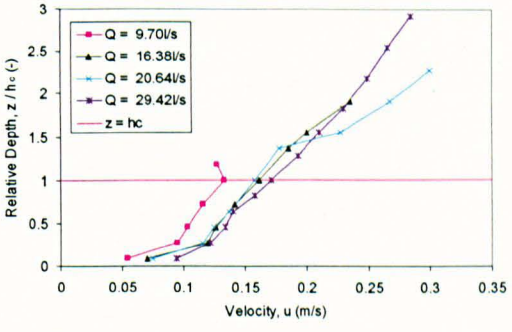

Figure 7-40 Vertical profile of primary velocities (Carex cropped to 5.5cm)

In Figure 7-39, profiles taken in emergent conditions (6.32l/s to 15.93l/s) exhibit uniform velocity profiles over the depth; and in submerged cases the velocity increases towards and over the top of the canopy. In the vegetated case presented in Figure 7-40 a region of uniform flow within the canopy is not present and the velocity increases over the entire flow depth.

7.2.6 Discussion of Velocity Profiles

7.2.6.1 Base Case

Section 7.2.1 shows that there is little variation in primary velocity across the channel (Figure 7-20). The channel walls are relatively smooth in comparison to the bed and so the influence of the channels walls does not extend greatly (<20mm, < 3.5% of the fully channel width) into the main flow.

Figure 7-22 shows that although strictly only applicable in the bottom 20% of the flow, the 'law of the wall' (see section 2.3.2.1) can well (R^2 = 0.99) describe the observed vertical velocity profile over the entire flow depth (Figure 7-22). Fitting the law of the wall gives a shear velocity (u*) value of 0.0314 m/s and a roughness height (k_0) of 0.000847 m. For the maximum flow rate, this shear velocity value is quite close to the value derived from the bed slope (

Equation 2-37) which is 0.0367 m/s (17% difference). Roughness height is usually derived from grain size (Equation 2-36), using a grain size, D_s, of 10mm (see section 5.2.3.1) gives a k_o value of 0.000332 m (39% difference from measured value)

Low levels of transverse velocities in the channel (Figure 7-23) indicate that secondary currents in the base case are negligible, which would be expected in a straight channel.

7.2.6.2 *Transverse Profiles of Velocity in Vegetation*

Transverse profiles of velocity through the vegetated canopies are displayed in section 7.2.2 and 7.2.3. Figure 7-41 compares the transverse profile of primary velocities taken at the maximum flow rate ≈ 29.5l/s for the reeds, Carex (within the canopy) and the base case.

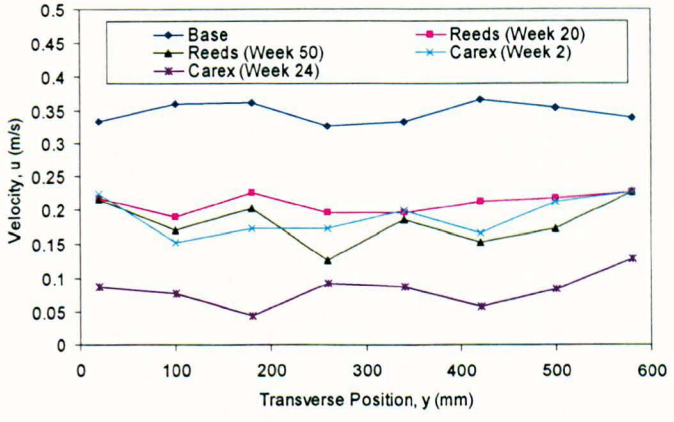

Figure 7-41 Comparison of transverse profiles of primary velocities in different vegetated cases (Q ≈ 29.5l/s)

It can be seen that the presence of vegetation retards the velocity profile with regard to the base case. The high age, large Carex plants (λ = 0.941) retard the flow to a greater extent than the low age, small (λ = 0.998) Carex/reeds cases. All profiles featured only a small amount of transverse velocity shear (i.e. difference in velocity over the cross section), although more differential advection would be expected close to the channel walls (the region close to the channel walls cannot be measured due to the size of the ADV probe). Although the presence of vegetation does retard the velocity profiles behind the vegetation elements to a small extent, there appears to be no dramatic change in the size of the transverse velocity shear between non-vegetated and vegetated cases. The addition of the vegetation has caused the fastest regions of flow to be at the edges of the channel as flow is forced around the vegetation.

The difference in velocity between the free flow zone and the canopy layer can be observed from the transverse profiles in section 7.2.4 (Figure 7-33 and Figure 7-34). The velocity difference is bigger for the high age, larger Carex plants. This supports the study of Poggi (2004) who found that the velocity difference between the two flow layers is bigger in canopies

which are more effective in slowing the canopy velocity (i.e. larger or denser canopies), forcing a larger quantity of flow over the canopy top.

In the case of the reeds (Figure 7-24 and Figure 7-25) and the larger Carex (Figure 7-31) the profile of velocity within the canopy is almost unchanged with discharge. This supports the observation made in section 7.1.6.6, regarding how the parameter dU/dQ becomes very small when the vegetation is stiff and the influence of the bed is negligible.

7.2.6.3 Vertical Profiles of Primary Velocity in Emergent Vegetation

The profiles of velocity in emergent flows are plotted in section 7.2.2 and 7.2.4. To provide a comparison between the testing cases, the profiles can be plotted together (Figure 7-42). In this case the maximum discharge is not used as the Carex would be in a submerged condition.

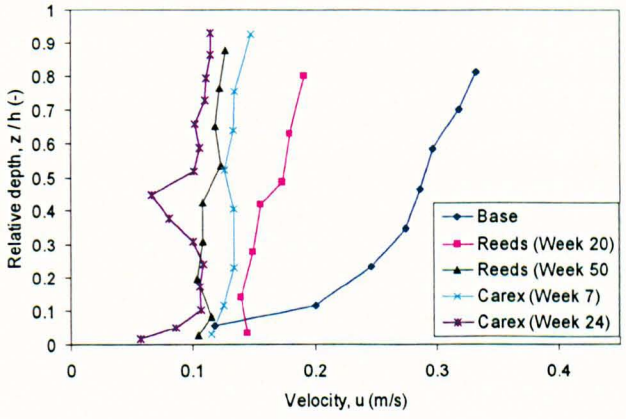

Figure 7-42 Comparison of vertical profile of primary velocities in different emergent vegetated cases ($Q \approx 20l/s$)

From Figure 7-42 it can be seen that within the canopy the presence of vegetation retards the profile of velocity with regard to the base case. This retardation effect, within the canopy, increases as the vegetation increases in age (and therefore density or size). Emergent vegetation exerts resistance over the entire flow depth; hence the profiles are roughly uniform and no longer obey the logarithmic law of the wall. In contrast to transverse shear, the presence of vegetation greatly reduces the magnitude of vertical velocity shear relative to the base case.

7.2.6.4 Submerged Vegetated Vertical Profiles of Primary Velocity

At the higher flow rates the Carex plants become submerged and two layer flow occurs. Figure 7-35 and Figure 7-36 demonstrate the change in the profile of velocity and flow structure when two layer flow arises. A faster region of flow becomes present towards and above the top of the

canopy. The flow above the canopy travels faster because of the lack of intruding vegetation elements resisting the flow. To better explain the structure of flow resistance it is necessary to plot the vertical velocity profiles with reference to the canopy top, h_c (Figure 7-43).

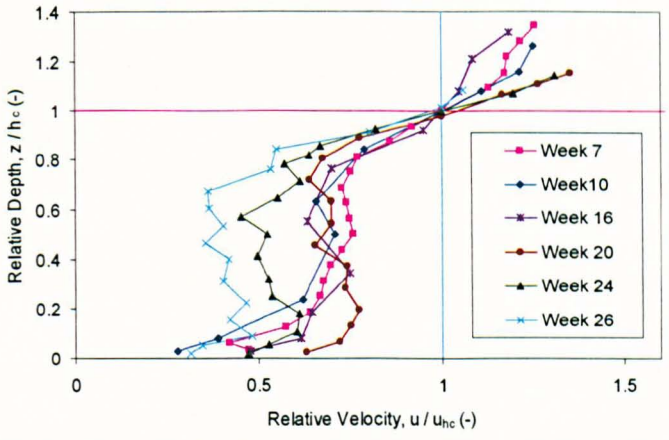

Figure 7-43 Vertical profile of primary velocities in growth phase Carex (Q = 29.5l/s)

Figure 7-43 displays the vertical profile of primary velocities at the maximum flow rate with reference to the canopy top in growth phase Carex. It is possible to identify the regions of flow as identified in section 3.2.2 (Figure 3-4), i.e. a wake zone (the region where velocity is constant with depth), a mixing layer (a linear increase in velocity above the wake zone) and the free flow (logarithmic) region above the canopy. The influence of the mixing layer extends some distance into the canopy layer and hence the velocity begins to increase at a depth, d_c below the canopy height. In can be observed that in the growth phase the wake zone takes up the majority of the flow depth. However, it is difficult to accurately define the flow regions using the velocity profiles alone.

The changing influence of boundary roughness can be observed in the Carex cases as the plants increase in age and grow in size. In low age Carex (i.e. week 7 – Figure 7-35) the velocity increases with distance above the bed until z/z_{max} of approximately 0.4, then it is roughly constant until the mixing layer at z/z_{max} of 0.8. In high age Carex (i.e. week 24 - Figure 7-36) this boundary influenced zone stops around $z/z_{max} = 0.05$. Hence, the influence of the bed on the velocity profile is reduced with increasing plant growth, as the drag from the vegetation becomes much larger than the resistance of the bed.

According to the analogy between submerged velocity profiles and mixing/shear layers, first proposed by Raupach et al. (1996) and explained in section 3.2.2 (Figure 3-4), the profiles should feature an inflection point at the canopy top ($z = h_c$). An inflection point can be defined mathematically as a point in which the second derivative of the function changes sign (Thomas and Finney, 1996). To determine the inflection point in the velocity profile a best fit line can be fitted to the profile of velocity, and the second derivative determined (Figure 7-44).

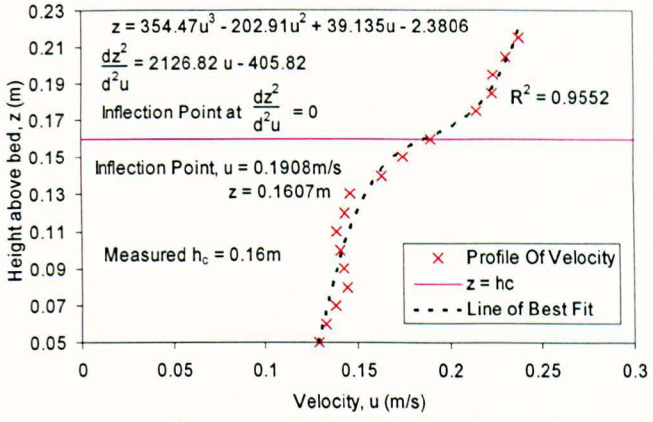

Figure 7-44 Determination of inflection point in vertical profile of velocity (Week 7 Carex, Q = 29.5l/s)

Figure 7-44 shows an example vertical profile of velocity taken in submerged Carex. The best fit third order polynomial is also plotted. By evaluating the second order derivative of the best fit line, the position of the inflection point can be determined. In this case the inflection point occurs at the point where u = 0.1908m/s, z = 0.1608m. The measured position of the canopy top (h_c) in this case is 0.16m above the bed. The inflection point in the velocity profile thus corresponds very well to the position of the canopy top, seemingly concurring with the Raupach et al. (1996) mixing layer analogy.

A third order polynomial can be accurately ($R^2 > 0.95$ in all cases) fitted to all vertical profiles of velocity in submerged growth phase Carex, although the quality of fit, and prediction of the canopy top, decreases in accuracy as the Carex grows and the available submergence ratio is lower. This is due to the fact that there are fewer points above the canopy top with which to define the line of best fit. The position of the inflection point in the profiles of velocity and the measured canopy height for growth phase Carex (conducted at the maximum flow rate) are presented in Table 18.

Table 18 – Comparison between measured canopy height and position of inflection in vertical profiles of primary velocity (In submerged growth phase Carex, Q ≈ 29.5l/s)

Test (Age)	Measured Canopy Height, h_c (m)	Position of Inflection (m)	Goodness of Fit, R^2	% Error between inflection and h_c
7	0.160	0.162	0.955	1.25
10	0.182	0.186	0.967	2.41
16	0.195	0.178	0.981	8.74
20	0.220	0.235	0.991	6.68
24	0.270	0.283	0.959	4.92
26	0.280	0.257	0.965	8.19

As the velocity inflection is located between the slow (canopy) and fast (free flow) regions of flow, the strength of the inflection $\left(\frac{du}{dz}_{hc}\right)$ should be an indicator to the relative difference

between velocities in the canopy and free flow layer, and hence the strength of the vertical shear acting over the flow depth. Measuring the differential advection (Δu) directly is difficult in this case, as many of the free flow layers are small (at high ages) and the ADV probe is unable to measure within 2cm of the free surface. According to the findings of Poggi et al. (2004) the strength of the velocity inflection at the canopy top becomes larger as the vegetated layer gains resistance, reducing the flow velocity within the canopy, and increasing the amount of flow over the canopy top. A stronger inflection at the canopy top will result in larger velocity gradients over the flow depth and hence larger vertical velocity shear. The strength of the velocity inflection can be characterised by the slope of the velocity profile at the canopy top (as measured from the vertical profiles of primary velocity). In the growth phase tests, the inflection strength parameter can be clearly related to the submergence ratio of the flow (Figure 7-45).

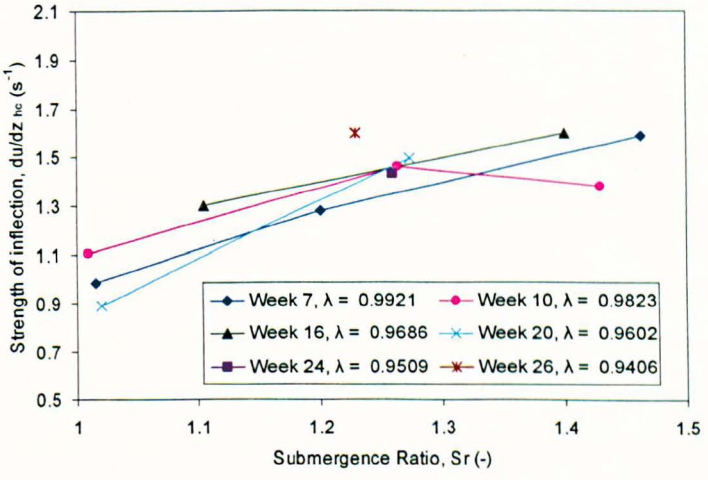

Figure 7-45 Strength of the velocity inflection in growth phase Carex

The strength of the velocity inflection tends to increase slightly with plant growth (and hence canopy resistance) but Figure 7-45 shows that it is most clearly related to submergence ratio. The greater the submergence ratio, the more developed the flow over the canopy top. If the flow over the canopy top can be assumed to act as boundary layer flow, average flow velocity is proportional to $R^{2/3}$ (from Manning's equation - Equation 2-11). Hence, increasing flow depth above the canopy will increase the size of the velocity inflection. For a submerged system with a constant canopy height and discharge (as in the study of Poggi et al., 2004), increasing the canopy size/density will lead to an increasing depth of submergence (as the flow resistance increases), and hence a greater velocity inflection at the canopy top. However in the current study, the Carex grow in height as well as size; the growth in height reduces the proportion of flow in the free flow zone (Figure 6-20), and so the effects of increasing canopy resistance cannot be linked directly to the strength of the inflection.

7.2.6.5 Cropped Vegetation

Cropping the vegetation creates a vegetated canopy with a high flow resistance but with a low height (leading to higher possible submergence ratios). Based on the findings of Poggi et al. (2004) and the dependency on submergence ratio discussed in section 7.2.6.4, it would be expected that this would lead to strong inflection points and high vertical shear. Figure 7-46 displays the vertical profile of primary velocities in each of the cropped vegetated cases. Figure 7-47 shows the average strength of the velocity inflection in each test.

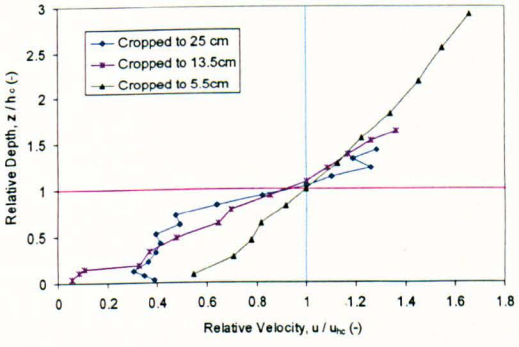

Figure 7-46 Vertical profile of primary velocities (Cropped Carex, Q = 29.5l/s)

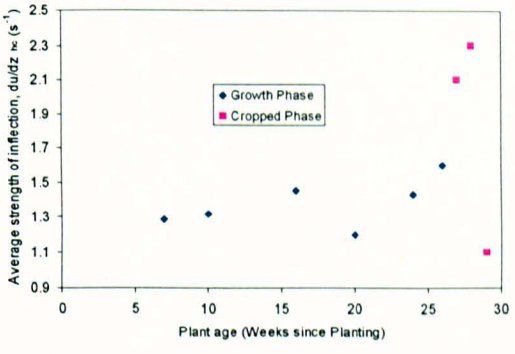

Figure 7-47 Average size of inflection point in growth and cropped phases

In the first two cropped cases (cropped to 25cm - week 27, cropped to 13.5cm - week 28) the high resistance caused by the canopy and the higher submergence ratios causes the strength of the inflection to be very high (Figure 7-47). High canopy resistance and high submergence ratios will lead to higher levels of vertical velocity shear in these cases. In the final cropped test (cropped to 5.5cm - week 29) the mixing layer penetrates to the bed, the wake zone disappears, and the velocity increases over the entire flow depth. This leads to a relatively weak inflection point at the canopy top.

Comparing Figure 7-46 with the vertical profile of primary velocities taken in growth phase Carex (Figure 7-43) shows that cropping the vegetation alters the relative sizes of the flow zones (outlined in Figure 3-4). More flow travels over the top of the canopy whilst the relative size of the wake zone is reduced.

7.2.6.6 Vertical Profiles of Transverse Velocity

Section 7.2.2 shows that the average magnitude of transverse velocities in the reeds case is approximately 2 % of the primary velocity, similar to the base case. Section 7.2.3 shows that the average level of transverse velocities in the Carex case reaches values which are approximately 10% of the primary flow velocity.

In section 5.3.5.2 it was described how the strength of the secondary circulations could be quantified my measuring the variations in the profiles of transverse velocity over the flow depth. The variance of each vertical profile of transverse velocities can be calculated and used to show the trend in the variation of transverse velocities over the flow depth with Carex growth (expressed as channel porosity). Figure 7-48 displays the standard deviation values of the vertical profiles of transverse velocities for the base case (channel porosity = 1) and for each case in the Carex growth phase. Each flow range is plotted as a separate series.

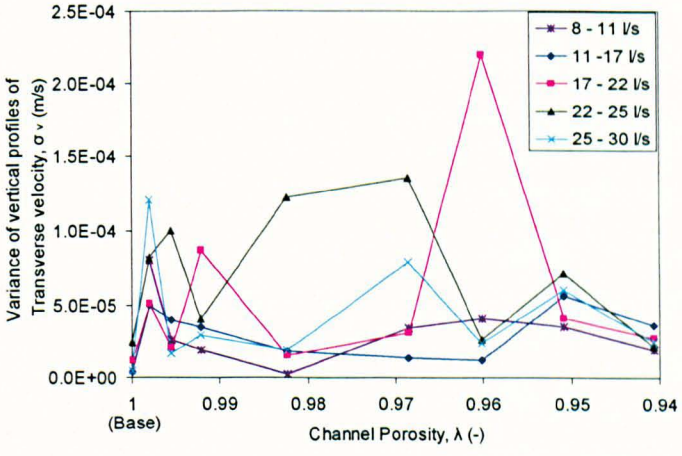

Figure 7-48 Variance of transverse profiles of velocity with channel porosity in growing Carex

The overall variation of transverse velocities over the depth varies little with plant porosity; however there is an overall increase relative to the variations observed in the base case. This effect may be due to the presence of wakes, and the fact that flow must travel around vegetation elements. The presence of higher transverse velocity variations over the depth would indicate higher secondary circulations which in turn may contribute to higher transverse mixing rates in the channel (see section 2.4.4.2).

7.2.6.7 Summary of Velocity Profile Discussion

The main conclusions to be drawn from the observations of the profiles of velocity are

- Despite the localised resistance effects of vegetation, velocity shear over the channel width is not greatly altered by the presence of either Carex or reeds in the channel.
- In emergent flows (and for the wake zone in submerged flow) the vertical profiles of primary velocity are roughly uniform over the flow depth. Vertical velocity shear in emergent flow is therefore much reduced in the vegetated case when compared to the base case.

- In submerged conditions flow travels faster over the canopy top than within the canopy, this results in vertical shear between the canopy and free flow zone. A mixing/shear layer is formed at the top of the canopy, with an inflection point in the velocity profile at the canopy top.

- The strength of the velocity inflection is related to the flow depth above the canopy (i.e. size of free flow zone and submergence ratio).

- Cropping the vegetation resulted in canopies with a high resistance subject to high submergence ratios. This resulted in strong inflection points. The region within the canopy where the velocity is uniform with depth (the wake zone) is reduced in size.

- Variations in transverse velocities over the depth (and hence secondary circulations) are greater in the Carex compared with the reeds and the base case conditions. There is no apparent trend in the variation in transverse velocities with Carex growth.

7.3 Turbulence Results and Discussion

This section presents the transverse and vertical profiles of Reynolds stress measured using the ADV probe in all of the vegetated and non vegetated cases tested. Turbulence and Reynolds stress was discussed in section 2.3. Both mass and momentum are transported throughout the flow regime by turbulence, and therefore an understanding of how the presence of vegetation changes the turbulence in the flow is important for determining the influence of vegetation on mixing. Profiles of Reynolds stress were taken in the same positions as the profiles of velocity (shown in Figure 5-16).To quantify the transport of mass and momentum over a transverse plane, the Reynolds stresses in the transverse profiles are calculated as $\rho\overline{u'v'}$, whilst to quantify the transport of mass and momentum over the vertical plane the Reynolds stresses in the vertical profiles are calculated as $\rho\overline{u'w'}$.

7.3.1 Turbulence in the Base Case

Figure 7-49 displays the transverse profile of Reynolds stress for each discharge tested in the base case. The Reynolds number of the flow has also been calculated for each flow rate using Equation 2-4 and is displayed in the legend.

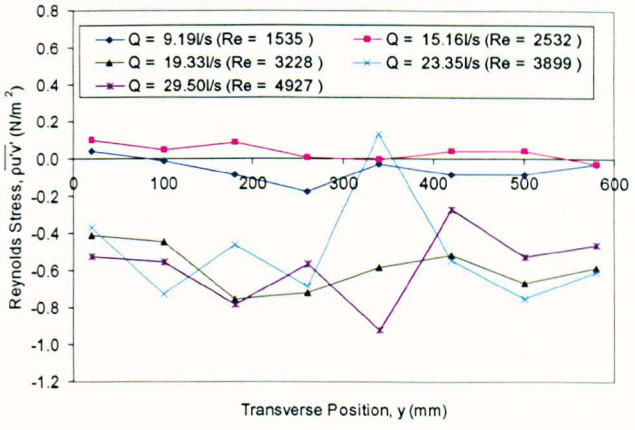

Figure 7-49 Transverse Profile of Reynolds Stress (Base Case)

According to Table 3 all tests apart from the lowest flow rate were conducted in fully turbulent flow. The lowest flow rate test was conducted in transitional flow conditions. Reynolds stress values are approximately uniform across the channel width. However, there is an observable change in Reynolds stress levels between the lowest two and highest three flow rates. This can be attributed to the fact that the bottom two profiles were not taken at the same proportion of the flow depth as the higher flow rates due to the clearance limitations of the ADV probe.

Figure 7-50 displays the vertical profile of Reynolds stresses for each discharge tested in the base case. The vertical profiles of Reynolds stress taken at 9.19l/s is not displayed due to insufficient measurements taken over the channel depth. Figure 7-51 compares the measured profile of Reynolds stress taken at the maximum flow rate with the theoretical distribution for open channel flow calculated using Equation 2-38, using a theoretical u* of 0.0368m/s calculated by Equation 2-37.

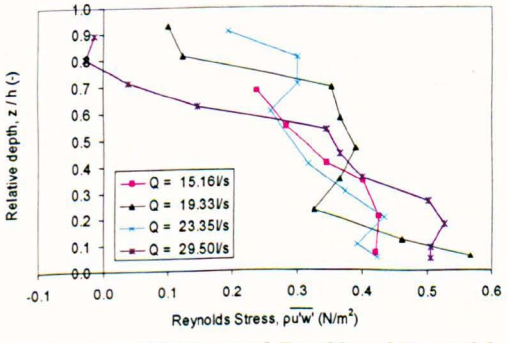

Figure 7-50 Vertical Profile of Reynolds Stress (Base Case)

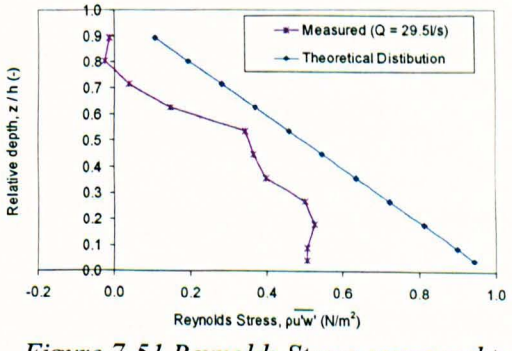

Figure 7-51 Reynolds Stress compared to theory (Base case, Q=29.5l/s)

As suggested by boundary layer theory, (see section 2.3.2.2) the profiles in Figure 7-50 exhibit a roughly linear trend from a maximum value at the bed to approximately zero at the free surface.

7.3.2 Turbulence in Reeds

Figure 7-52 and Figure 7-53 show the transverse profiles of Reynolds stress in low and high age reed cases respectively, for each discharge tested.

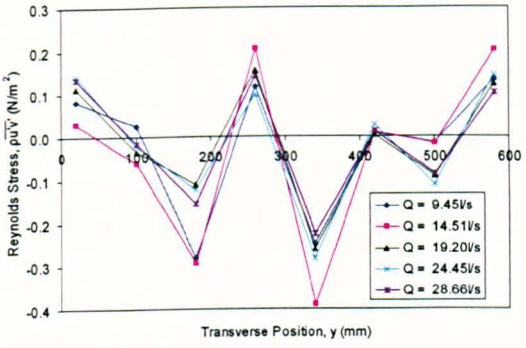

Figure 7-52 Transverse profile of Reynolds Stress (Reeds, week 20)

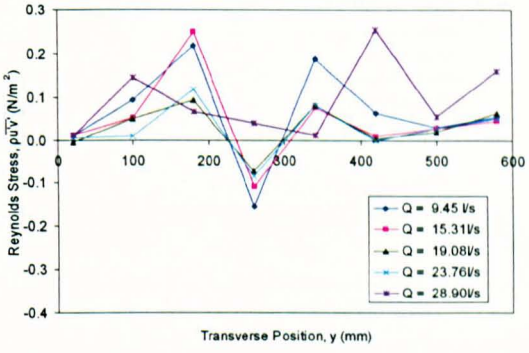

Figure 7-53 Transverse profile of Reynolds Stress (Reeds, week 50)

The profiles exhibit several spikes in Reynolds stress due to the wakes and eddies generated by the local presence of individual vegetation elements. In the high age (and therefore higher density) reeds case the magnitude of the spikes appears to be slightly smaller, with fewer regions of strong negative Reynolds stresses.

Figure 7-54 and Figure 7-55 show the vertical profiles of Reynolds stress in low and high age reed cases respectively, for each discharge tested.

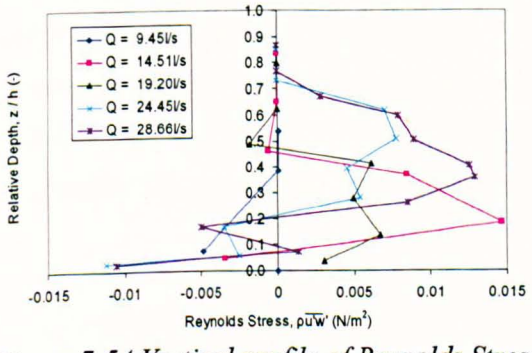

Figure 7-54 Vertical profile of Reynolds Stress (Reeds, week 20)

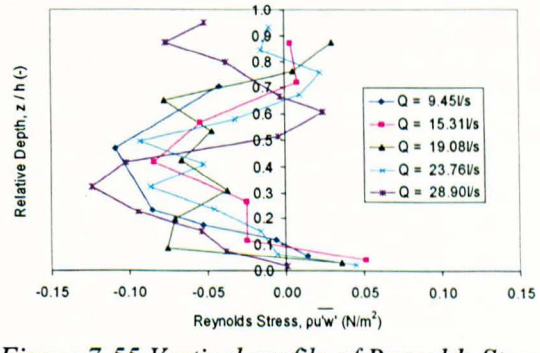

Figure 7-55 Vertical profile of Reynolds Stress (Reeds, week 50)

In both Figure 7-54 and Figure 7-55 there is no observable trend in Reynolds stress over the flow depth.

7.3.3 Turbulence in Emergent Carex

The transverse Reynolds stress profiles taken in the channel containing emergent Carex are presented in Figure 7-56 and Figure 7-57. Although at the highest flow rates the Carex are classified as submerged, all profiles displayed here are taken within the canopy and thus are

presented here for both completeness and to provide a comparison. Vertical profiles of Reynolds stress are displayed as part of the full Reynolds stress profiles in the submerged Carex section.

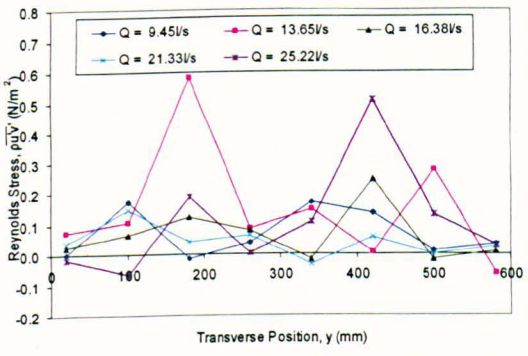

Figure 7-56 Transverse profile of Reynolds Stress (Carex, week 2)

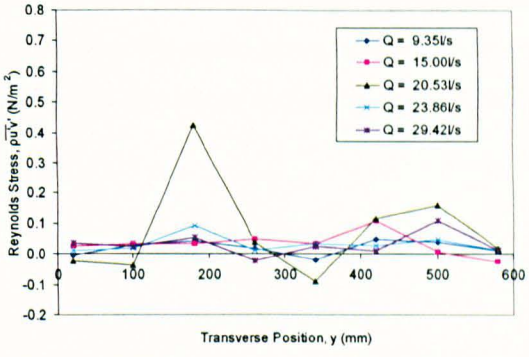

Figure 7-57 Transverse profile of Reynolds Stress (Carex, week 24)

Figure 7-56 and Figure 7-57 show the transverse profiles of Reynolds stress for each flow rate, in tests conducted 2 and 24 weeks after planting respectively. The profile taken in the low age, Carex plants exhibit spikes in Reynolds stress due to the presence of wakes and eddies generated by the vegetation elements. In the high age Carex plants the number and magnitude of these spikes is reduced.

7.3.4 Turbulence in Submerged Carex (Growth)

The transverse and vertical profiles of Reynolds stress taken in the channel containing submerged Carex are presented in Figure 7-58 and Figure 7-59. At the maximum flow velocity in tests conducted at week 7 and 20 transverse Reynolds stress profiles were taken above, as well as within the canopy. Profiles taken above the canopy were measured 2cm below the total flow depth. The profiles can be compared to the profiles taken within the canopy.

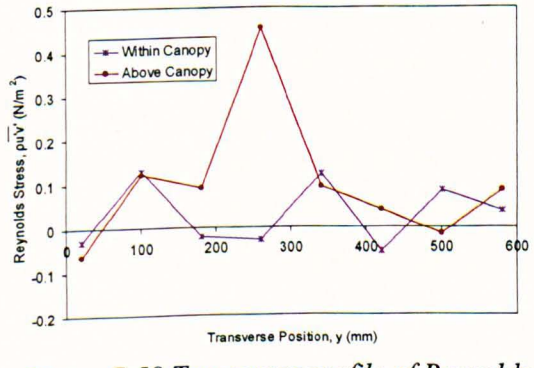

Figure 7-58 Transverse profile of Reynolds stress in and above canopy (Carex, Week 7)

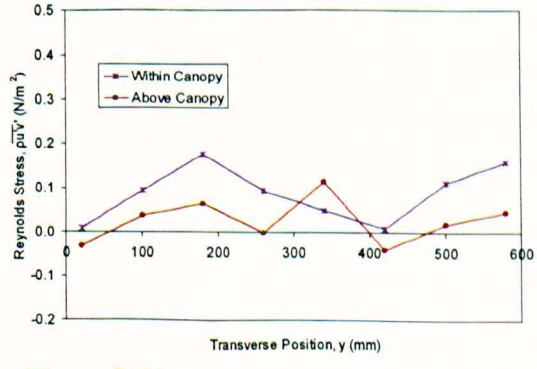

Figure 7-59 Transverse profile of Reynolds stress in and above canopy (Carex, Week 20)

Figure 7-58 and Figure 7-59 display the transverse profile of Reynolds stress in and above the canopy at the maximum flow rate (29.5l/s) in tests conducted 7 weeks and 20 weeks after

planting respectively. Apart from the occurrence of one spike in the profile taken in the smaller Carex case, there is little noticeable difference between the profiles.

Full vertical profiles of Reynolds stress were taken from week 7 onwards. Figure 7-60 and Figure 7-61 show the vertical profile Reynolds stress for each flow rate, in tests conducted 7 and 24 weeks after planting respectively. The vertical profiles of Reynolds stress in submerged flow are plotted with respect to the canopy height, h_c in order to provide an indication of the effect of submergence on the profiles.

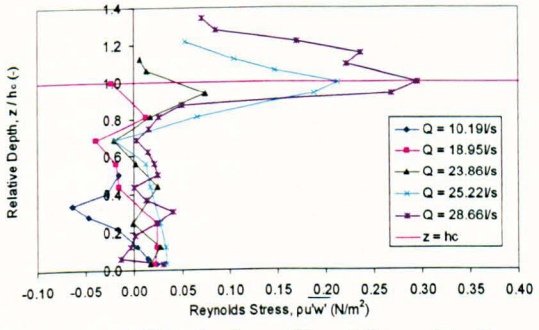

Figure 7-60 Vertical profile of Reynolds Stress (Carex, Week 7)

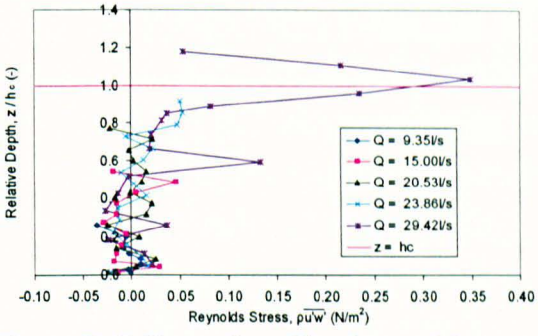

Figure 7-61 Vertical profile of Reynolds Stress (Carex, Week 24)

Profiles taken in emergent conditions (10.19l/s to 18.95l/s in week 7, 9.39l/s to 20.53l/s, week 24) exhibit negligible level of Reynolds stress over the depth. In submerged cases a higher region of Reynolds stress is observed towards the top of the canopy. Above the canopy top the levels of Reynolds stress decay towards the free surface. The measured Reynolds stress at the canopy top increases with flow rate in the week 7 test. The Reynolds stress values at the canopy top measured at the maximum flow rate are quite close in the tests conducted 7 and 24 weeks after planting (0.30 N/m^2 and 0.34 N/m^2), respectively.

7.3.5 Turbulence in Submerged Carex (Cropped)

The vertical Reynolds stress profiles taken in the channel containing cropped Carex are presented in Figure 7-62 and Figure 7-63. Transverse Reynolds stress profiles are not displayed as they were taken in similar conditions (similar stem diameters, porosities, discharge) to the Reynolds stress profiles taken at the last test in the growth phase. The lowest flow rate in the Reynolds Stress profile in the cropped to 5.5cm case is not displayed due to insufficient measurements taken over the channel depth.

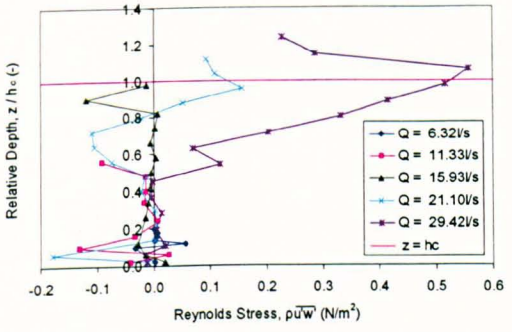

Figure 7-62 Vertical profile of Reynolds Stress (Carex cropped to 25cm)

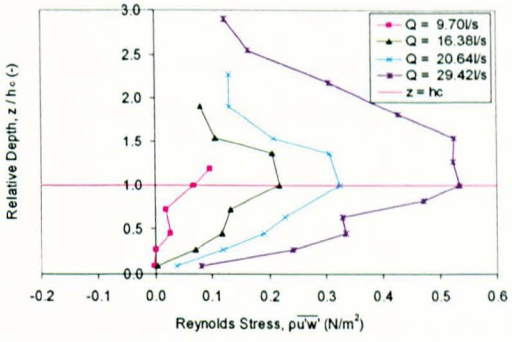

Figure 7-63 Vertical profile of Reynolds Stress (Carex cropped to 5.5cm)

Figure 7-62 shows the vertical profile of Reynolds stress taken after the Carex were cropped to a height of 25cm. Similarly to the growth phase tests, the profiles taken in emergent conditions (6.32l/s – 15.93l/s) exhibit negligible level of Reynolds stress over the depth. In submerged cases a higher region of Reynolds stress is observed towards the top of the canopy. Above the canopy the levels of Reynolds stress decay towards the free surface. Figure 7-63 shows the vertical profiles of Reynolds stress taken after the Carex were cropped to a height of 5.5cm. In this case there is no region of negligible Reynolds stress. The Reynolds stress values increase from the bed to the canopy top, h_c and then decrease to the free surface. In both cases the maximum value of Reynolds stress achieved increases with flow rate for each test; comparing growth phase (Figure 7-60 and Figure 7-61) to cropped phase (Figure 7-62 and Figure 7-63) shows that the Reynolds stress measured at the canopy top in the cropped phase are higher than in the growth phase ($0.3N/m^2$ in the growth phase, $0.5N/m^2$ in the cropped phase at maximum discharge).

7.3.6 Discussion of Turbulence

7.3.6.1 Base Case

Section 7.3.1 shows that in the base case there is little variation in transverse Reynolds stress across the channel (Figure 7-49). The vertical profile of Reynolds stress shows a roughly linear decay with distance away from the bed (Figure 7-50). This concurs with the shape of the theoretical distribution of shear stress in an open channel (see section 2.3.2.2). Having conducted this analysis it is now possible to calculate a bed shear velocity (u*) using three different methods.

1. By calculating the average shear velocity theoretically using Equation 2-37

2. By measuring the distribution of Reynolds stress the value of the shear stress at the bed, τ_0 can be determined by linear interpolation (assuming viscous stresses are negligible – see section 2.3.2). This can be converted to shear velocity using Equation 2-37.

3. Determining the best fit value of u* when fitting the velocity profiles to the measured vertical profiles of primary velocities (as in section 7.2.1)

Values of shear velocity derived from the different methods for all flow rates tested in the base case are presented in Figure 7-64.

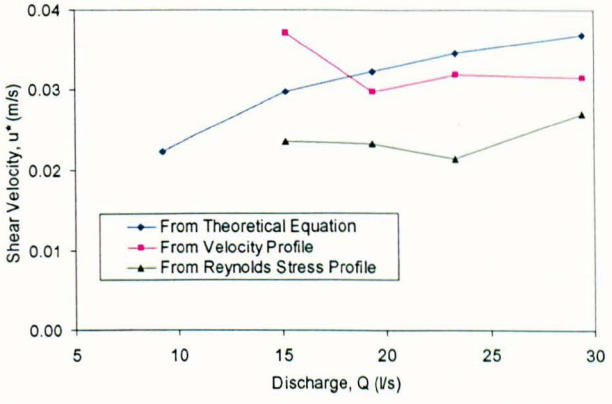

Figure 7-64 Comparison between different measurements of shear velocity (Base Case)

Babaeyan-Koopaei et al. (2002) also compared shear velocity calculated in a natural channel using the three methods listed above, finding a significant (≈ 30%) error between the theoretical (method 1) and measured values (methods 2 and 3). However, the recorded values from the turbulence and velocity profiles (method 2 and 3) were relatively close (≈ 8%). In this channel the difference between the Reynolds stress (method 2) and velocity derived shear velocity (method 3) values are quite large (≈ 20%). This must be due to error in the regression analysis when fitting a linear profile to the profile of Reynolds stress, and determining a best fit u* for the velocity profiles. The theoretical equation for shear velocity (method 1) determines average bed shear stress. Thus any discrepancy between the theoretical and measured values may be due to local bed effects acting close to the vertical profile measurement point.

7.3.6.2 *Transverse Profile in Vegetated Channels*

Transverse profiles of Reynolds stress through the vegetated canopies are displayed in sections, 7.3.2, 7.3.3 and 7.3.4. Profiles can be compared by plotting the transverse profiles of Reynolds stress taken at the maximum flow rate in the base case, reeds and Carex (within the canopy) (Figure 7-65).

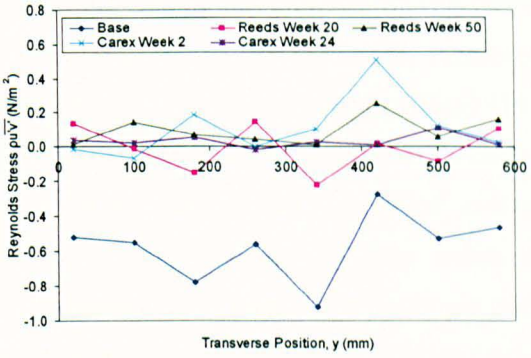

Figure 7-65 Comparison of transverse profile of Reynolds stress in different testing cases ($Q \approx 29.5l/s$)

Compared to the base case, the general levels of transverse Reynolds stress appears to be suppressed by the presence of vegetation, especially in the higher age (i.e. larger Carex, denser reeds) cases. This concurs with the findings of previous researchers such as Gambi et al. (1990), Leonard and Luther (1995) and Sand-Jensen and Penderson (1999) who also observed reduced Reynolds stress in vegetated canopies. This is caused by the plants absorbing momentum from the flow (see 3.2.1.1). In the low age Carex (λ = 0.998) Carex and the reeds cases there are several spikes in Reynolds stress which are generated by the wakes of the vegetation elements, while in the high age Carex (λ = 0.941) these spikes disappear. This may be due to the faster cross sectionally averaged velocity present in the younger Carex and reeds conditions which generates strong wakes and eddies behind vegetation elements. In the tests involving older, larger Carex plants the average canopy velocity is suppressed due to the high flow resistance (see section 7.1), and the size and strength of the turbulent wakes is reduced.

7.3.6.3 Vertical Profiles in Emergent Vegetated Channels

The vertical Reynolds stress profiles in emergent flows are plotted in sections 7.3.2, 7.3.3 and 7.3.4. To provide a comparison between the different vegetated and non vegetated cases the profiles can be plotted together (Figure 7-66). In this case the maximum discharge is not used as the Carex would be in a submerged condition.

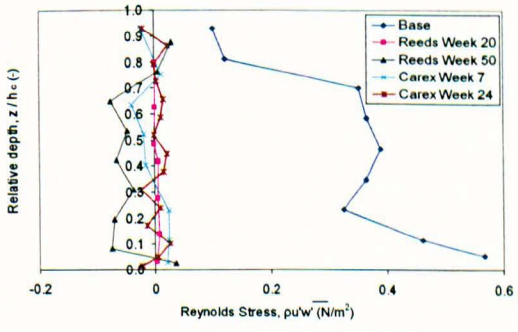

Figure 7-66 Comparison of vertical profile of Reynolds stress in different emergent testing cases ($Q \approx 20l/s$)

Figure 7-66 shows that within the canopy the presence of vegetation suppresses the levels of vertical Reynolds stress in comparison to the base case, measured Reynolds stress values becoming almost negligible. Similarly to the findings of Nepf (1999) the vertical Reynolds stress is approximately 3-4 times smaller than the transverse Reynolds stress in vegetated cases (average transverse Reynolds stress taken in Carex $\approx 0.12 N/m^2$, average vertical Reynolds stress taken in Carex $\approx 0.035 N/m^2$). This is because the stem wakes which are responsible for turbulence generation in vegetated flow create non isotropic turbulence, i.e. the vertical orientation of the plant stems generates transverse rather than vertical stem wakes.

Unlike the base case, in vegetated conditions there is no clear trend with depth and the position of maximum stress is no longer at the channel bed. The lower levels of vertical Reynolds stress in vegetated canopies means that the transport of mass and momentum over the channel depth is reduced relative to the base case.

7.3.6.4 *Vertical Profiles in Submerged Vegetated Channels*

Figure 7-67 shows the structure of the vertical Reynolds stress in the submerged growing Carex cases conducted at maximum flow rate. Figure 7-68 shows the structure of the vertical Reynolds stress in the submerged cropped Carex cases conducted at maximum flow rate. To examine the structure of Reynolds stress in submerged vegetated canopies it is necessary to plot Reynolds stress with reference to the canopy top h_c.

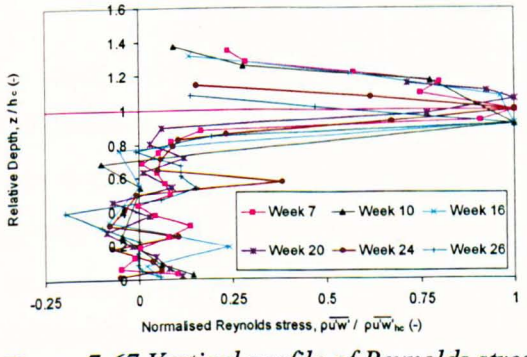

Figure 7-67 Vertical profile of Reynolds stress in growing Carex (Q = 29.5l/s)

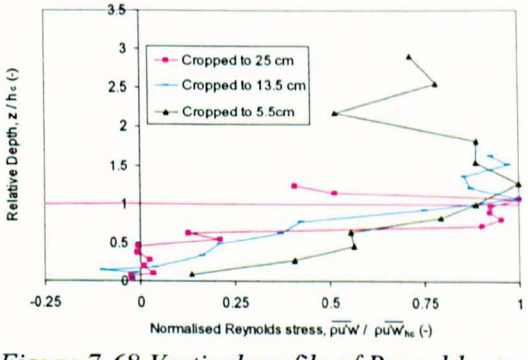

Figure 7-68 Vertical profile of Reynolds stress in cropped Carex (Q = 29.5l/s)

The vertical profiles of Reynolds stress exhibit a strong peak at the position of the canopy top. This height also coincides with the inflection in the velocity profile discussed in section 7.2.6.4. The profile of vertical Reynolds stress agrees well with the analogy to a shear layer as proposed by Raupach et al (1984) who also found a peak in Reynolds stress at the canopy top.

Using a combination of the vertical velocity and the Reynolds stress profiles the proportions of the wake zone, mixing layer and free flow layer (as shown in Figure 3-4, and discussed in

section 3.2.2.1) can be defined (Figure 7-69 and Figure 7-70). The exact definition of the mixing layer size is subjective but can be estimated to within 1-2cm.

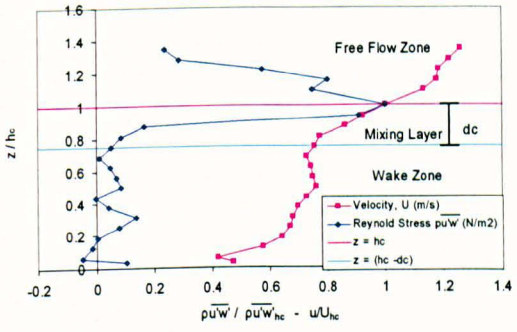

Figure 7-69 Flow Structure in Week 7 Carex Q = 29.5l/s

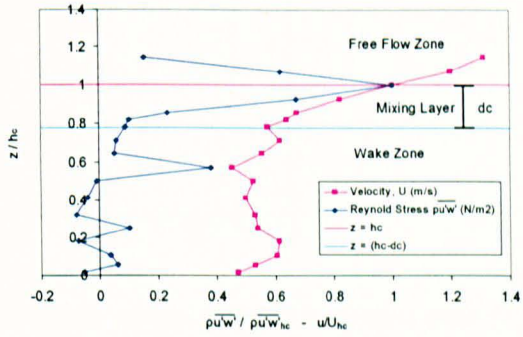

Figure 7-70 Flow Structure in Week 24 Carex Q = 29.5l/s

Figure 7-69 and Figure 7-70 show how the canopy height and mixing layer can be appraised from the profiles of velocity and Reynolds stress. The peak Reynolds stress and velocity inflection point coincide with the canopy top, h_c. The mixing layer penetration into the canopy, d_c can be defined as the distance between the canopy height h_c, downwards until the point where Reynolds stress becomes constant with depth. This value coincides with the distance in the vertical profile of velocity from h_c to where the velocity falls to the canopy layer velocity (U_c) (Figure 7-69 and Figure 7-70). The changing properties of the turbulent flow structure with plant growth can now be investigated.

7.3.6.5 Shear/mixing Layer Penetration Depth

As discussed in section 3.2.2 recent research (Nepf et al., 2007) has focused on how far turbulence from the shear layer penetrates into the canopy (i.e. the size of the mixing zone, d_c). This is important because within the mixing layer mass and momentum is transported relatively quickly over the depth (due to the high region of Reynolds stress) compared to the wake zone. As explained in section 2.4.2.4 vertical transport acts to reduce the magnitude of vertical shear dispersion. So the influence of the mixing layer will be important in understanding longitudinal mixing in submerged conditions. Comparing Figure 7-67 and Figure 7-68 it can be seen that the mixing layer penetrates to a greater extent in the cropped phase than the growth phase. Figure 7-68 shows that when the vegetation is cropped to 5.5 cm height the mixing layer penetrates to the bed and hence the wake zone is no longer present in this case. The average depth of penetration of the mixing layer can be plotted for each flow condition (Figure 7-71).

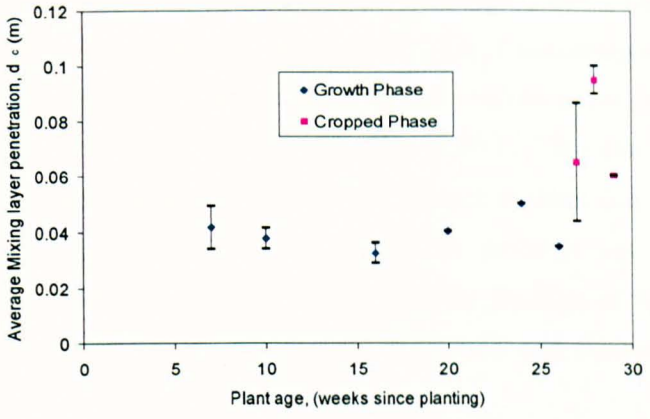

Figure 7-71 Average mixing layer penetration into canopy for each vegetated case

Figure 7-71 show the measured depths of mixing layer penetration into the canopy (values are averaged for each vegetated case). The turbulence from the mixing layer penetrates 3-5 cm into the canopy in the growth phase and approximately 6-9 cm in the cropped phase. The larger penetration in the cropped phase may be due to the changing morphology of the canopy top. The presence of flexible leaf elements in the growth phase may create a physical barrier between the canopy and free flow layers. This effect results in a smaller wake zone in the cropped phase as observed in Figure 7-68.

7.3.6.6 Reynolds Stress above the Canopy

The results can also be used to examine the Reynolds stress levels above the canopy top (Figure 7-72).

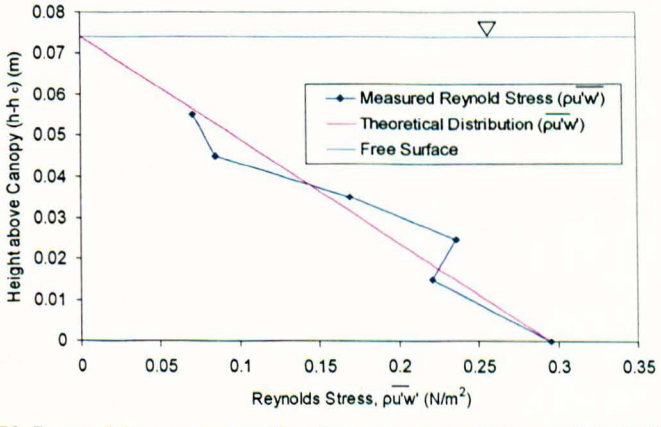

Figure 7-72 Reynolds stress profile above canopy (Carex, Week 7, Q=29.5l/s)

Figure 7-72 shows the Reynolds stress profile above the canopy for one submerged case. Above the canopy the Reynolds stress reduces in a linear manner to the free surface. If the free flow zone above the canopy is considered as a boundary layer (with depth $h-h_c$ and shear velocity derived from the Reynolds stress measured at h_c) the Reynolds stress profile in the free flow zone corresponds well with the linear theoretical relationship proposed in Equation 2-38.

However, if a canopy top shear velocity is calculated theoretically using Equation 3-30, then the Reynolds stress profile will be over predicted (Figure 7-73). Examining all tests in submerged flow it is found that Equation 3-30, provides shear velocity values at the canopy top (u^*_{hc}) 40% greater than those measured by the ADV probe (Figure 7-73). This may be due to either the probe not being positioned or aligned in exactly the correct position (i.e. not being positioned exactly at the canopy top), or that the position of the probe is not at a point which is representative of the entire flow field. This differs from the findings of Righetti and Armanini (2002) who found a difference of 8% between the theoretical and measured values of canopy top shear stress (u^*_{hc}).

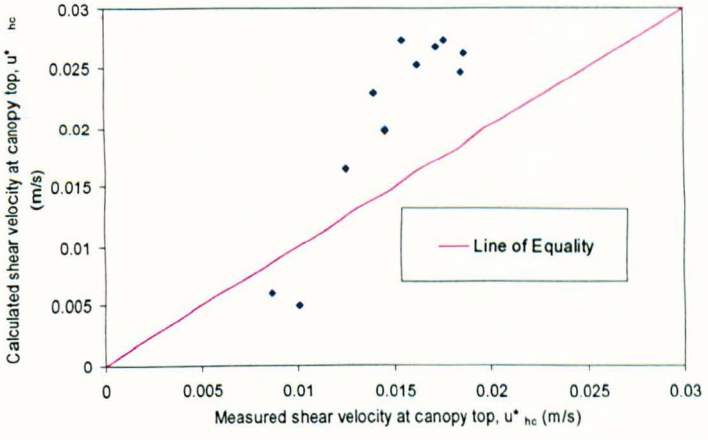

Figure 7-73 Comparison between measured and calculated u^*_{hc}

The strength of the Reynolds stress value at the canopy top in each vegetated case has been observed to increase with flow (Figure 7-60, Figure 7-62 and Figure 7-63). It is also noted that the recorded values are much higher in the cropped than the growth phase. It is anticipated that the canopy top Reynolds stress will be related to the strength of the velocity inflection, and in turn the depth of the free flow layer and the canopy resistance. A full study of the canopy top Reynolds stress and its related parameters is not within the scope of this work. Canopy top shear velocity (u^*_{hc}) will be assumed to be sufficiently well described by Equation 3-30.

7.3.6.7 *Effect of Plant Growth on Flow Structure*

To investigate the effect of plant growth and cropping on the changing proportions of the different zones within the flow, the position of the canopy height (from direct measurement) and the top of the wake zone has been plotted (by measuring the velocity and turbulence profiles) for each test (Figure 7-74).

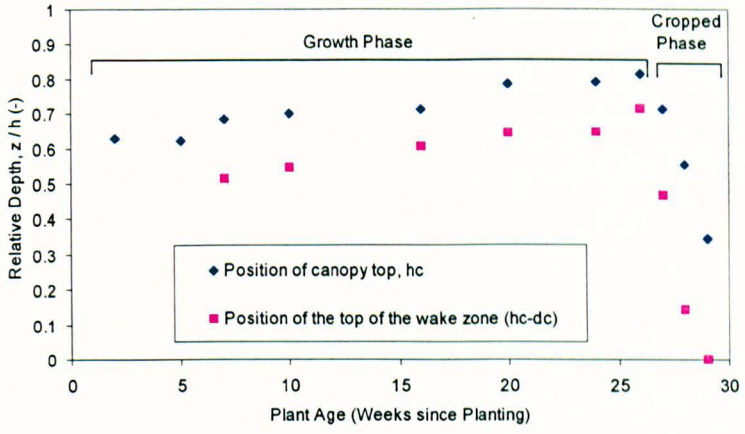

Figure 7-74 Proportion of flow inside the canopy and inside the wake zone for Carex tests conducted at maximum discharge (≈29.5l/s)

Figure 7-74 shows the proportion of the flow inside the canopy and inside the wake zone for each Carex test. The proportion of the flow both inside the canopy and the wake zone increases throughout the growth stage as the Carex increases in height. At the last growth stage the free flow zone comprises less than 20% of the entire flow. As the vegetation is cropped lower, the wake zone (between the bed and the mixing layer where uniform velocity profiles exist) is constricted. In the final cropped case (cropped to 5.5cm), conducted at week 29, this region disappears completely and the vertical profile of primary velocities becomes almost linear (Figure 7-46).

7.3.6.8 Summary of Turbulence Discussion

The main conclusions of the turbulence study can be summarised as

- The overall level of transverse Reynolds stress within the canopy is reduced in vegetated flows relative to the base case. However, spikes of high Reynolds stress are generated by the presence of stem wakes. As the cross sectionally averaged velocity becomes more suppressed with increasing plant age/size the size of these spikes reduces.

- In emergent conditions (and within the wake zone in submerged flow) the vertical Reynolds stress is much reduced relative to the base case, becoming almost negligible.

- In submerged canopies a mixing/shear layer will form between the canopy and free flow layer. The mixing layer is a region of high Reynolds stress and hence relatively rapid vertical transport occurs. The peak value of Reynolds stress occurs at the canopy top, in the same position as the velocity inflection observed in the vertical profiles of primary velocity.

- The Reynolds stress profile above the canopy behaves similarly to conventional boundary layer flow and decays in a linear manner to the free surface.

- The region of high Reynolds stress (mixing/shear layer) penetrates a distance (d_c) into the canopy. Mixing layer penetration is greater for the cropped phase than the growth phase.

- Throughout the growth phase the size of the wake zone increases, while the free flow zone decreases. As the vegetation is cropped, the size of the wake zone decreases and the free flow zone becomes larger. In the final test the wake zone disappears and the mixing/shear layer penetrates to the bed.

7.4 Transverse Mixing Results and Discussion

This section presents the results of the transverse mixing experiments conducted in the channel. Transverse mixing coefficients were measured using the Boxall and Guymer (2001) method, as detailed in sections 2.4.5.2, 5.3.9, and 6.3. Transverse mixing coefficients were measured from week 16 onwards in the Carex tests, in both high and low density reeds tests and in the base case.

7.4.1 Transverse Mixing in the Base Case

Figure 7-75 displays how transverse mixing increases with flow depth in the base case. Figure 7-76 presents transverse mixing as a function of hu*.

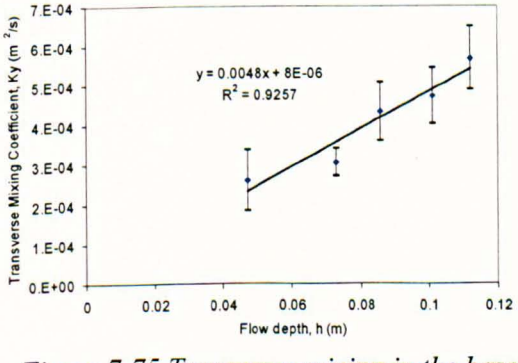

Figure 7-75 Transverse mixing in the base case against flow depth

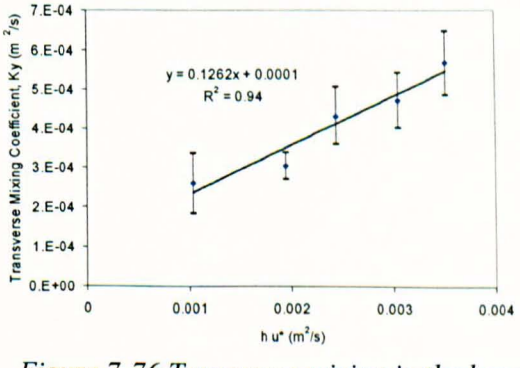

*Figure 7-76 Transverse mixing in the base case against hu**

As discussed in section 3.3.2.1, transverse mixing is conventionally scaled against the product hu*. The best fit linear relationship is plotted to provide a normalised K_y/hu* value of 0.126 for the base case.

7.4.2 Transverse Mixing in Reeds

Figure 7-77 shows the transverse mixing rates plotted against depth for each test conducted. Figure 7-78 shows the transverse mixing rates plotted against the conventional scaling product hu* for each test conducted. For comparison, the base case mixing rate ($K_y = 0.126hu^*$) is also plotted.

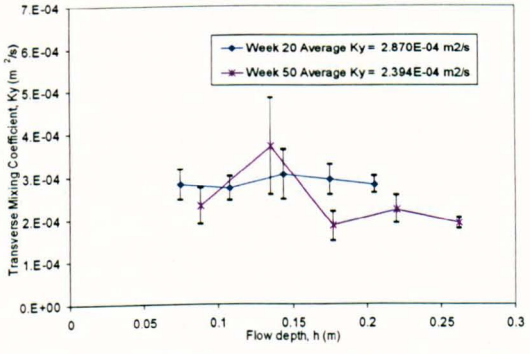

Figure 7-77 Transverse mixing in reeds against depth

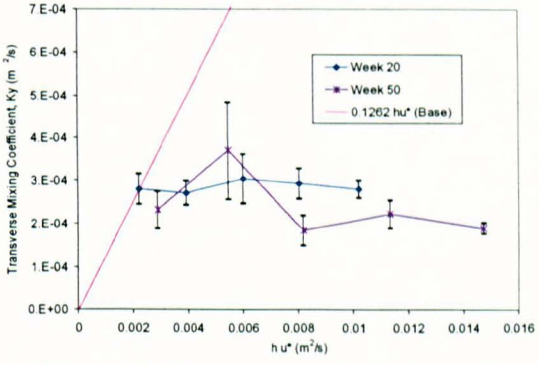

*Figure 7-78 Transverse mixing in reeds against hu**

Figure 7-77 and Figure 7-78 shows no trend in transverse mixing coefficient in reeds with either flow depth or the conventional scaling product hu*. As described in section 3.3.2 Fischer and Hanamura (1975) proposed that in channel featuring vertical roughness strips the transverse mixing is described more accurately as a product of channel velocity and strip (or in this case stem) diameter, S_d. In Figure 7-79 transverse mixing is plotted against the product US_d.

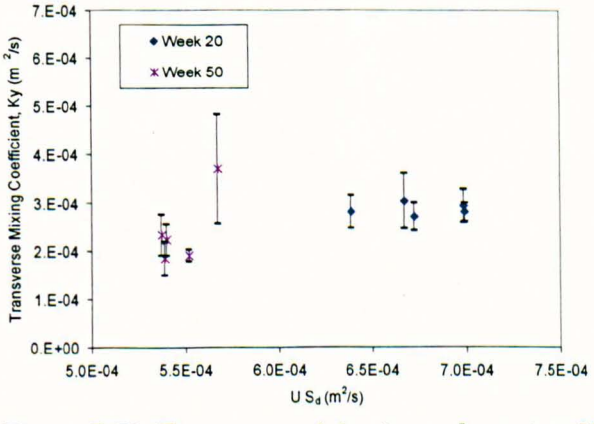

Figure 7-79 Transverse mixing in reeds against US_d

Figure 7-79 shows that over this range of US_d there is no observable trend in transverse mixing coefficient.

7.4.3 Transverse Mixing in Emergent Carex

Figure 7-80 shows the transverse mixing rates plotted against depth for each test conducted. Figure 7-81 shows the transverse mixing rates plotted the conventional scaling product hu* for each test conducted. For comparison the best fit base case mixing rate ($K_y = 0.126hu^*$) is also plotted.

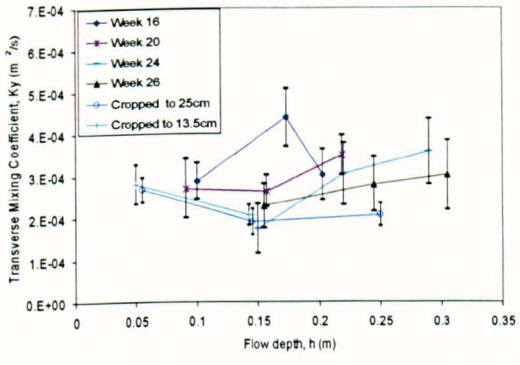

Figure 7-80 Transverse mixing in emergent Carex against depth

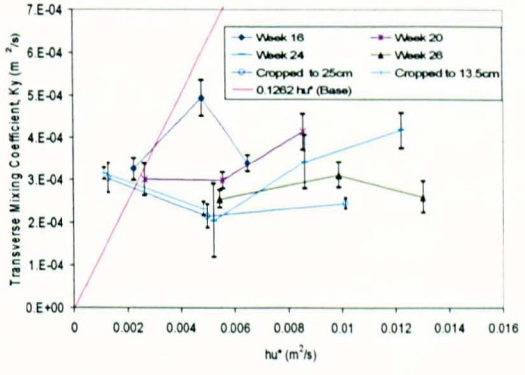

*Figure 7-81 Transverse mixing in emergent Carex against hu**

Figure 7-80 and Figure 7-81 shows that, as with the reeds there is no trend with either flow depth or the conventional scaling product hu*. Figure 7-82 shows transverse mixing plotted against the product US_d.

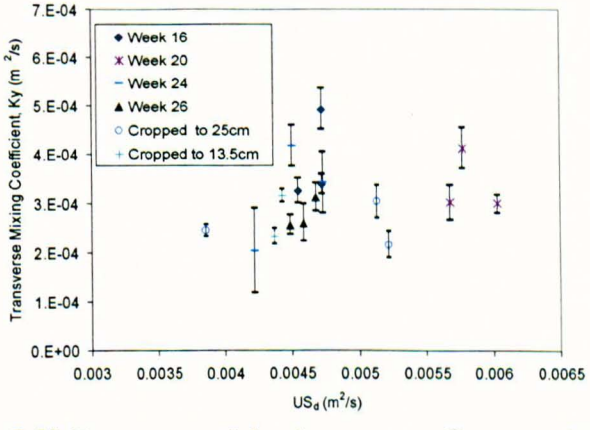

Figure 7-82 Transverse mixing in emergent Carex against US_d

Again, Figure 7-82 shows that over this range of US_d there is no observable trend in transverse mixing.

Figure 7-83 plots the average value of transverse mixing for each vegetated case (over all the flow rates conducted) against plant growth (expressed as channel porosity).

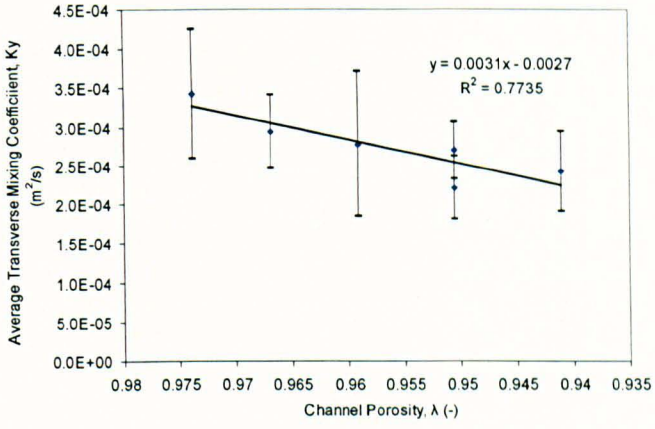

Figure 7-83 Average transverse mixing coefficient against channel porosity

Figure 7-83 shows that the transverse mixing coefficient decreases with decreasing channel porosity, suggesting that there may be an inverse relationship between Carex growth and transverse mixing.

7.4.4 Transverse Mixing in Submerged Carex (Growth and Cropped)

Figure 7-84 shows the transverse mixing rates plotted against depth for each test conducted. Figure 7-85 shows the transverse mixing rates plotted against the conventional scaling product hu* for each test conducted. For comparison the best fit base case mixing rate ($K_y = 0.126hu^*$) is also plotted.

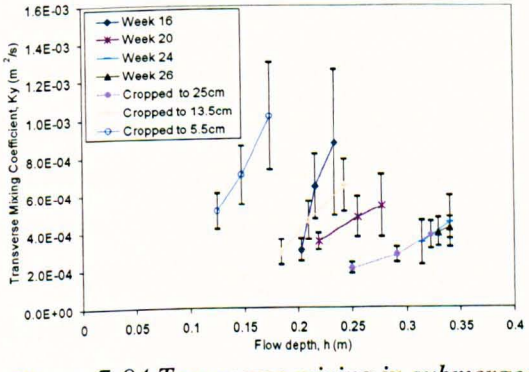

Figure 7-84 Transverse mixing in submerged Carex against depth

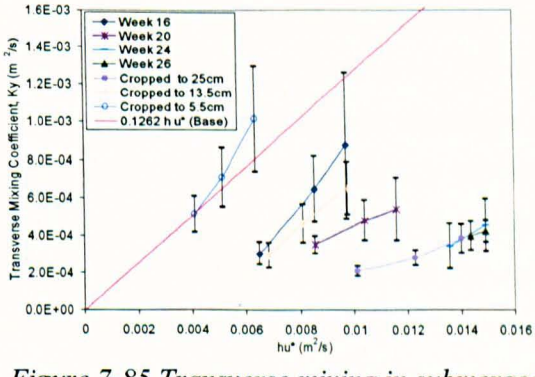

*Figure 7-85 Transverse mixing in submerged Carex against hu**

Figure 7-84 and Figure 7-85 shows that for each flow case there is a trend in transverse mixing with both flow depth and the product hu*. As discussed in section 0 the main origin of turbulence in submerged flow is at the canopy top, Reynolds stress decays to the free surface and the free flow layer acts as boundary layer flow, therefore a more suitable scaling product may be $(h-h_c)u^*_{hc}$. Figure 7-86 shows the transverse mixing rate plotted against the parameter $(h-h_c)u^*_{hc}$ for each test conducted (the parameter u* was derived using Equation 3-30).

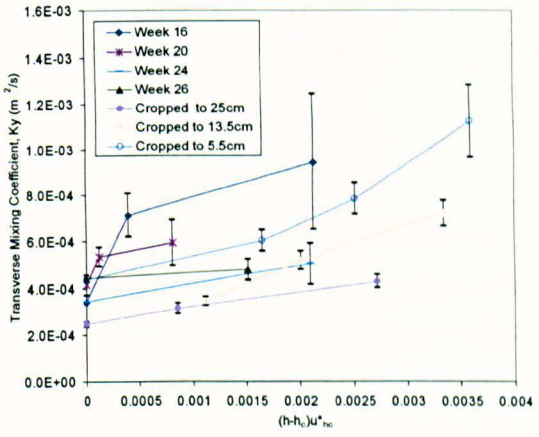

Figure 7-86 Transverse mixing in submerged Carex against $(h-h_c)u^*_{hc}$

Figure 7-86 shows there is a trend between the parameter $(h-h_c)u^*_{hc}$ and transverse mixing.

7.4.5 Discussion of Transverse Mixing

7.4.5.1 Base Case

In base case conditions the best fit value of K_y/hu^* is 0.126 which fits well with reported values for straight rectangular channels with no or negligible secondary currents (i.e. $\approx$ 0.13 from Rutherford, 1994, see section 2.4.6.2).

7.4.5.2 Emergent Conditions

Throughout the emergent flow conditions transverse mixing is approximately constant with flow depth. Figure 7-77 to Figure 7-82 show no clear relationship between either hu^* or US_d and transverse mixing in either the reeds or the Carex. As seen in section 7.3, adding vegetation to the channel suppresses the turbulence within the canopy. As a result the relationship between transverse mixing and bed shear velocity no longer exists. Roughly constant levels of turbulence and secondary currents (sections 7.2 and 7.3) through each vegetated case mean that the main drivers of transverse mixing alter little with discharge. Transverse mixing also does not seem to follow the theoretical relationship as proposed by Fischer and Hanamura (1975). However, for each flow case the range of US_d is small (at its greatest varying by 8% over the entire flow range) and experiments to establish a trend involving velocity should be undertaken over a larger range of velocities.

Figure 7-83 suggests that there may be a weak inverse relationship between plant growth and transverse mixing in Carex. This may be because larger canopies are able to suppress more turbulence by slowing average channel velocity, which would otherwise drive transverse mixing. This is supported by observing the transverse profiles of Reynolds stress as presented

and discussed in section 7.3, which show that in high age/size Carex the spikes in Reynolds stress produced by the stem wakes are suppressed.

7.4.5.3 Submerged Conditions

Once the plants become submerged the flow is split into two layers. Unlike in emergent flow the transverse mixing rates increase with flow depth and the product hu* (Figure 7-84 and Figure 7-85). As shown in section 7.3, in submerged flows turbulence is generated by the shear layer at the canopy top. Figure 7-86 shows that transverse mixing can also be scaled by the parameter $(h-h_c)u^*_{hc}$ which may provide a better description of the size and strength of the turbulence generated by the mixing layer. Figure 7-87 to Figure 7-89 show how each of the normalised coefficients change throughout the testing as the plants grow in size and the channel porosity decreases.

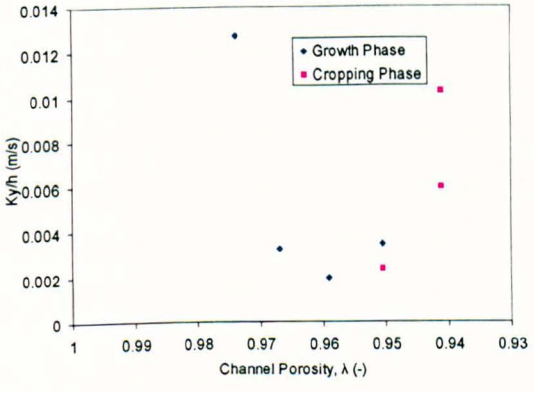

Figure 7-87 Normalised (h) transverse mixing with porosity

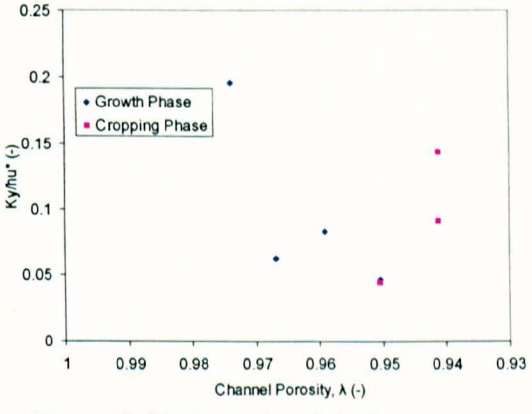

Figure 7-88 Normalised (hu) transverse mixing with porosity*

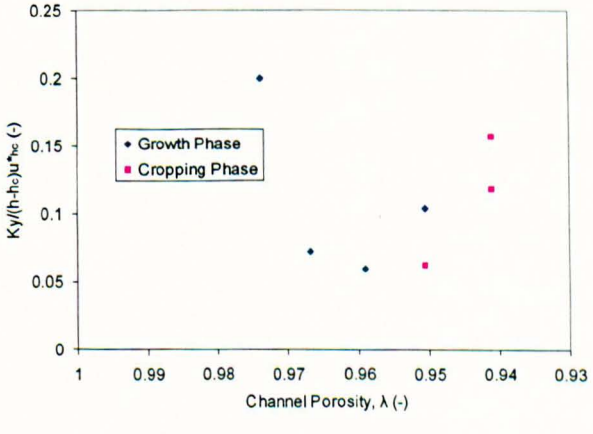

Figure 7-89 Normalised $((h-h_c)u^*_{hc})$ transverse mixing with porosity

In all cases the experiment conducted at the lowest stage of growth resulted in a normalised coefficient significantly higher than was found in the later tests. If the first experiment is disregarded as erroneous, the average and standard deviation of the normalised coefficients are presented in Table 19.

Table 19 – Normalised Transverse Mixing Coefficients in Flow through Submerged Carex

Coefficient	$\frac{K_y}{h}$ (m/s)	$\frac{K_y}{hu^*}$ (-)	$\frac{K_y}{(h-h_c)u^*_{hc}}$ (-)
Average	0.0045	0.0784	0.0954
Standard Deviation	1.78E-05	0.0556	0.0529

The coefficient varies the least when normalising by depth only, however this coefficient is not non dimensionalized, having units of m/s. The coefficient varies slightly less when normalising by the free flow layer than the whole flow. Further verification would require experiments to be conducted over a greater range of canopy heights and submergence ratios.

7.4.5.4 Summary of Transverse Mixing Discussion

Transverse mixing is driven by turbulence and secondary currents (see section 2.4.4.2). In the base case the secondary currents are relatively constant with discharge due to a lack of channel curvature (Figure 7-23). Turbulence is generated by the bed and is thus dependent on the size and strength of the turbulent eddies and is related to the product hu*.

In emergent vegetated flow turbulence is governed by the wakes acting behind vegetation elements, which decrease in size and strength as the vegetation increases in size/density and the velocity is increasingly suppressed. Secondary currents are present but are relatively constant with plant age (Figure 7-48). As a result

- In emergent conditions transverse mixing is no longer related to flow depth or the conventional scaling product hu*.
- Transverse mixing is roughly constant with flow depth.
- Despite evidence from previous research (Fischer and Hanamura, 1975, Tanio and Nepf, 2007) no relationship between transverse mixing and the product US_d was found.
- The average level of transverse mixing for each flow rate decreases as the Carex grow in size.

In submerged flow the main source of turbulence is the mixing layer (caused by velocity shear between the canopy and free flow zones).

- Mixing in submerged conditions follows a linear trend with both flow depth and hu*
- To describe turbulence generated by mixing/shear layer the scaling product $(h\text{-}h_c)u^*_{hc}$ is suggested

- Experiments show an equal variation in the non dimensionalized transverse mixing coefficients over the tests conducted.

7.5 Longitudinal Mixing Results and Discussion

In this section the results of the longitudinal mixing experiments conducted in the channel are presented. Details on the applicability of the models, reach choice, and example traces were presented earlier in section 6.5. In this section the influence of the vegetation on the mixing coefficients (the longitudinal mixing coefficient for the ADE and the dispersive fraction for the ADZ model) are investigated. Mixing coefficients presented are an average of 5 repeat tests, with error bars set at $\pm$ one standard deviation.

7.5.1 Longitudinal Mixing in the Base Case

Figure 7-90 displays how the longitudinal dispersion coefficient increases with flow depth. Figure 7-91 presents longitudinal mixing as a function of hu*.

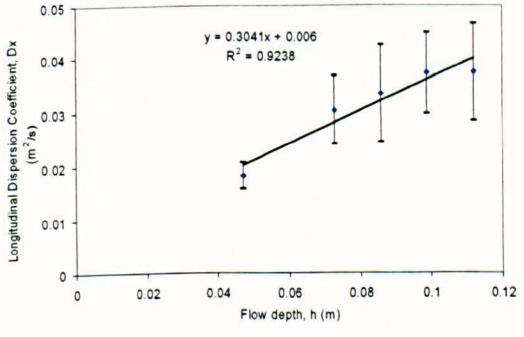

Figure 7-90 Dispersion coefficient in the base case against flow depth

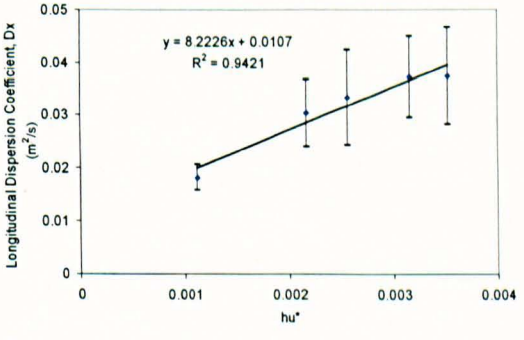

*Figure 7-91 Dispersion coefficient in the base case against hu**

As discussed in section 2.4.6.3, longitudinal mixing is conventionally scaled against the product hu*. The best fit linear relationship is also plotted and resulted in a normalised D_x/hu* value of 8.22 for the base case.

Figure 7-92 displays the relationship between dispersive fraction and flow depth. Figure 7-93 displays the relationship between dispersive fraction and discharge.

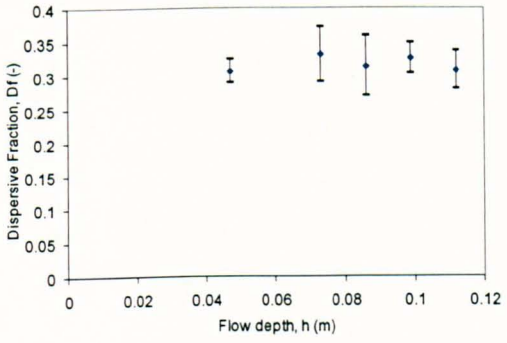

Figure 7-92 Dispersive fraction in the base case against flow depth

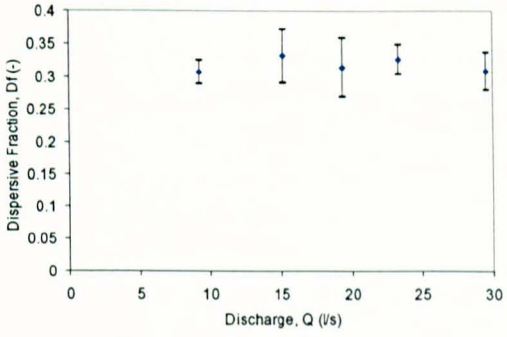

Figure 7-93 Dispersive fraction in the base case against discharge

Dispersive fraction remains roughly constant (Df $= 0.317 \pm 0.02$) for all flow cases.

7.5.2 Longitudinal Mixing In Reeds

Figure 7-94 and Figure 7-95 show the longitudinal mixing coefficient against flow depth and discharge respectively for all tests conducted in the reeds case. The base case results are also plotted for comparison.

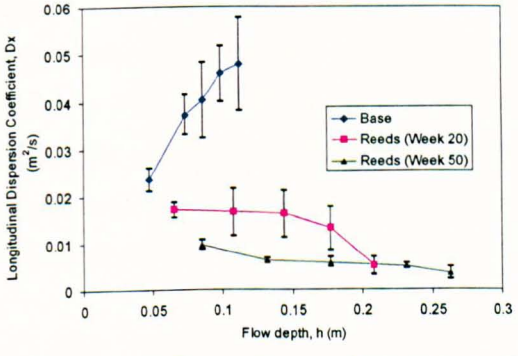

Figure 7-94 Dispersion coefficient in reeds against flow depth

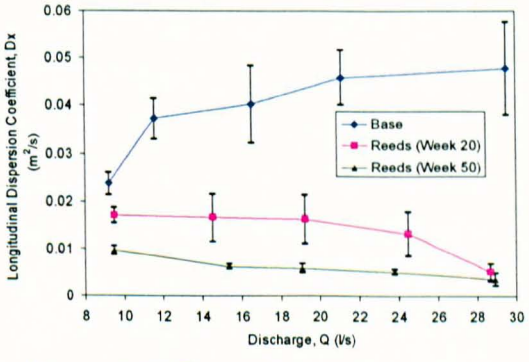

Figure 7-95 Dispersion coefficient in reeds against discharge

The plots show that the mixing coefficient in the vegetation is much lower (reduced by a factor of 2 to 4) than in the base case. In contrast to the base case the mixing coefficient in the reeds decreases slightly with flow depth and discharge. The average level of dispersion coefficient is lower in the tests taken 50 weeks after planting than those taken 20 weeks after planting.

Figure 7-96 and Figure 7-97 show the dispersive fraction against flow depth and discharge respectively for all tests conducted in the reeds case. The base case results are also plotted for comparison.

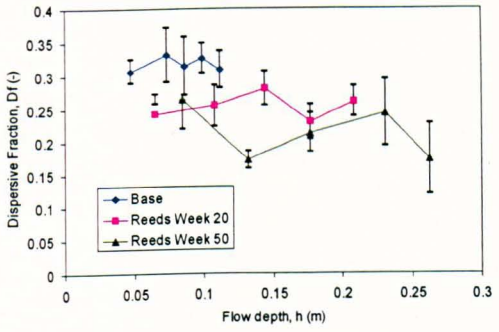

Figure 7-96 Dispersive fraction in reeds against flow depth

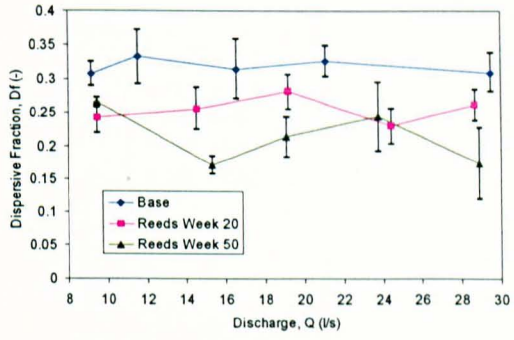

Figure 7-97 Dispersive fraction in reeds against discharge

The plots show that the dispersive fraction in the reeds is lower (≈ 30%) than in the base case. The reduction effect increases with the age of the reeds. Similarly to the base case, there is no trend in dispersive fraction with depth or discharge, though the variation of dispersive fraction over the range of flow is greater (≈ 30%).

7.5.3 Longitudinal Mixing in Growing Carex (Emergent and Submerged)

Figure 7-98 and Figure 7-99 show the longitudinal dispersion coefficient in Carex against submergence ratio and discharge respectively for tests conducted 2, 16 and 24 weeks after planting. In Figure 7-99 the base case condition is also plotted for comparison. Figure 7-100 shows the measured longitudinal dispersion coefficient for all tests conducted with each flow rate plotted as a separate series as a function of channel porosity. Stage is represented here by submergence ratio as it more clearly shows the effect of submergence.

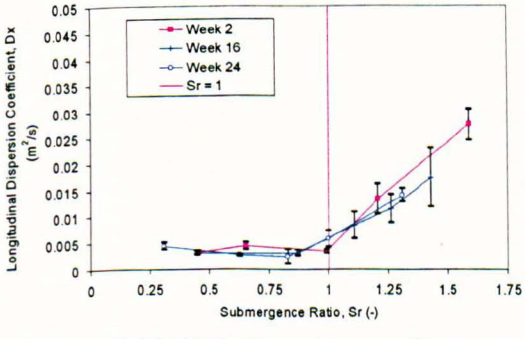

Figure 7-98 ADE dispersion coefficient in growing Carex with submergence ratio

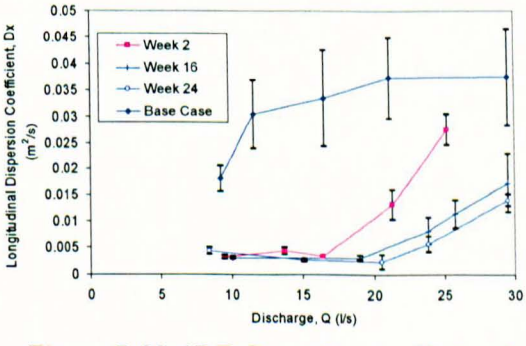

Figure 7-99 ADE dispersion coefficient in growing Carex with discharge

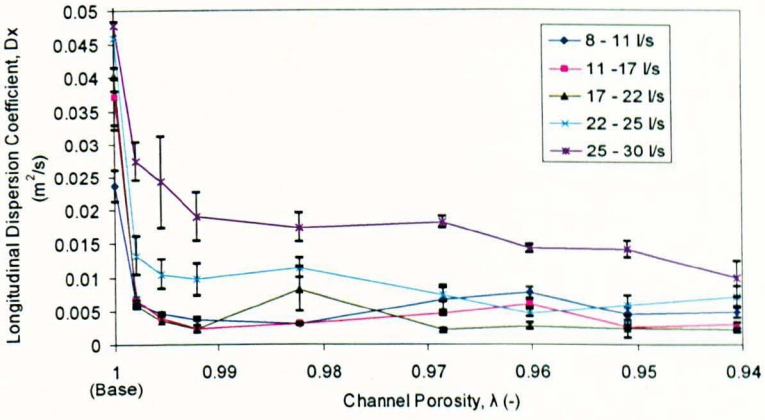

Figure 7-100 ADE dispersion coefficient in growing Carex with channel porosity

In emergent conditions (Sr < 1) the dispersion coefficient is much reduced (by a factor of 4 -5) when compared to the base case for all channel porosities. Mixing in these emergent flows is roughly constant with age and flow rate. Once the Carex become submerged (Sr > 1, at the maximum flow rate for all tests, and at the second highest flow rate in tests up to a porosity of 0.96) the dispersion coefficient increases rapidly with discharge. In all tests mixing is greatest at the maximum flow rate when the plants are submerged to the greatest extent (at the maximum flow rate). The peak value of mixing coefficient reached in each test deceases as the plants grow and the channel porosity decreases.

Figure 7-101 and Figure 7-102 show the dispersive fraction in Carex against submergence ratio and discharge respectively for tests conducted 2, 16 and 24 weeks after planting. In Figure 7-102 the base case condition is also plotted for comparison. Figure 7-103 shows the results for all mixing tests conducted with each flow rate plotted as a separate series as a function of channel porosity.

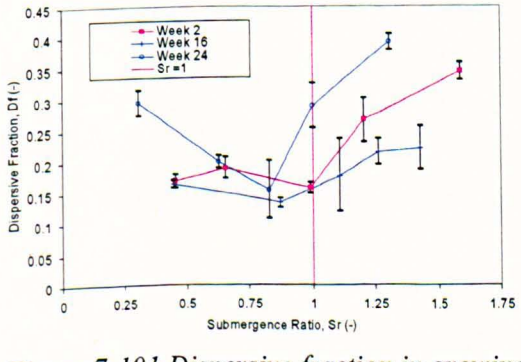

Figure 7-101 Dispersive fraction in growing Carex with submergence ratio

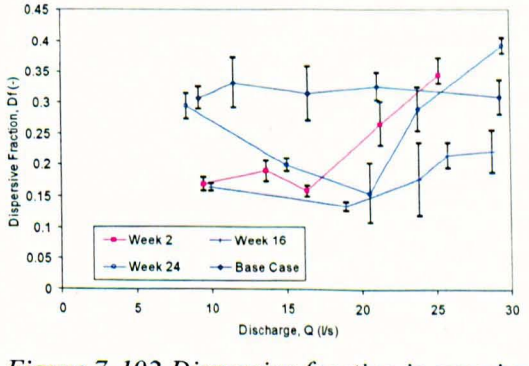

Figure 7-102 Dispersive fraction in growing Carex with discharge

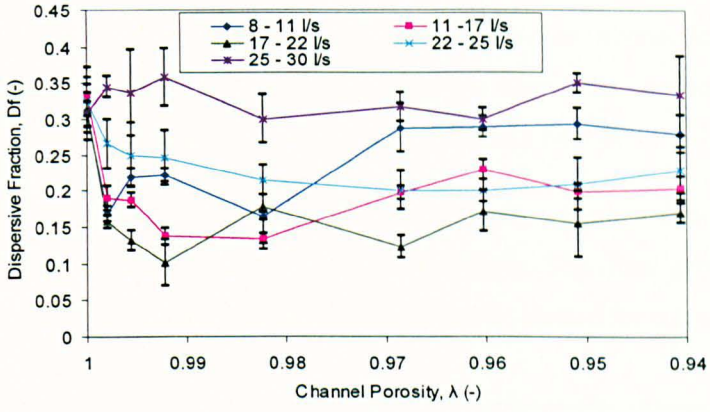

Figure 7-103 Dispersive fraction in growing Carex with channel porosity

In both Figure 7-101 and Figure 7-102 the dispersive fraction declines, or stays roughly constant, with flow rate/depth in the emergent phase, reaching a minimum at, or just before Sr = 1. After the plants become submerged the dispersive fraction rises, the maximum value of dispersive fraction occurring at the maximum flow rate. There does not appear to be a trend in dispersive fraction with channel porosity (Figure 7-103).

7.5.4 Longitudinal Mixing in Carex (Cropped)

Figure 7-104 and Figure 7-105 show the longitudinal dispersion coefficient against submergence ratio and discharge respectively for each of the cropped Carex cases. The final growing Carex test is plotted for comparison. In Figure 7-105 the base case is also plotted for comparison. Stage is again represented here by submergence ratio as it more clearly shows the effect of submergence.

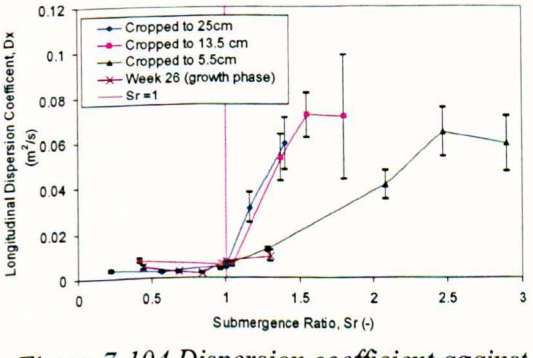

Figure 7-104 Dispersion coefficient against submergence ratio in cropped Carex

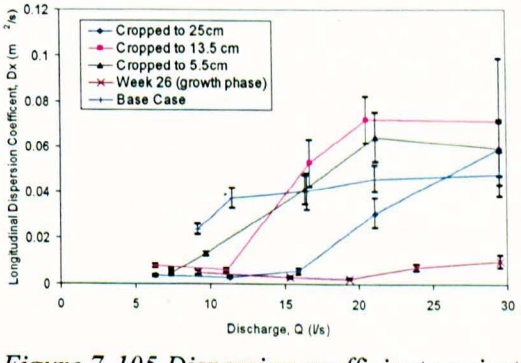

Figure 7-105 Dispersion coefficient against discharge in cropped Carex

In emergent cropped conditions the longitudinal dispersion coefficient behaves in a similar manner to the emergent growth phase Carex (i.e. much reduced levels compared to the base case), and in the submerged phase the dispersion increases with discharge/flow depth. However, in the cropped phase the dispersion coefficient again increases at a greater rate and reaches a higher value than in the growth phase. The dispersion coefficients reached at the maximum flow

rate in the three cropped cases are higher than the maximum value in the base case. The first two cropped (cropped to 25cm and 13.5cm) cases follow an almost identical trend with submergence ratio, while in the 5.5cm cropped case the dispersion coefficient increases with submergence at a lower rate, reaching a peak at approximately Sr = 2.5.

Figure 7-106 and Figure 7-107 show the dispersive fraction against submergence ratio and discharge respectively in each of the cropped Carex cases. The final growing Carex test is plotted for comparison. In Figure 7-107 the base case is also plotted for comparison.

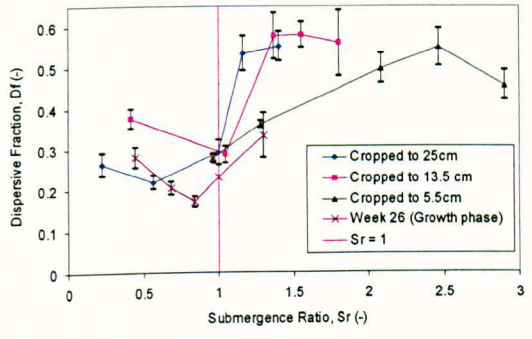

Figure 7-106 Dispersive fraction against submergence ratio in cropped Carex

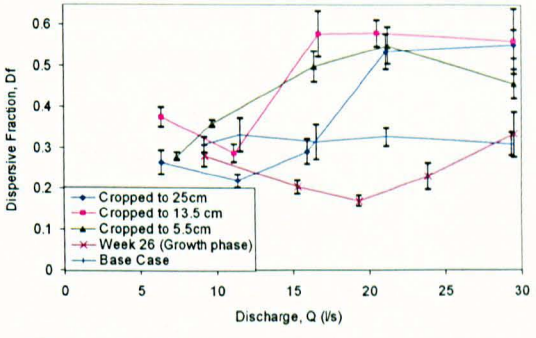

Figure 7-107 Dispersive fraction against discharge in cropped Carex

The dispersive fraction declines with flow rate/depth in the emergent phase, reaching a minimum at Sr = 1. After the plants become submerged the dispersive fraction rises, reaching a higher value than in the growth phase.

7.5.5 Discussion of Longitudinal Mixing

7.5.5.1 Base Case

In the base case there is a strong relationship between both h and hu* and longitudinal mixing coefficient. The best fit value of D_x/hu^* is 8.22 which is slightly higher than the theoretical value proposed by Elder (1959) for plane shear flow (5.26 - see section 2.4.4.4). However, this value does not include mixing due to transverse shear. Although the transverse velocity profiles (section 7.2) suggest that longitudinal mixing due to transverse shear will be small, the coefficient D_x/hu^* would still be expected to be slightly greater than 5.26.

The dispersive fraction remained constant with discharge and flow depth. This is in agreement with field data by Wallis et al., (1989a) who found that dispersive fraction was roughly constant with discharge.

7.5.5.2 Effect of Emergent Vegetation

The effect of vegetation on the velocity profiles and the subsequent reduction in velocity shear is presented in section 7.2. Although the transverse velocity shear is only changed slightly in vegetated canopies, the vegetation has a large impact on the vertical velocity shear. Vertical profiles of primary velocity being logarithmic in the base case (causing high velocity shear) changing to being almost uniform in the emergent vegetated cases (Figure 7-42). This effect reduces the magnitude of velocity shear in the channel and hence reduces the longitudinal spread of the tracer. This reduction in velocity shear has a significant impact on the mixing characteristics of the channel. It can be seen from sections 7.5.2 and 7.5.3 that in the case of both the reeds and the emergent Carex both the dispersion coefficient and dispersive fraction are much reduced relative to the base case.

7.5.5.3 Effect of Flow Depth/Discharge on Mixing

To observe any overall trends, all of the results from the emergent tests can be plotted. In Figure 7-108 to Figure 7-111 all dispersion coefficients and dispersive fractions measured in emergent vegetation are plotted against discharge and depth.

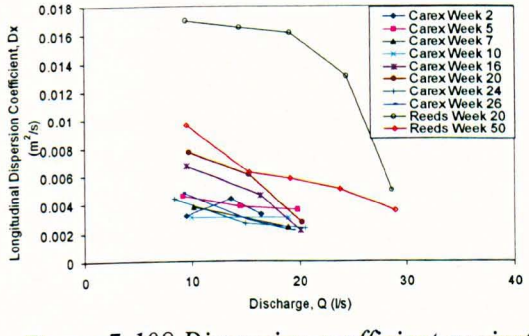

Figure 7-108 Dispersion coefficient against discharge in emergent Carex and reeds

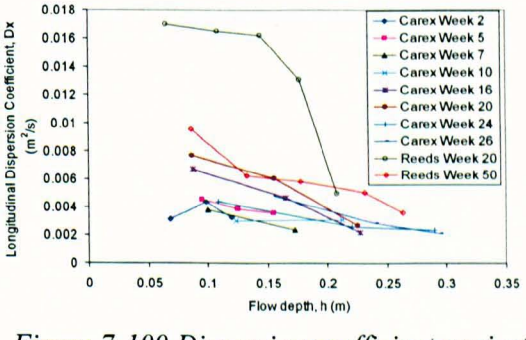

Figure 7-109 Dispersion coefficient against depth in emergent Carex and reeds

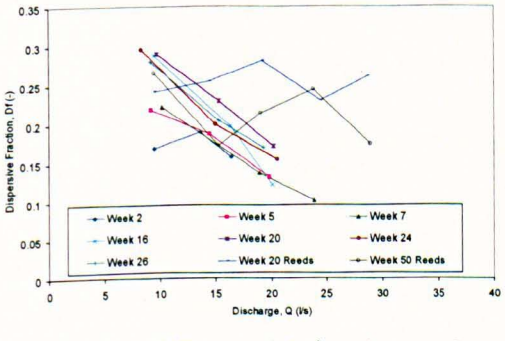

Figure 7-110 Dispersive fraction against discharge in emergent Carex and reeds

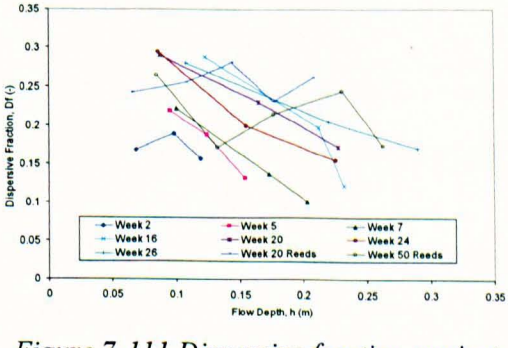

Figure 7-111 Dispersive fraction against depth in emergent Carex and reeds

In both reeds and Carex longitudinal mixing in emergent flow deceases with flow depth and discharge. This can be compared with the work of Nepf (1997) who linked flow velocity (and

discharge/depth) to longitudinal mixing coefficient, also finding an inverse relationship. In this case there is only a small variation in canopy velocity with flow rate (see section 7.1.6.6) and there is no relationship between velocity and dispersion coefficient or dispersive fraction. This trend may be due to the changing effectiveness of stem wakes with flow rate/depth. To evaluate the effects of the wakes on mixing processes such as velocity shear and trapping, velocity, turbulence and concentration measurements would be necessary at a smaller spatial scale than has been undertaken in this study.

7.5.5.4 *Effect of Growth*

Figure 7-112 and Figure 7-115 display all the dispersion coefficients and dispersive fractions taken in fully emergent (i.e. Sr << 1) Carex and reeds respectively against channel porosity (and hence plant growth) for each flow range.

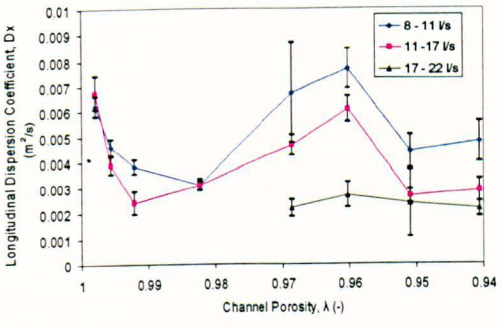

Figure 7-112 Dispersion coefficient in emergent Carex (Sr<<1)

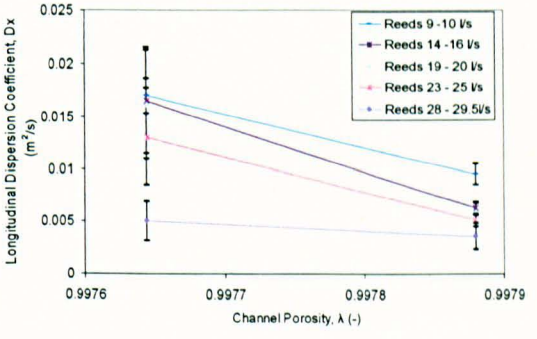

Figure 7-113 Dispersion coefficient in reeds (Sr<<1)

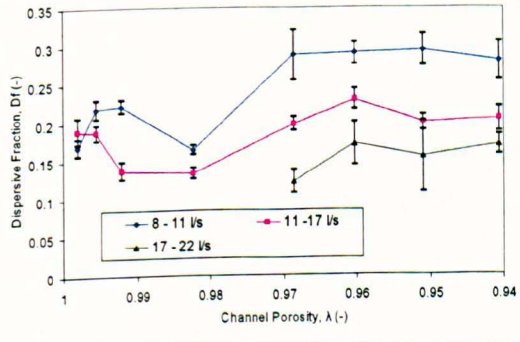

Figure 7-114 Dispersive fraction in emergent Carex (Sr<<1)

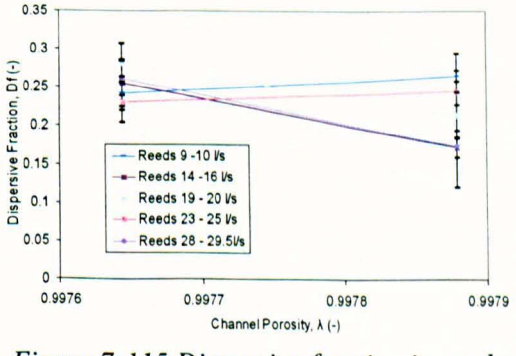

Figure 7-115 Dispersive fraction in reeds (Sr<<1)

In the Carex there is no consistent trend in mixing coefficient with channel porosity. All stages of Carex growth have the effect of decreasing the longitudinal dispersion coefficient by a factor of 4 to 5 relative to the base case. This suggests that all of the vegetative sizes tested have a similar impact on velocity shear in the channel, the subsequent increase in stem width/Carex size since the initial test had no additional impact on the mixing characteristics (if the flow remains in the emergent condition). Although section 7.2 shows that an increase in Carex size

reduces the average velocity within the canopy, the levels of vertical and transverse velocity shear remain roughly constant and hence there is no observable change in mixing.

This independence from age/porosity in the Carex case differs from the situation found in the reeds. This is due to the different growth pattern in the reeds, increasing in stem density rather than stem width with age. Although the dispersive fraction remains roughly constant with age in the reeds, it can be observed that the average level of longitudinal dispersion coefficient decreases with increasing age, and hence stem density (Figure 7-95 and Figure 7-113). The average longitudinal dispersion coefficient in the high age/density reeds case was approximately half the level of the low age/density reeds case. This trend is similar to that observed by Nepf et al. (1997) i.e. a decrease in mixing with increasing stem density. This trend was due to increasing stem density reducing the transverse velocity shear in the channel. Unfortunately due to the poor growth of the reeds and the subsequent lack of tests conducted, a clear trend between stem density and mixing cannot be established.

7.5.5.5 *Effect of Stem Reynolds Number*

Nepf et al. (1997) suggested that mixing in emergent canopies is linked to mechanical dispersion (see section 3.3.3). Mechanical dispersion is caused by the vegetation stem wakes diverting and delaying a proportion of the tracer mass. The effectiveness of this mechanical dispersion is dependent on the size and the strength of the turbulent wakes which form behind the vegetation elements. As discussed in section 3.1.2.5 such wakes are dependent on the stem Reynolds number. Thus if mechanical dispersion is a major influence on longitudinal dispersion a link between longitudinal mixing coefficient and stem Reynolds number would be expected.

Assuming that velocity shear is a product of the stem density and thus constant for each flow case (in emergent flow), for each vegetated case the longitudinal dispersion coefficient in emergent conditions should be linked to mechanical dispersion and hence the stem Reynolds number (Figure 7-116).

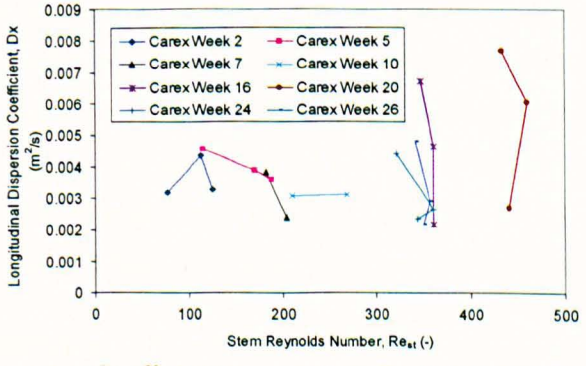

Figure 7-116 Dispersion Coefficient in emergent Carex against Stem Reynolds number

Figure 7-116 shows that there is no apparent relationship between mixing and stem Reynolds number, indicating that either mixing due to trapping is not the dominant source of mixing, or that the stem Reynolds number fails to describe the effectiveness of the stem wakes in spreading tracer.

7.5.5.6 Effect of Submerged Vegetation

In submerged Carex the mixing coefficients increase sharply relative to the emergent conditions. This is due to the presence of higher vertical velocity shear which arises from two layer flow. The small variation in mixing coefficients in emergent conditions and the sudden increase in mixing when the plants become submerged (i.e. in the presence of vertical shear) suggests that transverse shear is only a minor and relatively constant factor contributing to mixing in this system. This is as expected due to the relatively uniform velocities across the channel width.

Mixing in submerged flow is a more complex process than mixing in emergent conditions. The existence of distinct flow layers, dependent on the height and density of the canopy, leads to vertical shear over the flow depth. There are three main parameters that will influence the effectiveness of the vertical shear dispersion in submerged vegetation.

1. Magnitude of differential advection – A larger difference in velocity between the flow above and within the canopy will spread the tracer longitudinally at a faster rate

2. Transfer rate between the faster and slower regions of flow – Higher vertical transport reduces the effect of vertical shear by encouraging uniform concentration gradients over the depth.

3. Relative size of the fast and slow regions of flow – Zones of equal size will be the most effective in spreading tracer longitudinally.

In a channel featuring submerged vegetation the magnitude of differential advection will be dependent on the relative velocities of the canopy and free flow layers. The velocity within the canopy is limited by the balance between slope and vegetated drag. Assuming the free flow layer acts like a boundary layer flow (see section 7.1.6.7), velocity will depend on flow depth, slope and plant top roughness (Equation 2-11). Flow with a dense canopy (slowing flow within the canopy) and high submergence ratios (maximising flow above it) should therefore have a larger velocity differential and hence encounter larger vertical velocity shear.

Vertical transport or diffusivity is linked to the transport of mass and momentum throughout the flow (and hence Reynolds stress – see section 2.4.4.1). It has been observed in section 7.3 that

vegetation reduces Reynolds stress in the wake zone. This effect means that the wake zone becomes a storage zone where tracer becomes trapped, encouraging vertical shear and longitudinal mixing. In systems where the mixing layer penetrates to the bed, mass transport will occur more rapidly over the depth, reducing the effectiveness of vertical shear.

The relative zone size is a function of the submergence ratio of the flow. A submergence ratio of 2 represents equal zone size, and hence theoretically the most effective mixing system.

7.5.5.7 Mixing Coefficients in Growth Phase Submerged Carex

In all growth phase tests the vertical transport is limited by the presence of a wake zone (see section 7.3.4). Low levels of momentum transport in this zone means that vertical transport over the flow depth will be low, encouraging longitudinal mixing.

The relative zone size of the channel is directly related to the submergence ratio. In the growth phase the maximum measured submergence ratio was 1.6 (taken at the maximum flow rate in the week 5 Carex), and hence in the growth phase it is expected to see a positive trend between mixing and submergence ratio.

Mixing is also dependent on the magnitude of the velocity differential between the canopy and free flow zone. If it is correct to assume that the free flow layer is a form of boundary layer flow, the average flow velocity in the free flow zone will increase with flow depth/submergence ratio (section 2.3.2). Flow velocity in the canopy is limited by the presence of vegetative resistance, hence canopies with more flow resistance will encourage mixing in submerged systems by slowing flow within the canopy, whilst forcing more flow over the canopy top, increasing the velocity in the free flow zone and the velocity differential.

In this system however, the growth of the Carex not only increased the flow resistance but, by growing in height, decreased the available size of the free flow zone, and hence both the velocity of this zone and its relative size (Figure 7-74). To explore the influence of submergence ratio, Figure 7-117 plots the dispersion coefficients for all submerged growth phase Carex tests against submergence ratio. In Figure 7-118 the observed dispersive fraction for all submerged growth phase Carex tests are plotted against submergence ratio.

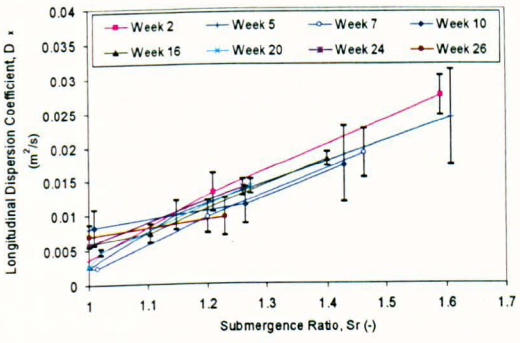

Figure 7-117 Submergence ratio and dispersion coefficient (submerged conditions)

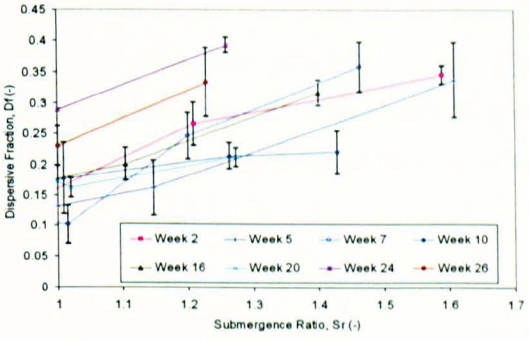

Figure 7-118 Submergence ratio and dispersive fraction (submerged conditions)

The observed mixing coefficients follow a roughly linear trend with submergence ratio, though the trend is clearer when mixing is expressed using ADE dispersion coefficient as opposed to the ADZ dispersive fraction. The increase in dispersion coefficient with submergence ratio is more rapid than the dispersive fraction. There is no observable trend with Carex age (and hence channel porosity and channel resistance – see section 7.1.6.5), indicating that the submergence ratio is the dominant parameter in this system (by both increasing the effectiveness of vertical shear by altering the relative zone size and increasing differential advection). As the submergence ratio itself is dependent of the resistance of the canopy and the flow rate, in systems with limited vertical transport mixing, longitudinal mixing will be primarily a function of discharge and canopy resistance.

7.5.5.8 *Effect of Cropping*

As seen in section 7.2.6.4, cropping the vegetation creates a canopy with high flow resistance but low heights. The lower canopy height means that more flow travels above the canopy in the free flow layer than in the growth phase tests (Figure 7-74). This combination of high retardance within the canopy and a greater proportion of flow above the canopy will cause conditions with a high velocity differential (Figure 7-47) and more equal relative zone sizes, conditions which had not been previously observed in the growth phase. As a result of this, in the first two cropped tests once the flow becomes submerged, the mixing coefficient reaches higher values than in the growth phase (Figure 7-104).

The tests where the vegetation was cropped to 25cm and 13.5cm follow an almost identical pattern with submergence ratios. This shows that in planting configurations with a similar flow resistance and turbulence structure, it is the degree of submergence that defines mixing. However, the cropped to 5.5cm case follows a different trend, with mixing coefficients increasing more slowly with submergence ratio. This is due to the different velocity and turbulence structure as observed in sections 7.2 and 7.3. Unlike in the first two cropped tests, in this case the mixing layer penetrates to the bed and in this case there is no wake zone. Vertical

transport over the flow depth therefore occurs much more rapidly and hence the effectiveness of vertical velocity shear and mixing is reduced in this case (see section 7.5.5.6). This demonstrates that dispersion is caused not only by the size and strength of the faster flowing region above the canopy (i.e. which can be linked to submergence ratio) but also because of the trapping effect of the wake zone.

7.5.5.9 Summary of Longitudinal Mixing Discussion

- In emergent conditions, the presence of vegetation encourages more uniform vertical velocity distributions and the resulting reduction in vertical velocity shear reduces the longitudinal mixing in the channel.

- As the stem density of the reeds increased the vegetation becomes more effective in encouraging uniform profiles of velocity, and hence shear dispersion and longitudinal mixing reduces with stem density.

- As the Carex grow the stem density does not increase, although the plants are more effective in reducing overall velocity, the effect on shear is negligible. Hence, there is no reduction in mixing with Carex growth in emergent conditions.

- A decrease in mixing with flow depth/discharge is observed. To investigate this further it is anticipated that measurements at smaller spatial scales are required to determine the effects of local stem wakes on the processes driving mixing in emergent conditions.

- In submerged flow, vertical velocity shear increases due to the presence of a faster flow zone over the canopy top. This vertical velocity shear causes increased mixing compared with the emergent case.

- The important parameters affecting the rate of mixing in submerged flow are the size of the differential advection between the canopy and free flow zone, the rate of vertical transport, and the relative size of the zones.

- Canopy flow resistance and submergence ratio determine the magnitude of the differential velocity and the relative zone size. The relative size of the wake zone determines the rate of vertical transport over the flow depth.

Chapter 8 - Review of Predictive Techniques

This chapter contains further analysis of the results presented in chapter 7. Specifically it uses the results collected to assess the suitability of the methods presented in chapter 3 to predict flow resistance and longitudinal mixing. Based on the work conducted new analysis methods are presented and tested.

8.1 Predicting Flow Resistance

8.1.1 Momentum Balance Models

8.1.1.1 Comparison of existing models (emergent case)

In this section the momentum based flow resistance models for emergent vegetation as presented in section 3.1.3.2 are compared with the measured stage discharge relationships through both reeds and Carex. The models of Stone and Shen (2000) and Jordanova et al. (2006) are discounted as the testing conditions do not comply with the specified constraints. The Carex did not achieve sufficient stem density required for the models. The model of Stone and Shen (2000) requires a minimum stem density of 113 stems/m^2 and the Jordanova et al. (2006) model requires the stem spacing to be no greater than 0.1m. The Carex had a stem density of 12.5 plants/m (equivalent to 20.8 plants/m^2) and were planted at a longitudinal spacing 0.2m. The reeds did not achieve a sufficient porosity and stem diameter required for the models. The model of Stone and Shen (2000) requires a maximum channel porosity of 0.995, and the Jordanova et al. (2006) model requires the stem diameter to be greater than 0.005m. The minimum porosity achieved in the reeds was 0.9979 and the reeds stem diameter was 0.003m.

The stage discharge relationships predicted by the James et al. (2004), Petryk and Bosmajian (1975) and Hoffman (2004) were compared with the measured stage discharge relationships (emergent conditions only) for each vegetated flow case. Figure 8-1 to Figure 8-4 compare the predicted stage discharge relationships for low and high age emergent Carex and reeds cases with the measured values. The best fit Manning's relationship for the base case channel is also plotted as a comparison. The parameters required for the models (such as stem diameter stem density and porosity) were measured directly (i.e. taken from Table 8). Once the predicted and measured stage discharge relationships are determined for each case, an average percentage error value between the measured and predicted depths can be determined for each flow case.

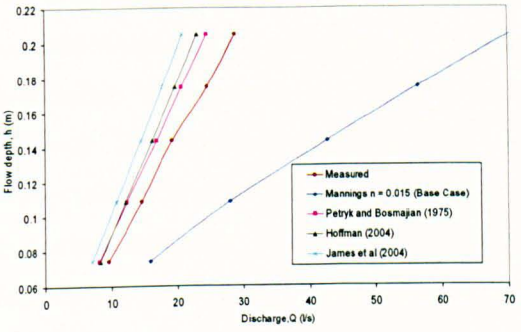

Figure 8-1 Stage discharge comparison in reeds (Week 20)

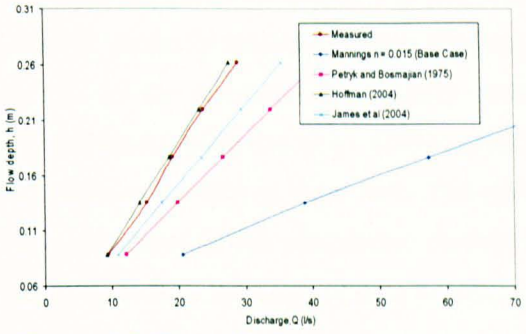

Figure 8-2 Stage discharge comparison in reeds (Week 50)

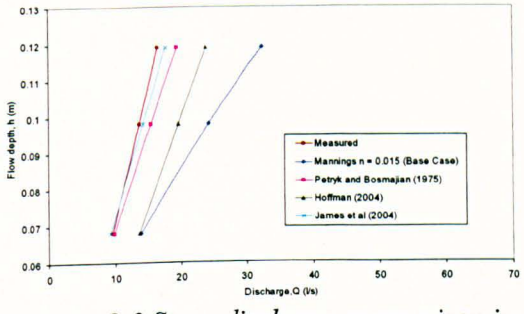

Figure 8-3 Stage discharge comparison in emergent Carex (Week 2)

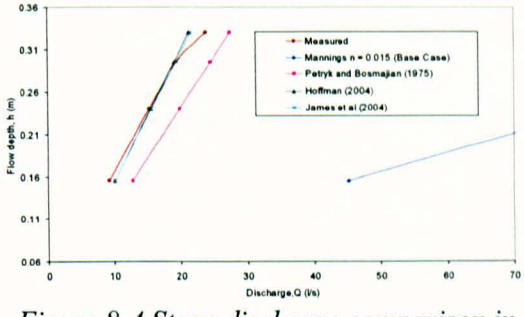

Figure 8-4 Stage discharge comparison in emergent Carex (Week 26)

In the week 20 reeds the models over-predict the flow resistance, whilst in the week 50 reeds the models under-predict the resistance (Figure 8-1 and Figure 8-2). In low age/porosity Carex the flow resistance models tend to under-predict the flow resistance of the channel (Figure 8-3). In high age/porosity Carex, apart from the Petryk and Bosmajian (1975) method, the models are quite accurate (Figure 8-4).

To quantify the accuracy of the resistance models over all tests the absolute percentage error between measured and predicted emergent stage discharge relationships can be plotted for each vegetated case (Figure 8-5 and Figure 8-6).

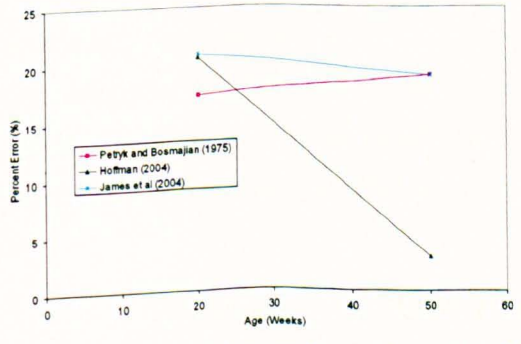

Figure 8-5 Model error through reeds with age

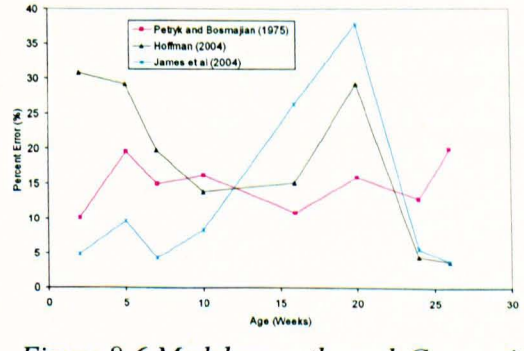

Figure 8-6 Model error through Carex with age

Figure 8-5 and Figure 8-6 displays the absolute average percentage error between each model and the measured values for each reeds and Carex tests respectively. In the reeds the models

over-predict the flow resistance in the week 20 tests, but the Hoffman (2004) become more accurate 50 weeks after planting. In the Carex the models generally predict the stage discharge relationship with an error of 5 - 25%. From weeks 2- 16 the resistance is generally under predicted. In the tests conducted at week 16 and 20, the model of James et al. (2004) greatly over-predicts the flow resistance, leading to errors of between 25-40% in these tests. The main theoretical distinction of the James et al. (2004) model compared to the other tested models is that the drag coefficient is higher (1.5). It may be that in these tests the value of drag coefficient is overestimated. The average error value over all tests for both Carex and reeds are presented in Table 20.

Table 20 – Average error (%) of flow resistance models

	Carex	Reeds
Petryk and Bosmajain (1975)	14.96	18.11
Hoffman (2004)	18.19	11.78
James et al. (2004)	12.52	19.92

In the Carex, the model of Hoffman (2004) has the largest average stage prediction error. This may be because of an inaccurate drag coefficient prediction or because of errors in the derivation. In the Reeds, the model of James et al. (2004) has the largest average stage prediction error. Again, this is most likely to be because the drag coefficient is overestimated in this case.

The models tested are all based on the momentum equation and so mathematically they are quite similar, each deriving vegetative drag from the drag equation (Equation 3-1), even though the vegetation 'density' is defined using different parameters ($\sum A_i$, NS_d and λ are all used). The main difference between the models is the drag coefficient provided by each author. As described in section 3.1.3.2 the drag coefficient value provided by Hoffman (2004) is based on the stem Reynolds number. Whilst drag coefficient value of James et al. (2004) and Petryk and Bosmajian (1975) are fixed (1.5 and 1 respectively). Whilst the models may be quite accurate in describing the flow resistance in one type of vegetation (in the case of James et al., 2004 - high density Carex) it may over or under predict flow resistance in the case of a different vegetation which has a different drag coefficient due to a differing morphology.

8.1.1.2 Model Sensitivity to Drag Coefficient

By using a constant drag coefficient or a coefficient based on an idealised cylinder, the momentum based models ignore any variation in resistance caused by different varieties of plant, and also how the resistance of the plant changes with flow due to streamlining. This problem has been recognised as the biggest limitation to the momentum based vegetated flow

resistance models (Green, 2005). To compare the models further the influence of the drag coefficient on the models has been explored.

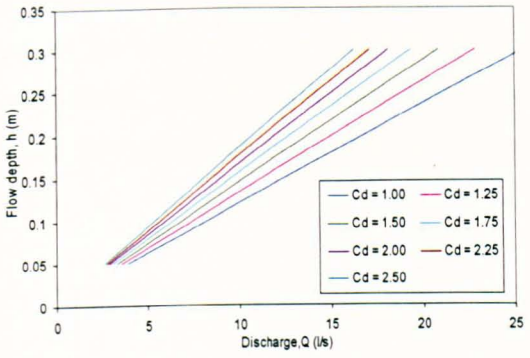

Figure 8-7 Flow depth predictions using different C_d (using James et al., 2004 equation)

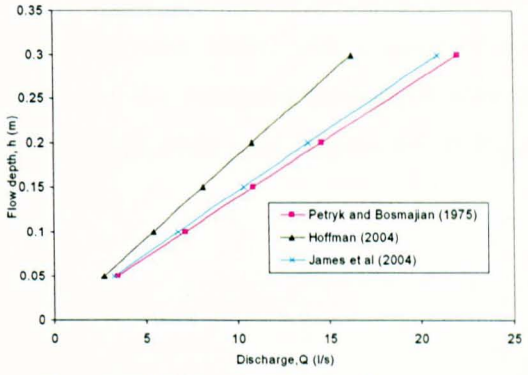

Figure 8-8 Flow depth predictions using different models with C_d = 1.5

Figure 8-7 shows the effect of using different drag coefficient values in conjunction with the James et al. (2004) model (conducted using N = 12.5 stems/m, S_d = 0.05m, S_o = 0.00123). In this case, an increase in drag coefficient from 1 to 1.5 (the difference in recommended drag coefficient values between the Petryk and Bosmajian (1975) and James et al. (2004) models) results in stage predictions which are 20% higher.

Figure 8-8 compares the models (conducted using N = 12.5 stems/m, S_d = 0.05m, S_o = 0.00123) if the drag coefficient is taken as a constant 1.5 in all cases. This illustrates the difference in the models if the variation due to choice of drag coefficient is removed. This remaining difference is due to the different variations in the derivation of each flow resistance model (detailed in section 3.1.3.2). For example, the Hoffman (2004) model includes a term to account for the fraction of the flow volume occupied by the plants; this differs from the equivalent term in the James et al. (2004) model and from the Petryk and Bosmajian (1975) model, which neglects this factor. In this case, the volume taken up by the plants is comparatively large (λ = 0.94 - based on final growth phase test) which causes a stage prediction 28% higher in the Hoffman (2004) model than the Petryk and Bosmajian (1975) model, however in the case of smaller plants or lower density cases, the effects of the flow volume difference is smaller. For example if the stem width is altered to 0.01m (λ = 0.99), the Hoffman (2004) model predicts a stage discharge relationship which is 15% lower then the Petryk and Bosmajian (1975) model. In this case the difference due to the different flow volumes is insignificant (due to the smaller plants). However in this, smaller vegetation, case the resistance from the bed becomes more significant in terms of total resistance (see section 3.1.2.1). Hence, in such a condition the difference in predictions is caused by the different derivations of resistance from the bed. Petryk and Bosmajian (1975) derives bed resistance by adding a contribution from Manning's equation,

while in the model of Hoffman (2004) the bed resistance is neglected (hence resulting in lower stage predictions).

To determine how the accuracy of the prediction is altered when different drag coefficient values are used, the stage discharge was calculated using each model with a range of drag coefficients. The average error between the predicted and the measured flow depth over the entire flow range can be plotted against the drag coefficient value used (Figure 8-9 to Figure 8-12).

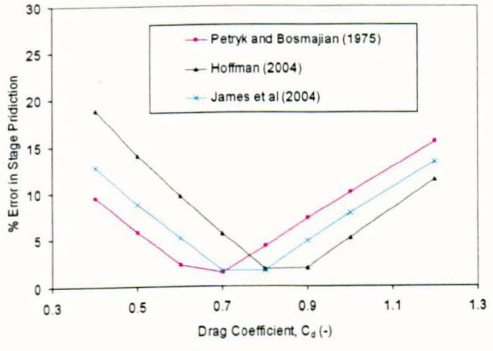

Figure 8-9 Error in flow depth predictions using different C_d (Week 20 Reeds)

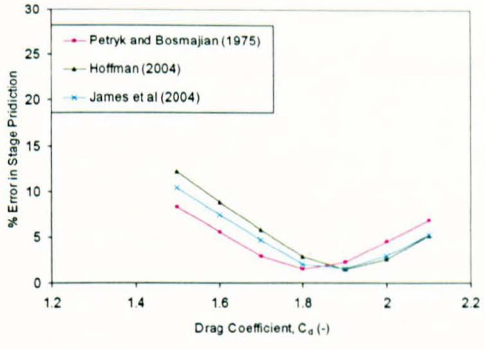

Figure 8-10 Error in flow depth predictions using different C_d (Week 50 Reeds)

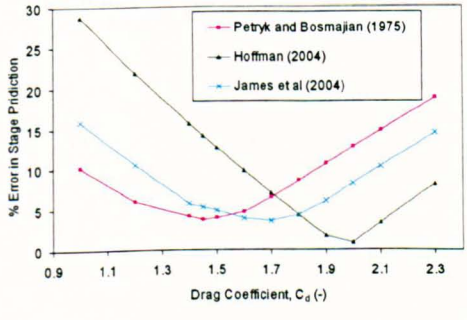

Figure 8-11 Error in flow depth predictions using different C_d (Week 2 Carex)

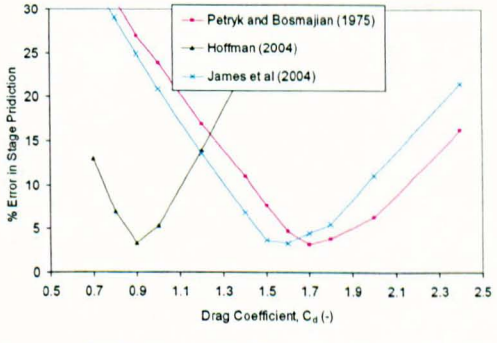

Figure 8-12 Error in flow depth predictions using different C_d (Week 26 Carex)

Figure 8-9 to Figure 8-12 display the error in stage prediction using each model for the high and low density Carex and reeds cases when different drag values are used. The optimum drag coefficient (i.e. resulting in the lowest error) varies depending on the model used and the type and age/ size of vegetation tested. The models have minima that indicate that they are potentially able to predict stage discharge relationships to within 5% error in all cases. Hence, provided a suitable selection of drag coefficient is made, such momentum balance models can provide a reasonable description of flow resistance in emergent vegetation. However, the minima values in Figure 8-9 to Figure 8-12 provide the optimum drag coefficient over the entire flow range. Although they vary with vegetation type/growth they do not take into account changes in drag as the plants become more streamlined with increasing flow. This explains why the minima % error values are generally higher in the case of the Carex (which are more

flexible) than in the other tests conducted with more rigid reeds (where the drag coefficient may not change as much due to low plant flexibility). To determine the how drag coefficient changes with plant age/size and flow rate, C_d must be calculated for each test conducted.

8.1.1.3 Determination of Drag Coefficient

Methods for determining drag coefficient based on observed flow conditions are discussed in section 3.1.3.3. Wu et al. (1999) defined the drag coefficient as

$$C_d = \left(Sr \frac{2gS_o}{U^2} \right) \frac{AL}{\Sigma A_i} \qquad \text{Equation 8-1}$$

The submergence ratio Sr is taken as 1 in emergent cases. Figure 8-13 and Figure 8-14 plot the drag coefficient in Carex and reeds according to Equation 8-1 against stem Reynolds number.

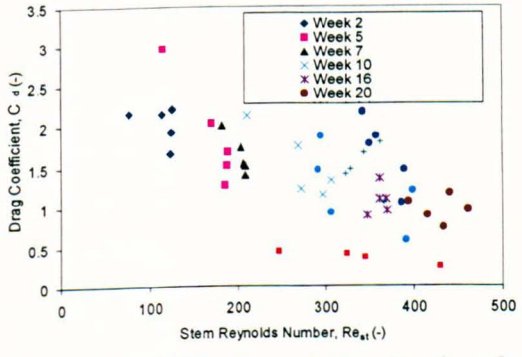

Figure 8-13 C_d - Re_{st} relationship though Carex (C_d from Wu et al., 1999)

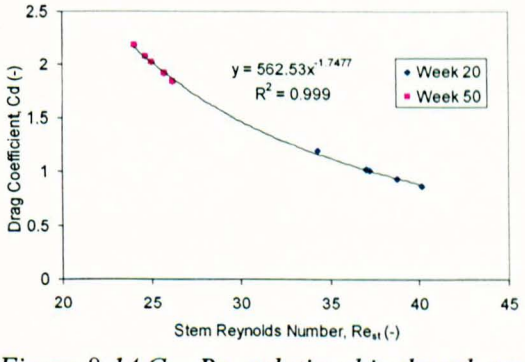

Figure 8-14 C_d - Re_{st} relationship though reeds (C_d from Wu et al., 1999)

Previous researchers (Wu et al. 1999, Jordanova et al., 2006) have found a power relationship between drag coefficient and stem Reynolds number, in the reeds (Figure 8-14) such a relationship exists, however in the Carex (Figure 8-13), although an inverse relationship between drag and stem Reynolds number is evident, no power law trend can be fitted. However, Equation 8-1 contains two assumptions which may make it inaccurate for the tests in this study. Firstly the influence of the bed resistance is ignored, which may lead to inaccuracies in the low age tests. Secondly, drag coefficient in Equation 8-1 is derived based on the cross sectionally averaged flow velocity, with an adjustment based on the submergence ratio of the flow. However no evidence has been provided to support this assumption, and it is preferable to use the canopy layer velocity when deriving drag in submerged conditions (Stone and Shen, 2000).

For improved accuracy it has been decided to derive drag coefficients which include the effects of the bed and avoids the use of cross sectionally averaged flow velocity in submerged cases.

By rearranging the momentum balance Equation 3-5) equation the bulk drag coefficient for each flow case can be determined. The momentum balance equation can be expressed as (for emergent conditions)

$$\rho g \lambda A S_o = 0.5 C_d \rho N A S_d U^2 + \tau_0 P \qquad \text{Equation 8-2}$$

Reproducing the Petryk and Bosmajain (1975) equation for bed shear stress τ_0 (Equation 3-9),

$$\tau_0 = \rho g U^2 n_b^2 \left(\frac{P}{A}\right)^{1/3} \qquad \text{Equation 8-3}$$

Substituting into Equation 8-2, eliminating fluid density, ρ and expressing wetted perimeter, P, as a function of flow area, A, and hydraulic radius, R, gives

$$gA\lambda S_o = 0.5 C_d N S_d A U^2 + g U^2 n_b^2 \left(\frac{1}{R}\right)^{1/3} A\left(\frac{1}{R}\right) \qquad \text{Equation 8-4}$$

To apply to all flow cases (emergent and submerged), the average flow velocity is replaced with canopy layer velocity, and the flow depth h is limited to h_c. Simplifying and rearranging gives

$$C_d = \frac{2g\left(\frac{S_o \lambda}{U_c^2} - n_b^2 \left(\frac{1}{R_c}\right)^{\frac{4}{3}}\right)}{N S_d} \qquad \text{Equation 8-5}$$

Where R_c = Hydraulic radius of canopy section (m)

U_c = Average velocity through canopy (m/s)

Similarly to the method of Stone and Shen (2002), in order to derive C_d in both emergent and submerged flow cases the U_c value has been taken from the measurements of velocity inside the wake zone. Although determining U_c based on the measurements may involve some error, it is felt that this approach is more theoretically justified than deriving a drag coefficient based on the cross sectionally averaged velocity. As with previous research (Jordanova et al., 2006, Hoffman, 2004) the drag coefficients are related to the stem Reynolds number. Figure 8-15 and

Figure 8-16 display the relationship between drag coefficient (from Equation 8-5) and stem Reynolds number for the Carex and reeds, together with the lines of best fit.

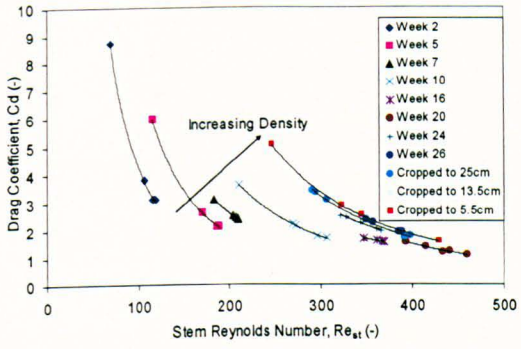

Figure 8-15 C_d - Re_{st} relationship though Carex (C_d from Equation 8-5)

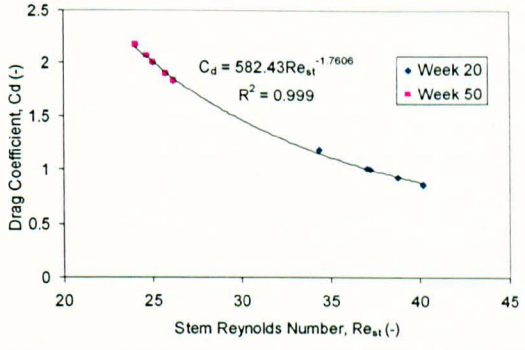

Figure 8-16 C_d - Re_{st} relationship though reeds (C_d from Equation 8-5)

In each case the drag coefficient can be described accurately (R^2>0.99) by a power relationship with stem Reynolds number. In stiff vegetation (reeds and high age Carex) the drag coefficient does not vary greatly. However, in young Carex the drag coefficient reduces significantly with stem Reynolds number, this is due to the greater bending and streamlining of the flexible Carex. For the Carex plants the C_d-Re_{st} relationship shifts as the plants becomes stiffer, as the plants approach maximum size the drag coefficient varies to a smaller extent and the C_d-Re_{st} relationship can be approximated by a single curve, even in cropped vegetation. The reed plants altered little between the low and high density tests and so the relationship can be described by a single curve. For each flow condition the C_d-Re_{st} relationship can be expressed as

$$C_d = \alpha \mathrm{Re}_{st}^{-k} \qquad \text{Equation 8-6}$$

However, to compare the drag coefficient to those listed in the review of Tsihrintzis, (2001) (Table 9) it must be converted to vegetal drag coefficient, from Equation 3-19.

$$C_d' = C_d \frac{\Sigma A_i}{AL} \qquad \text{Equation 8-7}$$

Wu et al. (1999) and Tsihrintzis, (2001) plotted the relationship between vegetal drag and flow, as opposed to stem, Reynolds number (Equation 3-21). The relationship between vegetal drag coefficient and (flow) Reynolds number for Carex and Reeds are displayed in Figure 8-17 and Figure 8-18.

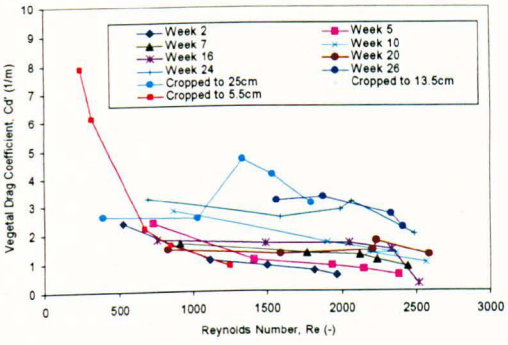

Figure 8-17 C_d' - Re relationship though Carex

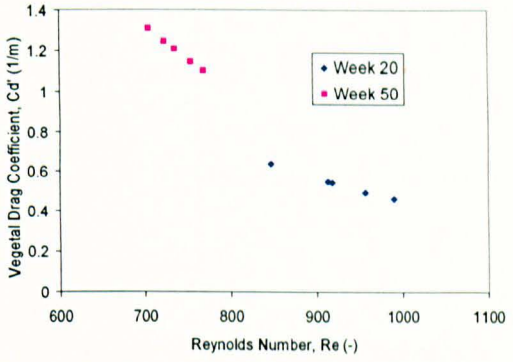

Figure 8-18 C_d' - Re relationship though reeds

As in the C_d–Re_{st} relationships presented in Figure 8-15 and Figure 8-16, drag coefficient declines with Reynolds number, however in this case the C_d–R_e curves no not resemble a power relationship. It is therefore not possible to compare the empirical coefficients provided by the power relationship with those listed in Table 9. The best fit coefficients α, and k which are defined by Equation 8-6 (i.e. from the relationships in Figure 8-15 and Figure 8-16) are presented in Table 21.

Table 21 – α and k values in Carex and reeds

	Reeds	Growth Phase (Age, Weeks)							
		2	5	7	10	16	20	24	26
α	582.43	70,745	106,650	143,894	210,207	291,243	307,214	337,658	369,484
k	1.76	2.012	2.012	2.015	2.010	2.018	2.008	2.007	2.008

	Cropped Phase (cropped to, cm)		
	25	13.5	5.5
α	361,238	381,601	388,868
k	2.004	2.000	2.004

The α and k values in reeds can be compared to those found by Jordanova et al. (2006) (who conducted drag experiments using harvested reeds stems, and also defined the empirical coefficients, α and k, based on stem Reynolds number and unmodified drag coefficient). Stems with full foliage attached resulted in α values ranging from 10 and 1241 and k values ranging between 0.38 and 0.8. The α value derived in the Reeds tests falls within this range (α = 582) whilst the k values are larger. This difference in k values may be due to different vegetation properties such as number of leaves (Jordanova et al., 2006 used harvested as opposed to growing reeds), or it may be because of the difference in experimental channel slopes (Jordanova et al. 2006, $S_o = 0.0005$; present study, $S_o = 0.00123$).

In the Carex the k values remain constant with growth ($k = 2.009 \pm 0.009$), however the α values can be related to plant growth (Figure 8-19).

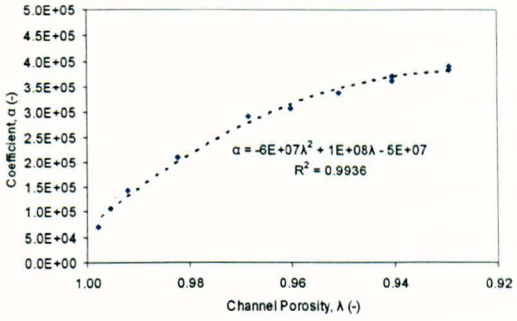

Figure 8-19 Relationship between α and Carex growth (expressed as channel porosity)

The coefficient α is clearly related to vegetation growth, the trend between α and channel porosity is well (R^2=0.994) represented by a polynomial relationship. This agrees with the observation of Tsihrintzis (2001), who also found a trend between α and vegetation density (although the relationship was with vegetal drag in his case). Based on this relationship, and the assumption that the k coefficient is roughly constant for the Carex at all stages of growth, there is potential to improve the accuracy of the drag models tested in section 8.1.1.1. To better represent the resistance caused by the vegetation under differing flow regimes, specified drag coefficients are replaced with those derived with Equation 8-6, using a constant k (based on the average value found) and an α based on plant growth. To test this method the stage discharge relationships predicted by the Petryk and Bosmajian (1975), Hoffman (2004) and James et al. (2004) models are recalculated for the growing Carex, but with a drag coefficient determined by the following relationship

$$C_d = \alpha \, \mathrm{Re}_{st}^{-2.009}$$

Equation 8-8

Where $\alpha = -6.33\times10^{7}\lambda^{2} + 1.08\times10^{8}\lambda - 5.45\times10^{7}$

As in section 8.1.1.1 the percentage error between the predicted and observed stage discharge relationships can be determined for each stage of growth in emergent conditions (Figure 8-20).

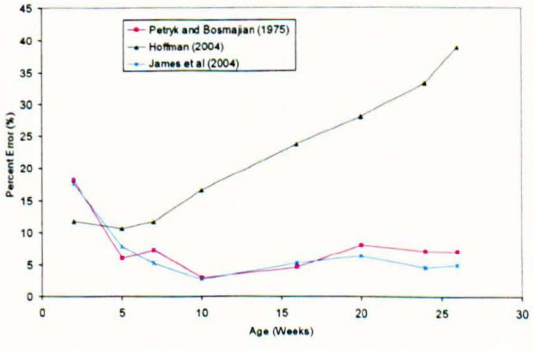

Figure 8-20 Model error through Carex with age using determined C_d- Re_{st} relationships

Given a C_d-Re_{st} relationship the model of James et al. (2004) predicts the observed stage discharge relationship to within 5% in most cases. This is an improvement on the original model (average error ≈ 13%). The remaining error may be caused by the use of the measured canopy velocity in the derivation of drag coefficient (section 8.1.1.3), which may not provide a true 'average' velocity (and therefore drag) representative of the entire channel (see section 7.1.6.1). The Petryk and Bosmajian (1975) model has a slightly higher error (5-10%) This may be because the Petryk and Bosmajian (1975) model neglects the area of the flow taken up by stems in its derivation. The model of Hoffman (2004) has the largest error (average error ≈ 25%), significantly overestimating the channel resistance, the error increases with Carex age. This large error may be due to the additional term (see section 3.1.3.2) in the model which accounts for the fraction of the flow volume occupied by the plants and the 'tortuous flow path'. This extra term appears to cause the model to overestimate resistance in the high age Carex cases.

As shown in 8.1.1.1, the use of one value of drag coefficient in conjunction with a momentum balance over the depth will lead to inaccuracies in the stage discharge prediction. These inaccuracies will be greater in flexible vegetation which has a greater ability to become more streamlined and adopt a lower drag coefficient as flow increases. It is therefore recommended that these momentum based models be used in conjunction with a C_d-Re_{st} relationship derived for a suitable vegetation type. It has been shown that use of such a relationship in predicting a suitable drag coefficient can considerably reduce the error between the predicted and observed stage discharge relationship. The James et al (2004) model has been identified as the most accurate model in this vegetated case.

8.1.2 Other Vegetated Resistance Methods

The other flow resistance models identified in section 3.1 are the relative roughness method and the n-UR approach. These models have also been tested against the measured data.

8.1.2.1 Relative Roughness Method

The relative roughness method is designed for use with submerged vegetation only and has been tested against the experiments conducted in submerged conditions. As described in section 3.1.3.5, Kouwen et al. (1969) proposed that flow above the vegetation canopy obeys the logarithmic law, and empirically fitted the logarithmic law by adjusting the origin intercept and the roughness parameter. By adjusting the parameters of the log law based on the stiffness and density of the vegetation an equation for flow velocity was derived. Reproduced from section 3.1.3.5,

$$\frac{U}{u*} = C_1 + C_2 Ln\left(\frac{h}{h_c}\right)$$ Equation 8-9

According to Equation 8-9 in submerged flow the parameter U/u* should be proportional to $Ln(h/h_c)$. For each individual flow case the roughness (C_1) and stiffness (C_2) parameters can then be defined. Figure 8-21 shows the relationship between $Ln(h/h_c)$ and U/u* for each submerged Carex test.

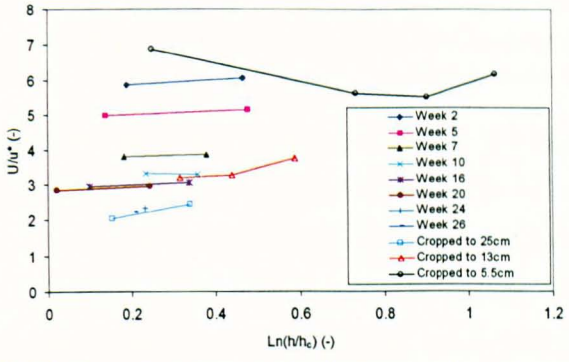

Figure 8-21 U/u against Ln (h/h_c) relationship in submerged Carex*

In many cases only two submerged tests were undertaken and so it is difficult to define a relationship, however, the parameter U/u* appears roughly constant with $Ln(h/h_c)$. Therefore defining the parameters C_1 and C_2 for use in Equation 3-22 is not possible. The Kouwen et al. (1969) model is probably more suitable for flow with higher submergence ratios such as grassed channel linings. Tests to verify such a method should involve a greater number of measurements.

8.1.2.2 n – UR Method

The principles of the n - UR method were introduced in section 3.1.3.1. The method is based on the hypothesis that flow resistance through vegetation is related to the product of average flow velocity and hydraulic radius. As the product UR increases the predicted resistance value decreases, as the vegetation becomes more streamlined, an effect that can be seen in the Carex flow resistance against depth plots (Figure 7-13). Five different n – UR curves have previously been produced, each suitable for a different type of vegetation (see Table 7). To evaluate this method the product UR can be calculated for each vegetated flow case and plotted against the calculated Manning's resistance coefficient. The resulting relationship can be compared to the published n – UR curves, equations for which have been published by Findlay and Ellul (1976) and Green and Garton (1983). Figure 8-22 and Figure 8-23 shows the relationship between n and the UR in the Carex and reeds tests respectively. In both of these cases the best fit n –UR

curve from Table 7 is 'Type E' which is the lowest retardance curve, suitable for Bermuda grass, this n – UR curve is also plotted in Figure 8-22 and Figure 8-23.

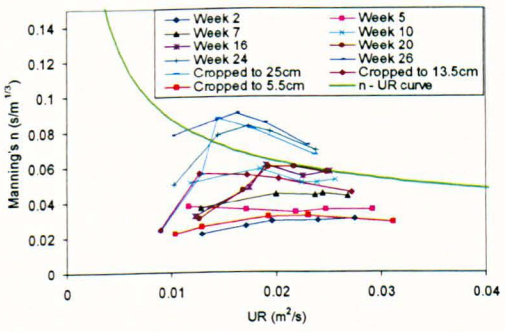

Figure 8-22 Comparison between n-UR curve and measured Carex data

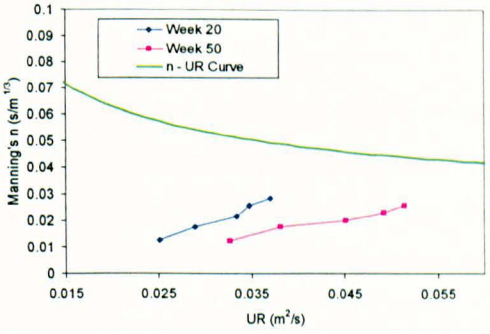

Figure 8-23 Comparison between n-UR curve and measured Reed data

From the observations that have been made it appears that there is a large variation between the best fit n-UR curve and the most of the experimental data. The UR curve over-predicts the Manning's n in most cases (apart from the final growth phase and the cropped to 25cm tests) This casts some doubt on the ability of the n-UR curve to accurately describe flow resistance in vegetated flows. However, the published n – UR curves do not include the range of UR that has been experimented on in these experiments. For example, in Chow (1959) the curves are provided for UR values between 0.1 and 30. It may be that the curves are more suitable for vegetated flows conducted within this range of UR; however the range of applicability of the curves has not been published.

8.1.3 New Submerged Flow Resistance Model

The relative roughness and n-UR approaches have failed to accurately predict the flow resistance of the vegetated channel for the tests conducted in submerged conditions and existing momentum based models are only applicable for emergent vegetation. A new method is therefore proposed which is based on a two layer approach.

It is proposed that submerged vegetation can be dealt with by splitting the flow into two layers. The bottom layer (i.e. flow through the vegetation $h < h_c$) is modelled in a similar way as flow though emergent vegetation in section 8.1.1, using a momentum balance approach but with an additional limiting factor $h = h_c$. Above this in the free flow zone, the flow can be modelled using boundary layer theory with the boundary being set at a height h_c above the bed. Total flow in the two layer system can be described as

$$Q = Q_{canopy} + Q_{abovecanopy} \qquad \text{Equation 8-10}$$

Converting Equation 8-10 using the continuity equation (Equation 2-1) gives

$$Q = U_c h_c b + Q_{abovecanopy} \qquad \text{Equation 8-11}$$

It has been shown that stage discharge relationships for emergent conditions can be accurately predicted by solving the momentum equation, provided a suitable value for drag coefficient is used. It is assumed that in submerged flow, velocity through the canopy zone can also be determined by the momentum equation. Applying the momentum equation (Equation 8-4) to the canopy zone only gives

$$g\lambda S_o = 0.5 C_d N S_d U_c^{\,2} + g U_c^{\,2} n_b^{\,2} \left(\frac{1}{R_c}\right)^{4/3} \qquad \text{Equation 8-12}$$

Solving for canopy velocity, U_c gives

$$U_c = \sqrt{\frac{g\lambda S_o}{\left(\frac{1}{R_c}\right)^{\frac{4}{3}} g n_b^{\,2} + 0.5 N S_d C_d}} \qquad \text{Equation 8-13}$$

Equation 8-13 is essentially a rearranged form of the James et al. (2004) flow resistance model, with an additional limiting factor $h = h_c$. In dense canopies (with negligible bed resistance - see section 7.1) the flow resistance from the bed is negligible and Equation 8-13 simplifies to

$$U_c = \sqrt{\frac{g\lambda S_o}{0.5 N S_d C_d}} \qquad \text{Equation 8-14}$$

In dense canopies velocity is dependent on the balance between stem size (density and width) and bed slope. If a constant C_d value is used (see section 8.1.1.3) then flow velocity becomes independent of discharge. In stiff vegetation such as reeds this approximation may be valid, and velocity and drag coefficient will remain roughly constant with depth. In flexible vegetation such as Carex, the constant velocity condition does not exist; the C_d will vary with velocity as the vegetation becomes more streamlined (see section 0). For optimum accuracy a C_d-Re_{st}

relationship should therefore be used. Using Equation 8-11 and Equation 8-13 the discharge in the free flow zone, $Q_{abovecanopy}$ can now be determined

$$Q_{abovecanopy} = Q - U_c h_c b \qquad \text{Equation 8-15}$$

Flow in the upper zone is treated like a boundary layer flow, hence Manning's relationship (Equation 2-11) applies. Applying Manning's equation to the free flow layer only gives

$$Q_{abovecanopy} = U_{ac} A_{ac} = \frac{1}{n_c} R_{ac}^{2/3} S_o^{1/2} h_{ac} b \qquad \text{Equation 8-16}$$

Where	R_{ac}	=	Hydraulic radius of free flow zone	(m)
	A_{ac}	=	Area of free flow zone	(m^2)
	U_{ac}	=	Average velocity in the free flow zone	(m/s)
	h_{ac}	=	Depth of free flow zone	(m)
	n_c	=	Canopy top roughness	($s/m^{1/3}$)

As detailed in Chow (1959), Manning's equation (Equation 2-11 and hence Equation 8-16) cannot be solved directly for the free flow zone depth, h_{ac}. However, a solution can be determined by an iterative approach. Equation 8-16 also requires knowledge of the canopy top roughness, n_c. From the stage discharge experiments conducted using submerged Carex as detailed in section 7.1, the Manning's n for growing Carex is 0.01 (see Figure 7-16), and for cropped Carex is 0.021 (see Figure 7-17). Once Equation 8-16 is solved for h_{ac} the total flow depth can be given as

$$h = h_c + h_{ac} \qquad \text{Equation 8-17}$$

The accuracy of this method can be tested on the gathered submerged Carex stage discharge data. The drag coefficient used to predict velocity in the canopy zone was based on the empirical relationship derived in section 8.1.1.3.

Table 22 – Measured and Predicted Flow Depths in Submerged Carex

Test (Age/Cropped to)	Discharge, Q (l/s)	Measured Flow depth, h (m)	Predicted Flow depth (m)	Error (%)
2	21.33	0.145	0.152	4.8
2	25.22	0.159	0.162	1.9
5	23.35	0.172	0.181	5.3
5	28.74	0.193	0.185	4.1
7	25.22	0.216	0.218	1.0
7	28.66	0.234	0.226	3.3
10	25.78	0.240	0.242	0.8
10	28.74	0.260	0.243	6.7
16	24.93	0.254	0.254	0.2
16	28.74	0.273	0.276	1.2
20	24.06	0.255	0.279	9.4
20	28.74	0.280	0.289	3.2
24	29.50	0.340	0.331	2.6
26	29.50	0.345	0.343	0.7
Cropped to 25cm	21.10	0.291	0.335	15.2
Cropped to 25cm	29.50	0.323	0.348	7.8
Cropped to 13.5cm	20.50	0.209	0.243	16.3
Cropped to 13.5cm	29.50	0.243	0.274	12.8
Cropped to 5.5cm	20.64	0.148	0.180	21.6
Cropped to 5.5cm	29.50	0.174	0.199	14.5

Table 22 shows the measured and predicted flow depth for submerged Carex for each test conducted at the flow rates above 20l/s (when the flow was sufficient to achieve canopy submergence). Over the growth phase the average error between the predicted and actual depth is 3.2%, in the cropped phase it is 14.7%.

The main difficulty in using this method in practice would be in the determination of three parameters

- Drag coefficient, C_d – Published C_d' – Re relationships exist (Table 9), however existing literature does not cover all vegetation types.

- Roughness coefficient of the canopy top, n_c – No literature exists and the Manning's n value would have to be estimated or evaluated through testing.

- Canopy height, h_c - For flexible vegetation h_c will reduce under flow. Deflected h_c can be related to force acting on the canopy (as Kujita and Hong; 1996), however little biomechanical data required for the necessary cantilever calculation exists.

One source of inaccuracy in the new approach is that it neglects the influence of the shear/mixing layer, assuming that the entire in canopy velocity is equal to wake zone velocity, U_c. It can be seen from the measured velocity profiles that in submerged flow (Figure 7-43) the portion of the velocity profile within the mixing layer has a greater velocity than U_c. The model

is therefore only suitable in cases where the wake zone occupies the majority of the canopy layer. This is the reason for the lack of accuracy in the cropped predictions, because the mixing layer takes up a larger proportion of the flow depth. In the case of the cropped to 5.5cm Carex the method does not provide accurate predictions (error of 14%). This is because the wake zone (where the velocity U_c is constant over the depth) does not exist due to the penetration of the mixing layer to the bed. In this case the flow is more accurately approximated as a rough boundary layer (Figure 8-24).

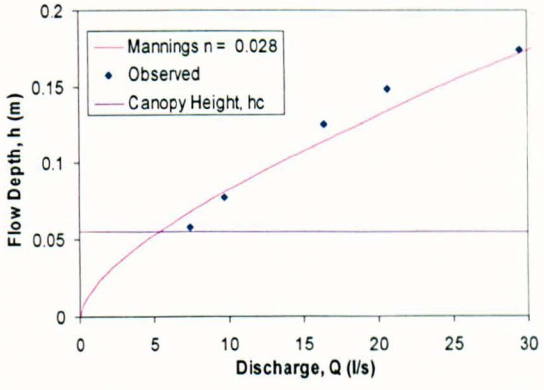

Figure 8-24 Stage discharge in canopy cropped to 5.5cm

Figure 8-24 shows that the stage discharge in the cropped to 5.5cm case can be reasonably well approximated by Manning's relationship ($R^2 = 0.98$, average error in depth prediction of 7%).

8.2 Predicting Vertical Profiles of Primary Velocity

This section looks at methods for predicting vertical profiles of primary velocity in vegetated flow.

8.2.1 Conceptual Model of Vertical Profile of Primary Velocity

Based on previous research as detailed in section 3.2 and observations of vertical profiles of primary velocity conducted in vegetated flow (section 7.2) a conceptual model can be proposed.

The flow profile in vegetated channels can be split into different zones where the velocity is influenced by different processes (Figure 8-25).

- Boundary Layer – Region (of size d_b) influenced by bed roughness, as the vegetation becomes more dense/larger the influence of the bed shrinks and this region becomes smaller (see section 7.2.6.4)

- Wake Zone – Velocity in this zone is dependent on the balance between vegetative drag and bed slope and can predicted using the momentum equation (Equation 8-13).

- Shear/Mixing zone – Velocity in this zone is likely to be dependent on the properties of the mixing layer as described in section 3.3.2.1; specifically mixing layer penetration, d_c, and free flow zone to canopy velocity differential, Δu.

- Logarithmic zone – As shown in section 3.2.2.2, previous studies suggest that velocity above the canopy can be described by a logarithmic distribution.

In emergent conditions the shear and the logarithmic zones do not exist, and the profile is mostly uniform over the depth. This is supported by observations of velocity profiles in reeds and emergent Carex in section 7.2. To predict a full vertical profile of velocity in submerged flow the velocity in each zone must be determined.

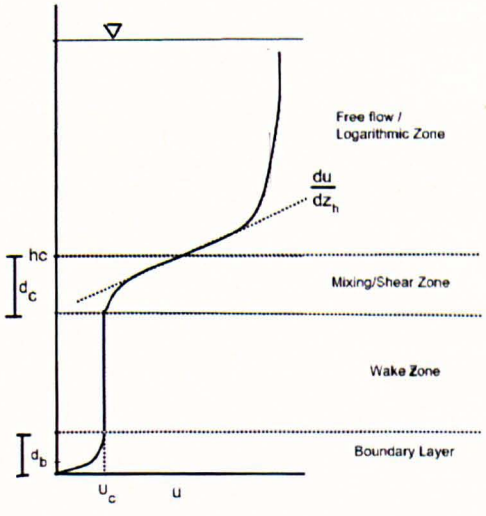

Figure 8-25 Conceptual Model of Vertical Profile of Primary Velocity through Submerged Vegetation

8.2.2 Boundary Layer and Wake Zone

As shown in 7.2.6, in canopies of sufficient density the boundary layer can be ignored, in this case the velocity from the bed to the bottom of the mixing layer (h_c-d_c) can be assumed to be uniform and equal to the velocity in the wake zone. Wake zone velocity is governed by the momentum balance between gravity and stem drag and can be found using the same momentum balance equation as in section 8.1.3 (Equation 8-13). In cases where the canopy is not of sufficient density for the boundary layer to be ignored then velocity in this region will depend on the bed roughness and canopy density.

8.2.3 Profile above Submerged Vegetation

Section 3.2.2.2 presented a number of equations derived by previous researchers to describe the velocity profile above the canopy (Table 10), all the profiles suggest a logarithmic relationship

exists. To determine which relationship is most suitable each equation can be tested against the measured profiles using optimised parameters (equivalent roughness height k_p and coefficient C) for each case.

Once the parameters are optimised many of the presented equations become identical. For example the equations of Christensen (1985) and Murota et al. (1984) provide an identical velocity profile given appropriate values for roughness height and coefficient C. However, three different forms of the velocity profile have been identified from Table 10. These are presented in Table 23 as Forms 1-3. A new equation incorporating the mixing zone penetration distance d_c (Form 4) is also proposed. This equation is based on the observation of the profiles of vertical velocity in submerged flow (section 7.2.6.4), specifically that flow velocity begins to increase above the canopy velocity, U_c, at a distance, d_c, below the canopy top. The different forms of the equation were tested against the measured velocity profiles taken above the canopy.

Table 23 – Forms of logarithmic profile above vegetation

Name	Equation	Suggested by
Form 1	$\frac{u}{u^*_{hc}} = \frac{1}{\kappa} Ln\left(\frac{z}{k_p}\right) + C$	Kouwen et al. (1969)
Form 2	$\frac{u}{u^*_{hc}} = \frac{1}{\kappa} Ln\left(\frac{z-h_c}{k_p}\right) + C$	Plate and Quraishi (1965) Christensen (1985)
Form 3	$\frac{u}{u^*_{hc}} = \frac{1}{\kappa} Ln\left(\frac{z-(h_c-z')}{k_p}\right) + C$	Klopstra et al. (1997) Watanabe and Kondo (1990)
Form 4	$\frac{u}{u^*_{hc}} = \frac{1}{\kappa} Ln\left(\frac{z-(h_c-d_c)}{k_p}\right) + C$	-

Examples of how the four forms of the logarithmic equation fit to the measured velocity profiles are presented in Figure 8-26 to Figure 8-29. The canopy top shear velocity, u^*_{hc} is provided by Equation 3-30. The coefficient C is 8.5 in all cases, k_p is optimised for each case to provide the best fit to the observed profiles.

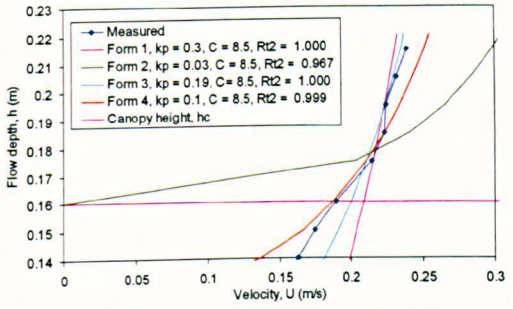

Figure 8-26 Measured and predicted velocity profile above canopy (Week 7 Growth Phase)

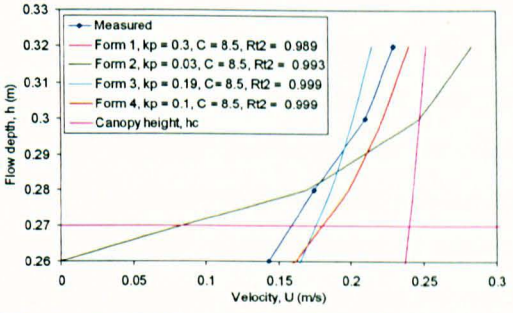

Figure 8-27 Measured and predicted velocity profile above canopy (Week 24 Growth Phase)

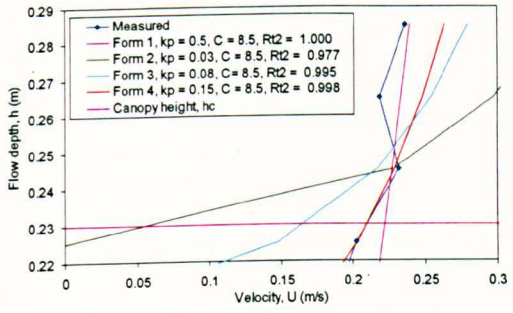

Figure 8-28 Measured and predicted velocity profile above canopy (Cropped to 25cm)

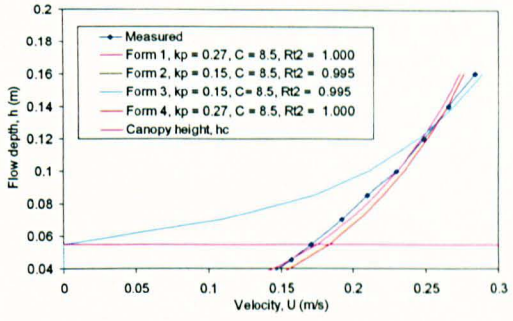

Figure 8-29 Measured and predicted velocity profile above canopy (Cropped to 5.5cm)

Over all of the tests conducted the profile of primary velocity above the canopy is described best by forms 3 and 4 (average Rt^2 for forms 3 and 4 is 0.99, and 0.99 respectively, as opposed to 0.989 and 0.97 for forms 1 and 2), where the zero plane displacement is positioned below the canopy top. In practice, the plant deflection parameter, z' required for form 3 may be easier to obtain (from measuring physical plant deflection) than mixing layer penetration, d_c (requiring the measurement of the profile of Reynolds stress) and hence form 3 may be the preferred equation. However, in stiff vegetation which experiences no bending (as in cropped to 5.5cm Carex - Figure 8-29), form 3 becomes close to form 2, and becomes inaccurate as it assumes a zero velocity condition at the canopy top. Figure 8-29 shows that in the cropped vegetation when the Carex is short and stiff (z'= 0) and d_c penetrates to the bed, form 4 tends toward form 1. In this case the measured velocity profile resembles a rough boundary layer, increasing over the entire flow depth (see Figure 7-40) and form 1 (and hence form 4) gives the closest fit as the zero velocity condition occurs at the channel bed. Therefore, from this point onwards, form 4 is used when predicting the profile of velocity above the canopy.

8.2.4 Velocity in the Mixing/Shear layer

Previous studies (see section 3.2.2) have reported that velocity increases above the wake zone, and an inflection point in primary velocity is present at the canopy height h_c. These studies have been confirmed by the velocity profiles measured in submerged Carex as a part of this work (section 7.2). The magnitude of the inflection is linked to the submergence ratio and the

velocity difference between the canopy and free flow layer (see section 7.2.6.4) so it is possible that the size of the inflection could be estimated using parameters such as canopy density, u^*_{hc}, Δu and submergence ratio. However, for simplicity it is proposed that between the wake zone and h_c the velocity can be approximated by linear trend, velocity increasing over the mixing layer from the wake zone to the free flow zone. However, a estimate of how far the mixing layer penetrates into the canopy, d_c, is still required. Nepf et al. (2007) suggests that d_c is related to the drag coefficient, canopy height and canopy density (Equation 3-29), and that the mixing layer would penetrate to the bed when $C_dNS_dh_c < 0.3$. The product $C_dNS_dh_c$ has been calculated for each flow case using the drag coefficient derived in section 8.1.1.3 and is plotted against relative penetration depth (Figure 8-30).

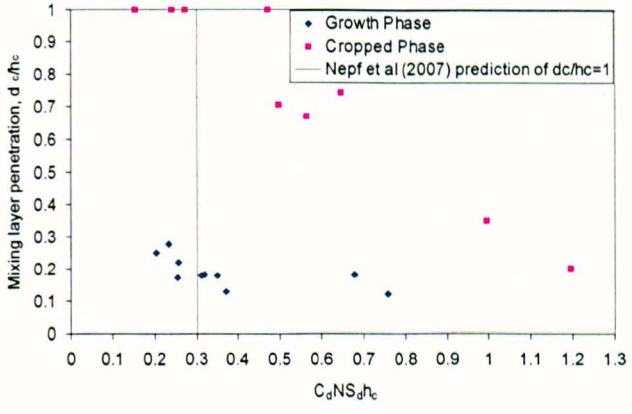

Figure 8-30 Mixing layer depth with $C_dNS_dh_c$

Figure 8-30 plots the relative mixing layer penetration against the parameter $C_dNS_dh_c$ for each test. In the growth phase the mixing layer depth remains roughly constant with $C_dNS_dh_c$ and does not penetrate to the bed ($d_c/h_c = 1$) when the product $C_dNS_dh_c < 0.3$ as suggested by Nepf et al. (2007). However; in the cropped phase the parameter d_c does seem to vary as predicted in Equation 3-29 and the mixing layer penetrates to the bed when $0.3 < C_dNS_dh_c < 0.5$. This difference may be due to the nature of the canopy top, the flexible nature of the growth phase plants acting as an additional barrier to the penetration of the mixing layer. Therefore whilst Equation 3-29 may be suitable for predicting mixing layer depth in fairly rigid, straight vegetation it may not be applicable to a wide range of vegetation types. Based on this analysis the Nepf's et al. (2007) relationship is not suitable for predicting d_c in most of the tests conducted in this study. Therefore, when required, mixing layer penetration depth is taken directly from experimental measurements.

8.2.5 Complete Velocity Profile in Submerged Flow

Using a combination of the momentum equation within the wake zone, and assuming a linear increase in velocity in the mixing zone and a logarithmic zone above h_c, it is possible to estimate

a complete velocity profile. For simplicity the boundary layer is ignored in all cases. To predict profiles of velocity in the submerged Carex, experimental measurements of mixing layer penetration d_c and canopy height h_c are used, together with Equation 8-13 for flow resistance/wake zone velocity. This still leaves one unknown parameter, the vegetation roughness height, k_p (to be used in velocity profile above the canopy - Table 23, form 4). To obtain this parameter an iterative approach is proposed. Firstly an initial k_p value is chosen and the velocity profile is then integrated over the flow depth to obtain a discharge value, Q_{est}. The estimated discharge Q_{est} can then be compared to the measured discharge, Q. The roughness parameter k_p can then be adjusted until Q_{est} converges to the measured discharge Q. Using the method detailed in this section the calculated velocity profile can be compared to measured velocity profiles taken in submerged Carex (example profiles displayed in Figure 8-31 to Figure 8-33 are taken at the maximum flow rate, Q=29.5l/s).

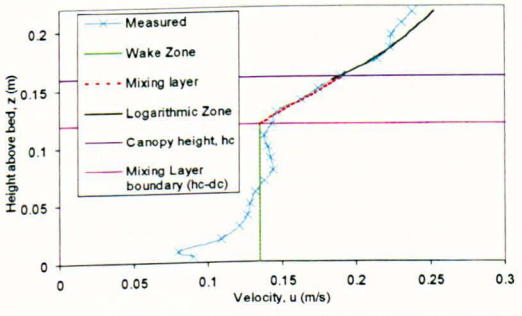

Figure 8-31 Measured and predicted vertical profile of velocity (Week 7- Growth Phase)

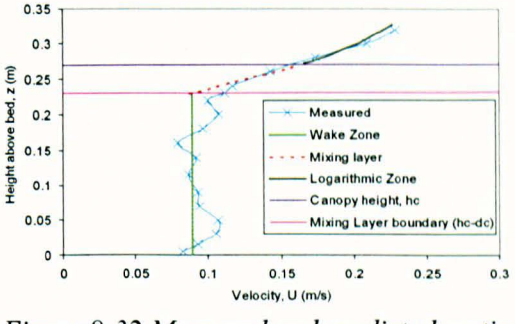

Figure 8-32 Measured and predicted vertical profile of velocity (Week 24- Growth Phase)

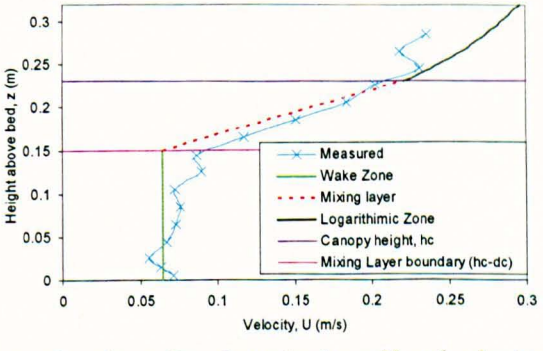

Figure 8-33 Measured and predicted vertical profile of velocity (Cropped to 25cm)

Figure 8-31 to Figure 8-33 show the predicted velocity and measured velocity profile for three different submerged flow conditions. The predicted profiles give a good approximation to the measured profiles in all cases. As with the submerged flow depth prediction method, the process relies on accurate values of d_c and h_c, which may be difficult to obtain in practical cases. In cases where the bed resistance is not insignificant there may be some inaccuracy close to the bed due to the omission of the boundary zone (Figure 8-31).

As with the flow depth prediction presented in section 8.1.3 the method is only applicable where the wake zone is of a significant size. If the mixing layer penetrates to the bed and the wake zone becomes insignificant (such as in the 5.5cm cropped case) it is more suitable to treat the flow as a boundary layer and assume a logarithmic velocity profile (Figure 8-34).

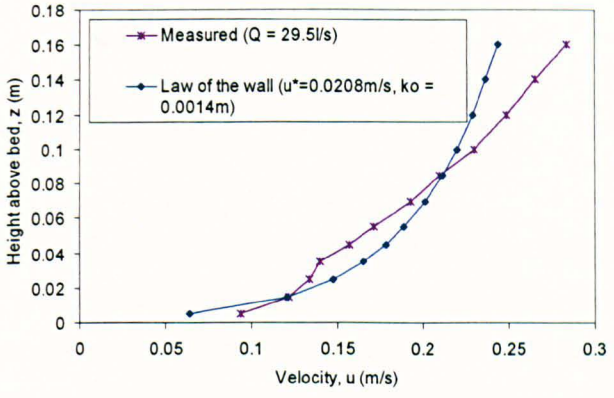

Figure 8-34 Measured and predicted velocity profile above canopy (Cropped to 5.5cm)

Figure 8-34 shows that the velocity profile in the 5.5cm cropped Carex can be roughly approximated ($R^2 = 0.85$) using the conventional logarithmic law for boundary layer flow.

In this section it has been shown that given knowledge of a canopy flow resistance, canopy height and mixing layer penetration it is possible to make an accurate estimation of the vertical profile of velocity in submerged canopies.

8.3 Predicting Longitudinal Mixing

This section compares the existing equations for predicting longitudinal mixing coefficients in vegetated flow with the measured values obtained from the testing program.

8.3.1 Emergent Conditions

Section 7.5 shows that longitudinal mixing experiments conducted in emergent conditions result in much reduced dispersion coefficients relative to the base case. This is due to the reduced magnitude of velocity shear in vegetated channels (see section 7.2) which would otherwise cause the tracer to disperse longitudinally. The literature review resulted in one equation provided by Lightbody and Nepf (2006) for predicting longitudinal dispersion coefficients in emergent vegetation.

8.3.1.1 Comparison with Lightbody and Nepf Model

As detailed in section 3.3.3.1, Lightbody and Nepf (2006) proposed that mixing in emergent vegetation was caused by velocity shear (from differential advection) and mechanical dispersion

(the physical presence of the plants separating tracer). It was proposed that these two processes can be summed together to provide a value for total longitudinal dispersion coefficient. Reproduced from section 3.3.3.1 the equation for longitudinal mixing in emergent canopies provided by Lightbody and Nepf (2006) is

$$\frac{D_x}{US_d} = \frac{e_z}{US_d}\overbrace{\left[\frac{d}{dz}\sqrt{\frac{C_d A_i}{C_d(z)A(z)}}\right]^2}^{A} x^2 + C_d^{3/2} \qquad \text{Equation 8-18}$$

The product 'A' represents the contribution from vertical velocity shear, and is calculated based on the distribution of mass and drag coefficient over the flow depth. Essentially it proposes that the distribution of velocity over the depth will be inversely related to the product of mass and drag coefficient. However, in practice the parameter A (vegetation mass and drag profile over the depth) is difficult to determine and has not been evaluated for the tests conducted in this thesis. However, it can be assumed that the mass and drag distribution of the reeds is uniform over the depth (as they are essentially uniform cylinders). By examining the vertical velocity profile within the reeds (section 7.2.2), it can be seen that the velocity is almost uniform over the depth which supports this assumption. Hence, mixing becomes purely due to mechanical dispersion and Equation 8-18 becomes

$$D_x = US_d C_d^{3/2} \qquad \text{Equation 8-19}$$

Using the drag coefficient values derived in section 8.1.1.3, the dispersion coefficient as predicted by Equation 8-19 can be compared to the measured longitudinal mixing coefficients in the reeds tests (Figure 8-35).

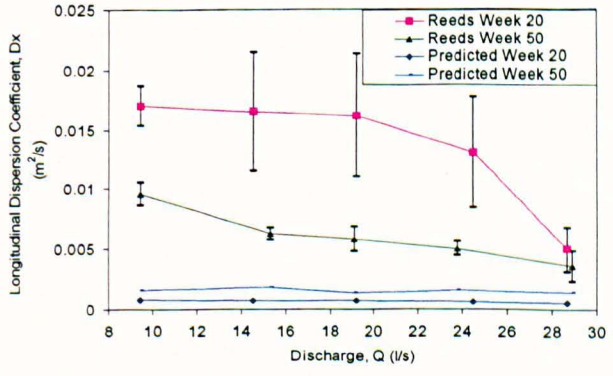

Figure 8-35 Comparison between Lightbody and Nepf (2006) model and measured values of longitudinal dispersion coefficient

Figure 8-35 shows that the model under predicts mixing by a factor of between 15 and 20. The equation of Lightbody and Nepf (2006) appears to not accurately predict mixing in this case.

Due to the uniform distribution of both mass and velocity over the depth in the reeds, the product 'A' in Equation 8-18 has been ignored. The model may be more suitable in cases where there is a significant change in mass, and therefore a non uniform velocity distribution, over the depth. However, in most practical cases this parameter will be difficult to determine accurately. This analysis suggests that mechanical dispersion as described by White and Nepf (2003) makes a relatively small contribution to total mixing in emergent canopies.

In emergent canopies the velocity shear and overall mixing are small relative to non vegetated channels (see section 7.5.5.2). To accurately predict mixing it may be necessary to accurately evaluate the mixing due to transverse velocity shear caused by the differential velocities induced by the stem wakes. This may be difficult to achieve accurately due to the small magnitude of both differential advection and resulting dispersion coefficients, and would require velocity measurements on a small spatial scale.

8.3.2 Longitudinal Dispersion Coefficient in Submerged Conditions

Mixing in submerged canopies is dependent on velocity shear, turbulence (affecting the vertical transport) and the submergence ratio (see section 7.5.5.6). The literature review resulted in one equation provided by Murphy et al. (2007) for predicting dispersion coefficients in submerged vegetation.

8.3.2.1 2-zone model in submerged flow

The model developed by Murphy et al. (2007) as presented in section 3.3.3.2 can be applied to the submerged Carex cases. As described in section 3.3.3.2 the model is based on the 2-zone Chickwendu model (section 2.4.7.1). Equation 3-43 is rewritten here as

$$D_x = \overbrace{\frac{(q_1 q_2)^2 (u_1 - u_2)^2}{\psi}}^{D_{Tran}} + \overbrace{q_2 \alpha (h - h_c) u^*_{hc}}^{D_2} \qquad \text{Equation 8-20}$$

Hence the mixing coefficient is described by a summation of mixing due to exchange between the canopy and the free flow zone (D_{tran}) and normal mixing in boundary layer flow above the canopy (D_2). Equation 8-20 has been derived for use in plane shear flow, with no mixing due to

transverse velocity shear. It is applicable to use the model in the current vegetated case because transverse shear has been shown to be only a minor influence on total mixing in submerged cases (see section 7.5.5.6).

The parameters used in the model have been obtained in the following way

- q_1 and q_2 (proportions of canopy and free flow) are obtained from depth and canopy height measurements.

- ψ, the transfer coefficient is dependent on the level of mixing layer penetration. As shown in section 7.3.6.7 in all cases except for the cropped to 5.5cm case the mixing layer (d_c) does not penetrate to the bed. Hence, in these cases ψ is derived from the empirical wake zone diffusivity equation (Equation 3-46) as presented in Lightbody and Nepf (2006) and recommend by Murphy et al. (2007). In the cropped to 5.5cm case ψ is derived from Equation 3-45 presented by Ghisalberti and Nepf (2005) as recommend by Murphy et al. (2007).

- (u_1-u_2), the difference in velocity between the free flow and wake zone, (Δu) can be obtained by velocity measurement, which is difficult in most practical cases. However, Murphy et al. (2007) suggests Δu can be related to the shear velocity at the canopy top, u^*_{hc} (Equation 3-28) reporting a goodness of fit parameter of $Rt^2 = 0.78$. In the current analysis, for optimum accuracy, Δu is evaluated both using Equation 3-28, and from the measurements taken with the ADV probe (the Δu parameter is measured taking average velocity above the canopy less the measured canopy velocity, U_c) . Hence, comparisons with measurements that were conducted at week 2 and 5 are not presented due to the lack of an accurate method of estimating Δu (complete vertical profiles were not taken at week 2 and 5).

- In plane shear flow the expression given by Elder (1959) should hold and hence α = 5.93 (see 2.4.4.3). However, as demonstrated in section 7.5.1, in the base case D_x/hu^* = 8.22, and so 8.22 will be used here as α.

Dispersion coefficients predicted by Equation 8-20 can be compared to measured values taken in submerged conditions. The measured and predicted coefficients are presented in Table 24 and Figure 8-36.

Table 24 – Predicted Dispersion Coefficients using Murphy et al. (2007) model

Test (Age/Cropped to)	Submergence Ratio, Sr	Measured D_x (m^2/s)	Predicted D_x (Using Equation 3-28) (m^2/s)	Error (%)	Predicted D_x (Using ADV) (m^2/s)	Error (%)
2	1.21	0.013	0.030	-21.2		
2	1.59	0.027	0.123	41.9		
5	1.15	0.011	0.034	25.4		
5	1.61	0.024	0.122	53.2		
7	1.20	0.010	0.081	72.1	0.012	16.1
7	1.46	0.019	0.195	77.3	0.029	34.4
10	1.01	0.008	0.089	80.4	0.008	-5.3
10	1.26	0.011	0.124	80.7	0.018	35.2
10	1.43	0.017	0.184	80.2	0.039	55.0
16	1.10	0.007	0.073	80.1	0.008	2.6
16	1.40	0.018	0.159	77.6	0.020	10.7
20	1.27	0.014	0.130	79.3	0.026	44.8
24	1.26	0.014	0.263	90.0	0.054	74.2
26	1.30	0.010	0.245	92.7	0.061	84.0
Cropped to 25cm	1.16	0.031	0.104	45.3	0.027	-14.7
Cropped to 25cm	1.40	0.059	0.547	80.2	0.139	57.4
Cropped to 13.5cm	1.37	0.053	0.170	49.6	0.155	66.0
Cropped to 13.5cm	1.55	0.072	0.155	22.2	0.086	16.4
Cropped to 13.5cm	1.80	0.071	0.765	81.3	0.617	88.5
Cropped to 5.5cm	1.28	0.013	0.010	-65.3	0.007	-96.0
Cropped to 5.5cm	2.08	0.041	0.048	-5.7	0.037	-10.0
Cropped to 5.5cm	2.47	0.064	0.064	-17.5	0.058	-10.6
Cropped to 5.5cm	2.90	0.059	0.085	22.3	0.073	19.0

Table 24 shows that the error between the predicted and measured values of dispersion coefficient are smaller if the Δu parameter is measured directly from the ADV measurements. The error of each prediction (using the ADV measurement) can be plotted against submergence ratio (Figure 8-36).

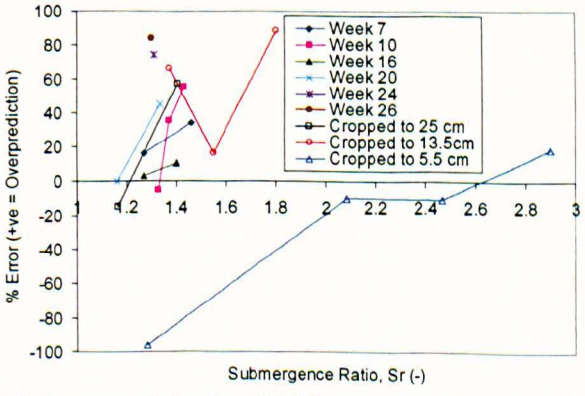

Figure 8-36 error (%) between Murphy (2007) model and measured values of longitudinal dispersion coefficient

Even when using direct measurement of the Δu parameter, the model does not suitably represent the observed values of dispersion coefficient (39% average error) in most cases. Though it should be noted that for the cropped cases the measured values of dispersion coefficient may not

be accurate due to the tracer not reaching the equilibrium zone before the start of the measurement reach in submerged conditions (see section 6.5.4).

The model does however work reasonably well in the case of the cropped 5.5cm high vegetation (predicting D_x to within 20% in 3 out of 4 tests), indicating that the model is more suitable in cases where the mixing layer penetrates to the bed. In this case the wake zone does not exist and the flow case is suitably modelled with a 2-zone equation Equation 8-20) where mixing can be expressed as a summation of mixing due to velocity shear in boundary layer flow plus a contribution from trapping within the mixing layer (Figure 8-37).

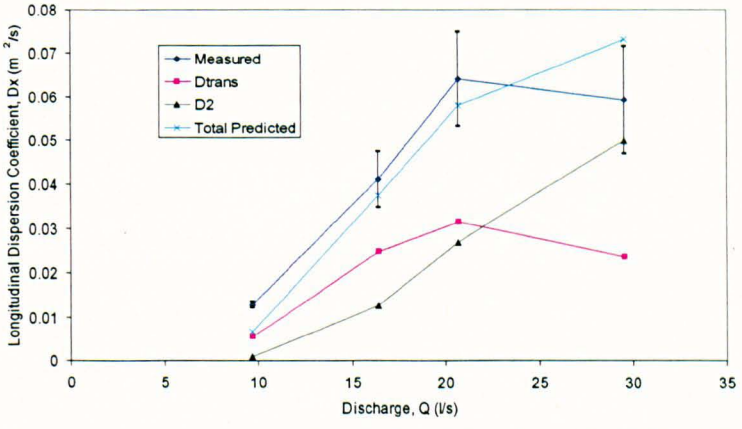

Figure 8-37 Prediction of dispersion coefficient from Murphy et al. (2007) (Equation 8-20) compared to measured values in 5.5cm cropped Carex case.

In more complex systems involving a wake, mixing and free flow zone (in the majority of the cases tested in this work) the model contains a number of simplifications which may be significant.

- The flow structure is simplified into two zones (i.e. within and above the canopy). And hence there is no distinction between the mixing layer and the wake zone.
- It assumes that the transfer coefficient between the canopy and the free flow zone can be described by the wake zone diffusivity. Mixing layer theory suggests relatively high levels of mass transfer occur at h_c, and thus a higher diffusivity than wake zone levels should be used.
- It ignores mixing in the wake zone

It is proposed that the model may be improved by using the full N-zone Chickwendu model together with knowledge of the vertical profile of velocity and Reynolds stresses.

8.3.2.2 Application of Chickwendu Method to Vegetated Flow

The Chickwendu method is described in section 2.4.7.1. Equation 2-136 is reproduced here as

$$D_x(N) = \overbrace{\sum_{j=1}^{N-1} \frac{(q_1 + q_2 \ldots + q_j)^2 \left[1 - (q_1 + q_2 \ldots + q_j)\right]^2 (u_{1j} - u_{(j+1)N})^2}{\psi_{j(j+1)}}}^{D_A} + \overbrace{\sum_{j=1}^{N} q_j e_{xj}}^{D_B} \qquad \text{Equation 8-21}$$

The Chickwendu method splits the flow into a number (N) of zones over the flow depth. Mixing in each zone is dependent on the rate of velocity shear between adjacent zones divided by a transfer coefficient (which represents mass transfer between the zones) (D_A) plus a contribution from diffusivity (D_B). In general mixing due to shear is much greater than that due to diffusivity, hence $D_A >> D_B$. The dispersion coefficient is the sum of mixing contributions ($D_A + D_B$) over the entire flow depth (i.e. over N zones).

The analysis only considers shear in one plane (i.e. in this case vertical rather than transverse shear is considered) therefore it can only be used when it can be assumed that mixing from one plane is insignificant. In this vegetated case mixing due to transverse shear can be judged to be negligible as tests conducted in this system have shown that the longitudinal mixing coefficient is only increased when strong vertical shear is present (see section 7.5.5.6). The method is not suitable for emergent canopies because velocity gradients within the canopy are very small and are difficult to predict without detailed measurements of the canopy morphology.

Equation 8-21 requires knowledge of the velocity, transfer coefficient and longitudinal diffusivity over the flow depth. Knowledge of the velocity profile can be provided by the methods detailed in section 8.2.5. The transfer coefficient for each zone, ψ_j is provided by Chickwendu (1986) as

$$\psi_j = \frac{2e_{zj}}{h^2(q_j + q_{j+1})} \qquad \text{Equation 8-22}$$

As described in section 2.4.4.1 diffusivity for each zone can be provided by (assuming a Schmidt number of 1)

$$e_{zj} = \frac{\tau_j}{\rho \frac{du}{dz}_j}$$ Equation 8-23

The diffusivity can therefore be evaluated from the Reynolds stress (assuming negligible viscous stresses) and velocity profiles. The profile of Reynolds stresses can be predicted using mixing layer theory as described in section 7.3.6. Using Equation 3-30 the Reynolds stress value at the canopy top, h_c can be estimated. From that point Reynolds stress decays linearly to zero at the free surface and to a canopy (or wake zone) Reynolds stress value, τ_c, in the wake zone (h_c-d_c).

If isotropic turbulence is assumed the diffusivity term (e_{xj}) required to calculate D_B in Equation 8-21 can be taken as

$$e_{xj} = e_{zj}$$ Equation 8-24

Thus the contribution from D_B can also be provided by Equation 8-23. However, modelling the wake zone with the N-zone method involves several complications. The assumption of a constant velocity (U_c) means that the parameter $\frac{du}{dz}$ is zero in the wake zone and Equation 8-23 becomes invalid. To overcome this it is assumed that mixing due to shear (D_A) is negligible in the wake zone and ignored, hence Equation 8-23 is no longer required within this zone. Due to the small velocity gradients present in the wake zone (see section 8.2.2) ignoring mixing due to shear is not expected to be a source of significant error.

Making the assumption of isotropic turbulence to validate Equation 8-24 may not be true due to the existence of non isotropic turbulence in vegetated canopies found by Nepf el al (1997). However, mixing due to diffusivity (D_B) is much smaller than mixing due to shear (D_A), and so this is again not expected to be a source of error. As Equation 8-23 is invalid within the wake zone, diffusivity in this zone may be estimated by Lightbody and Nepf's (2006) equation (Equation 3-32).

These assumptions mean that the wake zone effectively becomes one large model zone, with mixing due only to diffusivity. These simplifications meant that such a model cannot be used for canopies where the major source of mixing is not velocity shear between the wake zone and the mixing and free flow layers.

The method also requires an estimate of the wake zone Reynolds stress value, τ_c. For the current tests in submerged Carex the wake zone Reynolds stress (τ_c) can be taken as $0.035 N/m^2$ which is taken as a typical value from the Reynolds stress profiles presented in section 7.3.

A comparison of the parameters involved in the Chickwendu analysis for both plane shear and a submerged vegetation condition is presented in Figure 8-38. The contribution of each zone towards total mixing can also be examined. The largest contribution comes at around the point (h_c-d_c) because the velocity gradient, $\frac{du}{dz}$, is at its maximum and Reynolds stresses are low, hence the mass transfer rate (ψ) will be low, in turn leading to a large 'D_A' in Equation 8-21.

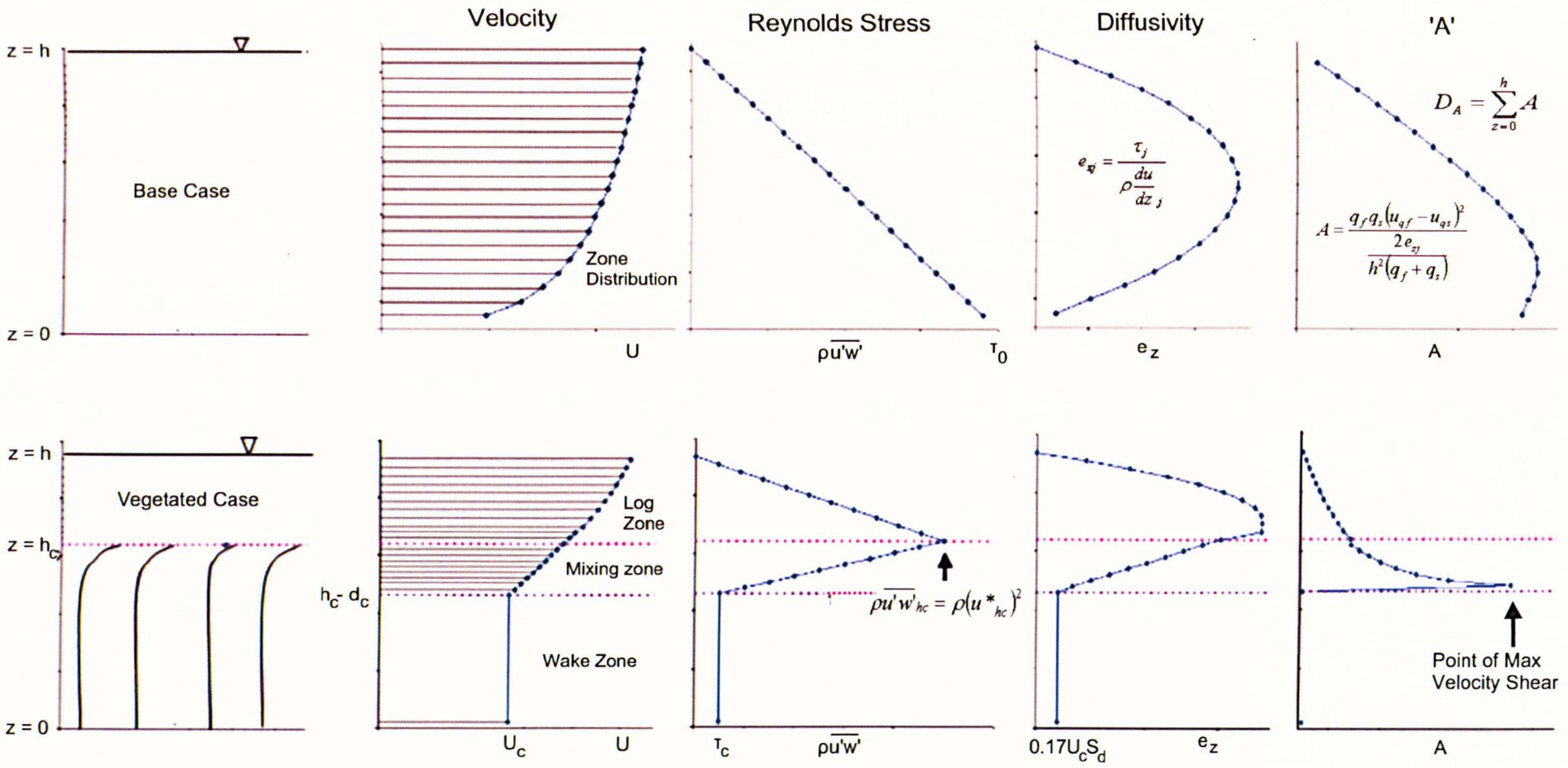

Figure 8-38 N-Zone Chickwendu model applied to plane shear flow and flow through submerged vegetation

8.3.2.3 Evaluation of new method

The predictions of longitudinal dispersion coefficient made by Equation 8-21 can be compared to the observed values in submerged Carex. It this case experimental values of flow depth, canopy height, mixing layer depth, and wake zone Reynolds stress are used in the prediction. Measured and predicted longitudinal dispersion coefficients are presented in Table 25 and Figure 8-39.

Table 25 – Predicted Dispersion Coefficients using full Chickwendu method

Test (Age/Cropped to)	Submergence Ratio, Sr	Measured D_x (m^2/s)	Predicted D_x (m^2/s)	Error (%)
2	1.21	0.013	0.013	-3.6
2	1.59	0.027	0.025	-10.0
5	1.15	0.011	0.009	-11.7
5	1.61	0.024	0.035	30.6
7	1.20	0.010	0.009	-2.8
7	1.46	0.019	0.019	0.5
10	1.26	0.011	0.012	3.5
10	1.43	0.017	0.017	-0.9
16	1.10	0.007	0.007	-3.2
16	1.40	0.018	0.019	4.8
20	1.02	0.005	0.004	-5.6
20	1.27	0.014	0.014	1.3
24	1.26	0.014	0.014	-0.3
26	1.30	0.010	0.010	5.4
Cropped to 25cm	1.16	0.031	0.030	-2.5
Cropped to 25cm	1.40	0.059	0.074	20.4
Cropped to 13.5cm	1.37	0.053	0.062	14.2
Cropped to 13.5cm	1.55	0.072	0.060	-20.1
Cropped to 13.5cm	1.80	0.071	0.104	31.5
Cropped to 5.5cm	1.28	0.013	0.015	17.0
Cropped to 5.5cm	2.08	0.041	0.038	-7.4
Cropped to 5.5cm	2.47	0.064	0.061	-4.9
Cropped to 5.5cm	2.90	0.059	0.045	-30.6

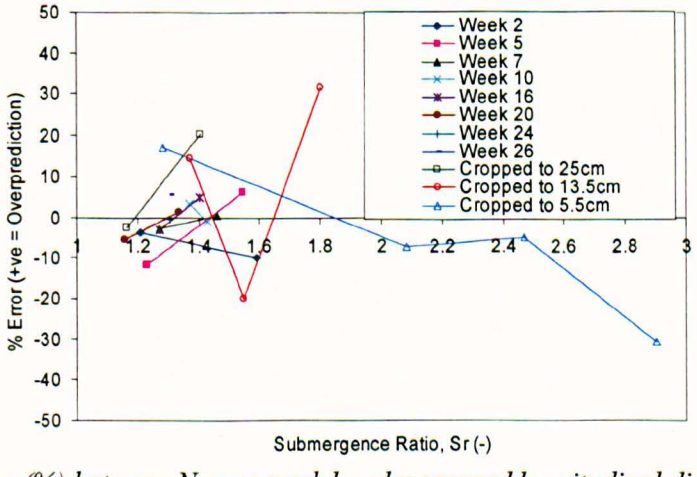

Figure 8-39 error (%) between N-zone model and measured longitudinal dispersion coefficient

Figure 8-39 shows that for the growth phase the new method provides more accurate predictions of the longitudinal dispersion coefficient than a simple two-zone model presented in section 8.3.2.1. Almost all predictions are within 10% of the measured value. More error was encountered when attempting to predict mixing in the cropped phase. However measured dispersion coefficients in the 25cm and 13.5cm cropped phases may be inaccurate due to the experiments not being conducted fully within the equilibrium zone. As shown in Figure 8-37 in cases where the mixing layer penetrates to the bed mixing is best modelled with a simpler 2 zone approach.

The main drawback with this method is the fact that measurements of d_c, and τ_c are required to make predictions. At present there is no method for predicting Reynolds stress within the canopy. Nepf et al. (2007) method for predicting mixing layer depth has been shown to be inaccurate for the currents tests in section 8.2.4.

8.3.3 *Dispersive Fraction in Submerged Conditions*

The concept of dispersive fraction was introduced in section 2.4.9.1 as a method to define a mixing parameter for the ADZ model. The dispersive fraction is defined as the ratio between the dead zone volume and the total volume in the reach. The larger the dead zone volume compared to the total volume of the flow, the larger the quantity of solute delayed compared to the main flow volume, and the greater the spreading of the solute.

In the vegetated channel experiments in this thesis the free flow volume has, in most cases, been smaller than the volume of flow travelling through the vegetated layer. In the vegetated case the main body of the flow within the vegetated layer can be seen to act as the trapped volume, whilst the solute of the free flow layer is separated from the main volume because of its faster flow. Thus in this case, as the volume of the free flow layer becomes larger in relation to the trapped volume within the vegetated layer, the greater the separation and hence the greater the mixing. The submergence ratio (Equation 3-2) of the flow describes this ratio between the depth of flow in and above the canopy. In submerged flow it has been shown that the rate of mixing is heavily dependent on the submergence ratio (see section 7.5.5.7), with mixing increasing with submergence ratio.

In such vegetated cases it may be possible to look at the dispersive fraction in a different way than is conventionally the case. A possible analogy to the dispersive fraction is the ratio between the size of the free flow and canopy flow zones. As it is the size of the free flow volume (rather than the size of the trapped volume) in relation to the volume of flow that determines the rate of mixing, a rearrangement of the normal dispersive fraction equation is required. It follows from Equation 2-149 that

$$Df = \frac{V_e}{V_R} = \frac{h - h_c}{h}$$ Equation 8-25

Effectively the free flow volume is viewed as the dead zone volume. As this is counterintuitive, it is best instead viewed as a separation volume rather than a dead zone volume. As this parameter is dependent only on the ratio between the two flow layers, it depends only on submergence ratio. It can be shown that

$$Df = \frac{h - h_c}{h} = \frac{Sr - 1}{Sr}$$ Equation 8-26

The dispersive fraction predicted by Equation 8-26 and measured values of submergence ratio can be compared to the measured value of dispersive fraction in submerged Carex (Figure 8-40 and Figure 8-41).

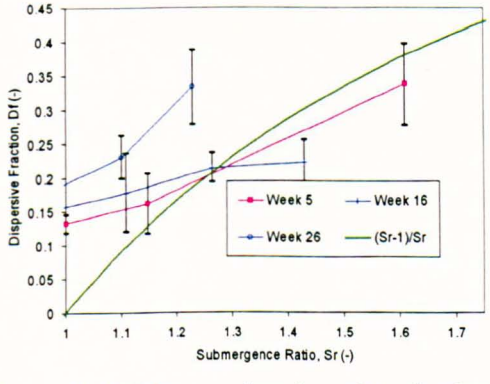

Figure 8-40 Measured and predicted values of dispersive fraction in the growth phase

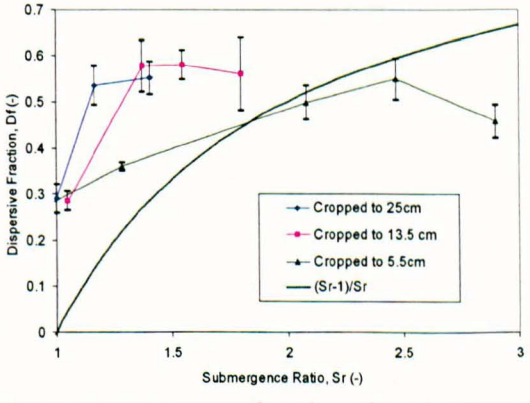

Figure 8-41 Measured and predicted values of dispersive fraction in the cropped phase

Figure 8-40 and Figure 8-41 show that Equation 8-26 predicts the trend in dispersive fraction, if not the precise values. The calculated dispersive fraction can be compared to all measured values observed in submerged conditions (Table 26 and Figure 8-42).

Table 26 – Predicted and Measured Dispersive Fraction in Submerged Conditions

Test (Age/Cropped to)	Submergence Ratio, Sr	Measured Df (-)	Predicted Df (-)	Error (%)
2	1.21	0.266	0.172	-54.2
2	1.59	0.345	0.371	7.1
5	1.15	0.162	0.128	-26.5
5	1.61	0.337	0.378	10.9
7	1.20	0.247	0.167	-48.0
7	1.46	0.358	0.316	-13.3
10	1.26	0.215	0.208	-3.0
10	1.43	0.221	0.300	26.3
16	1.10	0.201	0.094	-112.6
16	1.40	0.317	0.286	-10.8
20	1.27	0.212	0.214	0.9
24	1.26	0.392	0.206	-90.5
26	1.30	0.333	0.230	-45.0
Cropped to 25cm	1.16	0.534	0.141	-278.9
Cropped to 25cm	1.40	0.551	0.288	-91.4
Cropped to 13.5cm	1.37	0.577	0.270	-113.4
Cropped to 13.5cm	1.55	0.579	0.354	-63.6
Cropped to 13.5cm	1.80	0.559	0.444	-25.8
Cropped to 5.5cm	1.28	0.360	0.221	-63.1
Cropped to 5.5cm	2.08	0.498	0.520	4.3
Cropped to 5.5cm	2.47	0.549	0.595	7.7
Cropped to 5.5cm	2.90	0.456	0.655	30.4

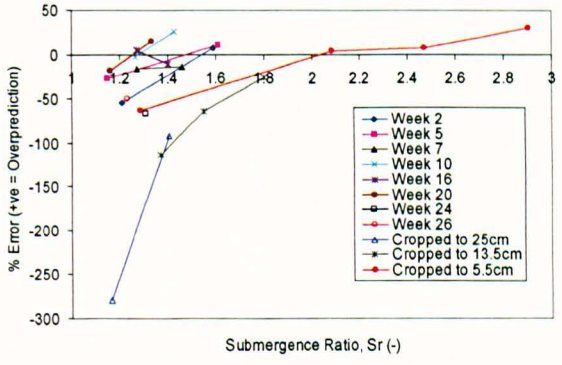

Figure 8-42 Comparison between predicted (Equation 8-26) and measured dispersive fraction

It can be seen from Table 26 and Figure 8-42 that the method only provides a rough estimate of measured dispersive fraction. The average percentage error between measured and predicted values in the growth phase is 26%, while in the cropped phase it is 66%. However, the method has the benefit of being relatively simple to evaluate, requiring only knowledge of the flow depth and canopy height. In flows with a higher degree of submergence the analogy of the free flow layer to the separation volume in Equation 8-26 will not be accurate. In cases where the majority of the flow is in the free flow layer it is the relative size of the trapped volume that determines the rate of mixing, therefore in this case the canopy flow should be considered as the ADZ (or separation) volume. The predicted dispersive fraction will then become equal to the inverse of submergence ratio and will become smaller as the proportion of flow trapped in the canopy decreases.

8.3.4 Methodology for Predicting Mixing Coefficients in Submerged Conditions

Throughout chapter 8 methods have been proposed to predict flow depth and velocity profiles in submerged and emergent conditions as well as mixing coefficients in submerged conditions. Linking this new knowledge together it is now possible to predict mixing coefficients in submerged flow based on knowledge of the basic channel and vegetation properties (discharge, channel slope, channel width, vegetation density, stem width, and canopy height) and some other flow and turbulence parameters which have been defined throughout this study.

8.3.4.1 Predicting Longitudinal Dispersion Coefficient

To predict longitudinal dispersion coefficient in submerged conditions, aside from the basic flow and channel parameters, the drag coefficient, canopy top roughness, mixing layer depth, canopy shear velocity, wake zone Reynolds stress and wake zone diffusivity are required. An outline of the methodology required to predict the dispersion coefficient is presented in Figure 8-43. The 'extra' parameters are detailed, together with recommended sources. It should also be noted that the full methodology listed in Figure 8-43 is only suitable in cases where the mixing layer does not penetrate to the bed and a wake zone exists. In cases where a wake zone does not exist, it is recommended that the longitudinal dispersion coefficient can be estimated using the Murphy et al. (2007) method outlined in section 8.3.2.1. In which case, the Murphy et al. (2007) model can be implemented once the flow depth, h has been determined.

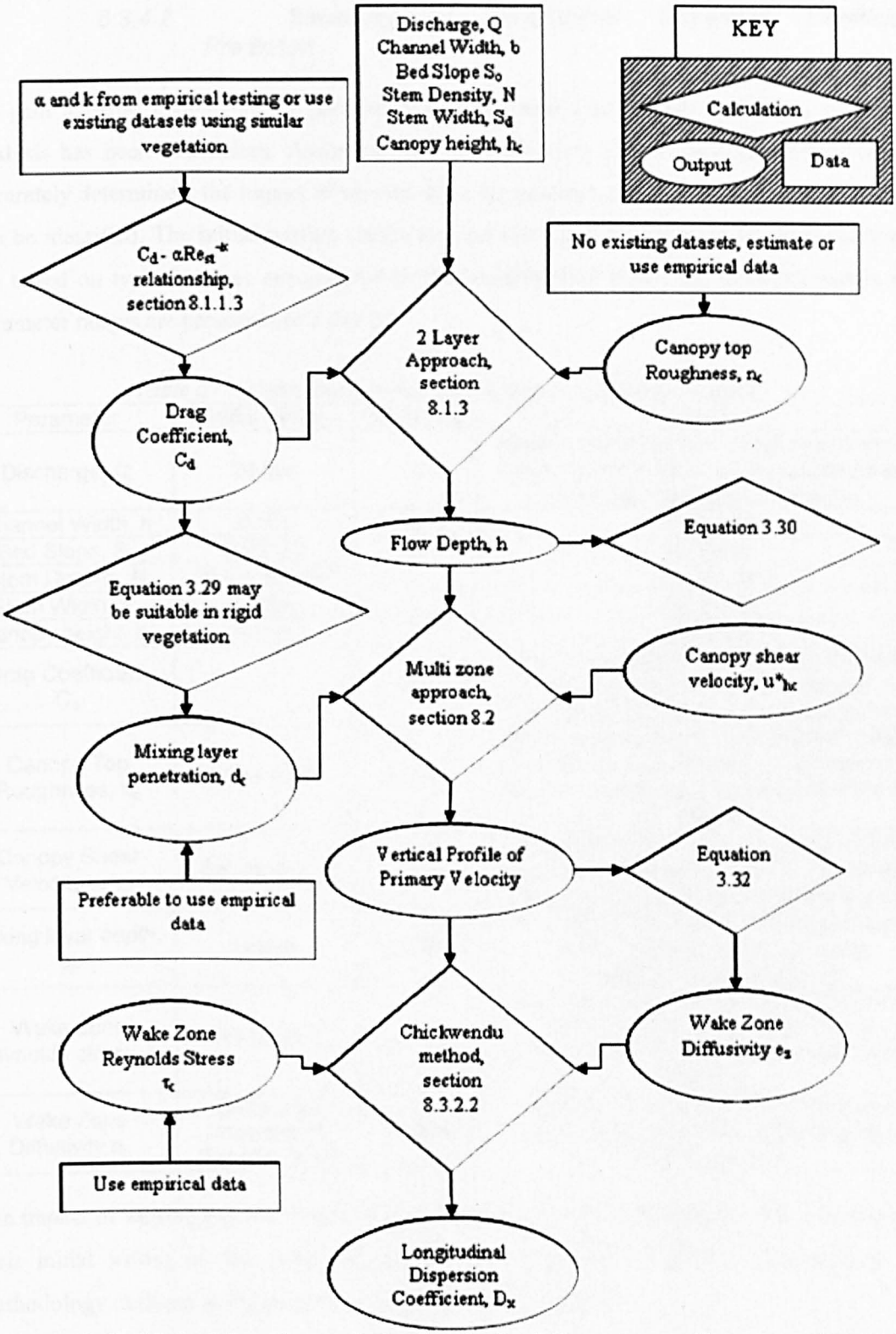

Figure 8-43 Methodology for predicting longitudinal dispersion coefficient in submerged vegetation

8.3.4.2 Sensitivity of Longitudinal Dispersion Coefficient Prediction

To gain a better insight on the performance of the new Chickwendu method, a sensitivity analysis has been undertaken. Assuming that the basic flow and channel parameters can be accurately determined, the impact of varying the extra parameters (C_d, n_c, d_c, u^*_{hc} and τ_c and e_c) can be identified. The initial starting conditions and the ranges of variation for each parameter are based on typical values encountered in this experimental study, the resulting values and parameter ranges are presented in Table 27.

Table 27 – Parameters in mixing coefficient sensitivity analysis

Parameter	Initial Value	Varied by	Notes
Discharge, Q	29.5l/s	0	Initial Value based on typical experimental value. Considered accurate measurement available therefore no variation.
Channel Width, b	0.6m	0	As above
Bed Slope, S_o	0.00123	0	As above
Stem Density, N	20.8 stems/m^2	0	As above
Stem Width, S_d	0.05m	0	As above
Canopy height, h_c	0.15m	0	As above
Drag Coefficient C_d	3	±75%	Initial Value based on typical experimental value. Variation based on typical experimental range of C_d in this study
Canopy Top Roughness, n_c	0.015 s/m$^{1/3}$	± 50%	Initial Value based on typical experimental value. Variation based on difference between growth and cropped experimental values
Canopy Shear Velocity, u^*_{hc}	Equation 3-30	± 45%	Equation 3-30 considered reasonable accurate, varied according to experimental values of Reynolds stress at canopy top
Mixing layer depth, d_c	0.04m	± 40%	Initial Value based on typical experimental value. Variation based on results throughout testing program
Wake Zone Reynolds stress, τ_c	0.035N/m^2	± 90%	Initial Value based on typical experimental value. Variation based on typical experimental range of values measured in this study
Wake Zone Diffusivity e_c	Calculated According to Equation 3-32	± 100%	Equation 3-32 considered best guess. Varied assuming reasonable degree of empirical error

The impact of varying each of the parameters separately (whilst keeping the other parameters at their initial value) on the predicted longitudinal dispersion coefficient (according to the methodology outlined in Figure 8-43) is presented in Figure 8-44.

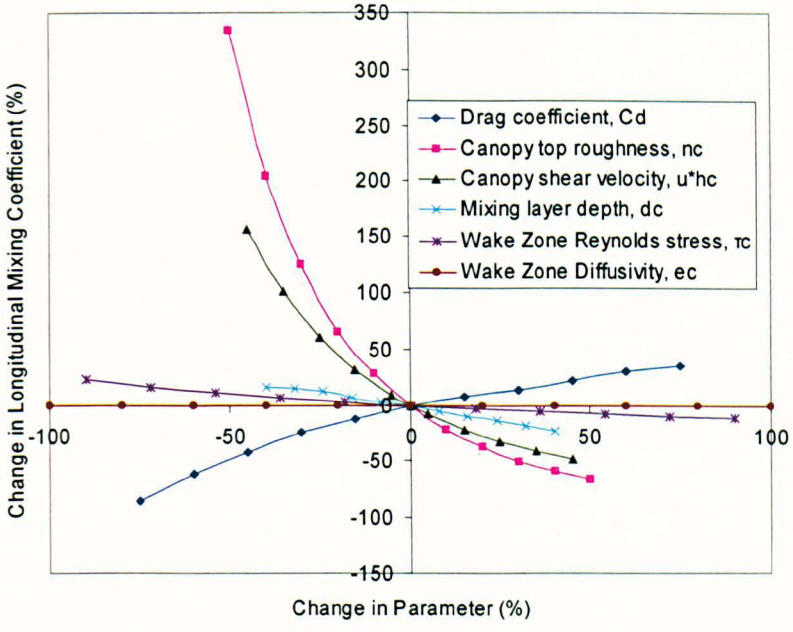

Figure 8-44 Effect of different parameters on longitudinal dispersion coefficient prediction using the methodology outlined in Figure 8-43

The prediction is highly sensitive to the drag coefficient and the canopy top roughness. These parameters are required at the beginning of the depth calculation process and thus have an impact on all of the other analysis processes. They are also the parameters that have an impact on the depth and velocity of the free flow zone and the submergence ratio of the flow. As shown in section 7.5.5.7, the submergence ratio had a strong influence on the observed mixing coefficients in submerged Carex, so the parameters which affect submergence ratio would be expected to have a large impact on the mixing coefficient.

The drag coefficient is inversely related to the flow rate and velocity of flow in the canopy zone, and thus is positively related to the amount (and so depth and velocity – according to boundary layer flow theory) of flow over the canopy top. In terms of the influence on vertical shear as explained in section 7.5.5.6, this directly impacts both the relative zone size and the differential velocity between the fast and slow zones of flow. Hence an increasing drag in the canopy leads to increasing mixing. Although not shown here, by the same logic increasing the density or size of the vegetation (if the other parameters are constant) will have a similar effect.

Canopy top roughness affects the depth and speed of flow in the free flow layer. By increasing roughness, the size of the free flow layer increased, but its velocity decreased. Although the increase in relative zone size will tend to encourage mixing, in this case the reduction in differential advection between the two zones is more significant and causes a reduction in mixing coefficient with canopy top roughness.

As they determine flow depth, drag coefficient and the canopy top roughness indirectly affect canopy shear velocity, which is used to determine the profile of Reynolds stresses, the transfer coefficient, ψ and the rate of vertical mass transport. As discussed in 7.5.5.7, vertical transport is an important factor in determining the rate of mixing. Hence, varying canopy shear velocity also has a large impact on the mixing coefficient. Increasing shear velocity leading to increasing vertical transport, reducing the effectiveness of shear dispersion and reducing mixing.

The mixing layer depth has a lesser but still significant effect, having an impact on both the vertical transport (as it determines the size of the mixing layer), and the shape of the velocity profile. Again a larger mixing layer encourages vertical transport, reducing the mixing coefficient.

At low deviations from the initial value, the prediction of dispersion coefficient is relatively insensitive to the wake zone Reynolds stress value assigned to the canopy. The wake zone Reynolds stress only has a minor impact on vertical transport in a limited region of the flow depth. However, at present the Reynolds stress has to be determined empirically and large errors (>15%) in the mixing coefficient are possible if the parameter is not determined to within 75%.

The wake zone diffusivity has an insignificant effect on predicted dispersion coefficient. The wake zone diffusivity only contributes to mixing due to diffusivity (D_B in Equation 8-21), which is insignificant compared to mixing due to shear, D_A.

The sensitivity of the prediction to drag coefficient and the canopy top roughness means that the uncertainty of the prediction can be greatly reduced if the flow depth is already known. This eliminates the requirement for canopy top roughness and drag coefficient in the methodology outlined in Figure 8-43.

8.3.4.3 Predicting Dispersive Fraction

A similar methodology can be constructed for dispersive fraction in submerged vegetation (Figure 8-45). As only the submergence ratio is required to make a prediction, this methodology is relatively simple when compared to the methodology for predicting longitudinal dispersion coefficients (Figure 8-43). The only parameters required, aside from the basic flow and channel parameters, being drag coefficient and canopy top roughness.

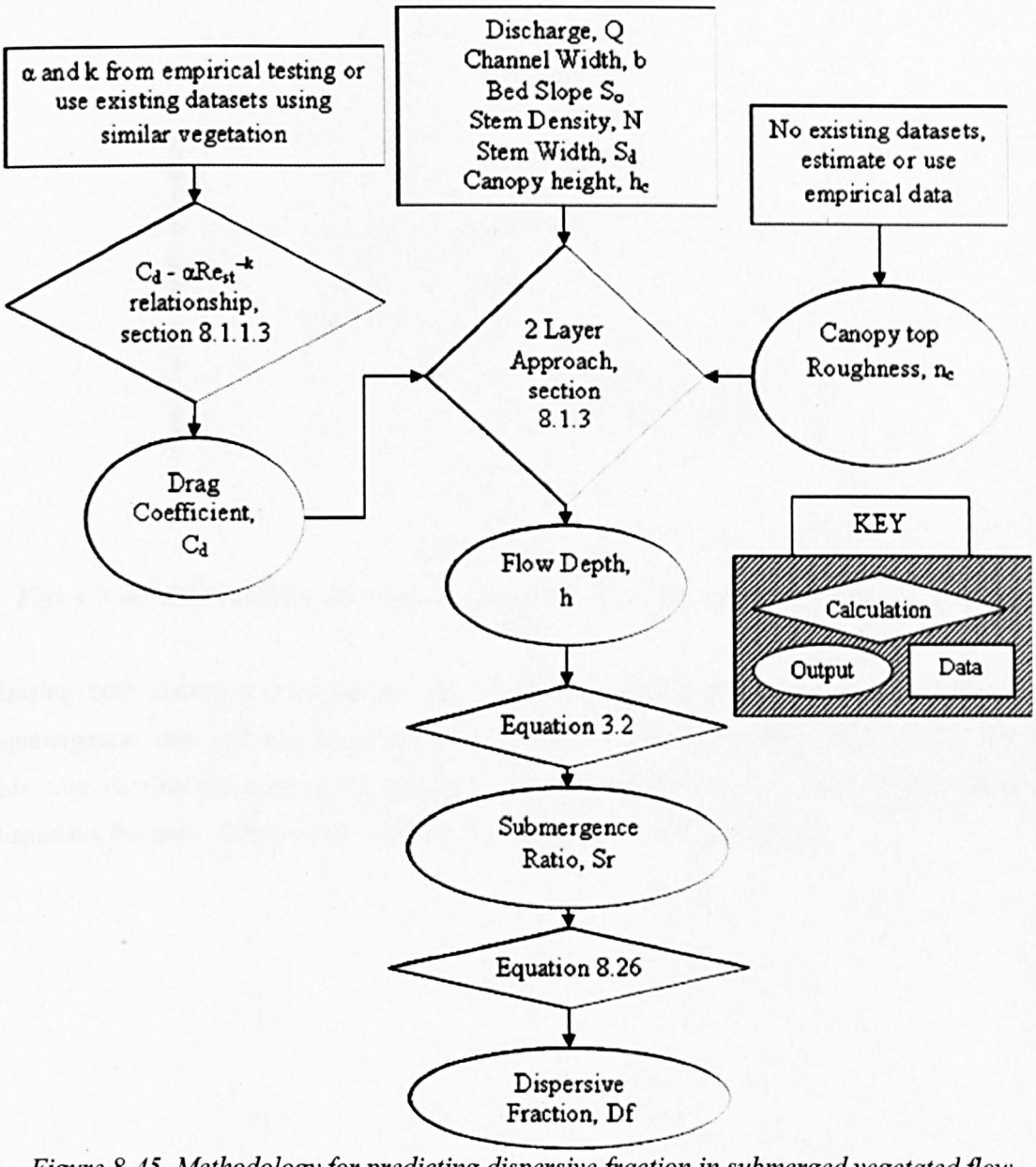

Figure 8-45 Methodology for predicting dispersive fraction in submerged vegetated flow

8.3.4.4 Sensitivity of Dispersive Fraction Prediction

As with the methodology for predicting longitudinal dispersion coefficients, (Figure 8-43) a sensitivity analysis has been carried out on the methodology for predicting dispersive fraction, as outlined in Figure 8-45. In this case only the drag coefficient and canopy top roughness have an impact on the predicted values, and thus are the only parameters varied. The initial starting conditions and the ranges of variation for the two parameters are identical to the sensitivity analysis conducted for the longitudinal mixing coefficient methodology (detailed in Table 27). The results of the sensitivity analysis are presented in Figure 8-46.

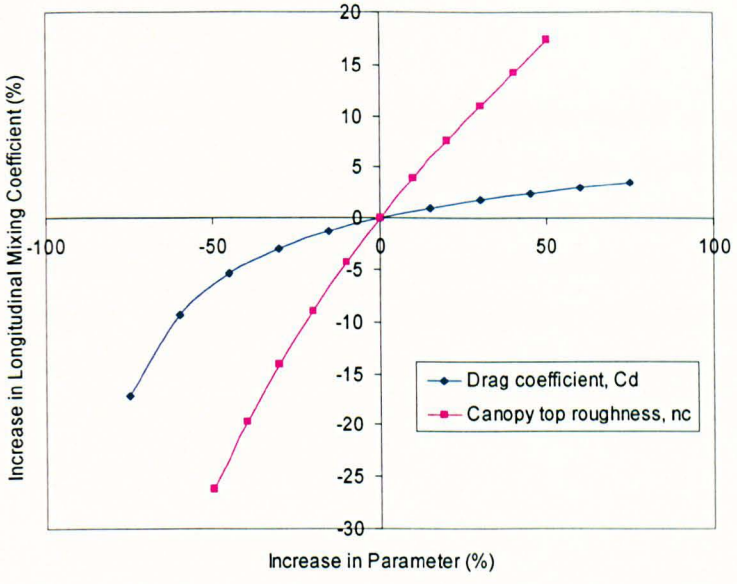

Figure 8-46 Effect of different parameters on dispersive fraction prediction using Equation 8-26

Raising both canopy top roughness and drag coefficient increases the depth of flow, the submergence ratio, and thus the predicted dispersive fraction (according to Equation 8-26). In this case varying the canopy top roughness has the largest impact on flow depth and thus dispersive fraction. However, the prediction is sensitive to both parameters.

Chapter 9 - Conclusions

The research objectives of this thesis were to investigate the impact of vegetation in open channel flow and mixing. Following a literature review (chapter 3), chapter 4 identified a number of specific research questions regarding flow resistance and mixing in vegetated flow. To answer these questions a detailed laboratory study was undertaken. The laboratory study measured flow resistance, velocity, turbulence and transverse and longitudinal mixing through two different vegetation types (reeds and Carex). Results were compared to base case conditions, where no vegetation was present. After completing the study and analysing the results the following conclusions have been made.

9.1 Flow Resistance

One of the research objectives identified was to assess the accuracy and practicality of existing flow resistance models. All previous models suggest that the presence of vegetation in a natural channel would increase the overall resistance, slowing the flow and increasing the flow depth. Experiments confirmed that the presence of vegetation in a channel considerably increased its flow resistance and reduced the channel flow carrying capacity. Experiments demonstrated how Manning's roughness coefficient, n, increased as the Carex grew in size and the reeds grew in density. Manning's n, from being approximately constant with depth in the base case, was found to change with flow depth, increasing with depth in emergent conditions, decreasing with depth once the vegetation became submerged.

This thesis has evaluated a number of existing methods for determining flow resistance in vegetated flow, including the n-UR method (Ree and Palmer, 1949), the relative roughness method (Kouwen, et al., 1969) and the drag approach (Petryk and Bosmajian, 1975). Although the n-UR approach provides useful insights into the behaviour of vegetation under flow (in particular the effect of streamlining in reducing the drag on the flow), the method did not accurately represent the vegetated channel resistance. The relative roughness approach was judged to be not applicable to the vegetation studied, being more suited to flow over vegetated channel linings with a high degree of submergence. It has therefore not been possible to verify the n-UR and the relative roughness methods using the tests conducted for this thesis. This research suggests that a momentum balance or drag approach has the potential to give a good description of flow resistance in vegetated channels featuring emergent vegetation. Its theoretical nature means that it has a wide range of applicability and can be suited to a number of vegetation types. Of the existing momentum based flow resistance models for emergent vegetation which have been tested, the model of James et al. (2004) provides the most accurate stage discharge predictions for the tests undertaken in this thesis.

However, the main practical issue with the momentum based approach is the selection of a suitable drag coefficient. The original model derived by Petryk and Bosmajian (1975) used a constant value of drag coefficient. In effect this ignores both the differences in drag of different vegetation types, and any streamlining effect where the drag of vegetation reduces due to the plants adopting a streamlined position. In canopies where the effect of the bed is negligible, this means that the model predicts velocity independently of discharge, and thus an increasing Manning's n with flow depth. This however directly contradicts the n-UR approach which, based on empirical evidence, shows how streamlining of vegetation reduces drag and hence resistance. In most cases it is clear that for accurate results the drag coefficient should be a function of flow. This research has confirmed that the drag coefficient can be related to the stem Reynolds number of the flow, provided that the empirical coefficients which characterise this relationship are known. In this case it has been identified that one of the coefficients is related to channel porosity. More work would be required to characterise how the empirical coefficients vary with further vegetation and channel characteristics, such as channel slope, and vegetation type and flexibility. Some work on this has been carried out (Tsihrintzis, 2001), however, a number of different approaches for characterising both drag coefficient and the C_d-Re relationship make comparison and application of the existing studies difficult. However, it is judged that such work is beneficial as this research has shown that the accuracy of the drag models can be improved provided a suitable C_d-Re_{st} relationship is used. Such a relationship is critical in flexible vegetation which has the ability to become more streamlined as the flow rate increases. In stiff vegetation not subject to bending, the change in drag coefficient will be less, yet it should still be taken into account, especially over a large flow range. This suggests that future work should focus on characterising the flow resistance properties of actual vegetation types, especially those which tend to be flexible and hence not subject to this constant drag/velocity condition.

Existing models for submerged flow are largely empirical in nature, and thus are constrained by only being applicable in conditions similar to those which they were derived for. Existing drag models for submerged vegetation were not verifiable in the experimental channel as the specified constraints were outside the experimental conditions. A novel two layer approach has been proposed which calculates the flow within the canopy using the drag approach and then the flow above the canopy using a conventional boundary layer resistance formula (Manning's equation). The total flow is calculated from the summation of the canopy layer and free flow layers. The model has been tested on observed data with good results. The method does however require an estimate of effective canopy top roughness, which may vary with vegetation type and density.

In practice the main issue with momentum based models is the difficultly in characterising the parameters required, such as drag coefficient, stem diameter and density. To bring such models into widespread practice, research is required into typical stem densities and diameters of the plants most likely to be found in waterways. The accurate use of momentum based drag methods also requires further determination of C_d-Re_{st} relationships and in the case of submerged vegetation, canopy top roughness.

9.2 Solute Mixing

9.2.1 Applicability of ADE and ADZ Models

The literature review concluded that comparatively little research had been conducted on the applicability of the one dimensional mixing models in vegetated flows. By measuring the goodness of fit of the ADE and ADZ models to the measured concentration profiles and the development of the moments of the measured concentration profiles in vegetated flow, the applicability of the one dimensional models has been judged and compared to the performance in the base case.

In emergent conditions, measured concentration profiles enter the equilibrium zone (in which Fickian mixing assumptions can be applied) closer to the injection point than in the base case. This indicates that any trapping mechanisms working in the wakes of the vegetation elements do not significantly delay the onset of Fickian conditions by imparting additional skew into the concentration profiles. The overall retardance effect of the vegetation slows the flow and means that Fickian conditions are reached sooner, in terms of distance. In the case of canopies with a high degree of retardance, measured profiles were approximately symmetrical prior to the measured mixing reach. It has been shown here that the one dimensional ADE and ADZ models effectively predict mixing in these conditions.

In submerged conditions, concentration profiles are dominated by vertical velocity shear, which imparts a high degree of skew. In such cases the advective zone is lengthened relative to a channel with emergent vegetation. However it was still possible to measure equilibrium zone mixing within the length of experimental channel available in this thesis. Once the plume entered this equilibrium zone its change could be accurately described using the ADE. The ADZ model's ability to predict skew means that it can be used sooner (in terms of distance from injection) than the ADE. In cases where the vegetation was cropped, increased levels of vertical velocity shear delayed the start of the advective zone beyond those observed in the base case and even beyond the length of the experimental channel.

For the purposes of this study it has been important to quantify how the presence of vegetation alters the advective zone distance in terms of distance from the injection point. It is envisioned that future research may concentrate on whether vegetation alters the advective zone distance in terms of time. This may give a better indication on the effect of vegetation trapping and velocity shear in vegetated flows on the advective zone length.

9.2.2 Effect of Vegetation on Mixing

The research aimed to discover how vegetation affects the rate of mixing, and how these effects change as the vegetation parameters (height, size and flexibility) alter with plant growth. To do this it has been necessary to measure not only mixing rates, but also profiles of velocity and Reynolds stress, as these influence the rate of velocity shear and mass transport in the flow.

9.2.2.1 Velocity and Reynolds Stress in Vegetated Flow

Velocity and turbulence measurements in vegetated flow conditions largely confirm trends proposed by existing research. The extra flow resistance causes profiles of primary velocity and Reynolds stress to be retarded within the canopy relative to the base case condition. The vertical orientation of plant stems generates wakes and eddies behind the vegetation elements, causing localised spikes of high transverse Reynolds stress. However the frequency and magnitude of these spikes decreased with plant growth as the plants increasingly retard the flow. The presence of wakes and eddies appeared to generate transverse Reynolds stress only, with the effect that vertical profiles of Reynolds stress became almost negligible in all vegetated cases. Tests conducted in submerged flow appeared to confirm the mixing layer analogy proposed by Raupach et al. (1996). A mixing layer with a region of high momentum exchange (high Reynolds stress) and an inflection in the velocity profile was observed at the top of the canopy. Below this mixing layer, within the canopy, a wake zone region (with a uniform velocity profile and low Reynolds stress) exists in most cases. However, in low canopies the wake zone may not exist and the mixing layer will penetrate to the bed. Above the mixing layer the flow resembled boundary layer flow, with Reynolds stress decaying to the free surface. The relationship between Reynolds's stress at the canopy top, the strength of the velocity inflection, and the depth of the free flow zone and flow resistance of the canopy requires further study with a more detailed number of measurements and higher submergence ratios.

A new method for determining the velocity profile over the entire flow depth has been proposed. The method splits the flow into a series of layers and combines momentum balance and boundary layer theory. The main challenge with this new method that is outstanding is that it requires accurate determination of the depth of the mixing layer, d_c.

9.2.2.2 *Transverse Mixing in Vegetated Flow*

The tests conducted indicate that the presence of vegetation has a significant effect on transverse mixing. For each vegetated case roughly constant levels of measured turbulence and secondary currents with flow mean that the main drivers of transverse mixing alter little with discharge. Hence, unlike non vegetated conditions, transverse mixing in emergent canopies is roughly constant with discharge and flow depth. Previous researchers (Fischer and Hanamura 1975, Tanio and Nepf, 2007) have reported that mixing is related to channel velocity. In these experiments, velocity varied only slightly over the flow depth for most experiments and hence no trend was evident. Transverse mixing appears to be inversely related to plant growth. This is possible as the magnitude of turbulent eddies (and hence momentum and mass exchange) behind vegetation elements reduces with plant growth due to a slower flow though larger, denser canopies.

In submerged canopies mixing over each test was found to vary with the product of depth and boundary shear stress. As turbulence in submerged canopies is generated by the shear between the canopy and free flow layer a new normalising parameter $(h-h_c)u^*_{hc}$ was proposed, which attempts to scale mixing by the strength of the turbulence in the mixing layer. Transverse mixing was found to be strongly related to the new parameter, although it did not offer significant improvement in quantifying the transverse mixing than the conventional hu^*.

9.2.2.3 *Longitudinal Mixing in Vegetated Flow*

In emergent flows the presence of vegetation had the overall effect of reducing longitudinal mixing relative to the base case. This is due to the effect of the vegetation on retarding the velocity profile, making it roughly uniform over the width and depth and hence reducing the magnitude of shear dispersion. Hence, there appears to be a negative relationship between longitudinal mixing and stem density. However, due to the poor growth of the reeds, the relationship between stem density and mixing coefficient has not been adequately explored. The exact prediction of mixing coefficients in emergent vegetation is not yet possible. A model proposed by Lightbody and Nepf (2006) based on mixing due to vertical shear dispersion (caused by a variation on plant mass over the depth) and wake trapping failed to accurately predict mixing coefficients. Due to the low levels of mixing encountered it is proposed that the prediction of mixing in emergent canopies would require the evaluation of profiles of velocity and turbulence at a smaller spatial scale than has been attempted in this thesis.

Mixing rates in submerged canopies are generally larger than in emergent vegetation due to the increased vertical velocity shear over the depth. However, in most cases the measured mixing coefficients were lower than in the base case. In cases with a high degree of velocity shear (such

as cropped vegetation with high submergence ratios) the observed mixing coefficients increased above those found in the base case. Submerged canopies are complex mixing systems, involving different flow layers (wake, mixing and free flow zones). The rate of mixing in such a system is dependent on their relative size, the difference in average velocity, and the rate of transfer of mass between these zones. All of which are dependent on the flow in the channel, the size of the mixing layer and the flow resistance of the vegetation in question. Of these parameters the most difficult to predict is the size of the mixing layer; which was found to be approximately constant in growth phase Carex, but to increase in the cropped Carex. A method for predicting mixing layer depth derived by Nepf et al. (2007) using rigid simulated vegetation was effective in predicting mixing layer depth in the relatively rigid cropped vegetation, yet failed to describe the penetration depth in the growth phase. This shows that future studies regarding mixing layer penetration should concentrate on characterising penetration depth for real (i.e. flexible) rather than rigid simulated vegetation. The study shows that the most critical parameter for longitudinal mixing is the submergence ratio of the flow, as this affects both the differential velocity and the relative zone size. This makes the evaluation of flow depth (and hence channel flow resistance) critical in the accurate evaluation of the mixing coefficients.

The tests conducted indicate that in cases where the wake zone is insignificant the mixing can be reasonable well predicted by a relatively simple 2-zone model such as the one proposed by Murphy et al. (2007). In such a case, the rate of longitudinal mixing is usually lower than a comparative case with a wake zone due to more rapid vertical transport reducing the magnitude of shear dispersion. However, in cases where a significant wake zone exists such a model involves simplifications in the transfer rates and relative zone sizes and thus performs less well. A more advanced method for predicting mixing coefficients in submerged canopies based on the N-zone Chickwendu (1986) model has been presented as part of this thesis. It has been tested against the measured data with good results. Although to make it practical, further work is required to characterise mixing layer penetration in real vegetation types and diffusivity levels inside vegetated canopies. A simple method to predict the ADZ mixing parameter, the dispersive fraction, has also been proposed. Based on the ratio between the canopy and free flow zones, whilst only providing rough estimates of dispersive fraction, it only requires knowledge of the flow depth and canopy height.

Unlike in this study flow in actual channels may have varying amounts of vegetation across the channel width (i.e. a channel with vegetated banks). In this case a tracer would be subject to transverse as well as vertical velocity shear. Obviously this would further complicate the mixing processes and a velocity shear analysis would have to be undertaken in the transverse instead of/as well as the vertical plane and would entail a more sophisticated 2D extension to the Chickwendu method.

Following the work conducted in this thesis, a full methodology to determine both longitudinal mixing coefficient and dispersive fraction in submerged canopies is now available. A sensitivity analysis for both determination of longitudinal mixing coefficient and dispersive fraction has been carried out. This shows that accurate determination of vegetation drag, canopy top roughness, canopy shear velocity and mixing layer penetration is essential for the accurate mixing coefficient determination. Further work is therefore required to characterise these parameters accurately for a wide range of submerged vegetated canopies.

9.3 Summary of Conclusions

To conclude, the main findings of this thesis are

- In emergent vegetation momentum balance models can provide an accurate description of the flow resistance provided an accurate estimation of the drag coefficient is made. This drag coefficient is a function of Reynolds number. Further work is required to characterise the C_d - Re relationship for each vegetation type and agree on a standardised method of drag and Reynolds number measurement.

- The thesis has demonstrated that a two layer approach can accurately predict flow resistance in submerged conditions. This method combines a momentum balance approach in the vegetated zone and boundary layer flow theory in the free flow zone. However as well as the estimation of the drag coefficient this method requires knowledge of the canopy top roughness.

- In emergent vegetation the concentration profiles become symmetrical a relatively short distance from the injection point and length of the advective zone is shortened compared to a non vegetated case. However in submerged flow the increased vertical shear means that skew persists a long distance downstream of the injection. This delays the start of the equilibrium zone when compared to emergent conditions.

- In emergent vegetation profiles of velocity become approximately uniform over the width and the depth of flow. This leads to a reduction in shear dispersion and a consequent reduction in the rate of longitudinal mixing.

- Mixing in submerged vegetation is dominated by vertical shear dispersion. Therefore for a given flow rate mixing is dependant on the submergence ratio of the flow and the rate of vertical mass transport. Vertical mass transport is dependant on the relative size and strength of the mixing layer which is generated at the top of the canopy. In canopies where the mixing layer penetrates to the bed, longitudinal mixing rates are lower as the greater vertical mass transport reduces the effectiveness of shear dispersion.

- The longitudinal dispersion coefficient in such a shear dominated flow can be predicted using an adapted Chickwendu (1986) approach, provided an accurate prediction of the channel flow resistance and the size and strength of the mixing layer are made.

- This work has shown that whilst studies using artificial vegetation have been useful in characterising the underlying mechanics of vegetated flow, methods for predicting flow resistance and mixing cannot ignore the extra variables introduced by the presence of real vegetation. Studies with artificial vegetation cannot characterise important variables such as the drag coefficient or mixing layer penetration depth in real vegetation. Therefore future work should concentrate on characterising the behaviour of real types of different vegetation.

Acknowledgements

I would like to acknowledge the help and support of the following persons

Joby Boxall for his excellent supervision and guidance, Ian Guymer for all of his input and sound advice. All the technicians who have helped me set up my laboratory work, particularly Paul Osborne who was never troubled my attempts (with varying degrees of success) to 'grow things' in an engineering lab. All the members of the PWG for their help and support, particularly to Sarah for being a sympathetic ear throughout the PhD. My girlfriend Alma for her patience, advice, support, encouragement and not to mention all the late night cooking. And finally my parents, without whom I never would have made it to the start of my PhD, nevermind the end.

References

Albertson, M.L., Barton, J.R. and Simons, D.B. (1960) "Fluid Mechanics for Engineers." Prentice Hall. Englewood Cliffs, NJ.

Babaeyan-Koopaei, K., Ervine, D. A., Carling, P. A. and Cao, Z. (2002) "Velocity and turbulence measurements for two overbank flow events in River Severn." *Journal of Hydraulic Engineering*, **128** (10): 891.

Bakhmeteff, B. A. (1936) "The Mechanics of Turbulent Flow." Princeton University Press, Princeton, 66.

Berrittella, M., Hoekstra, A. Y., Rehdanz, K., Roberto, R., and Tol, R. S. J. (2007) "The economic impact of restricted water supply: A computable general equilibrium analysis." *Water Research,* **41**(8): 1799.

Beer, T and Young, P.C. (1984) "Longitudinal Dispersion in Natural Streams." *Journal of Environmental Engineering,* **109** (5): 1049-1069.

Boussinesq, J. (1877), "Théorie de l'Écoulement Tourbillant", *Mem. Présentés par Divers Savants Acad. Sci. Inst. Fr.*, Vol. 23, pp. 46-50.

Boxall, J. B. (2000) "Dispersion of Solutes in Sinuous Open Channel Flows." Phd Thesis, University Of Sheffield, U.K.

Boxall, J. B. and Guymer, I. (2001) "Estimating transverse mixing coefficients." *Proceedings of the Institution of Civil Engineers: Water, Maritime and Energy,* **148**(4): 263.

Boxall, J. B. and Guymer, I. (2007) "Longitudinal mixing in meandering channels: New experimental data set and verification of a predictive technique." *Water Research,* **41**(2): 341.

British Standards, EN ISO 5167-4 (2003) "Measurement of Fluid Flow by Means of Pressure Differential Devices Inserted in Circular Cross-section Conduits Running Full – Part 4: Venturi Flumes."

Carollo, F. G., Ferro, V. and Termini, D. (2002) "Flow velocity measurements in vegetated channels." *Journal of Hydraulic Engineering,* **128**(7): 664.

Chadwick, A. and Morfett, J. (1994) "Hydraulics in Civil and Environmental Engineering." E & FN Spon.

Chatwin, P. C. (1973) "Calculation Illustrating Effects of the Viscous Sublyer on Longitudinal Dispersion." *Quarterly Journal of Mechanics and Applied Mathematics,* **26**(Part 4): 427.

Chen, C.L. (1976) "Flow resistance in broad shallow grassed channels." *ASCE Journal of Hydraulics Division,* **102**, pp. 307–322.

Chiew, Y., and Tan, S. (1992) "Frictional Resistance of Overland Flow on Tropical Turfed Slope." *Journal of Hydraulic Engineering,* **118**(1): 92-97.

Chikwendu, S. C. (1986) "Calculation of Longitudinal Shear Dispersivity Using an N-zone Model ans N Yields Infinity." *Journal of Fluid Mechanics,* **167**: 19.

Christensen, B. A. (1985) "Open Channel and Sheet Flow Over Flexible Roughness." *Proceedings of the 21st IAHR Congress.* Melbourne, Australia. 462–467.

Chow, V. (1959) "Open-Channel Hydraulics", Mcgraw-Hill.

Clapham, A. R., Tutin, T. G. and Moore, D. M. (1987) "Flora of the British Isles." Cambridge University Press.

Day, T. J. and Wood, I. R. (1976) "Similarity of the Mean Motion of Fluid Partials Dispersing in a Natural Channel." *Water Resources Research,* **12**(4): 666.

Deng, Z. Q., Bengtsson, F., Singh, V. P. and Adrian, D. D. (2002) "Longitudinal Dispersion in Single-Channel Streams." *Journal of Hydraulic Engineering,* **128**(10): 901.

Dennis, P. (2000) "Longitudinal Dispersion due to Surcharged Manholes." Phd Thesis, University Of Sheffield, U.K.

Doppler, C. (1842) - Über das farbige Licht der Doppelsterne und einige andere Gestirne des Himmels - Versuch einer das Bradleysche Theorem als integrirenden Theil in sich schliessenden allgemeineren Theorie (On the coloured light of the binary refracted stars and other celestial bodies - Attempt of a more general theory including Bradley's theorem as an integral part) Reprinted in: Kurt Bretterbauer et al.., (1988) "Christian Doppler, Leben und Werk". *Der Dopplereffekt*, Salzburg

Douglas, J. F., Gasiorek, J. M., Swaffield, J. A., Jack, L.B. (2005) "Fluid Mechanics - Fifth Edition." Pearson Education Limited, Harlow, England.

Dutton, R. J. (2005) "Modelling Transient Storage Processes." Phd Thesis, University Of Sheffield, U.K.

Einstein, H.A. and Banks, H. B. (1950) "Fluid Resistance of Composite Roughness." *Trans. Am. Geophys. Union,* **3**: 603-610.

Elder, J. W. (1959) "The Dispersion of Marked Fluid in Turbulent Shear Flow." *Journal of Fluid Mechanics,* **5:** 544-560.

El-Hakim, O. and Salama, M. M. (1992) "Velocity distribution inside and above branched flexible roughness." *Journal of Irrigation and Drainage Engineering,* **118**(6): 914.

Elliot, A. H. (2000) "Settling of fine sediment in a channel with emergent vegetation." *Journal of Hydraulic Engineering,* **126**(8): 570-577.

Findlay, G. H. and Ellul, G. A. (1976) "The application of computers to prepare design tables for grasses waterways and flumes." *Agricultural Engineering,* **Vol 5:** 20-24

Finnigan, J. (2000) "Turbulence in plant canopies." *Annual Review of Fluid Mechanics,* **32**: 519.

Fathi-Maghadam, M. and Kouwen, N. (1997) "Nonrigid, nonsubmerged, vegetative roughness on floodplains." *Journal of Hydraulic Engineering,* **123**(1): 167.

Fischer, H.B. (1967) "The Mechanics of Dispersion in Natural Streams." *Journal of the Hydraulics Division,* **93**(6):187-216

Fischer, H. B. (1973) "Longitudinal Dispersion and Turbulent Mixing in Open Channel Flow." *Annual Review of Fluid Mechanics,* **5**: 59-78.

Fischer, H. B. and Hanamura, T. (1975) "Effects of Roughness Strips on Transverse Mixing in Hydraulic Models." *Water Resources Research,* **11**(2): 362.

Fukuoka, S. and Sayre, W. W. (1973) "Longitudinal Dispersion in Sinious Channels." *Journal of the Hydraulics Division, ASCE,* **99**(HY1): 195.

Gambi, M.C., Nowell, A.R.M. and Jumars, P.A. (1990) "Flume observations on flow dynamics in Zostera marina (eelgrass) beds." *Marine Ecology Progress Series,* **61**: 159 –169.

Ghisalberti, M. and Nepf, H. M. (2004) "The limited growth of vegetated shear layers." *Water Resources Research,* **40**(7): 075021-0750212.

Ghisalberti, M. and Nepf, H. M. (2005). "Mass transport in vegetated shear flows." *Environmental Fluid Mechanics,* **5**(6): 527.

Goring, D. G. and Nikora, V. I. (2002) "Despiking acoustic doppler velocimeter data." *Journal of Hydraulic Engineering,* **128**(1): 117.

Gourlay, M.R. (1970) Discussion of: "Flow resistance in vegetated channels." by Kouwen N, Unny, T.E. and Hill, H.M. *Journal of the Irrigation and Drainage Division of the American Society of Civil Engineers* **96**(IR3): 351-357.

Green, J. C. (2005) "Modelling flow resistance in vegetated streams: Review and development of new theory." *Hydrological Processes,* **19**(6): 1245.

Green, J. E. P. and Garton, J. E. (1983) "Vegetation Lined Channel Design Proceedures." *Transactions of the ASCE,* **26**(2): 436:439.

Guymer, I. (1998) "Longitudinal Dispersion in a Sinuous Channel with Changes in Shape." *Journal of Hydraulic Engineering, ASCE,* Vol. **124**, No1, pp.33-40.

Haber, B. (1982) "Über den Erosionsbeginn bei der Überströmung von flexiblen Rauheitselementen." Mitteilungen des Leichtweiss-Institutes für Wasserbau der Technischen Universität Braunschweig. Heft 74.

Hall, B. R. and Freeman, G. E. (1994) "Study of hydraulic roughness in wetland vegetation takes a new look at Mannings' n." *The Wetlands Res. Prog. Bulletin,* US Army Corps of Engrs, Wtrwy. Experiment Station **4**(1): 1–4.

Hinze, J. O. (1964) "Turbulent Pipe Flow." *The Mechanics of Turbulence,* Gordon Breach, New York. 129-165.

Hoffman, M. R. (2004) "Application of a Simple Space-Time Averaged Porous Media Model to Flow in Densely Vegetated Channels." *Journal of Porous Media,* **7**(3): 183-191.

Holly, F. M. (1985) "Dispersion in Rivers and Coastal Waters – 1. Physical Principles and Dispersion Equations." Elisver, London, 1-37.

Jadhav, R. S. and Buchberger, S. G. (1995) "Effects of vegetation on flow through free water surface wetlands." *Ecological Engineering,* **5**: 481-496.

James, C. S., Birkhead, A. L., Jordanova, A. A. and O'Sullivan, J. J. (2004) "Flow resistance of emergent vegetation." *Journal of Hydraulic Research,* **42**(4): 390.

Jarvela, J. (2002) "Flow resistance of flexible and stiff vegetation: A flume study with natural plants." *Journal of Hydrology,* **269**(1-2): 44.

Jarvela, J. (2004) "Determination of flow resistance caused by non-submerged woody vegetation." *International Journal of River Basin Management,* **2**(1): 61-70.

Jarvela, J. (2005) "Effect of submerged flexible vegetation on flow structure and resistance." *Journal of Hydrology,* **307**(1-4): 233.

Jobson, H. E. and Sayre, W.W. (1970a) "Predicting Velocity Profiles in Open Channels." *ASCE,* 96 (HY10), 1983-1996.

Jobson, H. E. and Sayre, W.W. (1970b) "Vertical Transfer in Open Channel Flow." *ASCE,* 96 (HY3), 703-724.

Jobson, H. E. (1997) "Predicting travel time and dispersion in rivers and streams." *Journal of Hydraulic Engineering,* **123**(11): 971.

Jordanova, A. A., James, C. S. and Birkhead, A. L. (2006) "Practical estimation of flow resistance through emergent vegetation." *Water Management,* **159**(3): 173.

Kadlec, R. H. (1990) "Overland flow in wetlands. Vegetation resistance." *Journal of Hydraulic Engineering,* **116**(5): 691.

Kironoto, B. A. and Graf W. H. (1994) "Turbulence characteristics in rough uniform open-channel flow." *Proceedings of the Institution of Civil Engineers, Water Maritime and Energy,* **106**(4): 333.

Klopstra, D., Barneveld, H. J., Van Noortwijk, J. M. and Van Velzen, E. H. (1997) "Analytical model for hydraulic roughness of submerged vegetation." *Proceedings, Congress of the International Association of Hydraulic Research, IAHR,* San Francisco, CA, USA, ASCE, New York, NY, USA.

Kouwen, N., Unny, T. E., Hill, H. M., (1969) "Flow Redardance in Vegetated Channels." *Journal of the Irrigation and Drainage Division,* **95**(IR2): 329.

Kouwen, N. and Unny, T. E. (1973) "Flexible Roughness in Open Channels." *Journal of the Hydraulics Division,* **99**(HY5): 728.

Kouwen, N. and Li, R. M. (1980) "Biomechanics of vegetative channel linings." *Journal of the Hydraulics Division, ASCE,* **106** (HY6, Proc. Paper, 15464): 1085.

Kouwen, N. (1988). "Field estimation of the biomechanical properties of grass." *Journal of Hydraulic Research,* **26**(5): 559.

Kouwen, N. (1990) "Modern approach to the design of grassed channels." *Irrigation and Drainage - Proceedings of the 1990 National Conference,* p 160-167.

Kouwen, N. and Fathi-Moghadam, M. (2000) "Friction factors for coniferous trees along rivers." *Journal of Hydraulic Engineering,* **126**(10): 732.

Kutija, V. and Hong, H. T. M. (1996) "Numerical model for assessing the additional resistance to flow introduced by flexible vegetation." *Journal of Hydraulic Research,* **34**(1): 99.

Leonard, L. A. and Luther, M.E. (1995) "Flow hydrodynamics in tidal marsh canopies." *Limnology and Oceanography,* **40** pp. 1474–1484.

Li, R. M. and Shen, H. W. (1973) "Effect of tall vegetations on flow and sediment." *Journal of the Hydraulics Division,* **99**(HY5): 814.

Lightbody, A. F. and Nepf, H. M. (2006) "Prediction of near-field shear dispersion in an emergent canopy with heterogeneous morphology." *Environmental Fluid Mechanics,* **6**(5): 477.

Linder, K. (1982) "Der stromungswiderstand von Pflanzenbestanden" *Mitteil des Leichtweiß-Insistutes fur Wasserbau der TU Braunschweig,* Heft 75.

Lopez, F. and Garcia, M. (1998) "Open-channel flow through simulated vegetation: suspended sediment transport modeling." *Water Resources Research,* **34**(9): 2341.

Lui, H. (1977) "Predicting dispersion coefficient of streams." *Environmental Engineering Division, ASCE,* **103 (1)**, pp. 59–69.

Magazine, M. K., Pathak, S. K. and Pande, P. K. (1988) "Effect of bed and Side Roughness on Dispersion in Open Channels." *Journal of Hydraulic Engineering,* **114**(7): 766.

McNulty, A. J. and Wood, I. R. (1983) "Some Experimaental and Theoretical Results for the Dispersion from a Continuous Point Souce of Pollutant." *Proceedings - 8th Australasian Fluid Mechanics Conference,* Newcastle, Australia.

McQuivey, R. S. and Keefer, T. N. (1974) "Simple Method For Predicting Dispersion in Streams." *Journal of Environmental Engineering Division, ASCE.* **100**(EE4): 997.

Middleton, G. and Southard, J.B. (1984) "The Mechanics of Sediment Movement." *S.E.P.M.* **3**

Murota, A., Fukuhara, T. and Sato, M. (1984) "Turbulence structure in vegetated open channel flows." *Journal of Hydroscience and Hydraulic Engineering,* **2** 1 pp. 47–61.

Murphy, E., Ghisalberti, M. and Nepf, H. M (2007) "Model and laboratory study of dispersion in flows with submerged vegetation." *Water Resources Research,* **43**(5): 05438.

Nepf, H. M., Mugnier, C. G. and Zavistoski, R.A. (1997) "The Effects of Vegetation on Longitudinal Dispersion." *Estuarine, Costal and Shelf Science,* **44**: 675-684.

Nepf, H. M., Sullivan, J.A. and Zavistoski, R.A. (1997) "A model for diffusion within emergent vegetation." *Limnology and Oceanography,* **42**(8): 1735-1745.

Nepf, H. M. (1999) "Drag, turbulence and diffusion in flow through emergent vegetation." *Water Resources Research,* **35**(2): 479.

Nepf, H., Ghisalberti, M., White, B. and Murphy, E. (2007) "Retention time and dispersion associated with submerged aquatic canopies." *Water Resources Research,* **43**(4): W04422.

Nepf, H. M. and Vivoni, E. R. (2000) "Flow structure in depth- limited, vegetated flow." *Journal of Geophysical Research,* **105**(C12): 547-528.

Nokes, R. I. and Wood, I. R. (1987) "Turbulent dispersion of a steady of positively or negativley buoyant particles in two dimensions." *Journal of Hydraulic Research,* **25**(1): 103.

Newton, I. (1687) "Philosophiae Naturalis Principia Mathematica."

Nezu, I. (1977b) "Turbulence Intesities in Open Channel Flows." *Proc. of Japan Soc. Civil Engineers,* **261:** 67-76

Petryk, S. and Bosmajian, G. (1975) "Analysis of Flow though Vegetation." *Journal of the Hydraulics Division,* **101**(7): 884.

Plate, E. J. and Quraishi, A. A. (1965) "Modeling of Velocity Distributions Inside and Above Tall Crops." *Journal of Applied Meteorology,* **4**(3): 400.

Poggi, D., Porporato, A., Ridolfi, L., Albertson, J. D., and Katul, G. G. (2004) "The effect of vegetation density on canopy sub-layer turbulence." *Boundary-Layer Meteorology,* **111**(3): 565.

Pope, S.B. (2000) "Turbulent Flows", Cambridge University Press.

Prandtl, L. (1925) "Bericht ueber Untersuchungen zur ausgebileten Turbulenz." *ZAMM 5*, pp. 136–139.

Raupach, M. R., Finnigan, J. J. and Brunet, Y. (1996) "Coherent Eddies and turbulence in vegetation canopies: The mixing-layer analogy." *Boundary-Layer Meteorology,* **78**(3-4): 351.

Richter, K. M. (2003) "Constructed wetlands for the treatment of airport de-icer." Phd Thesis, University Of Sheffield, U.K.

Righetti, M. and Armanini, A. (2002) "Flow resistance in open channel flows with sparsely distributed bushes." *Journal of Hydrology,* **269**(1-2): 55.

Robert, A. (2003) "River Processes: A Introduction to Fluvial Hydraulics." Arnold.

Rutherford, J. C. (1994). "River Mixing." J Wiley and Sons Ltd.

Ree, W.O. and Palmer, V.J. (1949) "Flow of Water in Channels Protected by Vegetated Linings." *US Soil Conservation Bulletin,* **976**: 1-115.

Sand-Jensen, K. and Pedersen, O. (1999) "Velocity gradients and turbulence around macrophyte stands in streams." *Freshwater Biology,* Vol. **42**. Page 315 - 328.

Sayre, W.W. (1968) "Dispersion of Mass in Open Channel Flow." Phd Thesis, Colorado State University, Fort Collins.

Schiller, E.J. and Sayre, W.W. (1973) "Vertical Mixing of Heated Effluents in Open Channel Flow." *Report No. 148,* Iwoa Institue of Hydraluic Reaseach, University of Iowa.

Seo, I. W. and Cheong, T. S. (1998) "Predicting longitudinal dispersion coefficient in natural streams." *Journal of Hydraulic Engineering,* **124**(1): 25.

Seo, I. W. and Baek, K. O. (2004) "Estimation of the Longitudinal Dispersion Coefficient Using the Velocity Profile in Natural Streams." *Journal of Hydraulic Engineering,* **130**(3): 227.

Shaw, A. D. (2000) "The effect if suspended sediment concentration on the mixing of neutrally buoyant aqueous phase tracers in open channel flows." PhD Thesis, University Of Sheffield, U.K.

Shucksmith. J., Boxall, J. B., Guymer, I. (2007) "Importance of advective zone in longitudinal mixing experiments." *Acta Geophysica,* **V55**(1): 95.

Smart, P. L. and Laidlaw, I. M. J. (1977) "An evaluation of some fluorescent dyes for water tracing." *Water Resources Research,* **13:** 15-33.

Stefan, H. G. and Demetracopoulos, A. C. (1981) "Cells in Series Simulation of Riverine Transport." *Journal of the Hydraulics Division, ASCE,* **107**(6): 675.

Stephan, U. and Gutknecht, D. (2002) "Hydraulic resistance of submerged flexible vegetation." *Journal of Hydrology,* **269**(1-2): 27.

Stone, B. M. and Shen, H. T. (2002) "Hydraulic resistance of flow in channels with cylindrical roughness." *Journal of Hydraulic Engineering,* **128**(5): 500.

Taylor, G.I. (1921) "Diffusion by Continuous Movements". *Proc. London Math. Soc., Ser. 2,* **20:** 196-212

Taylor, R.P., Coleman, H.W and Hodge, B.K. (1985) "Prediction of turbulent rough-wall skin friction usinga discrete element approach." *Journal of Fluids Engineering,* **107.** pp 251-257.

Tanino, Y. and Nepf, H.M. (2007) "Experimental investigation of lateral dispersion in aquatic canopies." *Proceedings of the 32nd Congress of IAHR,* Venice, Italy.

Temple, D. M. (1986) "Velocity Distribution Coefficients For Grass-Lined Channels." *Journal of Hydraulic Engineering,* **112**(3): 193.

Temple, D.M., Robinson, K.M., Ahring, R.M. and Davis, A.G. (1987) "Stability design of grass-lined open channels." *Agric. Handbook 667,* Agric. Res. Service, U.S. Depatment of Agriculture, Washingtom, D.C.

Thomas, G.B. and Finney, R.L. (1996) "Calculus" Addison-Wesley Publishing Company Inc.

Tsihrintzis, V.A. (2001) Discussion of "Variation of roughness coefficients for unsubmerged and submerged vegetation" by Wu, F.-C., Shen, H.W., Chou, Y.-J., *ASCE Journal of Hydraulic Engineering* **131** (3) pp. 241–244.

Tsai, Y. H. and Holley, E. R. (1978) "Temporal Moments for Longitudinal Dispersion." *Journal of the Hydraulics Division, ASCE.* **104**(12): 1617.

Tsujimoto, T. and Kitamura, T. (1990) "Velocity profile of flow in vegetated-bed channels." *KHL Progressive Report, Hydraulics Lab., Kanazawa Univ.* **1**, pp. 43–55.

Tsuijimoto, T., Kitamura, T. and Fujii, Y. (1995) Hydraulic Resistance of Flow in Vegetated-bed Channels". *KHL Progressive Report,* Hydraulic Lab., Kanazawa University, **4**,43-55

Turner, A.K. and Chanmeesri, N. (1984) "Shallow flow of water through non-submerged vegetation." *Agricultural Water Management (Amsterdam),* **8**, pp. 375–385.

Valentine, E. M. and Wood, I. R. (1977) "Longitudinal Dispersion with Dead Zones." *Journal of the Hydraulics Division, ASCE,* **103**(9): 990.

Valentine, E. M. (1978) "The Effects of Boundary Roughness on Longitudinal Dispersion." PhD Thesis, University Of Canterbury, Christchurch.

Velasco, D., Bateman, A., Redondo, J. M. and Demedina, V. (2003) "An Open Channel Flow Experimental and Theoretical Study of Resistance and Turbulent Characterization over Flexible Vegetated Linings." *Flow, Turbulence and Combustion,* **70**(1-4): 69.

Wallis S.G., Guymer, I. and Bilgi, A. (1989a) "A practical engineering approach to modelling longitudinal dispersion." *Proceedings of the International Conference on the Hydraulic and Environmental Modelling of Coastal, Estuarine and River Waters*, University of Bradford, England, 19th-21th September, Gower Technical Press, pp 291-300.

Wallis, S. G., Young, P. C. and Bevan, K. J. (1989b) "Experimental investigation of the aggregated dead zone model for longitudinal solute transport in stream channels." *Proceedings of the Institution of Civil Engineers (London). Part 1 - Design & Construction,* **87**(2): 1.

Watanabe, T. and Kondo, J. (1990) "The infulence on canopy structure and density upon the mixing length within and above vegetation." *Journal of the Meteorological Society of Japan,* **68**(2): 227-235.

White, B. L. and Nepf, H. M. (2003) "Scalar transport in random cylinder arrays at moderate Reynolds number." *Journal of Fluid Mechanics,* (**487**): 43.

WinADV32. Ver 2.022. Public domain software, developed by Tony W Wahl, Water Resources Research laboratory, Bureau of Reclamation, Denver, Colorado.

Wilson, C. A. M. E., Stoesser, T. and Bates, P.D. (2005) "Modelling of Open Channel Flow through Vegetation." *Computational Fluid Dynamics: Applications in Environmental Hydraulics*, John Wiley & Sons, Ltd. p395.

Wilson, C. A. M. E. and Horritt, M. S. (2002) "Measuring the flow resistance of submerged grass." *Hydrological Processes,* **16**(13): 2589.

Wilson, C. A. M. E., Yagci, O., Rauch, H. P. and Olsen, N. R. B. (2006) "3D numerical modelling of a willow vegetated river/floodplain system." *Journal of Hydrology,* **327**(1-2): 13.

Wu, F. C., Shen, H. W. and Chou, Y. (1999) "Variation of roughness coefficients for unsubmerged and submerged vegetation." *Journal of Hydraulic Engineering,* **125**(9): 934.

Young, P., Jakeman, A. and McMurtrie, R. (1980) "An Instrumental Variable Method for Model Order Identification." *Automatica*, **16**: 281-294

Young, P.C. and Wallis, S. G. (1986) "The Aggregated Dead Zone Model for Dispersion in Rivers." *International Conference on Water Quality Modelling in the Inland Natural Environment*, Bornmouth, England, L1, pp 421-433.

Water demand figures in Table 1 taken from 'www.worldwatercouncil.org' viewed on 5 December 2007.

Images of Carex and reeds in nature taken from 'www.yarningdale.co.uk' viewed on 16 July 2007.